

D101.11: 5-856-1/ rep.

TM 5-856-1

DEPARTMENT OF THE ARMY TECHNICAL MANUAL

DESIGN OF STRUCTURES TO RESIST THE EFFECTS OF ATOMIC WEAPONS

WEAPONS EFFECTS DATA

RETURN TO GOV. DOCS. CLERK

This is a reprint of former EM 1110-345-413, 1 July 1959, including effective pages from Change No. 1 and 2. Redesignated TM 5-856-1 by DA Cir 310-28, 17 March 1965.

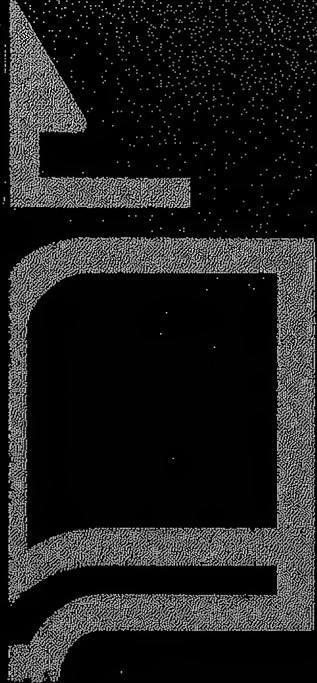


HEADQUARTERS, DEPARTMENT OF THE ARMY
NOVEMBER 1960

JULY 1959

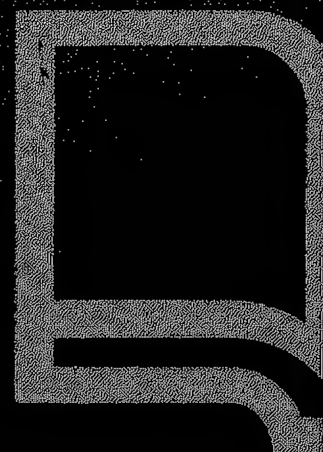
TAGO 9008A

U.S. SUPT. OF DOCS.



B5

101.11.5-856



A5



B5



A4



B5

B4

TM 5-856-1

HEADQUARTERS
DEPARTMENT OF THE ARMY
WASHINGTON, D.C., 1 July 1959

TM 5-856-1, is published for the use of all concerned.
By Order of the Secretary of the Army:

LYMAN L. LEMNITZER
General, USA
Chief of Staff

Official:
R. V. LEE
Major General, USA
The Adjutant General

ENGINEERING AND DESIGN

DESIGN OF STRUCTURES TO RESIST THE EFFECTS OF ATOMIC WEAPONS

WEAPONS EFFECTS DATA

TABLE OF CONTENTS

Paragraph		Page
	INTRODUCTION	
3-01	PURPOSE AND SCOPE	1
3-02	REFERENCES	1
	a. References to Material in Other Manuals of This Series	2
	b. Bibliography	2
	c. List of Symbols	2
3-03	RESCISSIONS	2
3-04	GENERAL	2
3-05	BLAST WAVE PHENOMENA	3
	a. Infinite Atmosphere	3
	b. Finite Height of Burst	10
3-06	SCALING BLAST PHENOMENA	19
	LOADING ON RECTANGULAR STRUCTURES WITHOUT OPENINGS	
3-07	LOADING ON STRUCTURES	19
	a. Diffraction and Drag Loading	21
3-08	LOADING ON CLOSED RECTANGULAR STRUCTURES	22
	a. Average Front Wall Overpressure \bar{P}_{front}	26
	b. Average Back Wall Overpressure \bar{P}_{back}	37
	c. Average Net Horizontal Overpressure \bar{P}_{net}	38
	d. Local Roof Overpressure P_{roof}	39
	e. Average Roof Overpressure \bar{P}_{roof}	42
	f. Local and Average Side Wall Overpressure P_{side} and \bar{P}_{side}	43
3-09	PROCEDURE FOR COMPUTATION OF LOADS ON CLOSED RECTANGULAR STRUCTURES	43
	a. Average Front Wall Overpressure vs Time	44
	b. Average Back Wall Overpressure vs Time	45
	c. Average Net Horizontal Overpressure vs Time	45
	d. Local Roof Overpressure vs Time	46
	e. Average Roof Overpressure vs Time	47

Paragraph

Page

	f. Local Side Wall Overpressure vs Time	48
	g. Average Side Wall Overpressure vs Time	48
3-10	NUMERICAL EXAMPLE OF COMPUTATIONS OF LOADS ON CLOSED RECTANGULAR STRUCTURE	48
	a. Average Front Wall Overpressure vs Time	48
	b. Average Back Wall Overpressure vs Time	49
	c. Average Net Horizontal Overpressure vs Time	50
	d. Local Roof Overpressure vs Time at Point x of Figure 3.35	50
	e. Average Roof Overpressure vs Time	51
	LOADING ON RECTANGULAR STRUCTURES WITH OPENINGS	
3-11	EFFECTS OF OPENINGS ON LOADING	53
	a. Average Exterior Front Wall Overpressure \bar{P}_{front}	54
	b. Average Interior Front Wall Overpressure $\bar{P}_{\text{i-front}}$	56
	c. Average Net Front Wall Overpressure $\bar{P}_{\text{f-net}}$	56
	d. Average Exterior Back Wall Overpressure \bar{P}_{back}	57
	e. Average Interior Back Wall Overpressure $\bar{P}_{\text{i-back}}$	58
	f. Average Net Back Wall Overpressure $\bar{P}_{\text{b-net}}$	62
	g. Average Exterior Roof Overpressure \bar{P}_{roof}	62
	h. Average Interior Roof Overpressure $\bar{P}_{\text{i-roof}}$	62
	i. Average Net Roof Overpressure $\bar{P}_{\text{r-net}}$	63
	j. Average Exterior Side Wall Overpressure \bar{P}_{side}	64
	k. Average Interior Side Wall Overpressure $\bar{P}_{\text{i-side}}$	64
	l. Average Net Side Wall Overpressure $\bar{P}_{\text{s-net}}$	64
3-12	PROCEDURE FOR COMPUTATION OF LOADS ON RECTANGULAR STRUCTURES WITH OPENINGS	65
	a. Average Exterior Front Wall Overpressure vs Time	65
	b. Average Interior Front Wall Overpressure vs Time	65
	c. Average Net Front Wall Overpressure vs Time	65
	d. Average Exterior Back Wall Overpressure vs Time	65
	e. Average Interior Back Wall Overpressure vs Time	66
	f. Average Net Back Wall Overpressure vs Time	66
	g. Average Exterior Roof Overpressure vs Time	66
	h. Average Interior Roof Overpressure vs Time	66
	i. Average Net Roof Overpressure vs Time	66
	j. Average Exterior Side Wall Overpressure vs Time	66
	k. Average Interior Side Wall Overpressure vs Time	67
	l. Average Net Side Wall Overpressure vs Time	67

Paragraph

Page

LOADING ON STRUCTURES WITH GABLED ROOFS

3-13	LOADING ON GABLED ROOFS	67
	a. Average Front Slope Roof Overpressure \bar{P}_{roof} Shock Front Parallel to Ridge Line	67
	b. Average Rear Slope Roof Overpressure \bar{P}_{roof} Shock Front Parallel to Ridge Line	70
	c. Average Overpressures, Shock Front Perpendicular to Ridge Line	70
3-14	PROCEDURE FOR COMPUTATION OF LOADS ON GABLED ROOFS	70
	a. Average Front Slope Roof Overpressure in First Bay vs Time, Shock Front Parallel to Ridge Line	70
	b. Average Rear Slope Roof Overpressure in First Bay vs Time, Shock Front Parallel to Ridge Line	71

LOADING ON EXPOSED STRUCTURAL MEMBERS

3-15	LOADING ON EXPOSED STRUCTURAL FRAMEWORKS	72
3-16	PROCEDURE FOR COMPUTATION OF LOADS ON EXPOSED STRUCTURAL FRAMEWORKS	74

LOADING ON CYLINDRICAL SURFACES

3-17	LOADING ON CYLINDRICAL ARCH SURFACES	75
	a. Cylindrical Arch Overpressure P_{cyl} , Axis Parallel to Shock Front	75
	b. Average End Wall Overpressure \bar{P}_{end} , Axis Parallel to Shock Front	84
	c. Local Cylindrical Arch Overpressure, Axis Perpendicular to Shock Front	84
	d. Average End Wall Overpressure, Axis Perpendicular to Shock Front	85
3-18	PROCEDURE FOR COMPUTATION OF LOADS ON CYLINDRICAL ARCHES	85
	a. Local Cylindrical Arch Overpressure vs Time, Axis Parallel to Shock Front	85
	b. Average End Wall Overpressure vs Time, Axis Parallel to Shock Front	86
	c. Local Cylindrical Arch Overpressure vs Time, Axis Perpendicular to Shock Front	86
	d. Average End Wall Overpressure vs Time, Axis Perpendicular to Shock Front	86

LOADING ON DOMES

3-19	LOADING ON SPHERICAL DOME SURFACES	86
3-20	PROCEDURE FOR COMPUTATION OF LOADS ON SPHERICAL DOMES	88

Paragraph		Page
	LOADING ON BURIED STRUCTURES	
3-21	LOADING ON BURIED STRUCTURES	88
	a. Local Roof Overpressure P_{roof}	93
	b. Average Roof Overpressure \bar{P}_{roof}	93
	c. Local Front and Back Wall Overpressures P_{front} and P_{back}	94
	d. Average Front Wall Overpressure \bar{P}_{front}	94
	e. Average Back Wall Overpressure \bar{P}_{back}	95
	f. Local Side Wall Overpressure P_{side}	95
	g. Average Side Wall Overpressure \bar{P}_{side}	95
	h. Overpressure on Underside of Buried Structure	95
3-22	PROCEDURE FOR COMPUTATION OF LOADS ON BURIED STRUCTURES	96
	RADIATION	
3-23	NUCLEAR RADIATION PHENOMENA	96
3-24	NUCLEAR RADIATION SHIELDING	100
	a. Initial Radiation Shielding	101
	b. Fallout Radiation Shielding	106
3-25	THERMAL RADIATION	107
	a. Phenomena	107
	b. Scaling	108
	c. Effect on Materials	108
	CRATERING	
3-26	CRATERING PHENOMENA	112
	BIBLIOGRAPHY	115
	APPENDIX A	
	TRANSONIC DRAG PRESSURES	
A-01	INTRODUCTION	119
A-02	GENERAL FEATURES OF THE FLOW	120
A-03	METHOD FOR COMPUTATION OF PRESSURES IN THE TRANSONIC RANGE	126
	a. Cases in Which the Initial Flow Is Supersonic	126
	b. Cases in Which the Initial Flow Is Subsonic	128

EM 1110-345-413
1 July 59

		Page
Paragraph		
A-04	NUMERICAL RESULTS FOR THE GIVEN CASES	129
A-05	REMARKS CONCERNING DOME OR CONICAL-SHAPED STRUCTURES	133
	REFERENCES	134

!

i

L

LIST OF SYMBOLS

A	Area of a structural member cross section (sq. in.) Tributary area of a structure for purpose of computing load (sq. ft)
A_B	Area of steel beam cross section, composite beam construction only (sq. in.)
A_b	Net area of the rear face of a rectangular structure with openings (sq. ft)
A_c	Area of concrete in cross section (sq. in.)
A_f	Area of flange of structural steel beam or girder (sq. in.) Net area of the exterior front wall of a rectangular structure with openings (sq. ft)
A_g	Cross section area of concrete column (sq. in.)
A_{gf}	Gross area of the exterior front face of a rectangular structure (sq. ft)
A_n	Area of each portion of the subdivided face of a rectangular structure with openings (sq. ft)
A_{of}	Area of openings in the front wall of a rectangular structure (sq. ft)
A_R	Net area of the back wall of a rectangular structure with openings (sq. ft)
A_r	Area of reinforcing steel bars parallel to steel beams in composite construction (sq. in.)
A_s	Area of tension steel in reinforced concrete member (sq. in.)
A_v	Area of one stirrup of the web reinforcement of a reinforced concrete member (sq. in.)
A_w	Area of web of steel beam (sq. in.)
A'_s	Area of compression steel in reinforced concrete member (sq. in.)
a	Clear distance between flanges of a steel beam (in.) Depth of compression area of concrete (in.) Short side dimension of two-way slabs (ft) Column spacing in flat slab construction (ft) Acceleration of mass (ft/sec ²)
$a_{g,1}, a_{g,2}, a_{g,n-1}, a_{g,n+1}$	Acceleration of the g^{th} floor mass at times $t_1, t_2, t_{n-1}, t_{n+1}$, respectively
$a_g(t)$	Acceleration of the g^{th} floor mass as a function of time
$a_1, a_2 \dots a_{n-1}, a_n, a_{n+1}$	Acceleration at time $t_1, t_2, t_{n-1}, t_n, t_{n+1}$, respectively

a'	Distance from edge "a" to centroid of the load on area "A"
a''	Distance from edge "a" to the centroid of the inertial force
B	Peak value of externally applied load Elastic stiffness coefficient for soil under rocking foundation
B_e	Equivalent peak value of the externally applied load
B_{gX}	Peak value of the effective load on the g^{th} floor mass of a multi-story building
B_g	Peak value of the external load, $f_g(t)$, on the g^{th} floor mass
b	Width of flange of steel beam (in.) Width of compression flange of reinforced concrete beam (in.) Long side dimension of two-way slabs (ft)
b_f	Flange width of channel section (in.)
b_s	Width of longitudinal web stiffener for steel beams (in.)
b'	Width of stem of reinforced concrete tee beam (in.) Width of flange of steel beam used in composite construction (in.) Distance from edge "b" to centroid of load on area "B"
b''	Distance from edge "b" to the centroid of the inertial force
C	Compression force developed in reinforced concrete member (kips) Static compression column influence factor for shear walls
C_c	Crater depth factor for underground burst
C_d	Dynamic compression column influence factor for shear walls Average drag coefficient
C_D	Local drag coefficient
C_m	Maximum ACI Code moment coefficient obtainable for any point on a slab (equation 6.52)
C_R	Ratio of maximum resistance to peak load, $C_R = R_m/B$
C_{gR}	Parameter defined by equation 5.94
C_s	Seismic wave velocity (fps)
C_T	Ratio of load duration to natural period of oscillation, $C_T = T/T_n$
C_t	Approximate coefficient for determining elastic truss deflection (varies with type of truss)
C_W	Ratio of maximum work done to absolute maximum work done, $C_W = \frac{W_m}{W_p}$
C'_D	Local drag coefficient for a cylindrical segment of infinite length
\bar{C}_{ij}	Value of determinate formed by omitting the row and column containing the coefficient C_{ij} from the matrix $[C]$

Symbols

EM 1110-345-413

1 July 59

c	Distance from neutral axis to the extreme fiber (in.) Cohesive strength of the soil as determined by conventional laboratory testing procedures (psi) The clear distance between compression flange and stiffener
c _o	Velocity of sound in undisturbed air (fps)
c _{refl}	Velocity of sound in the region of reflected overpressure (fps)
D	Diameter of a cylindrical segment or a spherical dome (ft) Diameter of the smallest longitudinal reinforcing bar (in.) Diameter of spiral core of a concrete column
D.L.F	Dynamic Load Factor = x_m/x_s
D.I.F	Dynamic Increase Factor for strength of materials
d	Depth of burst of bomb below ground surface (ft) Height of burst of bomb above ground surface (ft) Depth from the compression face of a beam or slab to the centroid of longitudinal tensile reinforcement (in.) Least lateral dimension of rectangular column (in.) Total depth of steel beam (in.) Over-all depth of truss (ft) Diameter or width of column capital in flat slab construction (ft) Diameter of circular reinforced concrete column (in.)
d'	Distance between centroids of compression and tensile steel in doubly reinforced concrete member
E	Modulus of elasticity, including Young's Modulus for steel and soil, of any structural material except concrete Energy absorbed by the equivalent system Explosive factor for cratering Compressive modulus of elasticity of concrete, kips/sq. in.
E _c	Initial tangent modulus of elasticity for concrete
E _f	Explosive factor for underground burst
E _g	Maximum allowable energy absorption for the g th story
e	Base of natural logarithms (2.718) Eccentricity of load, distance from gravity axis to point of application of load (in.) Center to center spacing of two trusses
e _c	Strain at failure (%)
e _s	Strain at initiation of strain hardening (%)
e _y	Strain at yield (%)
F	Horizontal force
F _{g(t)}	Sum of all external loads above the g th story, $f_g(t) + f_{g+1}(t) + \dots + f_n(t)$
F _n	Design lateral load on frame at time t _n

F_o	Summation of all external horizontal forces applied to structure, including foundation reactions
F_p	Pressure factor for underground burst Normal component of total passive resistance force (kips)
$F(t)$	Load applied to a structural element or system as function of time
f	Fiber stress (psi)
f_a	Column critical buckling stress (psi)
f_{ad}	Average stress at design level due to axial load (psi)
f_B	Dynamic yield strength for structural steel in composite beam construction only (psi)
f_b	Elastic buckling stress due to bending (psi)
f_{bd}	Maximum stress due to bending at design level for steel members subjected to axial load and bending (psi)
f_{dy}	Dynamic yield strength of steel (psi)
$f_{gx}(t)$	Effective load on the g^{th} floor of a multi-story structure as a function of time
f_i	Initial static stress (psi)
f_{ly}	Lower static stress (psi)
f_r	Dynamic yield strength for reinforcing steel for composite beam construction only (psi)
f_t	Tensile strength of concrete (psi)
$f(t)$	Load applied to a structural element of system as a function of time
f_{uy}	Upper static yield point stress (psi)
f_y	Static yield point stress
f_1, f_2, f_3	Factors used in the design of tee beams
$f_1(t), f_2(t), f_g(t)$	Load applied to the first, second, and g^{th} floors of a multi-story building as a function of time
f'_c	Static ultimate compressive strength of concrete
f'_{dc}	Dynamic ultimate compressive strength of concrete
G	Solidity ratio of truss Shear modulus of elasticity (psi)
G.Z.	Ground zero (point on ground below point of detonation of air burst)
g	Acceleration of gravity
H	Impulse per unit area, impulse per foot of length, or total impulse (kip-sec) Depth of footing or wall below the surface of the ground Height of shear wall to center of roof beam

Symbols

EM 1110-345-413

1 July 59

H_e	Equivalent impulse acting on the equivalent system (kip-sec)
H_{gt}	Total impulse of the external load on the g^{th} floor mass (kip-sec)
H_t	Total impulse of the external load (kip-sec)
h	Height (ft) Story height (ft) Column height (ft) Height of a structure above ground (ft) Maximum thickness of channel flange (in.)
h_c	Clear height of column (ft)
h_g	Height of the g^{th} story of a multi-story building (ft)
h_n	Clearing dimension for each portion of the subdivided front face of rectangular structure with openings (ft)
h'	Clearing height of a closed rectangular structure (ft) Vertical distance from roof to point under consideration for buried structure (ft)
h'_b	Weighted average buildup height of the exterior rear face of a rectangular structure with openings (ft)
h'_f	Weighted average clearing height for the exterior front face of a rectangular structure with openings (ft)
h'_{ib}	Weighted average clearing height for the interior rear face of a rectangular structure with the openings (ft)
h'_{if}	Weighted average buildup height for the interior front face of a rectangular structure with openings (ft)
I	Moment of inertia ($in.^4$ or ft^4)
I_A	Inertial force of "A" portion of two-way slab
I_a	Average of the gross and transformed moments of inertia ($in.^4$ or ft^4)
I_B	Inertial force of "B" portion of two-way slab
I_g	Moment of inertia of the gross section ($in.^4$ or ft^4)
I_t	Moment of inertia of the transformed section ($in.^4$ or ft^4)
I_l	Moment of inertia of rectangular section in concrete tee beam design ($in.^4$)
I_2	Moment of inertia of tee section in concrete tee beam design ($in.^4$)
$I_n = I(t_n)$	Velocity impulse at time, t_n
I_o	Mass moment of inertia of structure about axis of rotation "O"
j	Ratio of distance between centroid of compression and centroid of tension to the depth, d
K	Modulus of strain hardening

KE	Kinetic energy
(KE) _a	Kinetic energy of the actual system
(KE) _e	Kinetic energy of the equivalent system
K _f	Either load, mass, or load-mass factor for slab fixed on four sides
K _{ij}	(i = 1, 2, 3,...; j = 1, 2, 3....) Stiffness influence coefficient (kips/ft)
K _L	Load factor
K _{LM}	Load-mass factor
K _M	Mass factor
K _{Pc}	Normal component of passive pressure coefficient accounting for the cohesive effect of any soil having an internal friction equal to ϕ
K _{Po}	Normal component of passive pressure coefficient for any soil with internal friction angle equal to ϕ and with zero wall friction developed
K _{Pϕ}	Normal component of passive pressure coefficient for any soil with internal friction angle equal to ϕ and with maximum wall friction developed
K _R	Resistance factor
K _s	Either load, mass, or load-mass factor for slab simply supported on four sides
KT	Kiloton, 1000 tons
K _z	Either load, mass, or load-mass factor for special edge conditions
K _o	Ratio of the maximum average overpressure to the reflected overpressure existing on an inclined roof
K'	Beam equivalent length coefficient used in the design of steel beam columns
K''	Column length factor used in the design of steel columns and beam columns
k	Spring constant, force required to cause unit deflection of spring (kips/ft) Soil pressure factor (psi)
k _c	Soil constant for underground explosion (psi)
k _E	Effective spring constant (kips/ft)
k _e	Equivalent spring constant (kips/ft)
k _{ep}	Spring constant in the elasto-plastic range
k ₁ , k ₂ , ... k _g ...	Spring constants for the first, second, and the g th stories of a multi-story building (kips/ft)
k _g	Simplified notation of k _{g,g-1}

Symbols

EM 1110-345-413

1 July 59

k_{gi}	-Spring constant of the coupling spring between the g^{th} and the i^{th} floors of a multi-story building (kips/ft)
k'_{gi}	$k'_{gi} = -k_{gi}$
$k_{g1}, k_{g2}, \dots, k_{gn}$	Spring constants of the springs connecting m_g with the masses $m_1, m_2, \dots, m_1, \dots, m_n$
L	Span length of beam or truss (ft) Unsupported length of beam (ft) Length of a rectangular structure in the direction of propagation of the blast wave (ft) Length of a cylindrical segment along the cylinder axis (ft) Length of shear wall center to center of column steel Spacing of columns in each direction
L_i	Distance from the outside of the front face to the inside rear face of a rectangular structure with openings (ft)
L'	Distance from the front face of a rectangular structure to a point under consideration on the roof or sides in the direction of propagation of the blast wave (ft) Length between sections of zero and maximum moment being considered (composite beams)
M	Bending moment applied to a section Moment of forces on piles about their centroidal axis Resisting moment of soil on the footing per unit width
M_c	Bending moment at center line of a beam or slab
M_{cn}	Negative resisting moment in column per foot, flat slabs (kip-ft)
M_{cp}	Positive resisting moment in column strip per foot, flat slabs (kip-ft)
M_D	Maximum design moment in a member under axial load, P_D
M_{dy}	Dynamic bending moment
M_{ed}	Elastic dynamic buckling moment
M_m	Maximum bending moment
M_{fa}	Component in a plane perpendicular to edge "a" of the total resisting moment along the fracture lines bounding area "A," two-way slabs (kip-ft)
M_{fb}	Component in a plane perpendicular to edge "b," of the total resisting moment along the fracture lines bounding area B, two-way slabs (kip-ft)
M_{mn}	Negative resisting moment in middle strip per foot, flat slabs (kip-ft)
M_{mp}	Positive resisting moment in middle strip per foot, flat slabs (kip-ft)

1 July 59

M_n	Negative bending moment at support
M_o	Moment of all external forces on structure about axis of rotation "o"
M'_o	Summation of external moments about the point of rotation excluding footing projection moments
M_P	Plastic resisting moment under bending only
M_{Pcn}	Negative plastic resisting moment in column strip per foot, flat slabs (kip-ft)
M_{Pcp}	Positive plastic resisting moment in column strip per foot, flat slabs (kip-ft)
M_{Pfa}	Component of the total plastic bending moment capacity along the fracture line boundary of area "A" which is in a plane perpendicular to edge "a," or the total positive plastic bending moment capacity for a section parallel to edge "a," two-way slabs (kip-ft)
M_{Pfb}	Component of the total plastic bending moment capacity along the fracture line boundary of area "B" which is in a plane perpendicular to edge "b," or the total positive plastic bending moment capacity for a section parallel to edge "b," two-way slabs (kip/ft)
M_{Pm}	Plastic resisting moment at centerline of beam or slab
M_{Pmn}	Negative plastic resisting moment in middle strip per foot, flat slabs (kip-ft)
M_{Pmp}	Positive plastic resisting moment in middle strip per foot, flat slabs (kip-ft)
M_{pos}	Maximum positive bending moment (kip-ft)
M_{Ps}	Plastic resisting moment at support (kip-ft)
M_{Psa}	Total negative plastic bending moment capacity along edge "a," two-way slabs (kip-ft)
M_{Psb}	Total negative plastic bending moment capacity along edge "b," two-way slabs (kip-ft)
M_y	Yield resisting moment (kip-ft)
M_P^o	Plastic resisting moment per unit of width of slab (kip-ft/ft)
M_{Pmb}^o	Plastic positive bending moment capacity per unit width for short span, two-way slabs (kip-ft/ft)
M_{Psa}^o	Plastic negative bending moment capacity per unit width at center of edge "a" for long span, two-way slabs (kip-ft/ft)
M_{Psb}^o	Plastic negative bending moment capacity per unit width at center of edge "b" for short span, two-way slabs (kip-ft/ft)

Symbols

EM 1110-345-413

1 July 59

M_l	Moment at the intersection of the two-linear portions of the P vs M curve of a steel beam section (kip-ft)
M'_P	Theoretical plastic resisting moment (kip-ft)
m	Mass per unit length ($\text{kip-sec}^2/\text{ft}^2$) Point mass ($\text{kip-sec}^2/\text{ft}$) In concrete design: $f_{dy}/0.85 f'_{dc}$
	Total moving mass of structure and earth included between footings
	Number of fundamental dimensional quantities
m_e	Mass of the equivalent system ($\text{kip-sec}^2/\text{ft}^2$)
m_r	Mass of structure considered to rotate as well as translate
m_t	Total mass of the element or structural system under consideration ($\text{kip-sec}^2/\text{ft}$)
m_{te}	Total mass of the equivalent system ($\text{kip-sec}^2/\text{ft}$)
m_1, m_2, \dots, m_g	Mass of the first, second, and g^{th} floors of a multi-story building
N	Number of non-dimensional parameters Total number of shear connectors required between the points of zero and maximum moment of a composite beam Weighted number of piles in group
N_f	Ratio of the length of fixed-edge perimeter to the total perimeter
N_s	Ratio of the length of simply-supported perimeter to the total perimeter
n	Number of columns in a story Ratio of modulus of elasticity of steel to modulus of elasticity of concrete Number of dimensional variables Number of stories in a multi-story frame
P	Load or force (kips) Total dynamic load on slab (kips) Panel influence factor for shear walls
P_A	Total load on "A" portion of two-way slab (kips)
P_{av}	Average axial load acting on each of several columns of a frame (kips)
P_{back}	Local overpressure on the back face of a buried rectangular structure (psi)
P_B	Total load on "B" portion of two-way slab (kips)
P_c	Compression mode overpressure (psi)
P_{ca}	Uniform compressive pressure applied radially on arch
P_{cr}	Uniform radial pressure that produces buckling of arch

P_{cyl}	Local overpressure normal to the exterior surface of a cylindrical segment (psi)
P_D	Maximum axial load on column with given M_D (kips)
P'_D	Reduced maximum axial load for long columns
P_d	Deflection mode overpressure (psi) Total dynamic axial load
P_{dome}	Local overpressure normal to the exterior face of a spherical dome (psi)
P_e	Equivalent concentrated load for equivalent system (kips)
P_{ed}	Elastic dynamic buckling load (kips)
$P_e(t)$	Equivalent load on an element as a function of time
P_f	Average value of $P(t)$ for the far (or leeward) side of the arch (psi)
P_{front}	Local overpressure on the front face of a buried rectangular structure (psi)
P_g	Peak underground overpressure resulting at a given location from an underground burst (psi)
P_n	Total vertical load (blast plus static) on column Force acting at any time, t_n Average value of $P(t)$ for the near (or windward) side of the arch (psi)
P_P	Dynamic plastic axial load capacity of column
P_{refl}	Reflected shock wave overpressure for angle of incidence of zero degrees (psi)
$P_{r-\alpha}$	Reflected shock wave overpressure for angle of incidence other than zero degrees (psi)
P_s	Overpressure existing in the incident shock wave for any value of $t-t_d$ (psi)
P_{sb}	Overpressure existing in the incident shock wave when $t-t_d = t_b$ (psi)
P_{side}	Local overpressure on the exterior side walls of a rectangular structure
P_{so}	Initial peak incident overpressure (psi)
P_{soi}	Peak overpressure of the shock wave formed in the interior of a structure with openings (psi)
P_{stag}	Stagnation overpressure; the overpressure existing in a region in which the moving air has been brought completely to rest (psi)
P_v	Axial load on the columns of a frame due to the vertical live and dead loads (kips)

(ΣP_v)	The time average of the total vertical load on the column in the time interval $t_{ge} < t < t_{gm}$
\bar{P}_{back}	Average overpressure on the exterior back wall of a rectangular structure (psi)
\bar{P}_{b-net}	Average net overpressure acting on back wall of a rectangular structure (psi)
$(\bar{P}_{back})_{max}$	Peak value of the average overpressure on the exterior back wall of a rectangular structure (psi)
\bar{P}_{end}	Average overpressure on the closed ends of a cylindrical segment (psi)
\bar{P}_{f-net}	Average net overpressure acting on front wall of a rectangular structure (psi)
\bar{P}_{front}	Average overpressure on the exterior of the front wall of a rectangular structure (psi)
$\bar{P}_{i-front}$	Average overpressure on the interior front wall of a rectangular structure with openings (psi)
\bar{P}_{i-refl}	Reflected shock wave average overpressure in the interior of a rectangular structure with openings (psi)
\bar{P}_{i-roof}	Average overpressure on the interior roof of a rectangular structure with openings (psi)
\bar{P}_{i-side}	Average overpressure on the interior side walls of a rectangular structure with openings (psi)
\bar{P}_{net}	Net average horizontal overpressure exerted on a rectangular structure (psi)
\bar{P}_{r-net}	Average net overpressure acting on the roof of a rectangular structure (psi)
\bar{P}_{roof}	Average overpressure on the front slope of a gable roof (psi) Average overpressure on the exterior of a rectangular structure (psi)
\bar{P}'_{roof}	Peak average overpressure on the front slope of the first gable of a multi-gabled roof (psi)
\bar{P}_{s-net}	Average net overpressure acting inward on sidewall of rectangular structure (psi)
\bar{P}_{side}	Average overpressure on the exterior side walls of a rectangular structure (psi)
P_l	Axial load determined by the intersection of the two linear portions of the P vs M curve of a steel beam section (kips)
$P(t)$	Actual load on a structural element as a function of time
p	Ratio of tensile reinforcement in reinforced concrete members to concrete area, A_s/bd Uniformly-distributed load intensity

p_o	Critical steel ratio for reinforced concrete member
\bar{p}	Equivalent static load for an arch (psi)
p'	Ratio of volume of spiral reinforcement to the volume of the concrete core (out-to-out of spirals) of a spirally reinforced concrete column Ratio of compressive reinforcement in beams to the concrete area, A'_s/bd
Q	Statical moment of the section about the centroidal axis Strength of a shear connector in composite construction Radiant energy on a unit area (cal/cm^2)
q	Unit drag pressure produced by the incident shock wave (psi)
q_d	Dynamic design bearing pressure on soil (kips/ft^2)
q_m	Maximum bearing pressure on soil (kips/ft^2)
q_o	Maximum unit drag pressure produced by the incident shock wave (psi)
R	Radius of a spherical dome Total resistance of structural element or structural system (kips) Dosage of gamma radiation (roentgens) Crater radius (ft)
R_A	Total resistance of "A" portion of two-way slabs (kips)
R_C	Crater radius (ft)
R_c	Horizontal static load resistance of shear wall at first cracking
R_{dc}	Horizontal dynamic load resistance of shear wall at first cracking
R_e	Reynolds number of the high velocity wind in the incident shock wave Resistance of the equivalent system (kips)
R_g	Simplified notation of $R_{g,g-1}$, the resistance function developed between the g^{th} and $(g-1)^{\text{th}}$ floors of a multi-story building
\bar{R}_g	The average value of R_g in the time interval from 0 to t'_g
R_{gi}	Resistance function developed between the g^{th} and the i^{th} floors of a multi-story building (kips)
R_{gm}	Maximum resistance of the g^{th} story of a multi-story building (kips)
R_{go}	Resistance developed in the spring which connects m_g to the ground
R_{gt}	Total resistance acting on the g^{th} floor mass (kips)
R_m	Maximum resistance developed by a structural system (kips)
R_{mA}	Plastic resistance of the "A" portion of two-way slabs where the edge is fixed (kips)

Symbols

EM 1110-345-413
1 July 59

R_{mB}	Plastic resistance of the "B" portion of two-way slabs where the edge is fixed (kips)
R_{me}	Maximum resistance of the equivalent system (kips)
R_{mf}	Fictitious maximum resistance (kips)
R_n	Resistance of a structural element or system at time, t_n (kips)
R_u	Horizontal ultimate load resistance of a shear wall (kips)
R_y	Yield resistance of the structure (kips)
R_l	Resistance in the elastic range (kips)
R_{lm}	Maximum resistance in the elastic range (kips)
R_{lmA}	Maximum total resistance in the elastic range - "A" portion of two-way slabs (kips)
R_{lmB}	Maximum total resistance in the elastic range - "B" portion of two-way slabs (kips)
$R(t)$	Resistance as a function of time
$R_g(t)$	Resistance of the g^{th} story columns as a function of time
$[R_g(t)]_{eq}$	Time variation of the resistance of the equivalent single-degree-of-freedom dynamic system for the g^{th} story
R_o	Dosage of nuclear radiation without shielding (roentgens)
$R(x)$	Resistance as a function of displacement
r	Radius of gyration of section (in.) Resistance per unit length of a beam or per unit area of slab Ratio of web reinforcement = A_v/b_s Distance from point of explosion (ft) Roentgens Ratio of steel reinforcing placed perpendicular to the steel beam (in composite construction) in excess of that required to carry the slab bending stresses
\bar{R}_g	Average value of the resistance of the g^{th} story when the relative displacement between the g^{th} and the $g-1^{th}$ story is negative
S	Section modulus
SE	Strain energy absorption (kip-ft)
$(SE)_a$	Strain energy absorption of actual structure (kip-ft)
$(SE)_e$	Strain energy absorption of equivalent structure (kip-ft)
S'	Section modulus about the weak axis
s	Coordinate axis at 45° angle to x axis in x-y plane Spacing of stirrups and spacing of ties in reinforced concrete members (in.)

\bar{s}	Distance along s axis to centroid of loading (ft)
\bar{s}_I	Distance along s axis to centroid of inertia force (ft)
T	Duration of the external load (sec) Resultant tension force (kips)
T_c	Fundamental period of vibration for complete spherical shell of centroid thickness (sec)
T_n	Natural period of oscillation or fundamental period (sec)
T_{nd}	Lowest natural period of circular arch with pinned or fixed ends
T_{ni}	Natural period of the i^{th} mode of oscillation (sec)
T_r	Time or rise of a step-load (sec)
T_1, T_2, \dots, T_g	Time duration of the external loads on the first, second, and g^{th} floors of a multi-story building (sec)
$T_{1X}, T_{2X}, \dots, T_{gX}$	Time duration when the effective loads on the first, second, and g^{th} stories are negative (sec)
T'_{gn}	Period of oscillation of a fictitious system representing the g^{th} story (sec)
t	Thickness of concrete slabs (in.) Thickness of flange of beams (in.) Time measured after the arrival of the incident shock wave (sec) Time variable Thickness of deep beam web
t_a	Time of arrival, or time required for the shock wave to travel from the point of explosion to the chosen location (sec)
t_{av}	Average flange thickness of standard steel beam (in.)
t_b	Time required for overpressure on the rear face of a closed rectangular structure to rise from zero to its maximum value (sec)
t_c	Time required to clear the front face of a structure from the reflection effects (sec)
t_d	Time displacement factor; the time required for the shock front to travel from the frontmost element of a structure to the point or surface under consideration (sec)
t_e	Time at which the limiting elastic deflection is reached
t_f	Flange thickness of a WF steel beam (in.)
t_{ge}	Time at which the limiting elastic deflection of the g^{th} story is reached
t_m	Time required for the vortex generated at the front face of a structure to travel a distance L' across the structure (sec) Time required for maximum displacement of element or structure to occur (sec)
t_o	Duration of the positive phase of the incident shock wave (sec)

Symbols

EM 1110-345-413

1 July 59

t_r	Time of rise; time required for the overpressure in the incident shock wave to rise from zero to its maximum value (sec)
t_s	Thickness of stiffener (in.)
t_t	Time required for the shock to pass over the length of the structure (sec)
t_{ur}	Time of rise of an underground overpressure pulse (sec)
t_w	Web thickness of a steel beam or channel (in.)
t_{yp}	Time required to reach yield point of material (sec)
$t_1, t_2 \dots t_n, t_{n+1}$	Time sequence
$t_{1m}, t_{2m} \dots t_{gm}$	Time at which the maximum absolute displacements of the first, second and g^{th} floor masses are reached
t'_b	Time required for the overpressure on the exterior rear face of a rectangular structure with openings to rise from zero to its maximum value (sec)
t'_c	Time required to clear the front face of a structure with openings from reflection effects (sec)
t'_2, t'_g	Time at which the relative displacements X_2 and X_g , respectively, are equal to zero
t^-_n	Time immediately before t_n
t^+_n	Time immediately after t_n
t_{lag}	Time lag
Δt	Time interval used in numerical analysis
$\Delta t_n = t_{n+1} - t_n$	A time interval
U_o	Velocity of the incident shock front (fps)
U_{io}	Velocity of the shock front of the shock wave formed in the interior of a rectangular structure with openings (fps)
u	Particle velocity in the incident shock wave (fps) Bond stress per unit of surface area of bar in reinforced concrete design (psi)
V	Dynamic reaction (kips) Total shear (kips) Total vertical force on piles
V_A	Total dynamic reaction along one edge "a," two-way slabs (kips)
V_{av}	Average vertical shear in length, L' (kips)
V_B	Total dynamic reaction along one edge "b," two-way slabs (kips)
V_c	Total column load in flat slab design (kips)
V_m	Maximum shear capacity of web of deep beam section
V_{max}	Maximum vertical shear force (kips)

v	Vortex velocity (fps) Shear stress (psi)
v_{dy}	Dynamic shear yield strength
$v_{g,n} = v_g(t_n)$	Velocity of the g^{th} floor at time, t_n
v_m	Maximum shearing stress (psi)
$v_n = v(t_n)$	Velocity at time, t_n
v_n^+	Velocity at t_n^+
v_n^-	Velocity at t_n^-
v_o	Horizontal velocity of axis of rotation "O"
$v(t_e)$	Velocity of mass at time t_e
v_y	Static shear yield strength of steel (psi) Average unit shear stress in concrete (psi)
$v(t)$	Velocity as a function of time
W	Total energy yield of an atomic bomb expressed K _T of TNT required for an equivalent total energy yield Weight (lbs) Total load on element of structure (kips) Work done (ft-lbs) Dynamic peak blast load
W_a	Work done on the actual system (ft-kips)
W_e	Work done on the equivalent system (ft-kips)
W_g	Maximum work done on the g^{th} floor mass (ft-kips)
W_{gm}	Absolute maximum work done on the g^{th} floor mass (ft-lbs)
W_m	Maximum work done on the equivalent system by the equivalent load
W_p	Fictitious maximum work done on the equivalent system
$W(t)$	Work done as a function of time
w	Uniformly distributed load (kips/ft) Length of channel shear connector (in.) Width of front face of rectangular building (ft)
w_1	Weighting factor for vertical and batter piles
X	Relative displacement in a story of a multi-story building (ft)
X_{gm}	Maximum relative displacement in the g^{th} story (ft)
X_{gs}	Relative displacement of the mass g when the average external loads are applied statically
X_1, X_2, X_g	Relative displacement in the first, second, and g^{th} stories of a multi-story building (ft), $X_g = x_g - x_{g-1}$

x_{ge}	Limiting elastic relative displacement for the g^{th} story column (ft)
x	Distance the incident shock wave travels after impinging on the frontmost element of a cylindrical segment or spherical dome to any point being considered Deflection of a structural element or system (ft) Distance of any pile from the centroidal axis
x_c	Collapse deflection
x_e	Limiting elastic deflection (ft)
x_f	Forced solution of a dynamic system for a given external load
x_{ge}	Absolute displacement of the g^{th} floor at time t_{ge}
x_{gm}	Maximum absolute displacement of the g^{th} floor (ft)
$x_{g,n-1}, x_{g,n}, x_{g,n+1}$	Absolute displacements of the g^{th} floor at time, t_{n-1}, t_n , and t_{n+1}
x_m	Maximum displacement (ft)
x_{n-1}, x_n, x_{n+1}	Displacement at time t_{n-1}, t_n , and t_{n+1} , respectively
x_o	Initial displacement (ft) Horizontal displacement of axis of rotation "O"
x_s	Displacement of an elastic system subjected to the peak load B acting statically (ft)
$x(t_e)$	Displacement of a mass at time t_e
x_1, x_2, x_g	Absolute displacement of the first, second, and g^{th} floors of a multi-story building (ft)
\bar{x}	Distance to centroid parallel to x axis (ft)
\dot{x}_o	Horizontal velocity of axis of rotation "O"
\ddot{x}_o	Horizontal acceleration of axis of rotation "O"
\ddot{x}	Acceleration in the x direction (ft/sec ²)
y	Displacement or deflection of a structural system (ft)
y_a	Deflection of actual element (ft)
y_{ac}	Midspan deflection of actual element (ft)
y_c	Midspan deflection (ft)
y_e	Limiting elastic deflection (ft) Deflection of equivalent system (ft)
y_{ep}	Limiting deflection in the elasto-plastic range (ft)
y_m	Maximum displacement (ft)
y_n	Displacement at time, t_n (ft)

y_r	Vertical distance from axis of rotation "O" to mass centroid of rotating mass, m_r , of structure
y_1	Deflection at midspan of column strip - flat slab (ft)
y_2	Deflection at midspan of middle strip - flat slab (ft)
y_{1m}	Maximum elastic range deflection (ft)
y_{2m}	Maximum elasto-plastic range deflection (ft)
\bar{y}	Distance to the centroid parallel to y axis (ft) Vertical distance from axis of rotation "O" to mass centroid of total moving mass, m
\ddot{y}	Acceleration in the y direction (ft/sec^2)
\dot{y}	Velocity in the y direction (ft/sec)
\dot{y}_{cl}	Velocity of displacement of the center of the beam (ft/sec)
y	Increment of displacement (ft)
Z	Plastic modulus of the cross section (in.^3)
Z'	Plastic modulus of the cross section in the weak direction (in.^3)
z	Depth of the resultant compressive force in concrete tee beam
α	Angle of incidence between the normal to the surface and the direction of propagation of the blast wave (degrees) Central angle of the arch Deflection coefficient for two-way slabs Design load ductility reduction factor
α_o	Angular acceleration of structure about axis of rotation "O" (radians/sec^2)
β	Dimensionless ratio = $0.5P_{so}/14.7$ Ductility ratio
δ_b	Maximum bending deflection due to the application of a unit load (ft/kip)
δ_c	Shear wall lateral deflection at first cracking
δ_n	Sub-area clearing factor for rectangular structures with openings
δ_s	Maximum shear deflection due to the application of a unit load (ft/kip)
δ_u	Shear wall lateral deflection at ultimate resistance
δ_y	Deflection at theoretical yield (ft)
θ	Angle of inclination to the horizontal of a gabled roof (degrees) Parameter used to define the location of a point on the surface of a cylindrical segment or a spherical dome (degrees) End rotation of structural element Angular displacement

Symbols

EM 1110-345-413
1 July 59

θ_B	Joint rotation at bottom of column
θ_c	Rotation of beam at midspan (radians)
θ_o	Angular displacement of structure about axis of rotation "O"
θ_T	Joint rotation at top of column
μ	Viscosity of air in the incident shock wave (lb-sec/ft ²) Coefficient of friction
ν	Poisson's ratio
ρ	Mass density of air in the incident shock wave (lb-sec ² /in. ⁴)
ρ_s	Mass density of soil (lb-sec ² /in. ⁴ , or lb-sec ² /ft ⁴)
σ_{cr}	Critical buckling stress (psi)
ϕ	Parameter used to define the location of a point on the surface of a spherical dome Phase angle in the transient response (radians) Internal friction angle (degrees)
ϕ_i	Phase angle of the i th mode (radians)
γ	Unit weight of soil (lbs/cu. ft)
ω_o	Angular velocity of structure about axis of rotation "O" (radians/sec)

ENGINEERING AND DESIGN

DESIGN OF STRUCTURES TO RESIST THE EFFECTS OF ATOMIC WEAPONS

WEAPONS EFFECTS DATA

INTRODUCTION

3-01 PURPOSE AND SCOPE. This manual is one in a series issued for the guidance of engineers engaged in the design of permanent type military structures required to resist the effects of atomic weapons. It is applicable to all Corps of Engineers activities and installations responsible for the design of military construction.

The material is based on the results of full scale atomic tests and analytical studies. The problem of designing structures to resist the effects of atomic weapons is new and the methods of solution are still in the development stage. Continuing studies are in progress and supplemental material will be published as it is developed.

The methods and procedures were developed through the collaboration of many consultants and specialists. Much of the basic analytical work was done by the engineering firm of Ammann and Whitney, New York City, under contract with the Chief of Engineers. The Massachusetts Institute of Technology was responsible, under another contract with the Chief of Engineers, for the compilation of material and for the further study and development of design methods and procedures.

It is requested that any errors and deficiencies noted and any suggestions for improvement be transmitted to the Office of the Chief of Engineers, Department of the Army, Attention: ENGEB.

3-02 REFERENCES. Manuals - Corps of Engineers - Engineering and Design, containing interrelated subject matter are listed as follows:

DESIGN OF STRUCTURES TO RESIST THE EFFECTS
OF ATOMIC WEAPONS

EM 1110-345-413 Weapons Effects Data
EM 1110-345-414 Strength of Materials and Structural Elements
EM 1110-345-415 Principles of Dynamic Analysis and Design

EM 1110-345-416 Structural Elements Subjected to Dynamic Loads
EM 1110-345-417 Single-Story Frame Buildings
EM 1110-345-418 Multi-Story Frame Buildings
EM 1110-345-419 Shear Wall Structures
EM 1110-345-420 Arches and Domes
EM 1110-345-421 Buried and Semiburied Structures

a. References to Material in Other Manuals of This Series. In the text of this manual references are made to paragraphs, figures, equations, and tables in the other manuals of this series in accordance with the number designations as they appear in these manuals. The first part of the designation which precedes either a dash, or a decimal point, identifies a particular manual in the series as shown in the table following.

<u>EM</u>	<u>paragraph</u>	<u>figure</u>	<u>equation</u>	<u>table</u>
1110-345-413	3-	3.	(3.)	3.
1110-345-414	4-	4.	(4.)	4.
1110-345-415	5-	5.	(5.)	5.
1110-345-416	6-	6.	(6.)	6.
1110-345-417	7-	7.	(7.)	7.
1110-345-418	8-	8.	(8.)	8.
1110-345-419	9-	9.	(9.)	9.
1110-345-420	10-	10.	(10.)	10.
1110-345-421	11-	11.	(11.)	11.

b. Bibliography. A bibliography is given at the end of the text. Items in the bibliography are referenced in the text by numbers inclosed in brackets.

c. List of Symbols. Definitions of the symbols used throughout this manual series are given in a list following the table of contents.

3-03 RESCISSION. (Draft) EM 1110-345-413 (Part XXIII - The Design of Structures to Resist the Effects of Atomic Weapons, Chapter 3 - Weapons Effects Data.)

3-04 GENERAL. Atomic weapons may be exploded in the air, at ground level, or at various depths below the ground surface. The types of protected structures whose design are covered in this series of manuals are surface, shallow covered, and shallow buried structures. The major effects considered in protection against atomic weapons are:

- (1) Air blast
- (2) Nuclear radiation
- (3) Thermal radiation
- (4) Cratering
- (5) Ground shock.

Underground burst and cratering cause insignificant effects on a structure unless the structure is in close proximity to the burst. These effects have been given very limited coverage in this manual.

The air burst is the major factor in the determination of the required strength of a blast-resistant structure. To evaluate the loads on a structure it is necessary to develop the critical blast loading pattern, relative to each exposure of the surface of the structure. Pressure intensities will vary with respect to time, reckoned from the instant of arrival of the shock front.

Nuclear radiation is an important consideration in the design of protective structures. In some designs radiation shielding may govern the required thickness of concrete and earth cover whereas the blast effects will be the determining factor relative to the designs for structural strength and stability. Consideration should be given to both direct and residual radiation. Incendiary properties and heat insulation from thermal radiation should be given attention in selecting suitable materials for construction of protective structures.

3-05 BLAST WAVE PHENOMENA. a. Infinite Atmosphere. To simplify the presentation of air blast phenomena, the explosion in an atmosphere of infinite extent is first considered. Almost immediately after the detonation occurs, the expansion of the hot gases initiates a pressure wave in the surrounding air as represented roughly by the curve in figure 3.1(a). This shows the general nature of the variation of the overpressure (pressure above atmospheric) with distance from the explosion at a given instant during the early stages of shock formation. As the pressure wave moves outward from the center of the explosion, the following, or inner, part moves through a region which has been previously compressed and heated by the leading, or outer, parts of the wave. The pressure wave moves with the velocity of sound, and since this velocity increases with the temperature and pressure of the air through which the wave is moving, the inner part of the wave moves more rapidly and gradually overtakes the outer part, as shown in figure 3.1(b). The pressure wave front thus gets steeper and steeper, and within a very short period the pressure change becomes abrupt forming a shock front, as indicated in figure 3.1(c). At the shock front

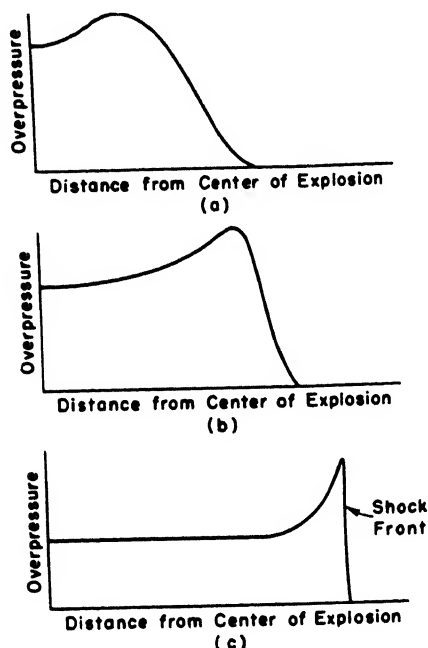


Figure 3.1. Overpressure during early stages of shock front formation

there is a sudden increase of pressure from normal atmospheric to the peak shock pressure and the advancing shock front becomes a moving wall of highly compressed air.

Initially, in the hot central region of the explosion the pressure exceeds atmospheric by a factor of many hundred thousand. The pressure distribution behind the shock front is somewhat as illustrated in figure 3.1(c). It shows the peak overpressure at the shock front, dropping rapidly in a relatively small distance to a value about one-half the shock front overpressure. The magnitude of the overpressure is essentially uniform in the central region of the explosion.

As the expansion proceeds, the pressure distribution in the region behind the shock front gradually changes. The overpressure is no longer constant but drops off continuously nearer the center. At later times when the shock front has progressed some distance from the center, a drop in pressure takes place below the initial atmospheric value at the center and a suction phase develops. The front of the blast wave weakens as it progresses outward and its velocity drops toward the velocity of sound in the undisturbed atmosphere. The sequence of events just described is depicted in figure 3.2. This shows the overpressure distribution in the blast wave as a function of the distance from the explosion at different stages in the expansion. When the suction phase is well developed, the overpressure in the blast wave resembles the heavily drawn curve in figure 3.2. The pressure variations in the blast wave from this time on can be considered in two different ways as

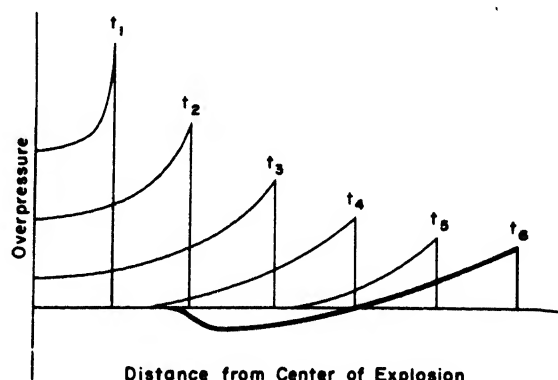


Figure 3.2. Variation of overpressure with distance at various times

1 July 59

shown in figures 3.3 and 3.4a.

First, the heavy curve of figure 3.2 has been redrawn in figure 3.3 to show the variation of overpressure with distance at a given time. The symbol P_{so} represents the peak overpressure, or shock intensity, in pounds per square inch and U_o represents the velocity of the shock front in feet per second. The arrows under the curve show the direction of movement of the air mass, or blast wind, in the positive and negative phases.

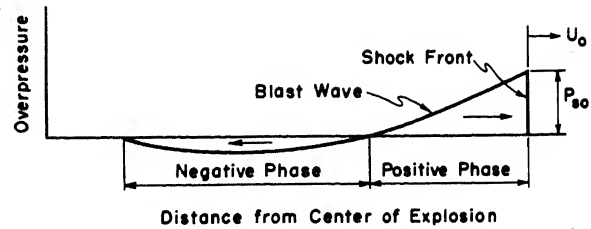


Figure 3.3. Variation of overpressure with distance at a given time

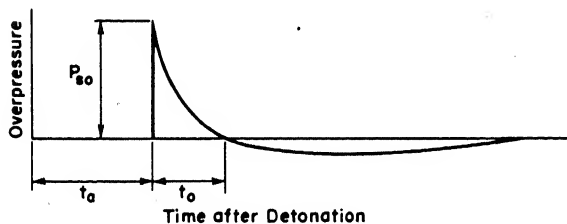


Figure 3.4a. Variation of overpressure with time at a given location

The peak overpressure in the positive phase is higher than the maximum overpressure in the negative phase. Consequently, the blast wind is of higher velocity in the positive phase than in the negative, or suction, phase.

Second, the pressure variations in the same wave may be considered at a point located a given distance from the explosion as indicated in figure 3.4a, which shows the variation of overpressure with time at a fixed location. The symbol t_a is the time of arrival, or the time in seconds for the shock front to travel from the center of the explosion to the given location, t_o is the duration in seconds of the positive phase, and P_{so} is as previously defined.

The rate of decay of the positive phase varies with respect to the magnitude of the peak overpressure. In figure 3.4b the rate of decays for various magnitudes of peak overpressures is expressed in terms of the ratio P/P_{so} to the ratio t/t_o , where P_s is the overpressure at time t after the arrival of the shock front. The peak negative overpressure is approximately one-eighth of the peak positive overpressure and the duration of the negative phase is approximately four times the duration of the positive phase of the blast.

The peak overpressure P_{so} in free air before the shock front

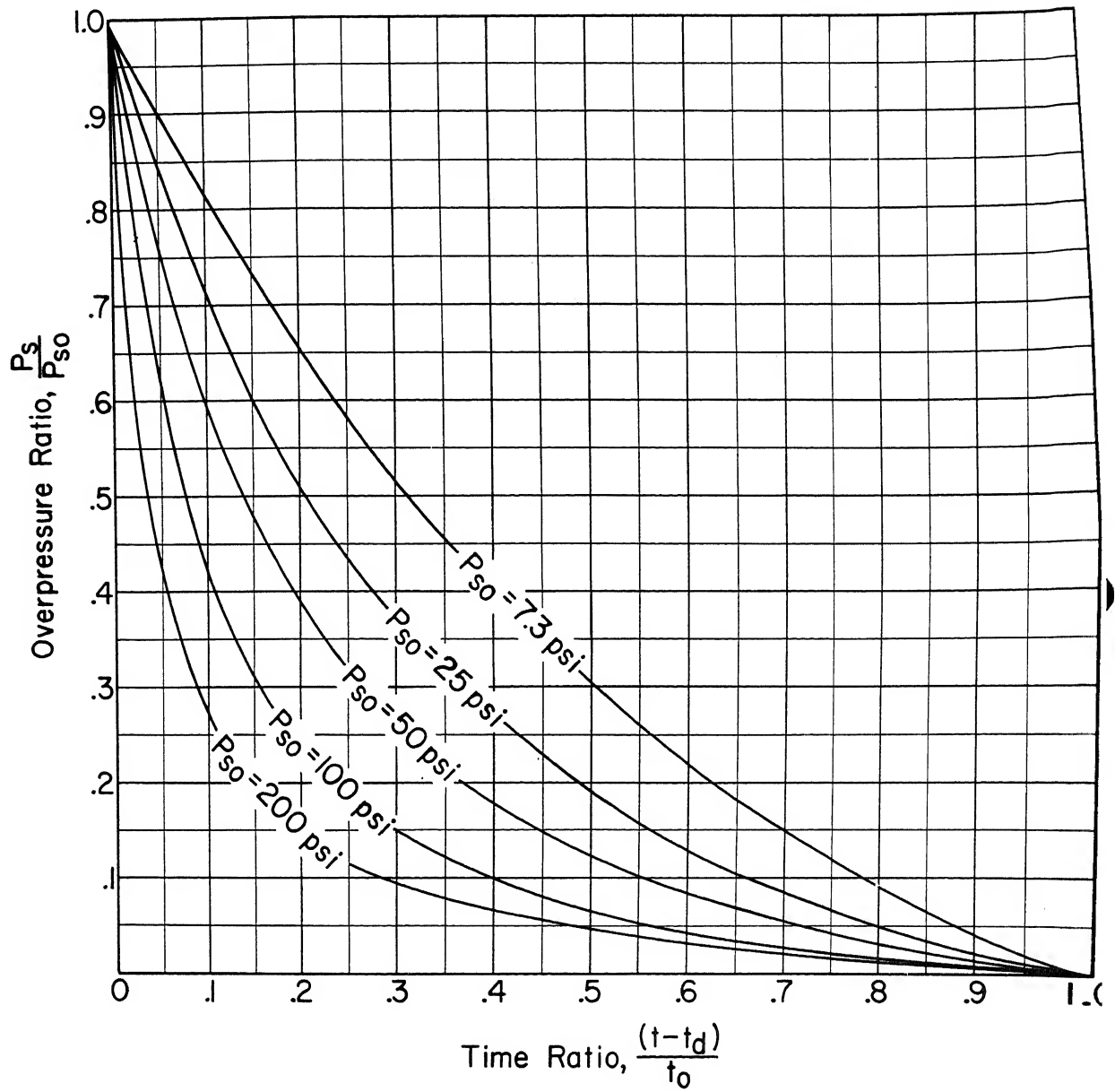


Figure 3.4b. Overpressure decay

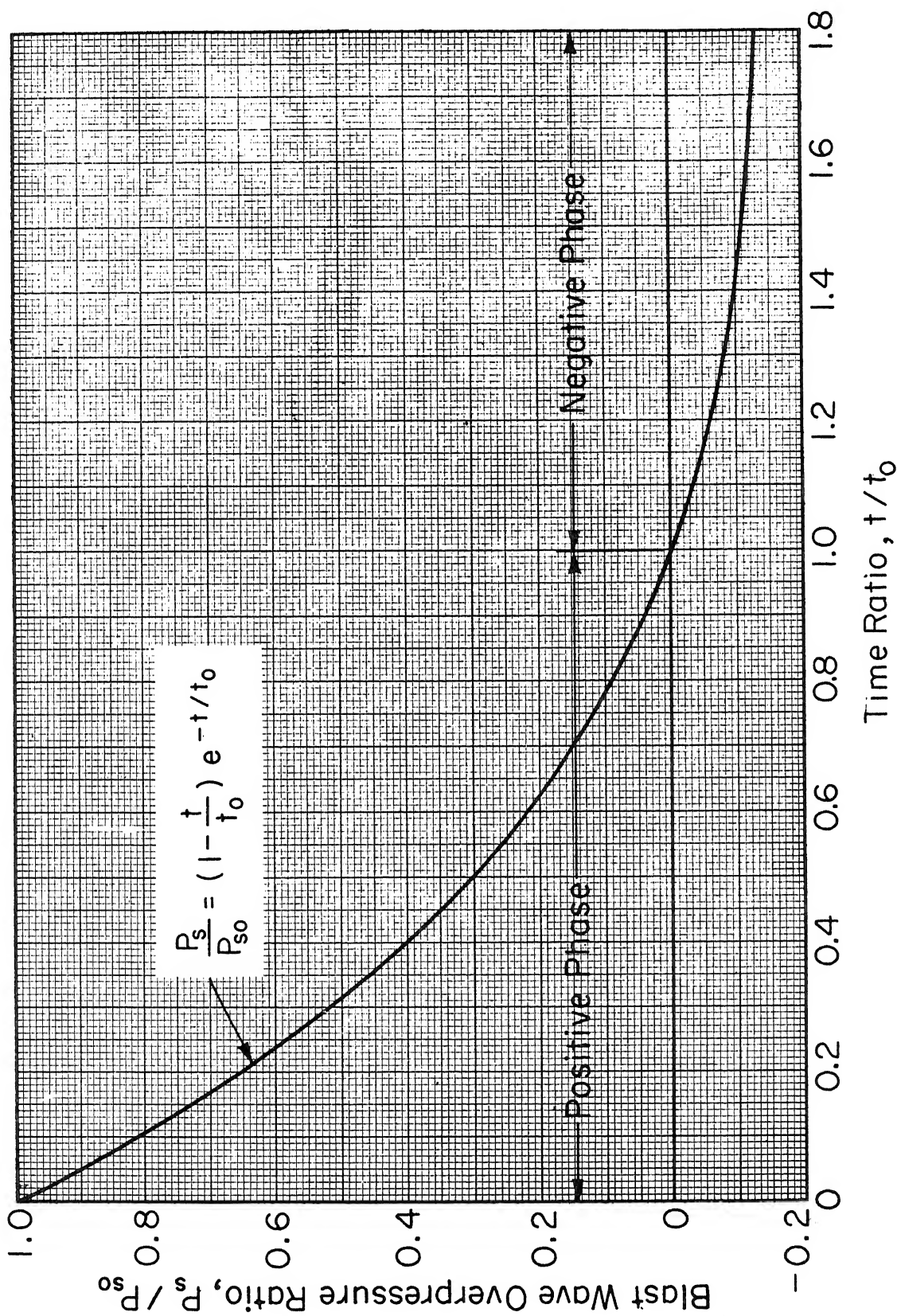


Figure 3.4c. Blast wave overpressure vs time ratios, 10-psi overpressure or less

Of

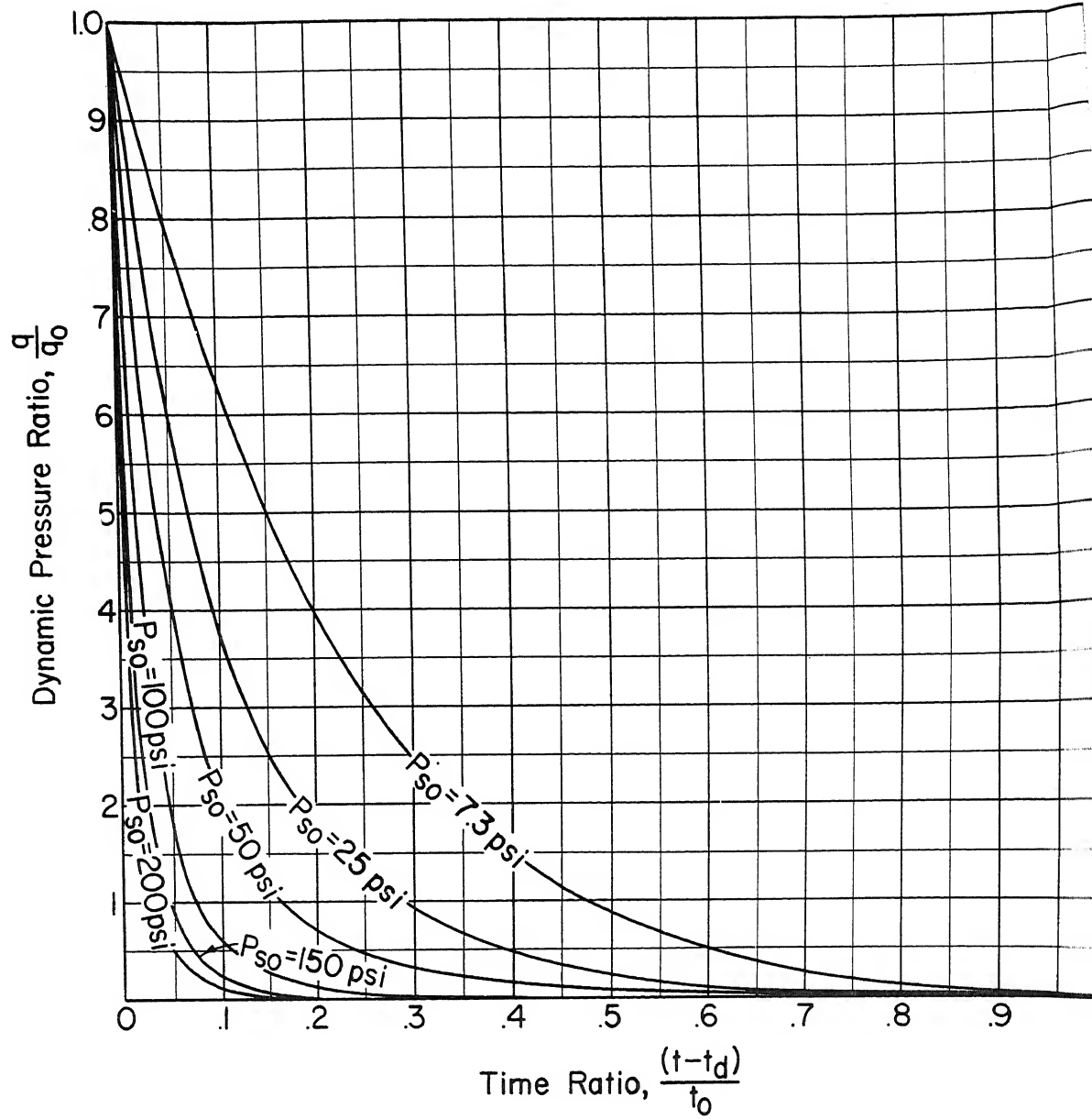


Figure 3.4d. Dynamic pressure decay

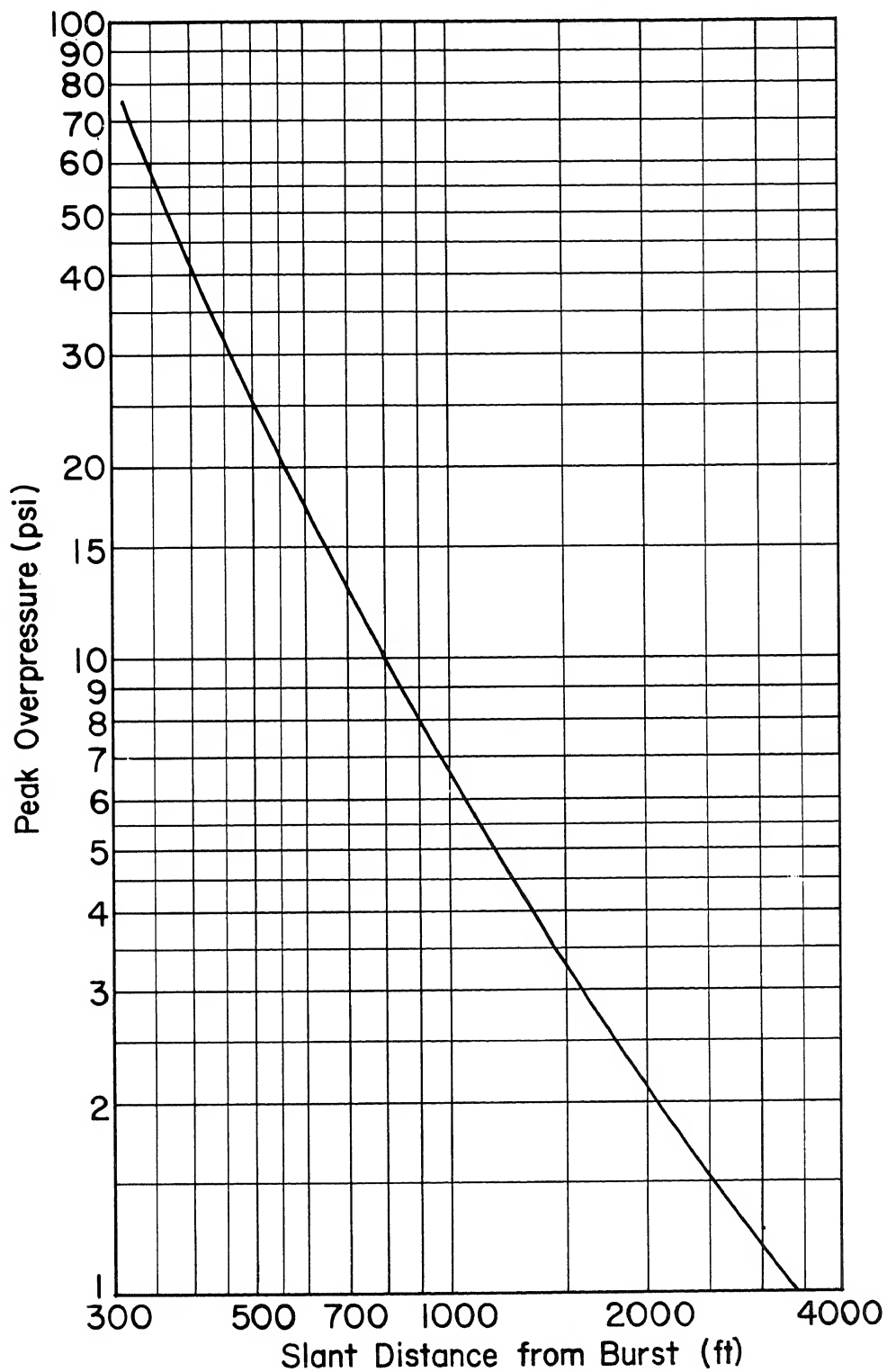


Figure 3.5. Peak overpressure for 1-KT free air burst by $2W$ assumption (taken from reference [36])

strikes the ground is a function of the distance from the point of burst and the yield of the weapon. Values for 1-KT bomb given in figure 3.5 are from curves given in reference [36] which are based on the supposition that a contact surface burst of W kilotons energy is equivalent in blast characteristics to an explosion of $2W$ kilotons high in the air and prior to reflection.

b. Finite Height of Burst. The discussion in the preceding paragraph deals with the air blast from an atomic bomb exploded in an atmosphere of infinite extent. A discussion follows relative to the influence of the surface of the earth on propagation and attenuation of the air blast.

If the bomb is detonated at a height h above the surface of the earth, the shock front will have the general configuration indicated in

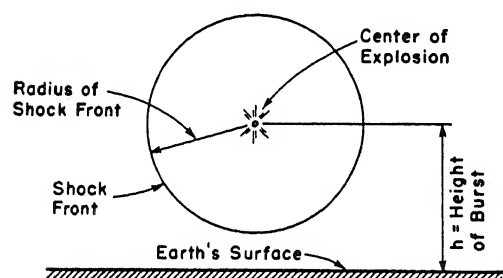


Figure 3.6. Shock front before striking ground surface

figure 3.6 during the brief time interval before it impinges upon the surface. The shock front is the same as if propagated in an atmosphere of infinite extent.

A short time later the radius of the shock front becomes greater than h , and a portion of the shock front impinges upon the earth's surface and

is reflected back, forming the reflected shock front illustrated in figure 3.7. The arrows at the incident and reflected shock fronts indicate the direction in which the blast waves are traveling. The location of the reflected shock front is roughly determined by drawing an arc with center located a distance h below the earth's surface and directly under the point of detonation, joining the points of intersection of the incident shock front with the earth's surface. The symbol α represents the angle of incidence of the shock front with the earth's surface. The reflected shock front overpressure $P_{r-\alpha}$ is a function of the

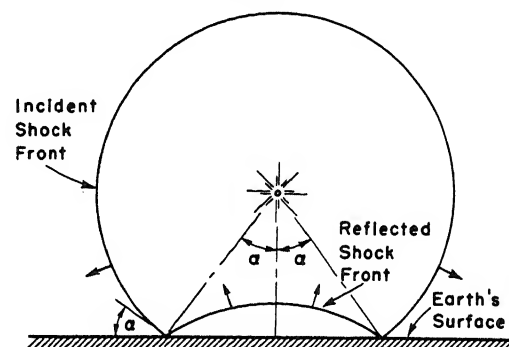


Figure 3.7. Shock front reflection at ground surface, α less than $45^\circ \pm$

incident shock overpressure P_{so} and the angle of incidence α [20].

The reflected shock front in figure 3.7 travels through the atmosphere at a higher velocity than the incident shock because it is traveling through a region of greater than atmospheric pressure and gradually overtakes and merges with it to form a single shock front called the Mach Stem as shown in figure 3.8. The fused shock front thus formed is normal to and travels parallel to the earth's surface. The Mach Stem formation is initiated when the angle of incidence α of the shock front becomes greater than approximately 45 degrees. Once formed, the height of the Mach Stem gradually increases as the radius of the shock front becomes greater.

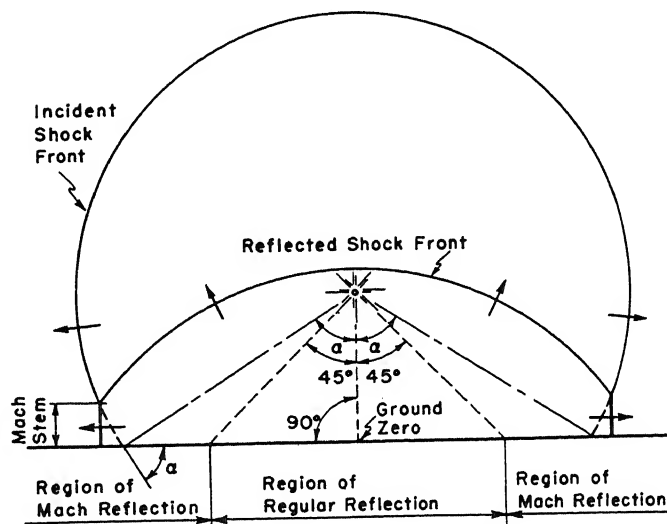


Figure 3.8. Shock front reflection when α is greater than $45^\circ \pm$

The region on the earth's surface within which α is less than 45 degrees, and no Mach Stem is present, is called the region of regular reflection, while the region for which α is greater than 45 degrees and a Mach Stem is present is called the region of Mach reflection. The importance of the Mach Stem phenomenon is that it results from the fusing of two shock fronts to form a single shock front of higher overpressure and of greater destructive potential to structures located in its path.

The shock front velocity U_o is a function of the peak overpressure P_{so} ; its value for standard atmospheric conditions is plotted in figure 3.9. The time of arrival t_a of the shock front at a given location is a function of the distance from the center of the explosion and the total energy yield of the weapon. The duration on the ground surface of the positive phase t_o of the blast wave is a function of the peak overpressure P_{so} and the total energy yield of the weapon. Values of the duration of the positive phase are plotted in figure 3.10a and in figure 3.10b.

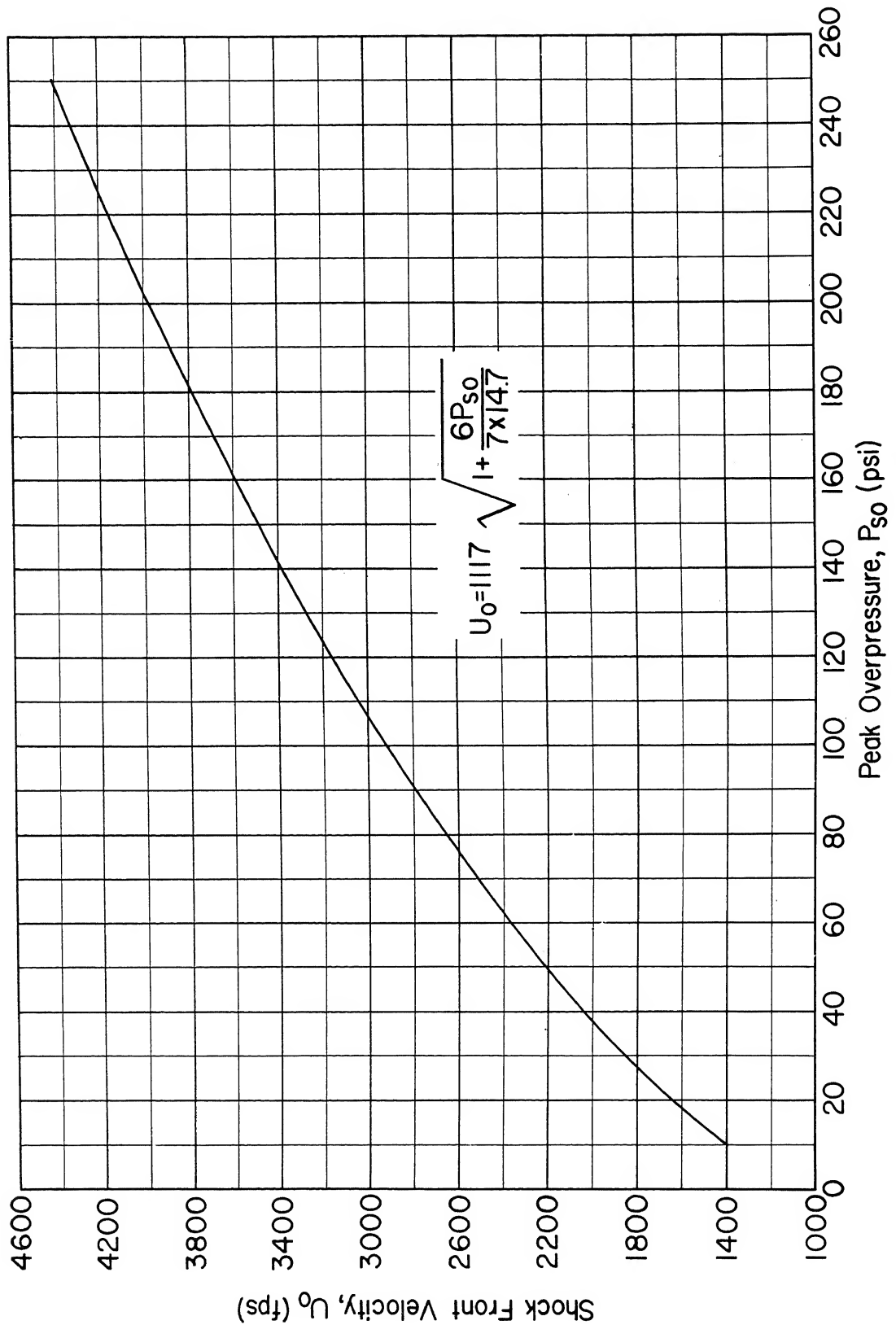


Figure 3.9. Shock front velocity vs peak overpressure

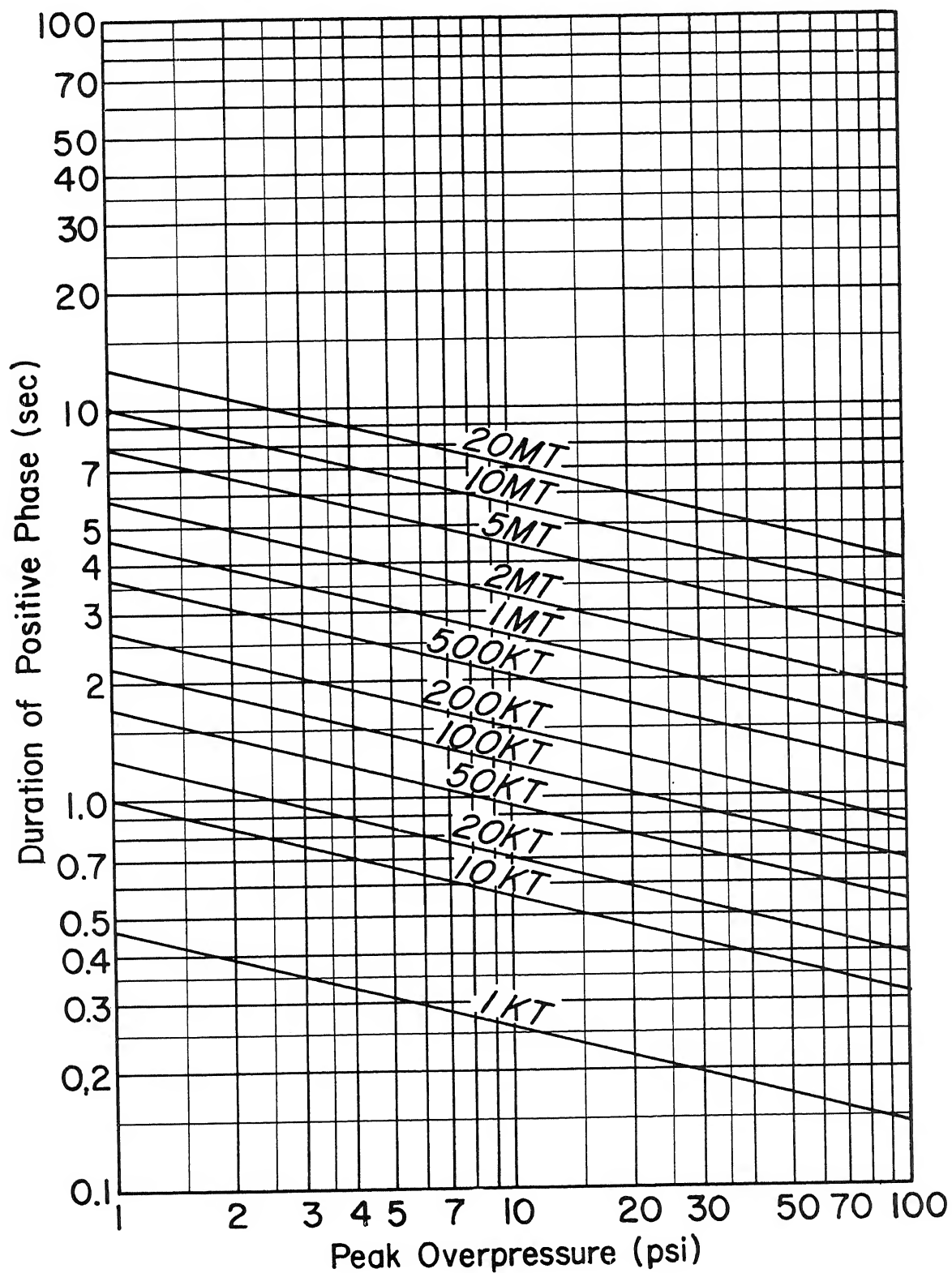


Figure 3.10a. Duration of positive phase--typical air burst

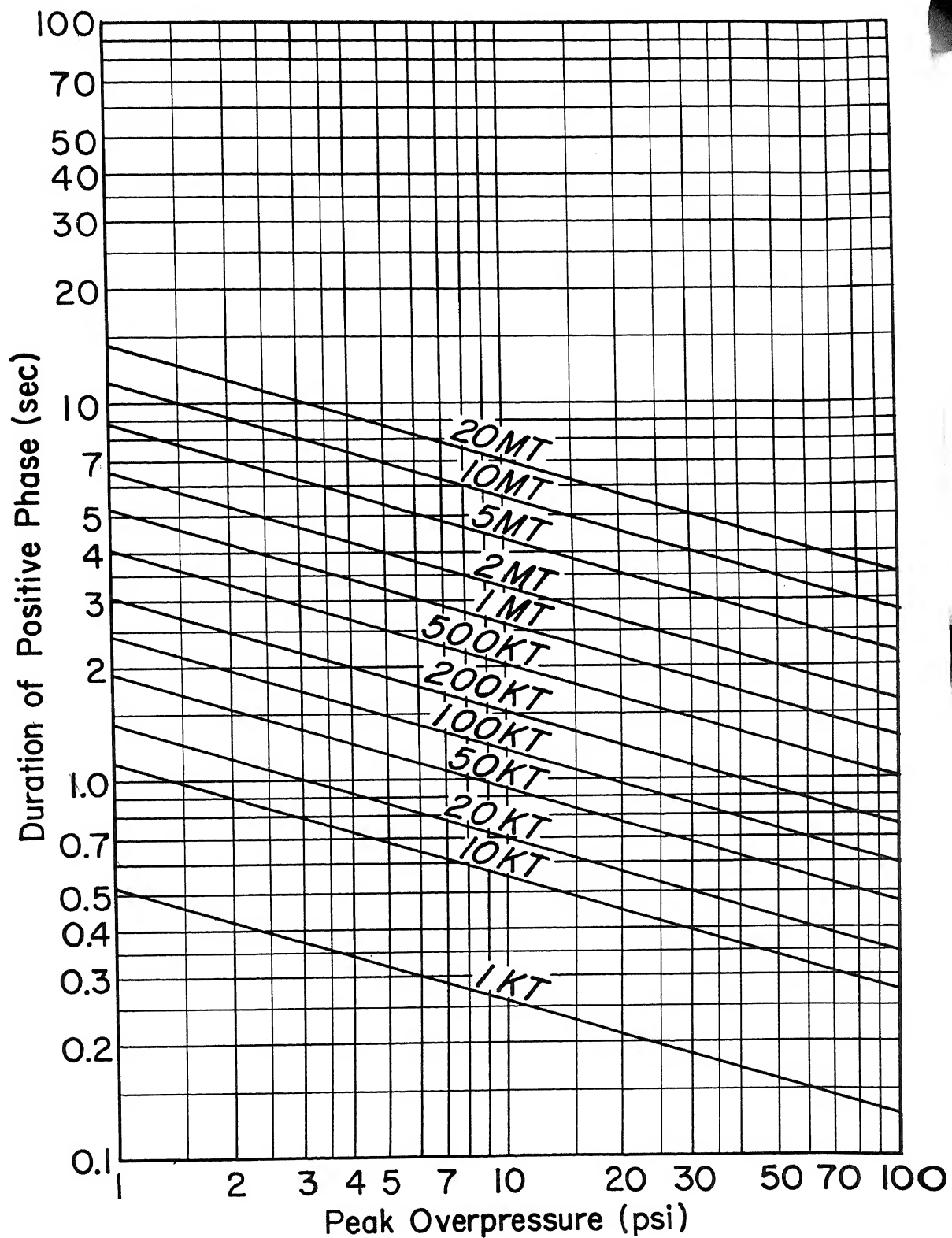


Figure 3.10b. Duration of positive phase--surface burst

Reflected overpressure ratio $P_{r-\alpha}/P_{so}$ is plotted in figure 3.11 as a function of the angle of incidence α of the shock front. This figure applies to an inclined shock front striking the earth's surface or to a vertical shock front striking a reflecting surface such as a wall of structure.

The peak overpressure P_{so} in the blast wave (shock front overpressure) at the ground surface plotted against distance from ground zero for various bomb sizes is given in figure 3.12a for a typical air burst and in figure 3.12b for a surface burst. The typical air burst is at a height above the ground which will maximize the target area covered by the 12-psi blast pressure level. This height probably cannot be attained by manned aircraft for the larger size bombs.

For other heights of burst P_{so} may be obtained from charts in reference [49], where the peak overpressure is plotted as a function of the height of burst and the horizontal distance from ground zero.

The variation of the overpressure in the blast wave on the ground with time can be determined in the same manner as for the bomb burst in an infinite homogeneous atmosphere. Equation 3.1 plotted as figure 3.4d is valid for ideal wave shapes which occur at approximately 10 psi or lower.

$$P_s = P_{so}(1 - t/t_o)e^{-t/t_o} \quad (3.1)$$

For higher overpressure levels the variation of overpressure with time at the ground level is usually irregular, due to thermal effects and to other modifying influences of the ground surface. Reference [49] contains data on these irregular wave forms. However, due to lack of data and the complexity of calculations involving irregular wave forms, the ideal wave forms that are given in figure 3.4c should be used for practical design purposes.

The dynamic pressure q due to the motion of the air particles in the blast wave is given by the relation $q = \rho u^2/2$ where ρ is the mass per unit volume of the air and u is the velocity of the air particles. The peak values of q at the ground surface plotted against distance from ground zero for various bomb sizes are given in figure 3.23b. The peak values of q plotted against the peak overpressure P_{so} are given in figure 3.23a.

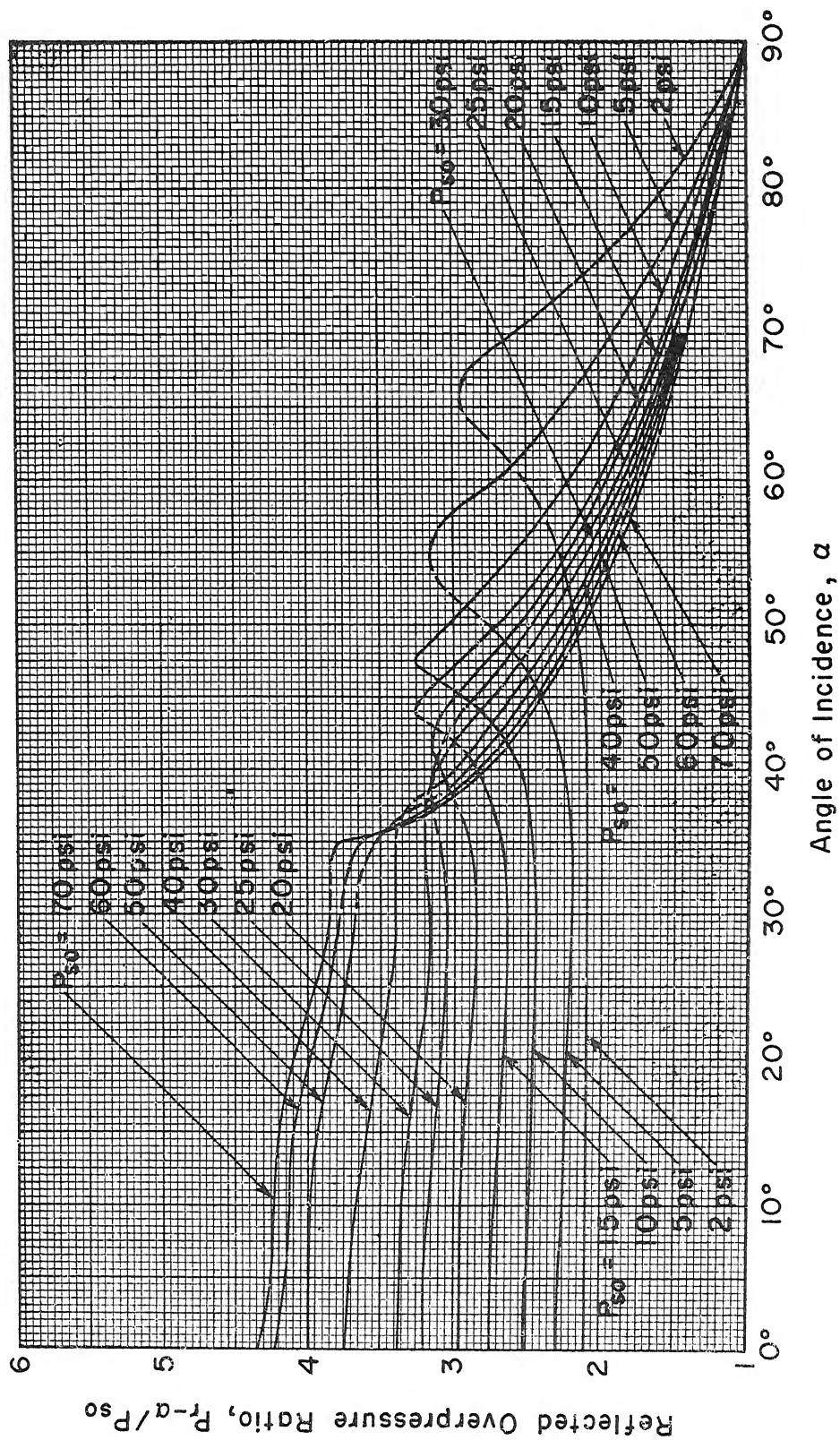


Figure 3.11. Reflected overpressure ratio vs angle of incidence

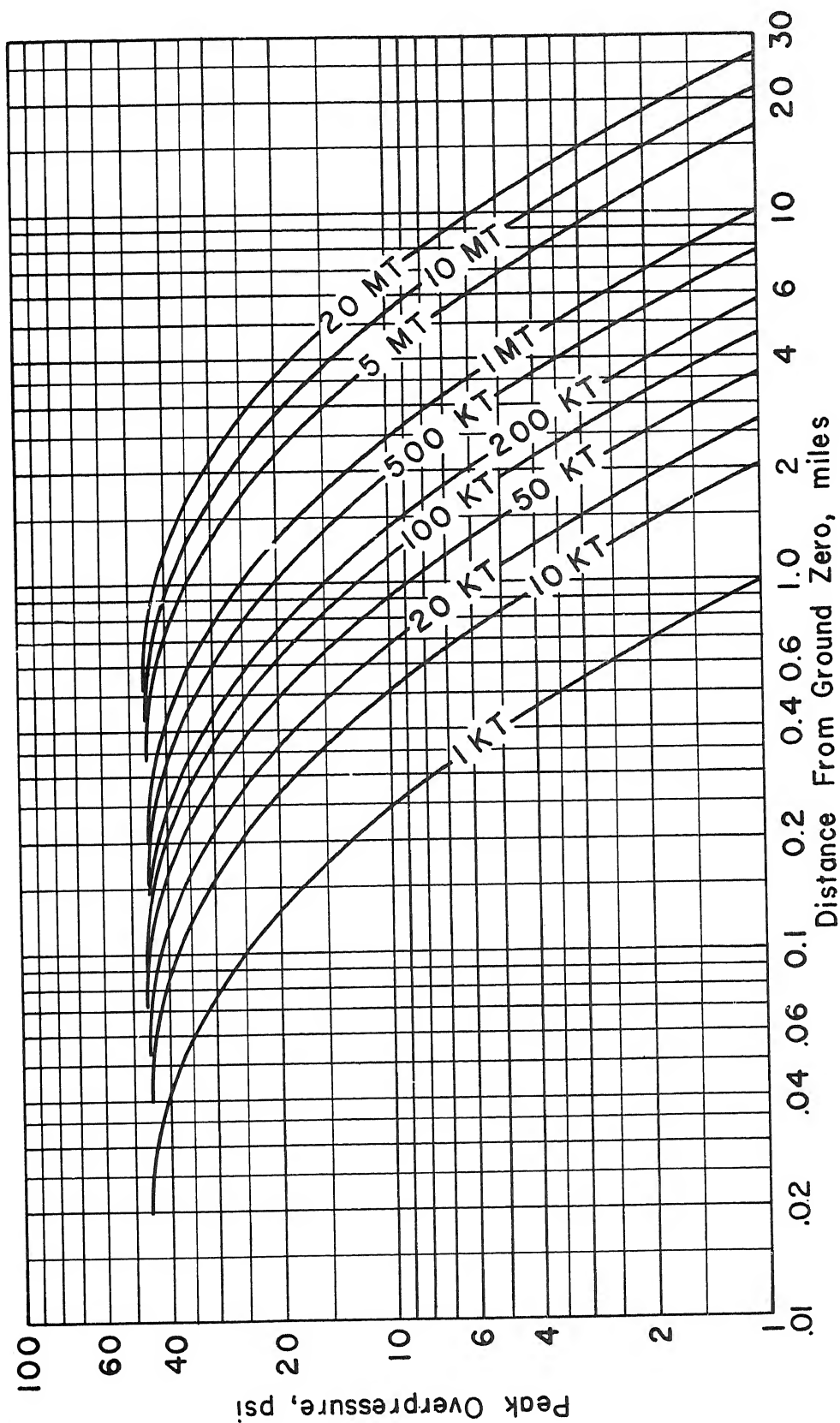


Figure 3.12a. Peak overpressure, typical airburst, height 650 ft $W^{1/3}$

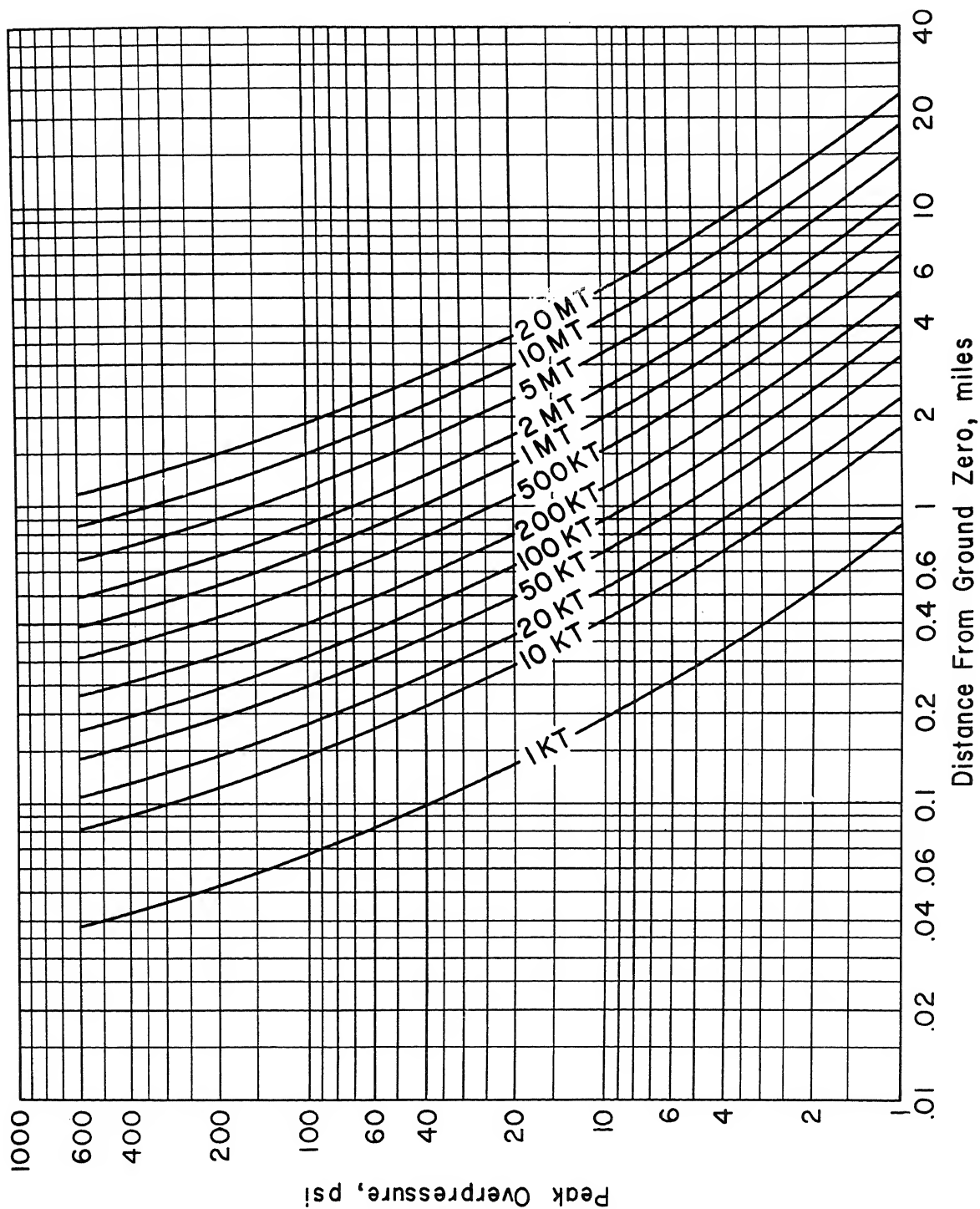


Figure 3.12b. Peak overpressure--surface burst

The rate of decay of the dynamic pressure is a function of the peak overpressure. Figure 3.4d shows variation in dynamic pressures for ranges of overpressures as a function of q/q_{so} at a fraction of time t/t_o ; where P_{so} is the overpressure and q_o is the peak dynamic pressure and q is the dynamic pressure at time t , after the arrival of the shock front.

3-06 SCALING BLAST PHENOMENA. It has been found that air blast phenomena such as the pressure and duration at different distances are related, for different strength bombs, according to the ratio of the cube root of the yield expressed in TNT. These relations are referred to as scaling laws.

These scaling laws state that if a given peak overpressure is experienced at distance r_1 from an explosion of a bomb of total energy yield W_1 the same peak overpressure will be experienced at distance r_2 from the explosion of a bomb of total energy yield W_2 where:

$$r_2 = r_1 \left(\frac{W_2}{W_1} \right)^{1/3} \quad (3.2)$$

The same scaling laws also state that while the peak pressures from the two bombs are equal to the two radii r_1 and r_2 , the durations of the blast pressure waves at the two points are different. If the duration of the positive phase of the pressure wave from the first bomb is t_{o1} at radius r_1 the duration of the positive phase t_{o2} of the pressure wave from the second bomb at distance r_2 will be:

$$t_{o2} = t_{o1} \left(\frac{W_2}{W_1} \right)^{1/3} \quad (3.3)$$

LOADING ON RECTANGULAR STRUCTURES WITHOUT OPENINGS

3-07 LOADING ON STRUCTURES. The manner in which the blast wave loads a structure varies with the ratio of the distance of the structure from ground zero to the height of the burst. The loading on a structure located within the region of regular reflection (figure 3.13) is greatly different in character from that for a structure located beyond this region. Since little or no data are available within the region of regular reflection and

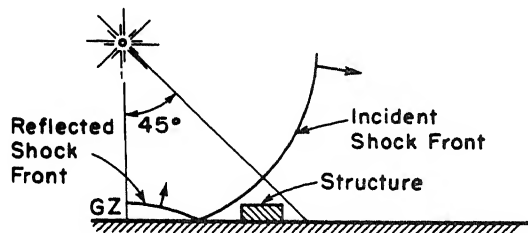


Figure 3.13. Structure located in region of regular reflection

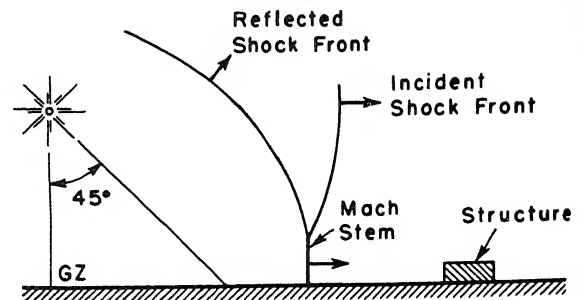


Figure 3.14. Structure located in region of Mach reflection

since a surface structure located in this region would be subject to such a high overpressure as to preclude a practical design, the procedures for the determination of loads are restricted to surface structures located outside the region of regular reflection (figure 3.14) where the Mach Stem is high enough to cover the structure.

The problem is that of computing the loading on a structure due to the impingement upon it of a blast wave traveling parallel to the surface of the earth. The structure is considered as being oriented with one face normal to the direction of propagation of the shock wave, since such an orientation produces the most severe loading on the structural elements. For the design of a structure so located, it is necessary to predict the overpressures which would exist on various portions of the structure as a function of time t measured after the shock front strikes the front wall.

The procedures developed in the following paragraphs for the determination of the loads on different types of structures are based on experimental results obtained from TNT and atomic explosions and from shock tube data. The computational methods presented are based on an interpretation of these experimental results and the equations given in connection with the loadings on a structure result from curve-fitting of measured data and should not be regarded as representing the development of any new theory. Nevertheless, every attempt has been made to make the empirical relationships consistent with such theory as now exists.

The following paragraphs are devoted to a general presentation of the procedures for the determination of the loads on structures of various types. Pertinent quantities are introduced and explained, and justification

for the methods employed is given as well as the bases for their conception. The general presentation for each type of structure is followed by a paragraph giving a step-by-step procedure by which the loads can be computed. Illustrative numerical examples are presented for the closed rectangular structures.

In using procedures presented herein, inconsistencies in loads computed may be encountered, particularly in the case of buried and semiburied structures and with peak overpressures greater than 25 psi. The lack of experimental data and an adequate theory in these regions requires use of engineering judgment and some degree of conservatism. Extrapolation and use of load data for peak overpressures greater than 25 psi are strictly an expediency and must be recognized as such by the engineer.

a. Diffraction and Drag Loading. The loading on aboveground structures resulting from the air blast produced by an air or surface burst may be considered to consist of a diffraction phase and a drag phase.

The diffraction phase of the loading is the term given to the initial phase of the blast loading on a structure when the reflected pressures associated with the air blast are acting on the structure. The time required for the blast wave to surround the structure completely and the presence of large reflected pressures on the front wall cause net lateral loads to be exerted on the structure as a whole in the direction of travel of the blast wave. The local and differential forces which act on the structure during the initial stages are defined as the diffraction phase loading.

The drag phase of the loading is the term given to the second phase of the loading on a structure due to the mass and velocity of the air particles in the blast wave after the envelopment of the structure by the wave front and the reflection effects have decayed. This phase of the loading is most important on open structural frameworks and on structures having small dimensions such as stacks, poles, chimneys, etc.

In general, the diffraction phase of the loading can be neglected and only the drag phase considered if the minimum dimension of the structure perpendicular to the direction of travel of the shock wave and the dimension of the structure parallel to the direction of travel of the blast wave are less than approximately 5 ft. Because of such short dimensions,

the duration of the diffraction phase is very short. The larger the loaded area the greater is the time required for the transient reflection effects to decay and reach the relatively steady condition of the drag phase. The longer the duration of the reflection effects the more important is the diffraction phase of the loading. In all cases except when a precursor exists, the pressures on any portion of the structure existing during the diffraction phase are greater than during the drag phase.

Large quantities of heated dust may be raised by the thermal radiation before the arrival of the blast wave. The air near the ground is also heated by the thermal radiation and this may cause a precursor wave to form ahead of the main shock. Test results indicate that when precursors form there is usually a dust-laden atmosphere present and the dynamic pressures are much larger than when there is no precursor. These high dynamic pressures are usually observed in the high overpressure regions.

3-08 LOADING ON CLOSED RECTANGULAR STRUCTURES. The type of structure for which the loading predictions of this section are applicable is illustrated in figure 3.15. The behavior of the blast wave upon striking a closed rectangular structure is depicted in figure 3.16(a), (b), (c), and (d). This figure illustrates the position of the shock front and the behavior of the reflected and diffracted waves at successive times during the passage of the blast wave over the center portion of the building (figure 3.15). As the shock front strikes the wall of the building (figure 3.16(a)) a reflected blast wave is formed and the overpressure on this wall is raised to a value in excess of the peak overpressure in the incident blast wave. This increased

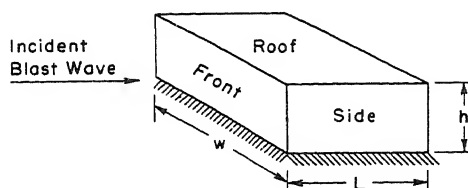


Figure 3.15. Closed rectangular structure

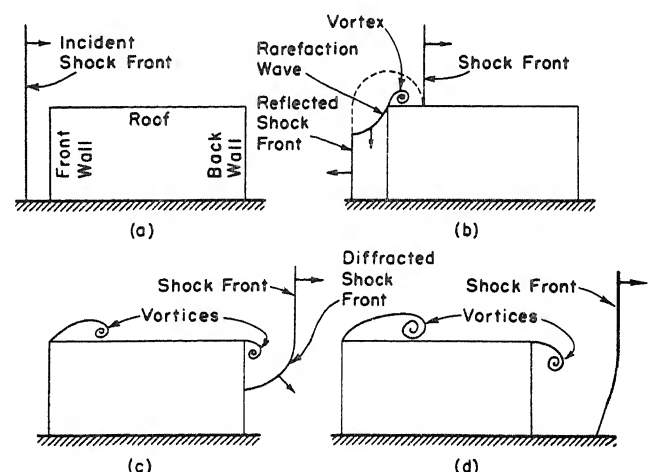
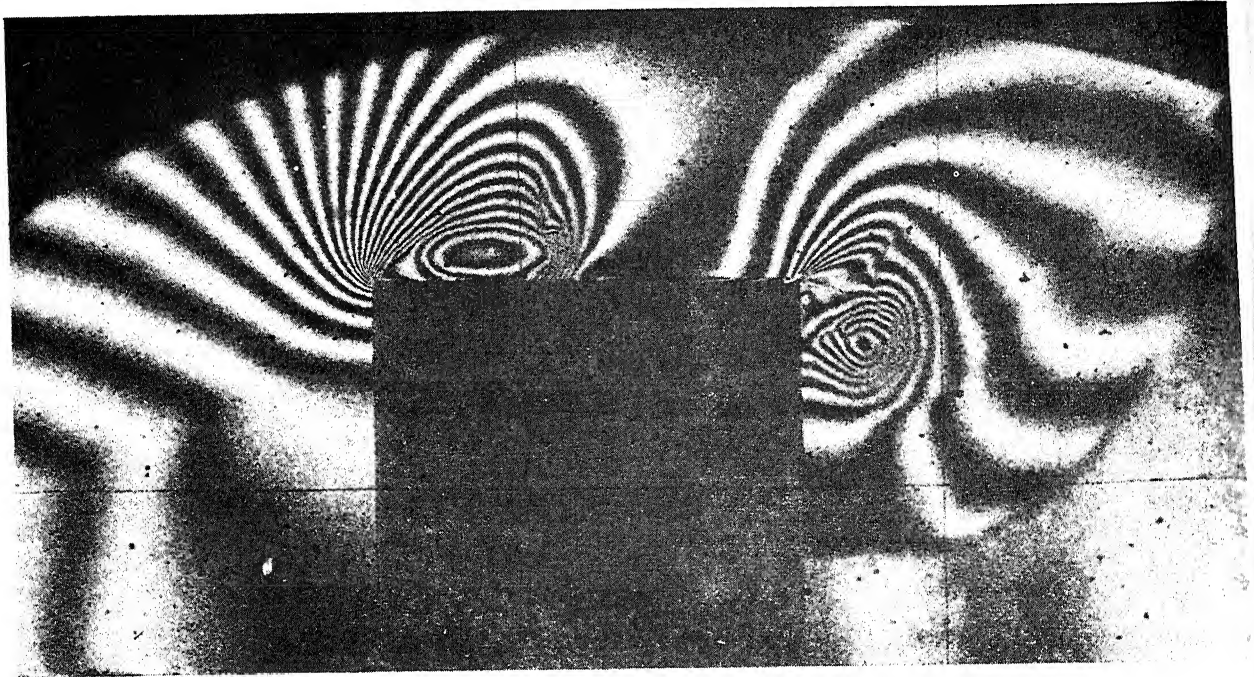


Figure 3.16. Behavior of blast wave along center portion of closed rectangular structure

overpressure is called the reflected overpressure and is a function of the peak overpressure in the incident blast wave and the angle of incidence of the shock front with the front wall which is zero degree in this case. At the instant the reflected shock front is formed, the lower overpressure existing in the incident blast wave adjacent to the top edge of the front wall initiates a rarefaction wave (figure 3.16(b)), or a wave of lower overpressure than that which exists in the reflected blast wave. This rarefaction wave travels with the speed of sound in the reflected blast wave toward the bottom of the front wall. Within a short time, called the clearing time, the rarefaction wave enfeebls the reflected blast wave to such an extent that its effect is no longer felt and reduces the overpressure existing on the front wall to a value that is in equilibrium with the high-velocity air stream associated with the incident blast wave. The overpressure on the front wall when equilibrium with the high-velocity air stream is reached is equal to the stagnation overpressure at the base of the front wall and an overpressure somewhat less than that in the blast wave at the top edge of the front wall. The stagnation overpressure is defined as that overpressure existing in a region in which the moving air has been brought completely to rest causing the pressure intensity to be increased by the loss in momentum of the air particles.

At some time after the shock front strikes the front wall of the structure, equal to the length of the structure divided by the shock front velocity, the shock front reaches the back edge of the structure and starts spilling down toward the bottom of the back wall (figure 3.16(c)). The back wall begins to experience increased pressures as soon as the shock front has passed beyond it. The effect is first observed at the top portions of the back wall and proceeds toward the bottom. A vortex, which is a region of air spinning about an axis at a high speed with low overpressures existing at its center because of the venturi effect, is created on the back wall and grows in size, traveling toward the base from the top edge and also moving away from the wall (figure 3.16(b) and figure 3.17). The maximum back wall overpressure develops slowly as a result of the vortex phenomena and the time required for the back wall to be enveloped by the blast wave.



*Figure 3.17. Photograph of a blast wave passing over a square block.
Light and dark bands represent contours of constant pressure*

As the shock front passes beyond the front wall (figure 3.16(b)) the overpressure exerted on the roof of the structure is initially raised to a value nearly equal to the overpressure existing in the incident blast wave. However, the air flow caused by the pressure difference between the reflected overpressure on the front wall and the blast wave overpressure on the roof causes the formation of a vortex along the top edge of the front wall. The vortex travels with a gradually decreasing intensity along the roof of the structure (figure 3.16(c)) at a slower rate than the shock front velocity. It causes a decay of the overpressures built up by the incident blast wave. After the passage of this vortex, the higher overpressures in the blast wave again become dominant and cause a second build-up of overpressures along the roof.

If a horizontal section through the structure is considered as shown in figure 3.18, it will be found that the blast wave produces effects similar to those produced on the roof, front, and back walls as indicated in figure 3.16. The major effects which should be noted are:

(1) The formation of rarefaction waves at each end of the front wall of the structure which travel toward the center to relieve the higher reflected pressures on the front wall;

(2) The diffracted wave fronts at the rear edges of the side walls which travel toward the center of the back wall;

(3) The vortices which form on the side walls near the front edges and travel slowly toward the back;

(4) The vortices which form at the ends of the back wall and travel slowly toward its center.

In determining the loads on a structure, it is convenient to use the instant at which the shock front impinges on the front face as a reference for time ($t = 0$). In adopting this convention, it is necessary to introduce a time-displacement factor t_d which is the time required for the shock front to travel from the front face of the structure to the surface or point under consideration. Figure 3.19 illustrates this convention. In this figure, $t - t_d$ is the time after the shock front has passed a given location on the structure and determines the overpressure P_s in the incident blast wave at that location.

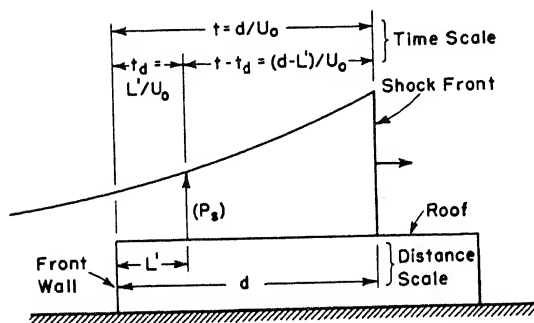


Figure 3.19. Time-displacement factor convention

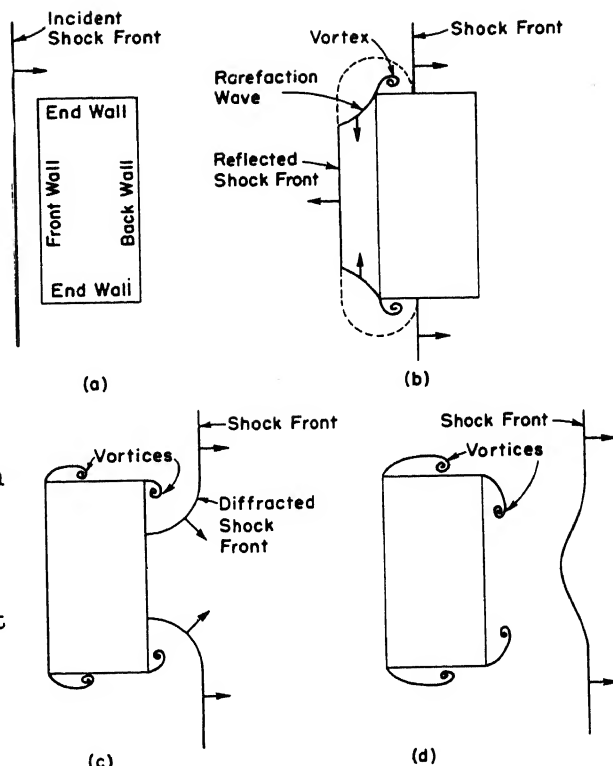


Figure 3.18. Behavior of blast wave along horizontal section through closed rectangular structure

For example, the time-displacement factor for a given location on the roof a distance L' from the front face of the structure is $t_d = L'/U_0$.

The total loading on any face of a cubical structure is equal to the algebraic sum of the respective

overpressures or reflected overpressures combined with the dynamic pressures. The later pressures are due to the wind effects of suspended particles and are referred to as "drag" loading which may result in either positive or negative corrections depending on the orientation of the surface with respect to the direction of travel of the shock front.

a. Average Front Wall Overpressure \bar{P}_{front} . At the moment the incident shock front strikes the front wall, the overpressure on the front wall is immediately raised from zero to the reflected overpressure P_{refl} . Reflected overpressure is plotted in figure 3.20 for zero angle of incidence as a function of the peak overpressure of the incident shock front. The value of P_{refl} from figure 3.20 is the same as $P_{r-\alpha}$ for $\alpha = 0^\circ$ using figure 3.11. The incident shock front continues its motion over the top of the structure, while the reflected shock front moves away from the front of the building in the opposite direction. Initially, the air pressure between the reflected shock front and the front wall is higher than the pressure behind the incident shock front. This causes air to move around to the sides and over the top of the structure into the lower pressure zone behind the incident shock. The rarefaction waves thus formed move from the end and top edges toward the center of the front face with the speed of sound for the pressure existing in this region of reflected overpressure [1].

For the range of shock strengths used in the Princeton shock tube experiments [4] which correspond to peak shock overpressures of 2 to 50 psi in a standard atmosphere, it has been found that the time required to clear the front face of reflection effects is determined by the dimensions of the front face and the peak overpressure of the incident shock wave. This clearing time t_c is given by the relation:

$$t_c = 3h'/c_{\text{refl}} \quad (3.4)$$

where

h' = clearing height, taken as the full height of the front face or half its length whichever is the smaller

c_{refl} = velocity of sound in the reflected region, plotted as a function of the peak overpressure of the incident shock wave in figure 3.21

During the time required to clear the front wall of reflection effects, the average overpressure on the front wall decreases from the

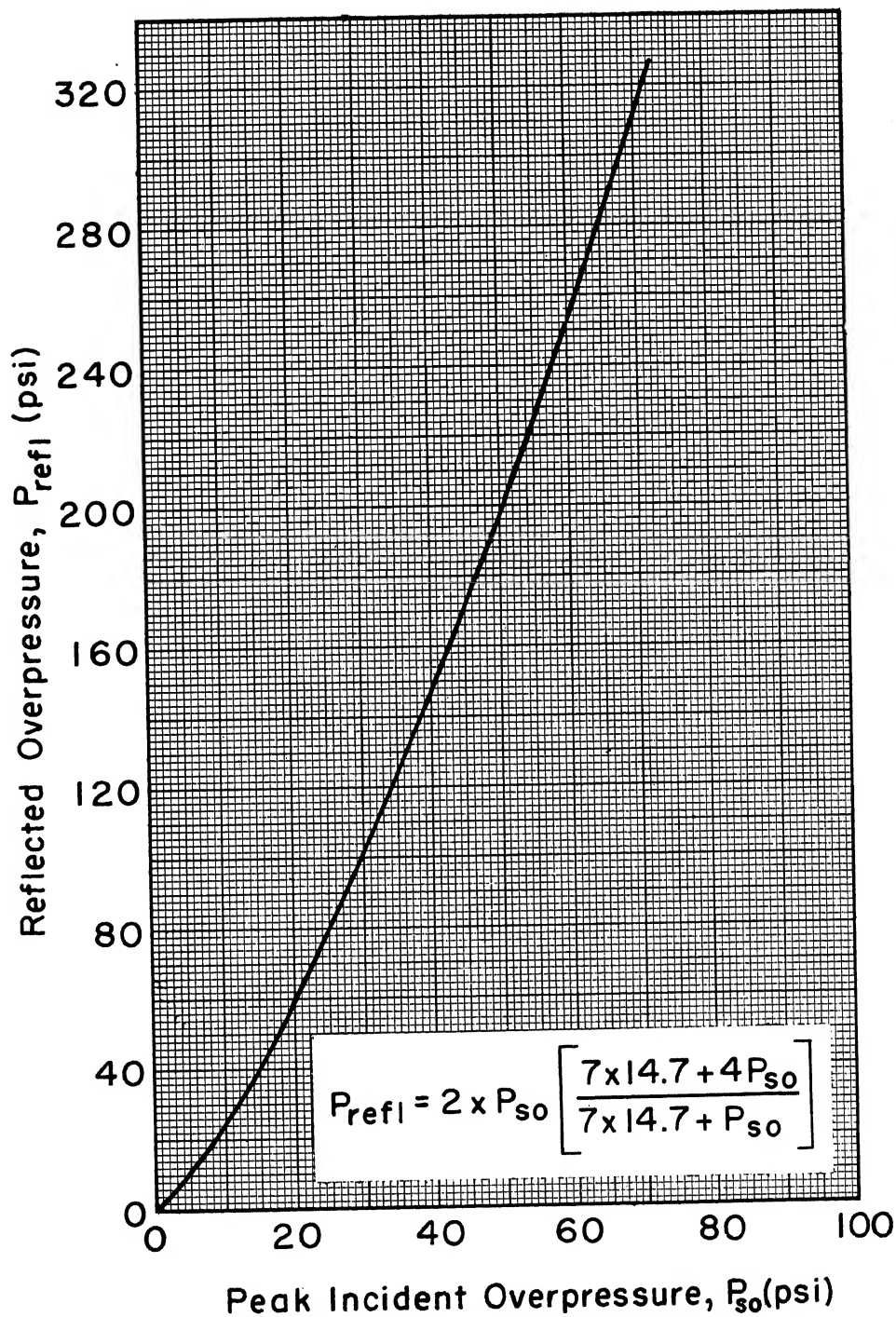


Figure 3.20. Reflected overpressure vs peak incident overpressure for normal reflection

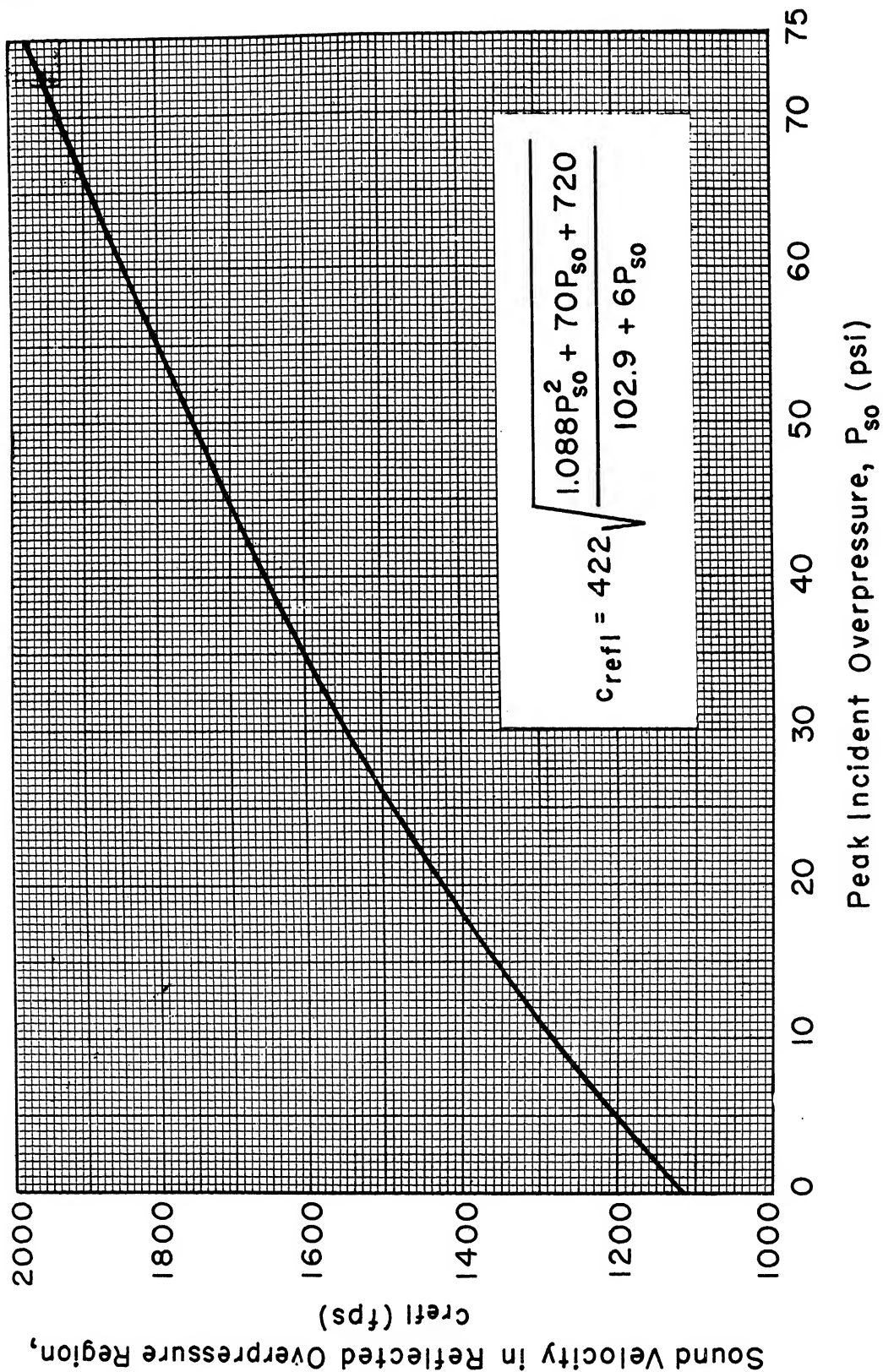


Figure 3.21. Velocity of sound in reflected overpressure region vs peak incident overpressure

reflected overpressure to a value given by the following equation:

$$\bar{P}_{\text{front}} = P_s + 0.85q \quad (3.5)$$

where P_s = overpressure in the incident blast wave at the front wall at any time $t - t_d$ as given by the equation

$$P_s/P_{so} = \left[1 - (t - t_d)/t_o \right] e^{-(t - t_d)/t_o} \quad (3.6)$$

Equation (3.6) is plotted in figure 3.22, and tabulated in table 3.1, where the ratio P_s/P_{so} is given as a function of $(t - t_d)/t_o$. This equation is similar to equation (3.1) with $(t - t_d)$ substituted for t .

In paragraph 3-05b the dynamic pressures associated with high overpressures were discussed. These pressures were evaluated in figure 3.23a. The rates of overpressure decay and dynamic pressure decay were set forth in figures 3.4b and 3.4c.

Design requirements for aboveground frame structures are usually for peak overpressures of 10 psi or less. The use of equations (3.6), (3.7a), and 3.7c following and tables 3.1 and 3.2 will be applicable and convenient.

The quantity q in equation (3.5) is the dynamic pressure due to the motion of air particles in the incident blast wave at any time $(t - t_d)$ and is given by $q = \rho u^2/2$ where ρ is the mass per unit volume of the air and u is the velocity of the air particles. Values of dynamic pressures vs overpressures for the theoretical (without precursor) and precursor condition are given in figure 3.23a. It will be noted that the values are about the same for each case up to about 10-psi overpressure. The dynamic pressure vs distance for miles for various weapon sizes is given in figure 3.23b.

$$q = 14.7 \left[\frac{\frac{5}{14} (P_s/14.7)^2}{1 + \frac{1}{7} (P_s/14.7)} \right] \quad (3.7a)$$

Peak dynamic pressure q for use when overpressures are less than 10 psi or where there are no precursor effects considered is given by the equation

$$q_o = 14.7 \left[\frac{\frac{5}{14} (P_{so}/14.7)^2}{1 + \frac{1}{7} (P_{so}/14.7)} \right] \quad (3.7b)$$

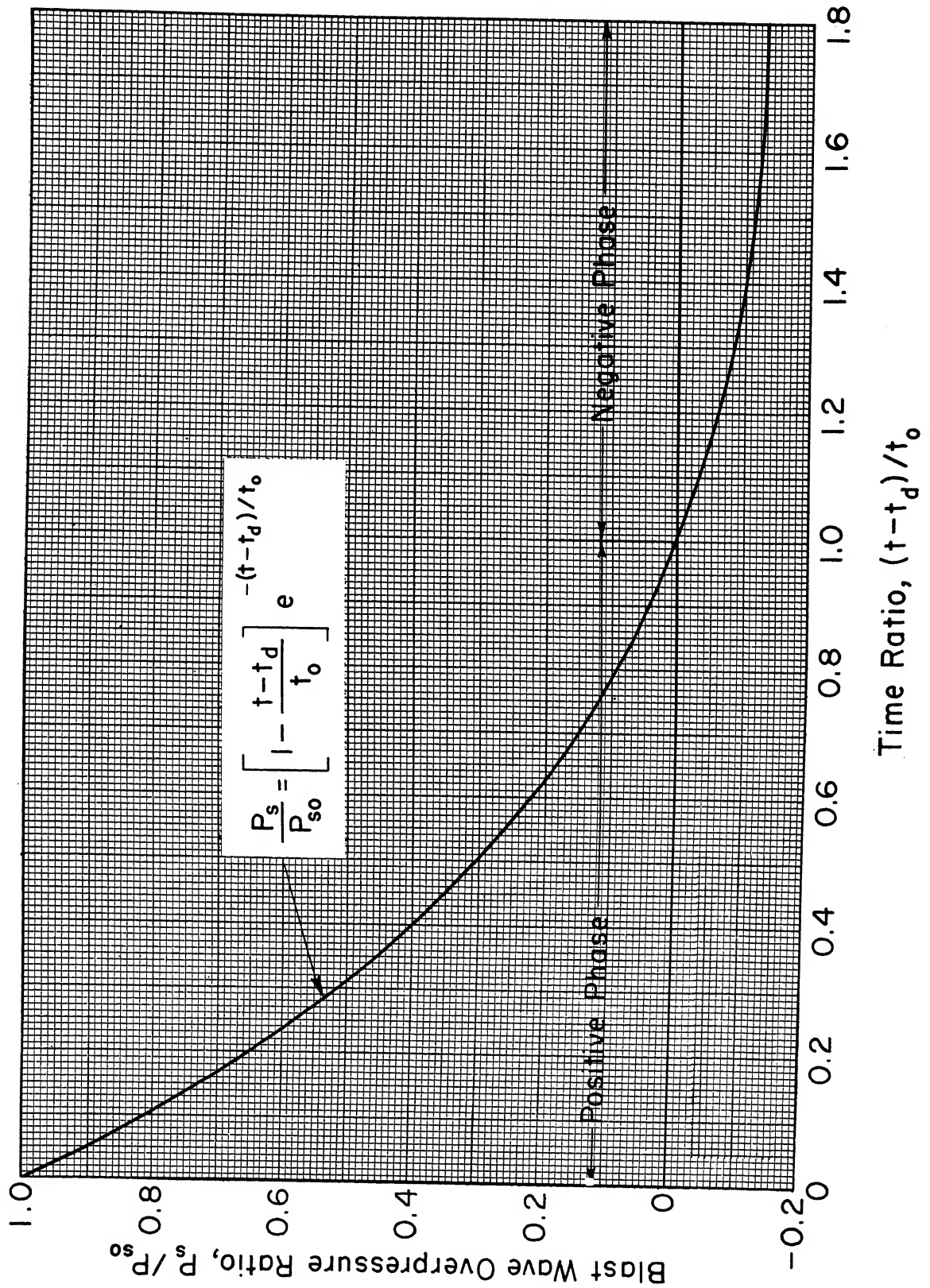


Figure 3.22. Blast wave overpressure ratio vs time ratio

Table 3.1. Blast Wave Overpressure Ratio vs Time Ratio

$(t - t_d)/t_o$	P_s/P_{so}	$(t - t_d)/t_o$	P_s/P_{so}	$(t - t_d)/t_o$	P_s/P_{so}
0.00	1.000	0.30	0.519	0.60	0.220
0.01	0.980	0.31	0.506	0.61	0.212
0.02	0.961	0.32	0.494	0.62	0.204
0.03	0.941	0.33	0.482	0.63	0.197
0.04	0.922	0.34	0.470	0.64	0.190
0.05	0.904	0.35	0.458	0.65	0.183
0.06	0.885	0.36	0.447	0.66	0.176
0.07	0.867	0.37	0.435	0.67	0.169
0.08	0.849	0.38	0.424	0.68	0.162
0.09	0.832	0.39	0.413	0.69	0.155
0.10	0.814	0.40	0.402	0.70	0.149
0.11	0.797	0.41	0.392	0.71	0.143
0.12	0.780	0.42	0.381	0.72	0.136
0.13	0.764	0.43	0.371	0.73	0.130
0.14	0.748	0.44	0.361	0.74	0.124
0.15	0.732	0.45	0.351	0.75	0.118
0.16	0.716	0.46	0.341	0.76	0.112
0.17	0.700	0.47	0.331	0.77	0.106
0.18	0.685	0.48	0.322	0.78	0.101
0.19	0.670	0.49	0.312	0.79	0.095
0.20	0.655	0.50	0.303	0.80	0.090
0.21	0.640	0.51	0.294	0.81	0.085
0.22	0.626	0.52	0.285	0.82	0.079
0.23	0.612	0.53	0.277	0.83	0.074
0.24	0.598	0.54	0.268	0.84	0.069
0.25	0.584	0.55	0.260	0.85	0.064
0.26	0.571	0.56	0.251	0.86	0.059
0.27	0.557	0.57	0.243	0.87	0.054
0.28	0.544	0.58	0.235	0.88	0.050
0.29	0.531	0.59	0.227	0.89	0.045
$\frac{P_s}{P_{so}} = \left[1 - \frac{(t - t_d)}{t_o} \right] e^{-(t - t_d)/t_o}$				0.90	0.041
				0.91	0.036
				0.92	0.032
				0.93	0.028
				0.94	0.023
				0.95	0.019
				0.96	0.015
				0.97	0.011
				0.98	0.008
				0.99	0.004
				1.00	0.000

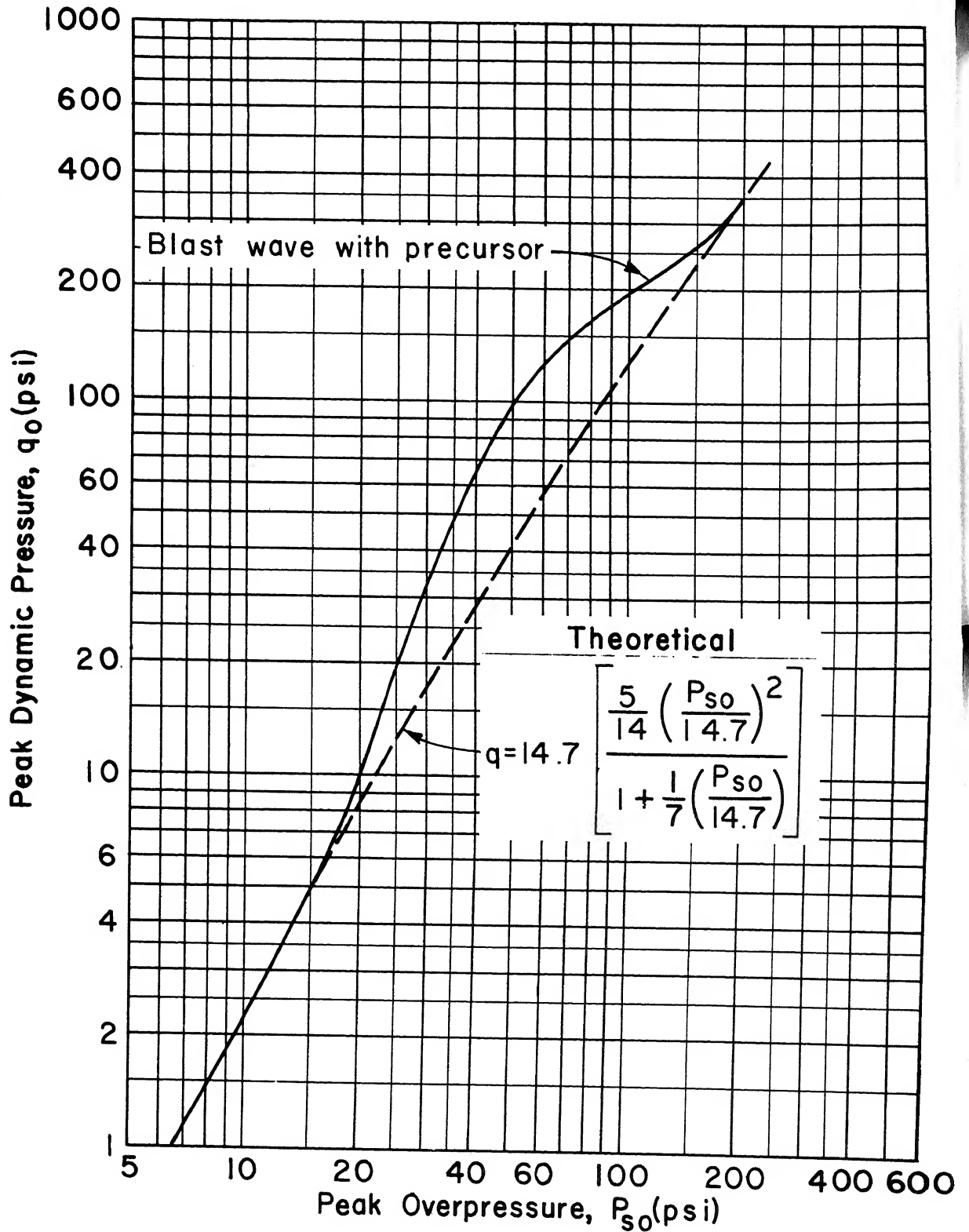


Figure 3.23a. Peak dynamic pressure vs peak incident overpressure

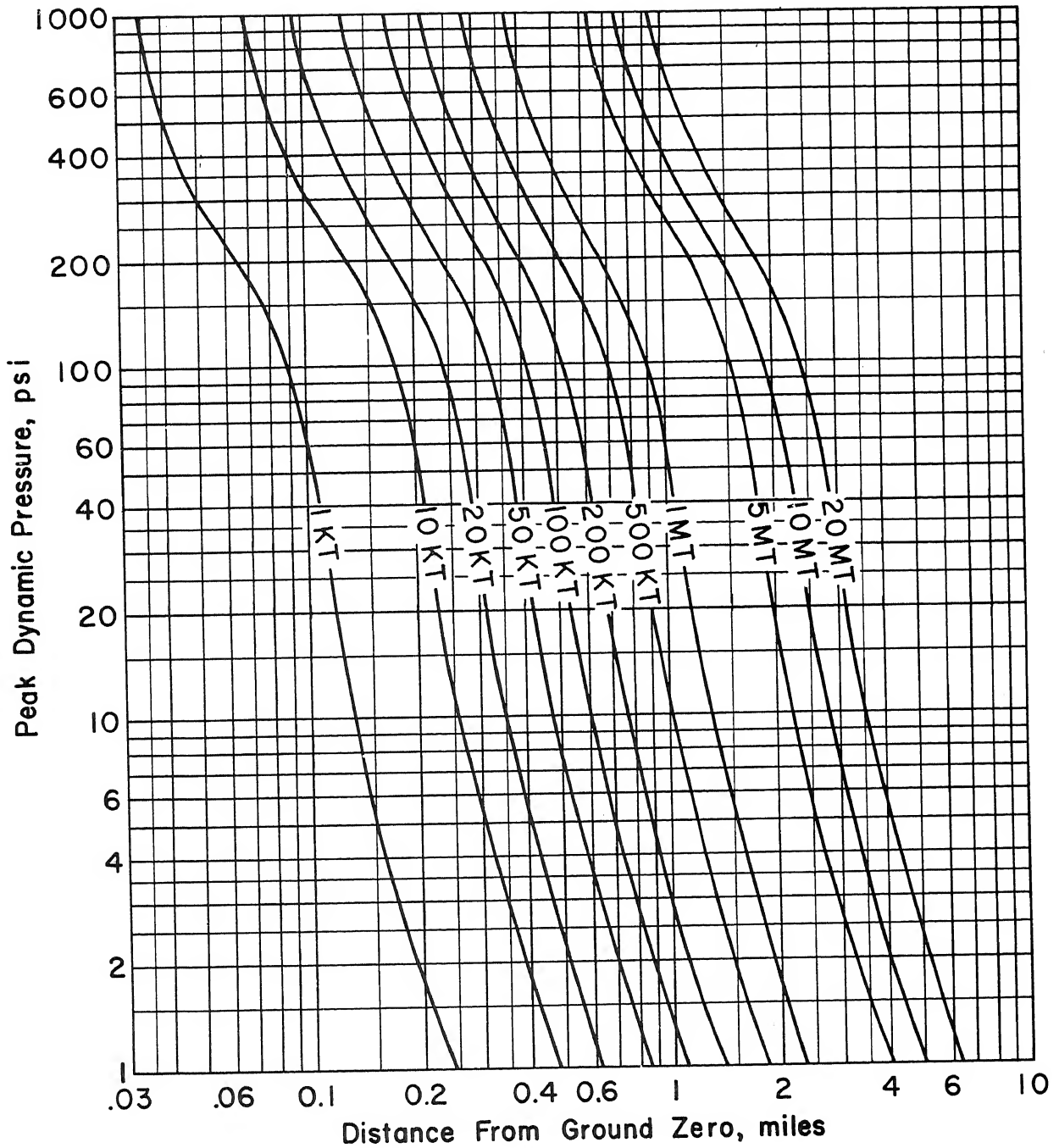


Figure 3.23b. Dynamic pressure for surface burst

To obtain q as a function of time for overpressures less than 10 psi it is convenient to use the ratio q/q_0 , plotted in figure 3.24 and tabulated in table 3.2 as a function of $(t - t_d)/t_0$, from the following expression

$$\frac{q}{q_0} = \left[1 - \left(\frac{t - t_d}{t_0} \right) \right] e^{-3.5(t - t_d)/t_0} \quad (3.7c)$$

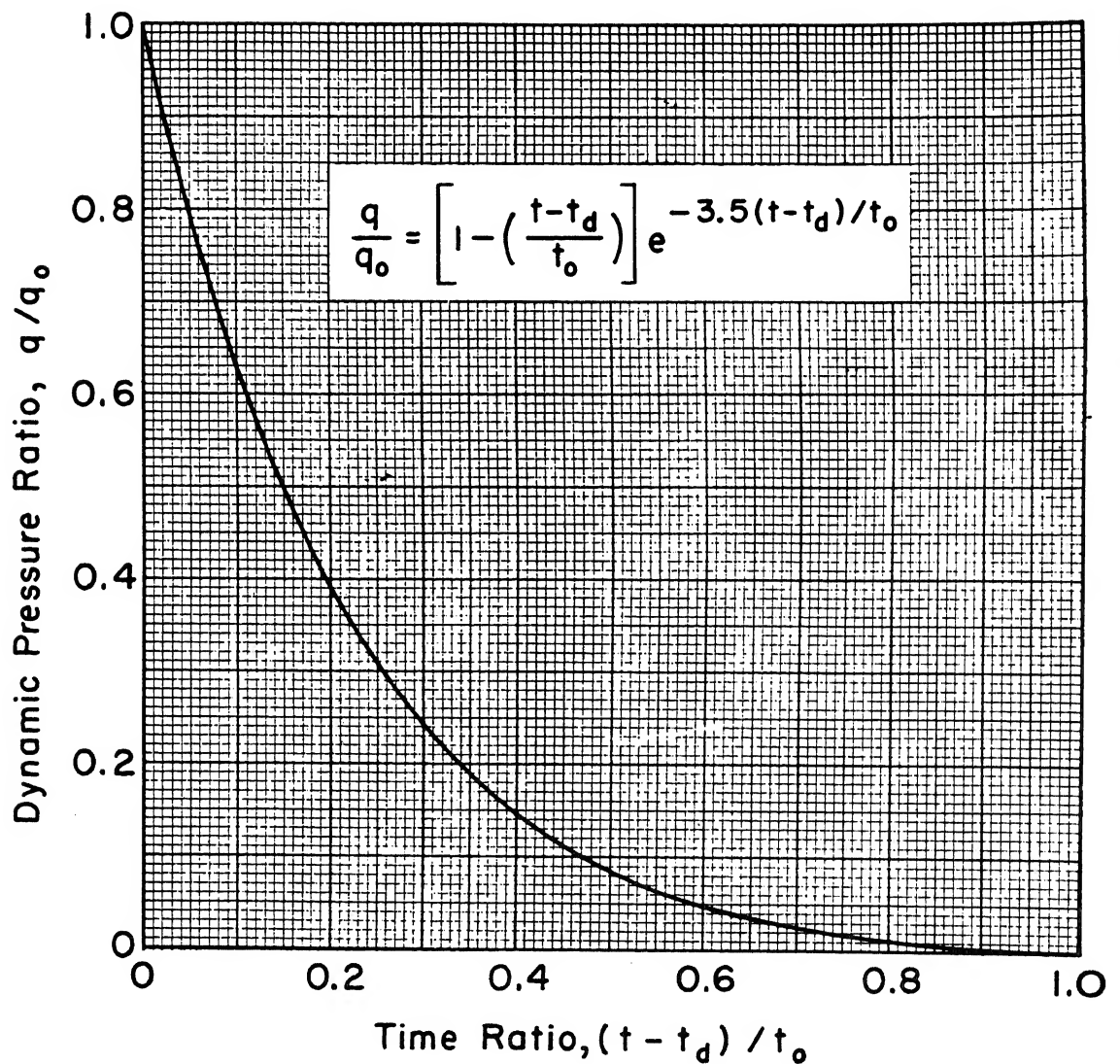


Figure 3.24. Dynamic pressure ratio vs time ratio

Table 3.2. Dynamic Pressure Ratio vs Time Ratio

$(t - t_d)t_o$	q/q_o	$(t - t_d)t_o$	q/q_o	$(t - t_d)t_o$	q/q_o
0.00	1.000	0.30	0.245	0.60	0.049
0.01	0.956	0.31	0.233	0.61	0.046
0.02	0.914	0.32	0.222	0.62	0.043
0.03	0.873	0.33	0.211	0.63	0.041
0.04	0.835	0.34	0.201	0.64	0.038
0.05	0.798	0.35	0.191	0.65	0.036
0.06	0.762	0.36	0.182	0.66	0.034
0.07	0.728	0.37	0.173	0.67	0.032
0.08	0.695	0.38	0.164	0.68	0.030
0.09	0.664	0.39	0.156	0.69	0.028
0.10	0.634	0.40	0.148	0.70	0.026
0.11	0.606	0.41	0.141	0.71	0.024
0.12	0.578	0.42	0.133	0.72	0.022
0.13	0.552	0.43	0.127	0.73	0.021
0.14	0.527	0.44	0.120	0.74	0.020
0.15	0.503	0.45	0.114	0.75	0.018
0.16	0.480	0.46	0.108	0.76	0.017
0.17	0.458	0.47	0.102	0.77	0.016
0.18	0.437	0.48	0.097	0.78	0.014
0.19	0.417	0.49	0.092	0.79	0.013
0.20	0.397	0.50	0.087	0.80	0.012
0.21	0.379	0.51	0.082	0.81	0.011
0.22	0.361	0.52	0.078	0.82	0.010
0.23	0.344	0.53	0.074	0.83	0.009
0.24	0.328	0.54	0.070	0.84	0.008
0.25	0.313	0.55	0.066	0.85	0.008
0.26	0.298	0.56	0.062	0.86	0.007
0.27	0.284	0.57	0.059	0.87	0.006
0.28	0.270	0.58	0.055	0.88	0.006
0.29	0.257	0.59	0.052	0.89	0.005
$\frac{q}{q_o} = \left[1 - \left(\frac{t - t_d}{t_o} \right) \right] e^{-3.5(t - t_d)/t_o}$				0.90	0.004
				0.91	0.004
				0.92	0.003
				0.93	0.003
				0.94	0.002
				0.95	0.002
				0.96	0.001
				0.97	0.001
				0.98	0.001
				0.99	0.000
				1.00	0.000

For the front wall overpressures, $t_d = 0$, hence $t - t_d = t$, where t measures the time after the instant at which the shock front impinges on the front wall.

Using the above quantities, the curve of average front wall overpressure \bar{P}_{front} versus time may be determined. Figure 3.25 shows a typical front wall average overpressure curve. The curve a-b-c is defined by

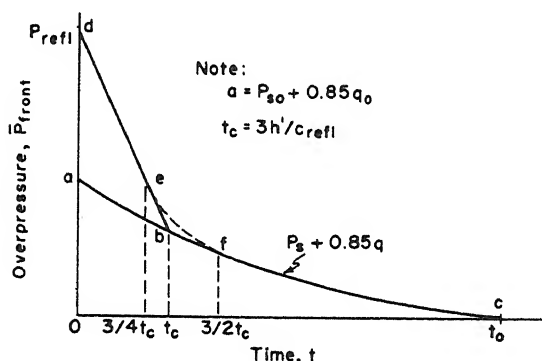


Figure 3.25. Average front wall overpressure vs time-closed rectangular structure

equation (3.5). Point d, the reflected overpressure, is connected by a straight line to point b, the average overpressure at time $t - t_d = t_c$. Since the resulting discontinuity at point b is not compatible with actual behavior of the loads on the front face, these two curves are smoothed by fairing in curve e-f as shown. The curve of average over-

pressure versus time on the front wall is then defined as curve o-d-e-f-c.

The foregoing method for determining the curve of average overpressure versus time on the front wall is based on the assumption that the time required for the overpressure in the incident shock wave to rise from zero is negligible.

If this is not the case, the time required for the peak overpressure to rise from zero, called the time of rise t_r , must be taken into account. This is accomplished by first computing the average front face overpressure for a zero time of rise as described above. Curve o-d-e-f-c of figure 3.26 illustrates the average front wall overpressure computed for a zero time of rise. Locate point g with time coordinate t_r and overpressure coordinate P_{refl} . Join points o and g with straight line

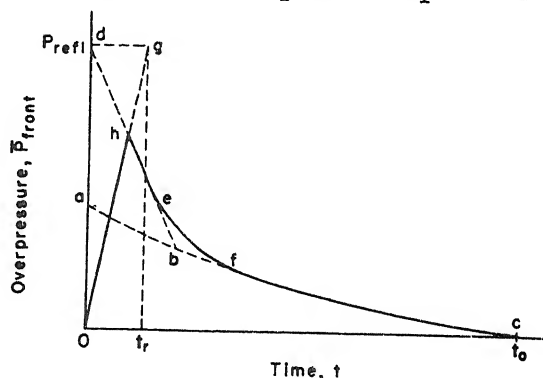


Figure 3.26. Graphical procedure for evaluating reduced average front wall overpressure due to time of rise of incident shock wave

intersecting d-e-f at h. The average front wall overpressure for time of rise t_r is given by curve o-h-e-f-c.

The overpressure on the front wall of a structure is not uniformly distributed. The maximum value occurs at the mid-point of the base and the minimum value occurs along the edges. Those portions of the front face nearest to the edges are cleared of the reflection effects in a shorter time than the remainder of the front face and the overpressure existing at those points is lower, following the clearing stage. The net effect of this vertical and horizontal variation is negligible and of questionable value for design purposes. Hence, the front wall loading is assumed to be distributed uniformly over the front wall surface. For the same reasons, the rear wall loading given next is assumed to be uniformly distributed over the rear wall.

b. Average Back Wall Overpressure \bar{P}_{back} . For the back wall, the time-displacement factor t_d is L/U_o , where L is the length of the building in the direction of propagation of the shock and U_o is the shock front velocity.

When the shock front crosses the rear edge of the structure, the foot of the shock spills down the back wall. The overpressures on the back wall behind this diffracted wave are considerably less than those in the incident blast wave due to the vortex which develops at the top and travels down the wall. A period of time longer than that required for the travel of this diffracted shock to the bottom of the wall must pass before the back wall average overpressure reaches its peak value. The time required for this build-up to occur, t_b , measured from the instant at which the shockwave reaches the back wall is equal to $4h'/c_o$, where h' is the clearing height of the back wall, taken equal to either the full height of the back wall or half the width of the building, whichever is the smaller, and c_o is the velocity of sound in undisturbed air, 1115 fps.

The peak value of the average overpressure on the back wall after this build-up has been completed is:

$$(\bar{P}_{back})_{max} = P_{sb} (1/2) \left[1 + (1 - \beta)e^{-\beta} \right] \quad (3.8)$$

where P_{sb} is the incident blast wave overpressure at the back wall at time $t - t_d = t_b$; $(\bar{P}_{back})_{max}$ is the peak value of the average overpressure

on the back wall which occurs at time $t = t_d + t_b$; $\beta = 0.5P_{so}/14.7$; and $e = 2.7183 =$ base of natural logarithms. It is assumed that P_{so} in the incident blast wave does not diminish in strength as the wave passes over the structure.

Figure 3.27a illustrates the variation of the ratio \bar{P}_{back}/P_s with time. For times in excess of $t = t_d + t_b$, the relation is given by the following equation:

$$\frac{\bar{P}_{back}}{P_s} = \frac{(\bar{P}_{back})_{max}}{P_{sb}} + \left[1 - \frac{(\bar{P}_{back})_{max}}{P_{sb}} \right] \left[\frac{t - (t_d + t_b)}{t_o - t_b} \right]^2 \quad (3.9)$$

where t_o is the duration of the positive phase.

Figure 3.27b shows a typical back wall average overpressure curve.

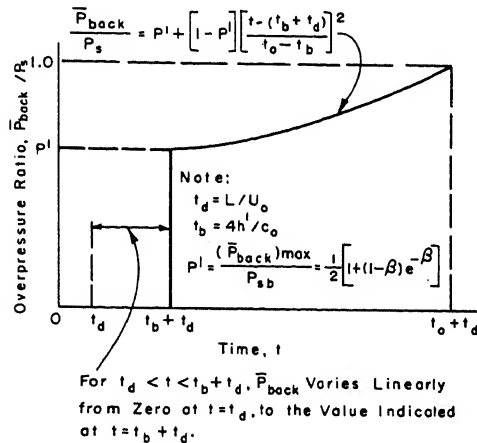


Figure 3.27a. Average back wall overpressure ratio vs time--closed rectangular structure

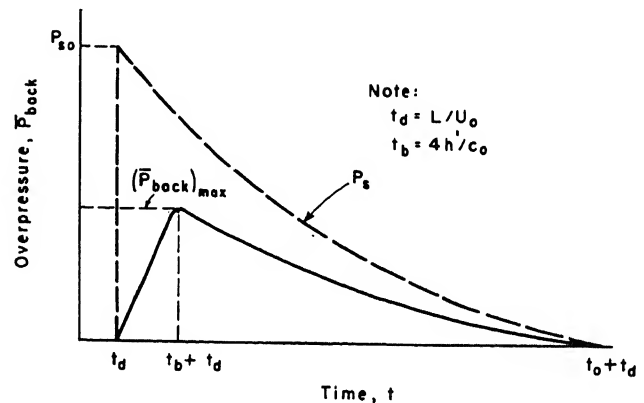


Figure 3.27b. Average back wall overpressure vs time--closed rectangular structure

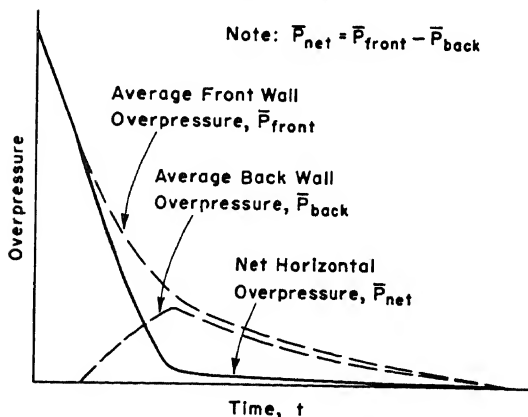


Figure 3.28. Net horizontal overpressure vs time--closed rectangular structure

c. Average Net Horizontal Overpressure \bar{P}_{net} . Considering as positive all overpressures exerted on the structure and directed toward the interior,

$$\bar{P}_{net} = \bar{P}_{front} - \bar{P}_{back} \quad (3.10)$$

where \bar{P}_{net} , \bar{P}_{front} , and \bar{P}_{back} are given in terms of time t . Figure 3.28 illustrates graphically the variation of the net average horizontal overpressure with time.

d. Local Roof Overpressure P_{roof} . The procedure developed for prediction of overpressures on the roof of a structure is based primarily on curve-fitting of the Princeton and Michigan shock tube data [4 through 13]. Pressures calculated by this procedure have been found to agree satisfactorily with overpressure records obtained in the GREENHOUSE structure testing program and the Sandia HE tests [6].

During the passage of the blast wave across the structure, low pressure areas develop on the roof and side walls due to vortex formation as indicated in figure 3.16 and figure 3.18. Shock tube data indicate that this vortex detaches itself from the front edges and moves across the structure with gradually increasing speed. Vortices are formed all along the front edges of the roof and sides of the structure, that is along a-b-c-d of figure 3.29. At corners b and c where they are aligned at 90° to each other, the vortices tend to interfere with each other and to move away from the roof and wall surfaces. This results in a diminution of the effects of the vortices at these edges which proceeds along the axes of the vortices from corners b and c as the vortices move toward the rear of the roof. Consequently the regions on the roof and side walls which are strongly affected by the vortices do not extend to all edges of the roof, but are triangular or trapezoidal in shape as indicated in figure 3.29.

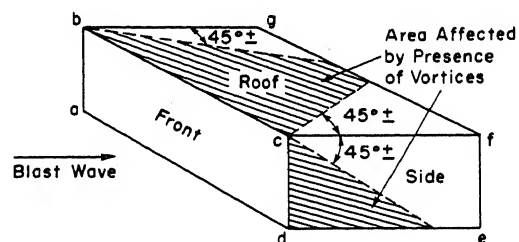


Figure 3.29. Areas on roof and sides most affected by vortex action

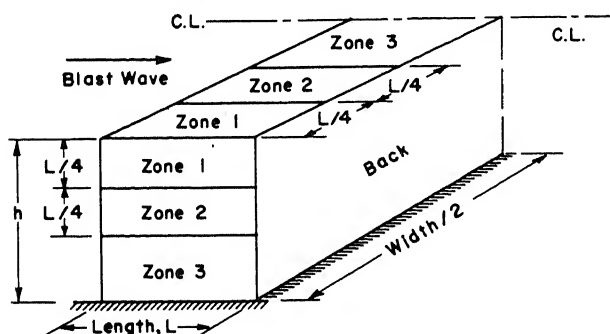


Figure 3.30. Location of loading zones on roof and sides of structure

These observed results indicate a variation of overpressures on the roof in a direction parallel to the shock front in addition to a variation along the roof in the direction of propagation of the wave. Although this lateral variation is a smooth one, the roof and side walls have been divided into three zones as illustrated in figure 3.30 to facilitate computation of local

pressures. Although only the location of the zones on the roof is discussed below, the zones on the side wall are similarly located as shown in figure 3.30.

Zone 1. This zone is a strip on the roof extending from the sides toward the center line a distance equal to one-quarter of the length L of the building.

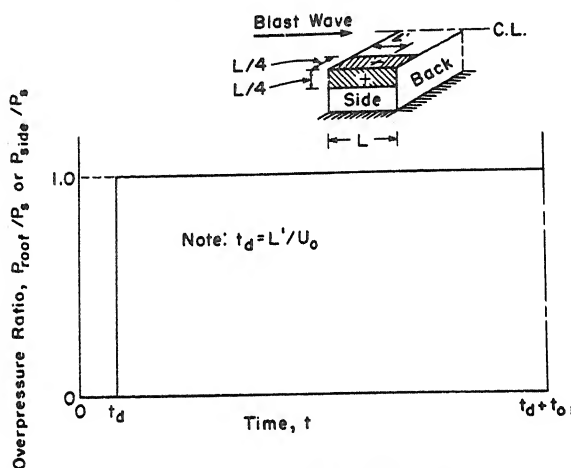


Figure 3.31. Local roof or side wall overpressure ratio vs time, Zone 1--closed rectangular structure

for any point in Zone 1 is equal to the overpressure-time curve for the incident blast wave displaced in time by factor $t_d = L'/U_o$. This is consistent with observed vortex disintegration as illustrated in figure 3.29.

Zone 2. This zone is a strip on the roof of width equal to one-quarter of the length of the structure measured from the edge of Zone 1 toward the center of the roof.

Figure 3.32 is a plot of the ratio P_{roof}/P_s for any point a distance L' from the front edge

Figure 3.31 is a plot of P_{roof}/P_s , the ratio of the local overpressure at any point on the roof in terms of time t to the overpressure in the incident blast wave where $t_d = L'/U_o$ is the time-displacement factor, equal to the time required for the shock front to travel a distance L' , the distance from the front edge of the roof to the point under consideration.

Figure 3.31 indicates that the local overpressure versus time curve

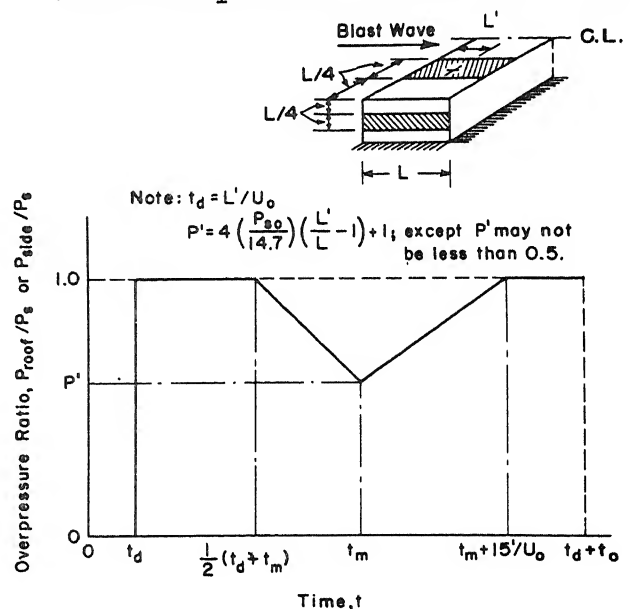


Figure 3.32. Local roof or side wall overpressure ratio vs time, Zone 2--closed rectangular structure

of the roof. Here again, P_{roof} and P_s incorporate the time-displacement $t_d = L'/U_o$. t_m is given by equation (3.11).

Zone 3. This zone includes all points on the roof not included in Zones 1 and 2. Figure 3.33 is a plot of the ratio P_{roof}/P_s for all points in this zone. Zone 3 is essentially a region of two-dimensional shock phenomena for which considerable data are available [4, 5, 9, 10, 11, 12, and 13].

The effects of the vortex travel across the roof of the structure are confined to Zones 2 and 3. The difference in the overpressure existing in these zones is due to the assumed severity of the vortex effects.

As the shock front passes over the point being considered, the local overpressure is raised to the overpressure in the incident blast wave. This equality between local and incident blast wave overpressures is maintained until the vortex developed at the front edge of the roof detaches itself and moves toward the rear edge, causing a decrease from the overpressure in the incident blast wave at the point being considered. The local overpressure reaches its minimum value at the time that the vortex is over the point in question. The time required for the vortex to travel the distance L' is

$$t_m = L'/v \quad (3.11)$$

where v is the vortex travel velocity, obtained from a reduction of the data in reference [4] and given by the relation

$$v = \left(0.042 + 0.108 \frac{L'}{L} \right) U_o \quad (3.12)$$

The value of the ratio of P_{roof}/P_s at time $t = t_m$ is

$$P' = P_{\text{roof}}/P_s = 4(P_{so}/14.7) \left(\frac{L'}{L} - 1 \right) + 1.0 \quad (3.13)$$

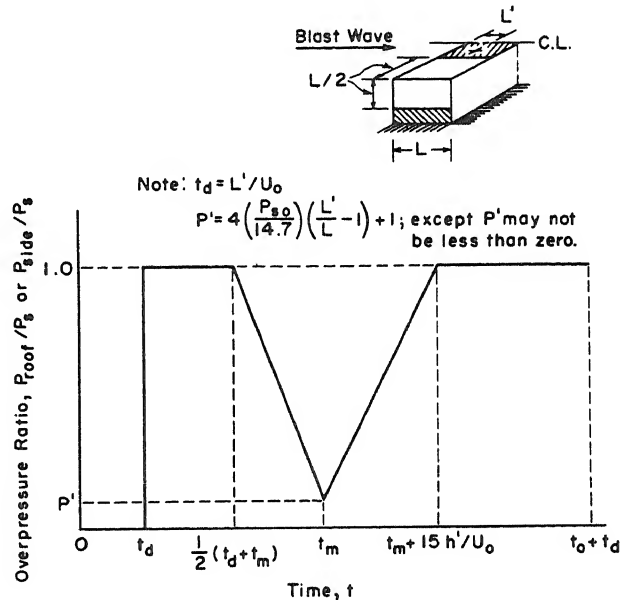


Figure 3.33. Local roof or side wall overpressure ratio vs time, Zone 3--closed rectangular structure

For points located in Zone 2 the minimum value of equation (3.13) is 0.5; for points located in Zone 3 the minimum value is zero.

As soon as the vortex has passed the point in question, the local overpressure starts to build up until at time $t = t_m + 15h'/U_0$ (where h' is the clearing height of the structure) it is once again equal to the overpressure in the incident shock wave.

e. Average Roof Overpressure \bar{P}_{roof} . Having established the variation of local overpressure, the average overpressure on the roof at any time could be obtained by the summation of the local overpressure curves over the entire roof at a given time t . If there were no lateral variation of local overpressures, such a method could be used to develop a general procedure applicable to all structures. However, the presence of this lateral variation complicates any procedure to such a degree that only the limiting case for Zone 3 loading is considered. The ratio of the average

NOTE: $P'' = 0.9 + 0.1(1.0 - \frac{P_{s0}}{4.7})^2$; except P'' may not exceed 1.0
 $P' = 2.0 - (\frac{P_{s0}}{4.7} + 1)(\frac{h'}{L})^{1/3}$ or $0.5 + 0.125(2 - \frac{P_{s0}}{4.7})^2$
 whichever is smaller; except P' may not be less than zero.

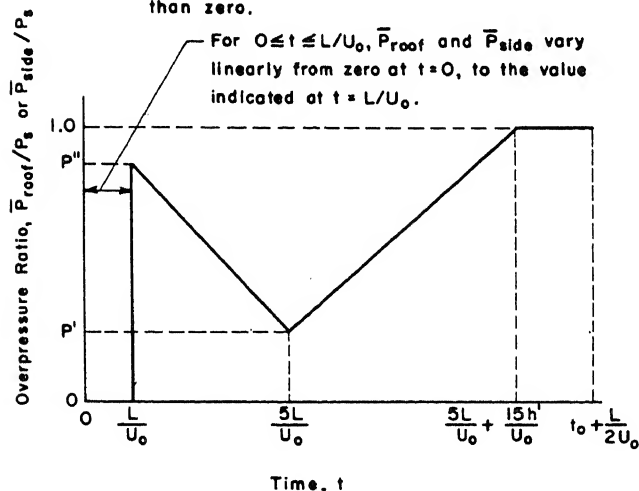


Figure 3.34. Average roof or side wall overpressure ratio vs time, Zone 3-- closed rectangular structure

the shock front to travel the length of the building is small compared to the duration of the positive phase. For values of $(L/U_0)/t_0$ less than 0.1 this assumption is reasonable.

A further restriction which must be imposed is due to the importance

age roof overpressure \bar{P}_{roof} to the overpressure of the incident blast wave existing at the center of the roof P_s is plotted in figure 3.34 for times in excess of time $t = L/U_0$ where P_s incorporates the time-displacement $t_d = L/2U_0$. The average overpressure on the roof varies linearly from zero at time $t = 0$ to the value of \bar{P}_{roof} given in figure 3.34 at time $t = L/U_0$. The assumption that \bar{P}_{roof} can be expressed as a proportion of P_s is valid only if the time required for

of the lateral variation of overpressures on the roof. If the width of the structure normal to the direction of travel of the shock wave is greater than twice its length, the average roof overpressures as determined by figure 3.34 are satisfactory. For a structure whose width is less than its length, the average roof overpressure for times greater than time $t = L/U_0$ is more correctly given by the relation

$$\bar{P}_{\text{roof}} = P_s \quad (3.14)$$

where P_s incorporates the time-displacement $t_d = L/2U_0$. The average roof overpressure varies linearly from time $t = 0$ to the value calculated by equation (3.14) at time $t = L/U_0$. For structures which are approximately square in roof plan, neither method is the more correct and an average of the two should be used. If a more accurate value of the average overpressure on a portion of the roof, such as a roof slab, is desired, this may be obtained by computing the local overpressure at two or three points on the slab and obtaining the weighted average as a function of their common time t .

f. Local and Average Side Wall Overpressure P_{side} and \bar{P}_{side} . On the basis of test data it has been observed that the sides of a structure are loaded in the same manner as is the roof, and that figures 3.31 to 3.34 determined for the roof of a structure apply equally well to the sides.

The side walls are divided into three zones, as shown in figure 3.30, for the determination of local overpressures P_{side} . Figures 3.31 to 3.33 present these local overpressures in the form P_{side}/P_s , where P_{side} and P_s incorporate the time-displacement $t_d = L'/U_0$. L' is the distance from the front edge of the side wall to the point under consideration.

The average overpressure on the side is given as the ratio $\bar{P}_{\text{side}}/P_s$ in figure 3.34, where P_s is the overpressure in the incident blast wave with a time-displacement $t_d = L/2U_0$. This figure is applicable only if the height h of the side wall is greater than half the length L . If this restriction is not satisfied the average overpressure on the side is more correctly given by the relation

$$\bar{P}_{\text{side}} = P_s \quad (3.15)$$

3-09 PROCEDURE FOR COMPUTATION OF LOADS ON CLOSED RECTANGULAR STRUCTURES.

The following paragraphs present a series of step-by-step general procedures

for the computation of the blast wave overpressures on the various portions of a closed rectangular structure.

Step 1. Given data: Size of weapon; distance of proposed structure from ground zero; exterior dimensions of structures.

Step 2. Determine P_{so} for the given data from figure 3.12a or 3.12b using the scaling relations of paragraph 3-06 as necessary.

Step 3. Determine t_o , knowing P_{so} , by applying the scaling relation of equation (3.3) to figure 3.10a or 3.10b.

Note that all the quantities listed in Step 1 are not necessary to determine the loading on any structure if P_{so} and t_o plus the exterior dimensions of the structure are given.

a. Average Front Wall Overpressure vs Time. Step 1. Determine P_s for a sequence of times t_1, t_2, t_3 , etc., from table 3.1 or figure 3.22 for $t_d = 0$.

Step 2. Determine P_{refl} , knowing P_{so} , from figure 3.20.

Step 3. Determine the clearing height of the front wall h' . This is equal to the full height of the front wall or half its width, whichever is the smaller.

Step 4. Determine c_{refl} , knowing P_{so} , from figure 3.21.

Step 5. Determine t_c from the relation $t_c = 3/h'c_{refl}$.

Step 6. Determine q_o , knowing P_{so} , from figure 3.23.

Step 7. Determine q for a sequence of times t_1, t_2, t_3 , etc., from table 3.2 or figure 3.24.

Step 8. Determine $(P_s + 0.85q)$ for the sequence of times used in Steps 1 and 7 above. The following headings systematize the calculations of Steps 1 to 8.

time, t	t/t_o	q/q_o	q	P_s/P_{so}	P_s	$P_s + 0.85q$
(1)	(2)	(3)	(4)	(5)	(6)	(7)

Column (1) is a set of times ranging from $t = 0$ to $t = t_o$ sufficient in number to allow drawing of the curve of $P_s + 0.85q$.

Column (3) is values obtained from table 3.2 or figure 3.24 for the values of t/t_o in column (2).

Column (5) is values obtained from table 3.1 or figure 3.22 for the values of t/t_o in column (2).

1 July 59

Step 9. Plot the curve of \bar{P}_{front} vs time as illustrated in figure 3.25.

b. Average Back Wall Overpressure vs Time. Step 1. Determine U_o , knowing P_{so} , from figure 3.9.

Step 2. Determine t_d , from the relation $t_d = L/U_o$.

Step 3. Determine t_b , from the relation $t_b = 4h'/c_o$, where $c_o = 1115$ fps and h' is either the full height of the back wall or half its length, whichever is the smaller.

Step 4. Determine P_{sb} at time $t - t_d = t_b$ from table 3.1 or figure 3.22.

Step 5. Determine $(\bar{P}_{\text{back}})_{\text{max}}$ at time $t = t_d + t_b$ from the relation $(\bar{P}_{\text{back}})_{\text{max}} = \frac{1}{2} P_{sb} \left[1 + (1 - \beta)e^{-\beta} \right]$; where $\beta = 0.5P_{so}/14.7$.

The average overpressure on the rear face varies linearly from zero at time $t = t_d$ to $(\bar{P}_{\text{back}})_{\text{max}}$ at time $t = t_d + t_b$.

Step 6. Determine the values of $\bar{P}_{\text{back}}/P_s$ for a sequence of times in excess of $t = t_d + t_b$ from the relation

$$\frac{\bar{P}_{\text{back}}}{P_s} = \frac{(\bar{P}_{\text{back}})_{\text{max}}}{P_{sb}} + \left[1 - \frac{(\bar{P}_{\text{back}})_{\text{max}}}{P_{sb}} \right] \left[\frac{t - (t_d + t_b)}{t_o - t_b} \right]^2$$

Step 7. Determine the values of P_s for the sequence of times in Step 6, and hence the values of \bar{P}_{back} . The following tabular headings systematize the work in Steps 6 and 7.

time, t	$t - t_d$	$(t - t_d)/t_o$	P_s/P_{so}	P_s	$\bar{P}_{\text{back}}/P_s$	\bar{P}_{back}
(1)	(2)	(3)	(4)	(5)	(6)	(7)

Column (1) is a sequence of times ranging from $t = t_b + t_d$ to $t = t_o + t_d$.

Column (4) is a set of values obtained from table 3.1 or figure 3.22 for the values listed in column (3).

Column (6) is the values calculated from the relation in Step 6 for the times given in column (1).

Step 8. Plot the curve of \bar{P}_{back} vs time as illustrated in figure 3.27b.

c. Average Net Horizontal Overpressure vs Time. Step 1. Knowing

\bar{P}_{front} and \bar{P}_{back} for a sequence of times t_1, t_2, t_3 , etc., determine $\bar{P}_{\text{net}} = \bar{P}_{\text{front}} - \bar{P}_{\text{back}}$ for each value of t .

Step 2. Plot the curve of \bar{P}_{net} vs time as illustrated in figure 3.28.

d. Local Roof Overpressure vs Time. The step-by-step procedure listed below is for a point located within Zone 3 (see figure 3.30) of the roof. The procedure for Zone 2 is similar except that figure 3.32 applies instead of figure 3.33, and the value of the ratio P_{roof}/P_s at time $t = t_m$ (Step 4) may not be less than 0.5. The procedure for Zone 1 involves a simple computation of P_s at various times using table 3.1 or figure 3.22 as illustrated in figure 3.31.

Step 1. Determine $t_d = L'/U_o$.

Step 2. Determine the vortex velocity v from the relation

$$v = \left(0.042 + 0.108 \frac{L'}{L} \right) U_o$$

Step 3. Determine $t_m = L'/v$.

Step 4. Determine the value of the ratio P_{roof}/P_s at time $t = t_m$ from the relation $P_{\text{roof}}/P_s = 4(P_{so}/14.7) \left(\frac{L'}{L} - 1 \right) + 1.0$, except that the minimum permissible value of this ratio is zero. The ratio P_{roof}/P_s decreases linearly from 1.0 at time $t = (t_d + t_m)/2$ to P_{roof}/P_s at time t_m and increases linearly to 1.0 at time $t = t_m + 15h'/U_o$; for all other times the value of the ratio is 1.0.

Step 5. Determine the value of the ratio P_{roof}/P_s for a sequence of times between time $t = t_d$ and time $t = t_d + t_o$.

Step 6. Determine P_s for the sequence of times in Step 5.

Step 7. Determine P_{roof} from Steps 5 and 6. The following tabular headings systematize the work in evaluating P_{roof} .

time, t	$t - t_d$	$(t - t_d)t_o$	P_s/P_{so}	P_s	P_{roof}/P_s	P_{roof}
(1)	(2)	(3)	(4)	(5)	(6)	(7)

Column (1) is a sequence of times ranging from $t = t_d$ to $t = t_d + t_o$.

Column (4) contains the values obtained from table 3.1 or figure 3.22 for the values in column (3).

Column (6) contains the values obtained in Step 4 above.

1 July 59

Step 8. Plot the curve of P_{roof} vs time from the values in column (7) as illustrated in figure 3.33.

e. Average Roof Overpressure vs Time. The step-by-step procedure listed below is for a structure for which figure 3.34 is applicable, as explained in paragraph 3-08e.

Step 1. Determine $t_d = L/2U_o$.

Step 2. Determine the value of $\bar{P}_{\text{roof}}/P_s$ at time $t = t_d + L/2U_o$

from the relation $\bar{P}_{\text{roof}}/P_s = 0.9 + 0.1 \left(1.0 - \frac{P_{so}}{14.7}\right)^2 \leq 1.0$

Step 3. Determine the value of $\bar{P}_{\text{roof}}/P_s$ at time $t = 5L/U_o$ from

the equations $\bar{P}_{\text{roof}}/P_s = 2.0 - \left(\frac{P_{so}}{14.7} + 1\right) \left(\frac{h'}{L}\right)^{1/3}$ or $\bar{P}_{\text{roof}}/P_s = 0.5 + 0.125 \left(2 - \frac{P_{so}}{14.7}\right)^2$ whichever gives the smallest value, but not less than zero.

Step 4. At time $t = 5L/U_o + 15h'/U_o$ the value of $\bar{P}_{\text{roof}}/P_s$ is one. $\bar{P}_{\text{roof}}/P_s$ varies linearly between the values computed in Steps 2, 3, and 4, and remains equal to one for times greater than $t = 5L/U_o + 15h'/U_o$.

Step 5. Determine the values of $\bar{P}_{\text{roof}}/P_s$ for a sequence of times greater than $t = L/U_o$ by interpolating between the values computed above.

Step 6. Determine P_s for the sequence of times used in Step 5.

Step 7. Determine \bar{P}_{roof} from Steps 5 and 6. The following tabular headings systematize the work in evaluating \bar{P}_{roof} .

time, t	$t - t_d$	$(t - t_d)/t_o$	P_s/P_{so}	P_s	$\bar{P}_{\text{roof}}/P_s$	\bar{P}_{roof}
(1)	(2)	(3)	(4)	(5)	(6)	(7)

Column (1) is a sequence of times ranging from time $t = L/U_o$ to time $t = t_o + t_d$.

Column (4) contains the values obtained from table 3.1 or figure 3.22 for the values in column (3).

Column (6) contains the values obtained from Step 5 for the times in column (1).

Step 8. Plot the curve of \bar{P}_{roof} vs time as illustrated in figure 3.34. Note that \bar{P}_{roof} varies linearly from zero at time $t = 0$ to the computed value at time $t = L/U_0$.

f. Local Side Wall Overpressure vs Time. The local side wall overpressure for a point in Zone 3 of the side is computed by use of Steps 1 to 8 of paragraph 3-09d. The procedure for Zone 2 is similar except that figure 3.32 applies instead of figure 3.33, and the value of the ratio P_{roof}/P_s at time $t = t_m$ (Step 4) must not be less than 0.5. The procedure for Zone 1 involves a simple computation of P_s at various times using table 3.1 or figure 3.22 as illustrated in figure 3.31.

g. Average Side Wall Overpressure vs Time. The average side wall overpressure for a structure for which figure 3.34 is applicable is computed by use of Steps 1 to 8 of paragraph 3-09e.

3-10 NUMERICAL EXAMPLE OF COMPUTATIONS OF LOADS ON CLOSED RECTANGULAR STRUCTURE.

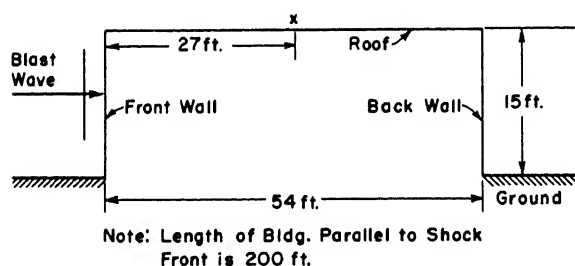


Figure 3.35. Exterior proportions--closed rectangular structure

Data: 18 KT typical airburst.

3000 ft distance from ground zero.

Exterior dimensions of problem structure (figure 3.35).

From figure 3.12 $P_{so} = 10$ psi.

From figure 3.10a $t_{o1} = 0.262$ (1 KT for 10 psi).

For an 18-KT weapon, $t_o = 18^{1/3} (0.262) = 0.685$ sec.

a. Average Front Wall Overpressure vs Time. Step 1. For $P_{so} = 10$ psi from figure 3.20, $P_{\text{refl}} = 25.3$ psi.

Step 2. From figure 3.35, $h' = 15$ ft.

Step 3. For $P_{so} = 10$ psi from figure 3.21, $c_{\text{refl}} = 1290$ fps.

Step 4. $t_c = 3h'/c_{\text{refl}} = 3(15)/1290 = 0.0349$ sec.

Step 5. For $P_{so} = 10$ psi, from figure 3.23, $q_o = 2.23$.

Steps 6 through 8. In table following.

t	t/t_o	q/q_o	q	P_s/P_{so}	P_s	$P_s + 0.85q$
0	0	1.000	2.23	1.000	10.00	12.12
0.0685	0.10	0.634	1.40	0.814	8.15	9.48
0.137	0.20	0.397	0.89	0.655	6.55	7.40
0.2055	0.30	0.245	0.55	0.519	5.19	5.71
0.274	0.40	0.148	0.33	0.402	4.02	4.33
0.3425	0.50	0.087	0.19	0.303	3.03	3.21
0.411	0.60	0.049	0.11	0.220	2.20	2.30
0.4795	0.70	0.026	0.06	0.149	1.49	1.55
0.548	0.80	0.012	0.03	0.090	0.90	0.93
0.6165	0.90	0.004	0.01	0.041	0.41	0.42
0.685	1.00	0.000	0.00	0.000	0.00	0.00

Sample calculation of typical entry in table: For $t/t_o = 0.40(0.685)$
 $= 0.274$.

From table 3.2 for t/t_o
 $= 0.40$, $q/q_o = 0.148$
 $q = 0.148(2.23) = 0.33$ psi

From table 3.1 for t/t_o
 $= 0.40$, $P_s/P_{so} = 0.402$
 $P_s = 0.402(10) = 4.02$ psi
 $P_s = 0.85q = 4.02 + 0.85(0.33)$
 $= 4.33$ psi

Step 9. Plot the curve as shown in figure 3.36(a).

b. Average Back Wall Overpressure vs Time. Step 1. For $P_{so} = 10$ psi, from figure 3.9, $U_o = 1403$ fps.

Step 2. $t_d = L/U_o = 54/1403$
 $= 0.0385$ sec.

Step 3. $t_b = 4h'/c_o$
 $= 4(15)/1115 = 0.538$ sec.

Step 4. For $(t - t_d)/t_o$
 $= 0.0538/0.685 = 0.0785$, from table 3.1, $P_s/P_{so} = 0.852$,
 $P_s = P_{sb} = 10(0.852) = 8.52$ psi.

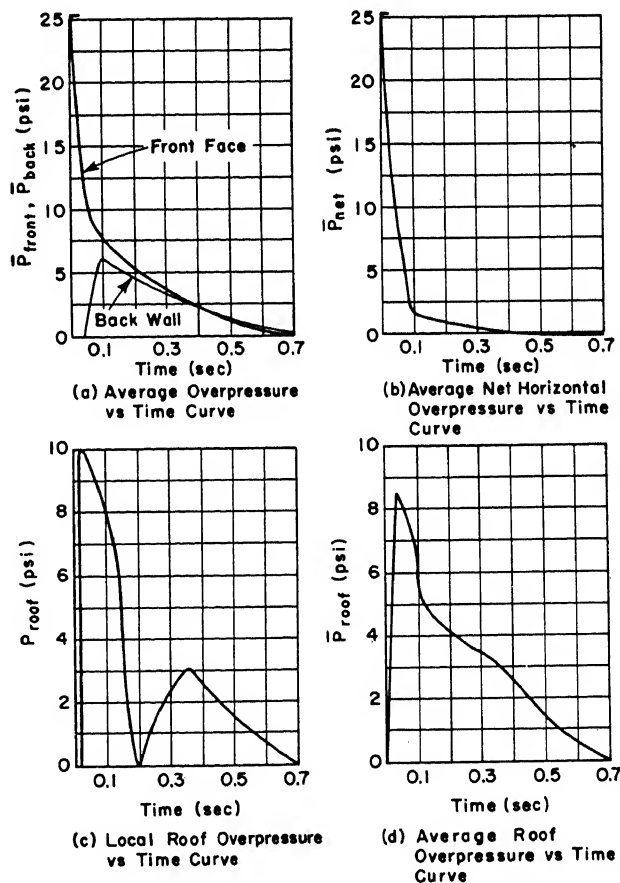


Figure 3.36. Overpressure vs time curves--closed rectangular structure

EM 1110-345-413
1 July 59

Step 5. $(P_{\text{back}})_{\text{max}} = P_{\text{sb}} \left[1 + (1 - \beta)e^{-\beta} \right] / 2$ where $\beta = 0.5P_{\text{so}}/14.7$.
 $\beta = 0.5(10)/14.7 = 0.34$

$$(P_{\text{back}})_{\text{max}} = 8.52 [1 + 0.47] / 2 = 6.26 \text{ psi}$$

Steps 6 and 7. In table following.

t	$t - t_d$	$(t - t_d)/t_o$	P_s/P_{so}	P_s	$\bar{P}_{\text{back}}/P_s$	\bar{P}_{back}
0.0923	0.0538	0.079	0.850	8.50	0.735	6.26
0.1070	0.0685	0.1	0.814	8.14	0.735	5.98
0.1755	0.137	0.2	0.655	6.55	0.740	4.85
0.2440	0.2055	0.3	0.519	5.19	0.750	3.89
0.3125	0.274	0.4	0.402	4.02	0.767	3.08
0.3810	0.3425	0.5	0.303	3.03	0.790	2.39
0.4495	0.411	0.6	0.220	2.20	0.820	1.80
0.5180	0.4795	0.7	0.149	1.49	0.855	1.27
0.5865	0.548	0.8	0.090	0.90	0.897	0.81
0.6550	0.6165	0.9	0.041	0.41	0.947	0.39
0.7235	0.685	1.0	0	0	1.000	0

Sample calculation of typical entry in table above:

For $(t - t_d)/t_o = 0.5$, $t = 0.5(0.685) + 0.0385 = 0.3810$

From table 3.1, for $(t - t_d)/t_o = 0.5$, $P_s/P_{\text{so}} = 0.303$

$$P_s = 0.303(10) = 3.03 \text{ psi}$$

For $(t - t_d)/t_o = 0.5$

$$\begin{aligned} \bar{P}_{\text{back}}/P_s &= (\bar{P}_{\text{back}})_{\text{max}}/P_{\text{sb}} + \left[1 - (\bar{P}_{\text{back}})_{\text{max}}/P_{\text{sb}} \right] \left[\frac{t - (t_d + t_b)}{t_o - t_b} \right]^2 \\ &= 6.26/8.52 + \left[1 - 6.26/8.52 \right] \left[\frac{0.3810 - (0.0385 + 0.0538)}{0.685 - 0.0538} \right]^2 \\ &= 6.26/8.52 + \left[1 - 6.26/8.52 \right] [0.2887/0.6312]^2 \\ &= 0.790 \end{aligned}$$

$$\bar{P}_{\text{back}} = 3.03(0.79) = 2.39 \text{ psi}$$

Step 8. Plot the curve as shown in figure 3.36(a).

c. Average Net Horizontal Overpressure vs Time. Step 1. Determine values of \bar{P}_{front} and \bar{P}_{back} at times $t = 0.00, 0.05, 0.15, 0.20, \dots, 0.65, 0.70$, from figure 3.36(a) and determine $\bar{P}_{\text{net}} = \bar{P}_{\text{front}} - \bar{P}_{\text{back}}$ for each time.

Step 2. Plot curve of \bar{P}_{net} vs time as shown in figure 3.36(b).

d. Local Roof Overpressure vs Time at Point x of Figure 3.35.

Step 1. $t_d = L'/U_o = 27/1403 = 0.0192 \text{ sec.}$

Step 2. $v = \left(0.042 + 0.108 \frac{L'}{L}\right)U_o = [0.042 + 0.108 (0.5)] 1403$
 $= 134.7 \text{ fps.}$

Step 3. $t_m = L'/v = 27/134.7 = 0.200 \text{ sec.}$

Step 4. At time $t = t_m$, $P_{\text{roof}}/P_s = 4(P_{so}/14.7) \left(\frac{L'}{L} - 1\right) + 1$
 $P_{\text{roof}}/P_s = 4(10/14.7)(27/54 - 1) + 1 = -0.36 < 0.$

Therefore, $P_{\text{roof}}/P_s = 0$ at time $t = 0.200$

$P_{\text{roof}}/P_s = 1.00$ at time $t = t_m + 15h'/U_o$

Steps 5 through 8. In table following. (Note that in the computations in table all times in columns (1) and (2) are calculated from assumed values in column (3) except at times $t = t_m = 0.200$, $t = \frac{1}{2}(t_d + t_m) = \frac{1}{2}(0.0192 + 0.200) = 0.1096$, and $t = 0.3602$.)

t	$t - t_d$	$(t - t_d)/t_o$	P_s/P_o	P_s	P_{roof}/P_s	P_{roof}
0.0192	0	0	1.000	10.00	1.0	10.00
0.0877	0.0685	0.1	0.814	8.14	1.0	8.14
0.1096	0.0904	0.132	0.761	7.61	1.0	7.61
0.1562	0.137	0.2	0.655	6.55	0.483	3.16
0.200	-	-	-	-	0	0
0.2247	0.2055	0.3	0.519	5.19	0.154	0.80
0.2932	0.274	0.4	0.402	4.02	0.583	2.34
0.3602	0.3410	0.498	0.305	3.05	1.0	3.05
0.3617	0.3425	0.5	0.303	3.03	1.0	3.03
0.4302	0.411	0.6	0.220	2.20	1.0	2.20
0.4987	0.4795	0.7	0.149	1.49	1.0	1.49
0.5672	0.548	0.8	0.090	0.90	1.0	0.90
0.6357	0.6165	0.9	0.041	0.41	1.0	0.41
0.7042	0.685	1.0	0	0	1.0	0

Sample calculation of typical entry in table above:

For $(t - t_d)/t_o = 0.4$, $t = 0.4(0.685) + 0.0192 = 0.2932 \text{ sec}$

From table 3.1, for $(t - t_d)/t_o = 0.4$, $P_s/P_{so} = 0.402$

$P_s = 0.402(10.0) = 4.02 \text{ psi}$

Since P_{roof}/P_s varies linearly from 0 at $t = 0.200$ to 1.0 at $t = 0.3602$

$P_{\text{roof}}/P_s = (0.2932 - 0.200)/(0.360 - 0.200) = 0.583$

$P_{\text{roof}} = 0.583(4.02) = 2.34 \text{ psi}$

Step 7. Plot the curve as shown in figure 3.36(c).

e. Average Roof Overpressure vs Time. Step 1. $t_d = L/2U_o$
 $= 54/2(1403) = 0.0194 = 0.0194 \text{ sec.}$

Step 2. At time $t = L/2U_o + t_d = 0.0388 \text{ sec}$

$$\bar{P}_{\text{roof}}/P_s = 0.9 + 0.1(1.0 - P_{s0}/14.7)^2 = 0.9 + 0.1(1.0 - 10/14.7)^2 = 0.910$$

(i.e., this value may not exceed one).

Step 3. At time $t = 5L/U_0 = 0.1928$ sec. Compute $2.0 -$

$$\left(1 + \frac{P_{s0}}{14.7}\right) \left(\frac{h'}{L}\right)^{1/3} = 2.0 - \left(1 + \frac{10}{14.7}\right) \left(15/54\right)^{1/3} = 0.902 \text{ and } 0.5 +$$

$$0.125 \left(2 - \frac{P_{s0}}{14.7}\right)^2 = 0.5 + 0.125 \left(2 - \frac{10}{14.7}\right)^2 = 0.717$$

Since $0.717 < 0.902$, $\bar{P}_{\text{roof}}/P_s = 0.717$.

Step 4. At time $t = 5L/U_0 + 15h'/U_0 = 0.1928 + 0.1604 = 0.3532$ sec

$$\bar{P}_{\text{roof}}/P_s = 1.$$

Steps 5 through 7. In table following.

t	$t - t_d$	$(t - t_d)/t_o$	P_s/P_{s0}	P_s	$\bar{P}_{\text{roof}}/P_s$	\bar{P}_{roof}
0.0388	0.0194	0.0283	0.944	9.44	0.910	8.58
0.0879	0.0685	0.1	0.814	8.14	0.848	6.90
0.1176	0.137	0.2	0.655	6.55	0.762	4.99
0.1928	0.1734	0.252	0.581	5.81	0.717	4.17
0.2249	0.2055	0.3	0.519	5.19	0.774	4.01
0.2934	0.274	0.4	0.402	4.02	0.894	3.60
0.3619	0.3425	0.5	0.303	3.03	1.0	3.03
0.4304	0.411	0.6	0.220	2.20	1.0	2.20
0.4989	0.4795	0.7	0.149	1.49	1.0	1.49
0.5674	0.548	0.8	0.090	0.90	1.0	0.90
0.6359	0.6165	0.9	0.041	0.41	1.0	0.41
0.7044	0.685	1.0	0	0	1.0	0

Sample calculation of typical entry in table above: For $(t - t_d)/t_o = 0.1$, $t = 0.1(0.685) + 0.0194 = 0.0879$ sec

From table 3.1 for $(t - t_d)/t_o = 0.1$, $P_s/P_{s0} = 0.814$
 $P_s = 0.814(10) = 8.14$ psi

Since $\bar{P}_{\text{roof}}/P_s$ varies linearly from 0.910 at $t = 0.0388$ sec to 0.717 at $t = 0.1928$ sec

$$\begin{aligned} \bar{P}_{\text{roof}}/P_s &= 0.910 - \left(\frac{0.0879 - 0.0388}{0.1928 - 0.0388}\right) (0.910 - 0.717) \\ &= 0.910 - 0.0491(0.193)/0.1540 \\ &= 0.848 \end{aligned}$$

$$\bar{P}_{\text{roof}} = 0.848(8.14) = 6.90 \text{ psi}$$

Step 8. Plot the curve as shown in figure 3.36(d).

LOADING ON RECTANGULAR STRUCTURES WITH OPENINGS

3-11 EFFECTS OF OPENINGS ON LOADING. For the determination of the loads on rectangular structures with openings it is necessary to consider all structures as falling into one of two categories.

Category (1). Structures having open interiors free of walls and other obstructions so as to allow relatively unhindered propagation of the blast wave through the interior of the structure, once it has entered through windows or otherwise. It is assumed that the percentage of back face openings is approximately equal to the percentage of front face openings.

Category (2). Structures having interior walls and other construction which would prevent free propagation of the blast wave through the interior of the structure.

Those structures falling into Category (2), above, are analyzed in a manner similar to that for the case of closed rectangular structures when determining the net translational forces acting on the structure. Net loads on exterior and interior portions of these structures may be computed as are the loads for structures falling into Category (1), with suitable interpretation of the various structural dimensions involved. The determination of the loads on structures with relatively open interiors, Category (1), is described below for approximately equal percentages of openings in the front and back walls.

The sequence of phenomena following the impingement of a shock wave on a rectangular structure with openings can be briefly summarized in the following paragraphs.

When the shock front strikes and reflects from the front wall, the overpressure on that wall rises to the reflected overpressure. Rarefaction waves immediately move in from the outside edges of the wall, clearing the reflected overpressures.

Windows and doors in the front wall will probably break under the reflected overpressure, though not instantaneously. However, they generally will break before the clearing is complete; hence, part of the clearing will occur through the window openings, allowing high pressure air to flow

into the interior. This sudden release of high pressure will cause shocks to form in the interior. These inside shocks, formed at each opening, will spread downstream from each opening and will tend to combine into a single shock front. This interior shock is, initially, weaker than the incident shock.

Meantime the incident shock front has moved past the front wall and is sweeping across the exterior roof and sides. The shock then moves across the exterior of the back wall of the structure from the sides and from above, building up the overpressure on that surface.

For those structures which have no interior partitions to obstruct the passage of the shock through the interior, the shocks entering at the front openings will move through the structure raising the overpressures on the inside surfaces as they are covered.

a. Average Exterior Front Wall Overpressure \bar{P}_{front} . The time required for reflected overpressures to clear on the front of a solid wall struck by a shock wave is expressed in multiples of the time necessary for a rarefaction wave to sweep the wall once, h'/c_{refl} . When walls with numerous openings are considered, however, clearing can take place around the edges of the openings. This necessitates a modification of the method of determining clearing times because the rarefaction wave travels a much shorter distance to cover the wall.

The distance h'_f is introduced as the weighted average distance the rarefaction wave must travel to cover the wall once, assuming immediate

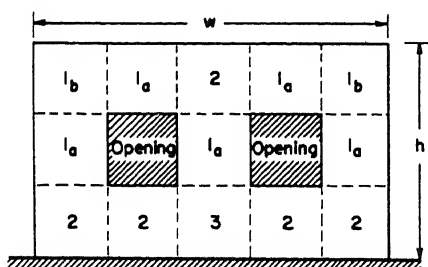


Figure 3.37. Subdivision of a typical wall with openings to determine weighted average clearing height

access of the incident shock to the interior of the structure. As shown in figure 3.37 the front face is divided into rectangular areas, determined by the location and dimensions of openings considering the directions along which the area can be cleared in the shortest possible time. These areas are labeled in the following manner:

Step 1. Label l_a , all areas cleared from two opposite sides.

Step 2. Label l_b , all areas cleared from two adjacent sides.

Step 3. Label 2, all areas cleared from one side.

Step 4. Label 3, all remaining areas.

The weighted average clearing height is then:

$$h'_f = \sum \frac{\delta_n h_n A_n}{A_f} \leq h' \quad (3.16)$$

where A_f = net area of front face (wh less openings)

A_n = area of each portion of the subdivided front face, except openings

h_n = for areas 1_a , the average distance between the sides from which clearing occurs

= for areas 1_b and 3, the average height or width, whichever is smaller

= for areas 2, the average distance between the side from which clearing occurs and the side opposite

δ_n = the area clearing factor.

= 1/2 for areas 1_a

= 1 for areas 1_b

= 1 for areas 2

= 1 for areas 3

Σ = the notation to represent the summation of the $\frac{\delta_n h_n A_n}{A_f}$ term for all areas

$h' = h$ or $w/2$, whichever is the smaller

The time required to clear the front face of a structure with openings of reflection effects t'_c can now be evaluated from the relation

$$t'_c = 3h'_f/c_{refl} \quad (3.17)$$

Windows in a structure will not be immediately blown out; GREENHOUSE data (see page 72, reference 15) indicates that the window-breaking time is of the order of a millisecond or less. This time, however, is too short to be of any practical importance in computing the loading on the structure. Therefore, it is assumed that the windows fail as soon as they are struck by the shock front and do not affect the loading computation.

The time curve of the average outside front wall overpressure on the net wall area can be constructed by the methods outlined in paragraph 3-08a and illustrated in figure 3.25 using the clearing time as defined by equation (3.17).

b. Average Interior Front Wall Overpressure $\bar{P}_{i\text{-front}}$. The average interior overpressure on the inside of the front wall $\bar{P}_{i\text{-front}}$ initially builds up in a similar manner as the average overpressures on the exterior back wall of a closed structure, except the vortices are located all around the inside edges of all openings. The build-up is linear from zero at time $t = 0$ to the peak overpressure P_{soi} (see paragraph 3-11e and figures 3.41 and 3.42) of the interior shock at time $t = 4h'_{if}/c_o$, where h'_{if} is the weighted average build-up height of the interior front wall computed from equation (3.16) but with all quantities interpreted as applying to the interior surface of the front wall. The overpressure is maintained and builds up again when the interior shock is re-lected back from the rear wall to a peak value which is dependent on the size of the structure. Equilibrium is

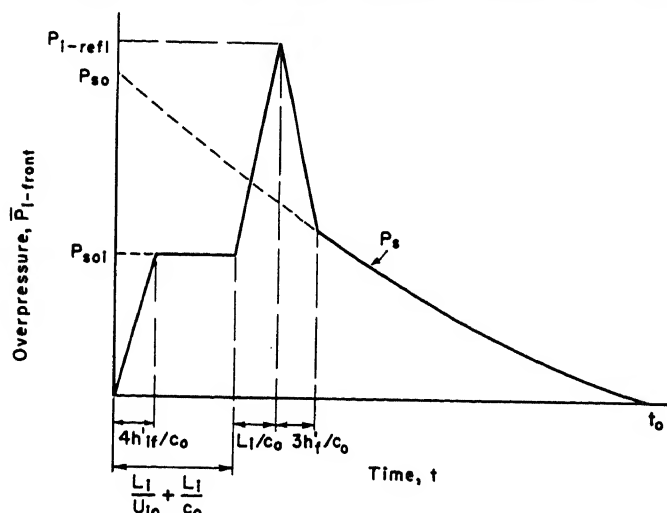


Figure 3.38. Average interior front wall overpressure vs time--small rectangular structure $(L_i/U_{io}) < 0.1t_o$

then attained when the overpressure within the interior reaches P_s ; P_s being the blast wave overpressure existing on the outside of the structure. Figure 3.38 illustrates the overpressure vs time curve for the inside front face of those structures in which $L_i/U_{io} < 0.1t_o$, and figure 3.39 for those in which $L_i/U_{io} > 0.1t_o$.

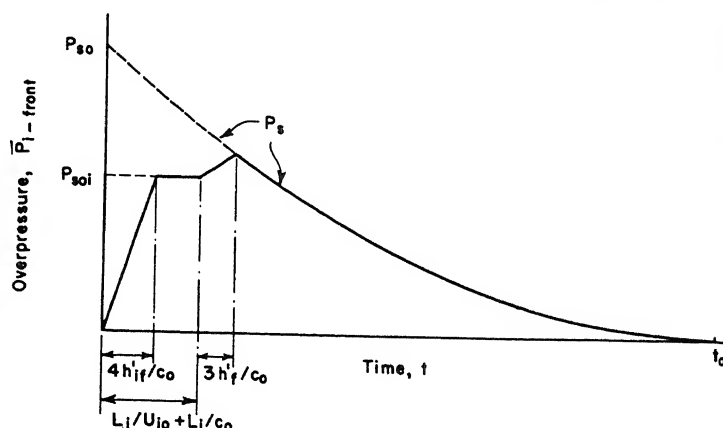


Figure 3.39. Average interior front wall overpressure vs time--large rectangular structure $(L_i/U_{io}) > 0.1t_o$

c. Average Net Front Wall Overpressure $\bar{P}_{f\text{-net}}$. The average net overpressure acting on the

front wall \bar{P}_{f-net} is determined by subtracting the interior front wall overpressure from the exterior front wall overpressure on a common time basis according to the equation

$$\bar{P}_{f-net} = \bar{P}_{front} - \bar{P}_{i-front} \quad (3.18)$$

where \bar{P}_{f-net} , \bar{P}_{front} , and $\bar{P}_{i-front}$ are given in terms of t . Figure 3.40 illustrates

graphically the variation of the average net front wall overpressure with time.

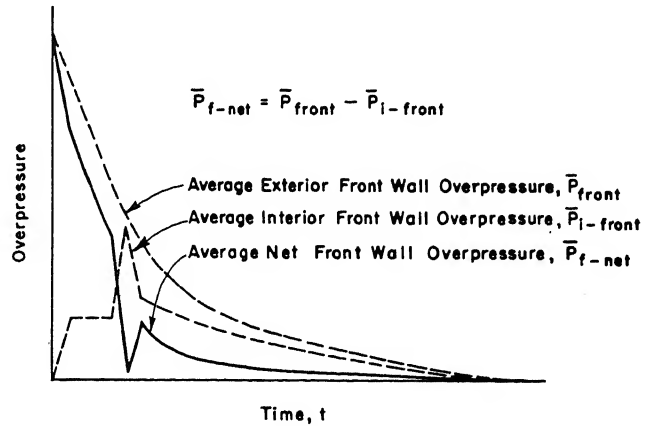


Figure 3.40. Average net front wall overpressure vs time--rectangular structures with openings

d. Average Exterior Back Wall Overpressure \bar{P}_{back} . A time lag is present between build-up of pressure on the back wall due to the time required for the blast wave to travel the length of the structure. Until the windows or window frames in the back wall fail, the back wall loads behave in the same manner as those on the back wall of a closed structure. After the windows break the back wall loading is affected by the vortices formed at all of the edges of the rear openings due to the interior blast passing through the openings at the same time that the exterior wave sweeps the rear face. If it is assumed that the windows blow out instantaneously over the entire structure, i.e., the window-breaking times are zero, the build-up time for pressures over the rear face is

$$t'_b = 4h'_b/c_o \quad (3.19)$$

where h'_b is the weighted average build-up time of the rear face, defined by

$$h'_b = \sum \frac{\delta_n h_n A_n}{A_R} \leq h' \quad (3.20)$$

A_R is the net area of the back wall (gross area less openings)

δ_n , h_n , A_n are as defined in paragraph 3-11a

h'_b is computed in the same manner as h'_f (the weighted average clearing height of the front face)

The average overpressure vs time curve for the outside rear face can

be computed by the methods outlined in paragraph 3-08b and illustrated in figure 3.27 using the build-up times as given in equation (3.19).

e. Average Interior Back Wall Overpressure \bar{P}_{i-back} . The presence of openings in the front wall of a structure permits a portion of the incident shock to enter through these openings, producing an interior shock wave weaker than the incident, which becomes approximately plane as it travels the length of the interior. That portion of the interior shock not passing through the back wall openings is reflected by the back wall, according to the laws of normal reflection and returns toward the front. Quick clearing occurs on the inside and vortices form at edges of openings on the outside as the blast wave passes out through openings.

In the prediction of inside pressures the structure is assumed to be smooth. Structural features which do not follow this idealization are neglected as regards their influence on the determination of interior loads. These features include interior columns along side walls, pipe sections which cross the interior, etc. The peak overpressure of the interior shock wave P_{soi} is dependent upon the overpressure of the incident shock wave and the percentage of window openings. Figure 3.41 is a plot of P_{soi} vs P_{so} for different values of the ratio of the area of openings in the front face to the gross area of the front face A_{of}/A_{gf} . Figure 3.42 is a plot of P_{soi} vs A_{of}/A_{gf} for various peak incident overpressures. These curves are based upon data reduced by the Armour Research Foundation [17] from shock tube tests performed at the University of Michigan [16] and at Princeton University [18].

The inside back wall remains unloaded until time $t_d = L_1/U_{i0}$, where L_1 is the distance from the outside of the front wall to the inside rear face and U_{i0} is the velocity of the inside shock front which is plotted in figure 3.9. The overpressure on this wall is then instantaneously raised to the reflected overpressure value \bar{P}_{i-refl} given in figure 3.20.

The presence of openings in the back wall prevents the maintenance of this reflected overpressure and, hence, there is a linear decay to a value approaching the drag pressure in the inside blast wave. The time required for this decay is a function of the number and size of openings in the back wall and of the size of the structure. For relatively small structures

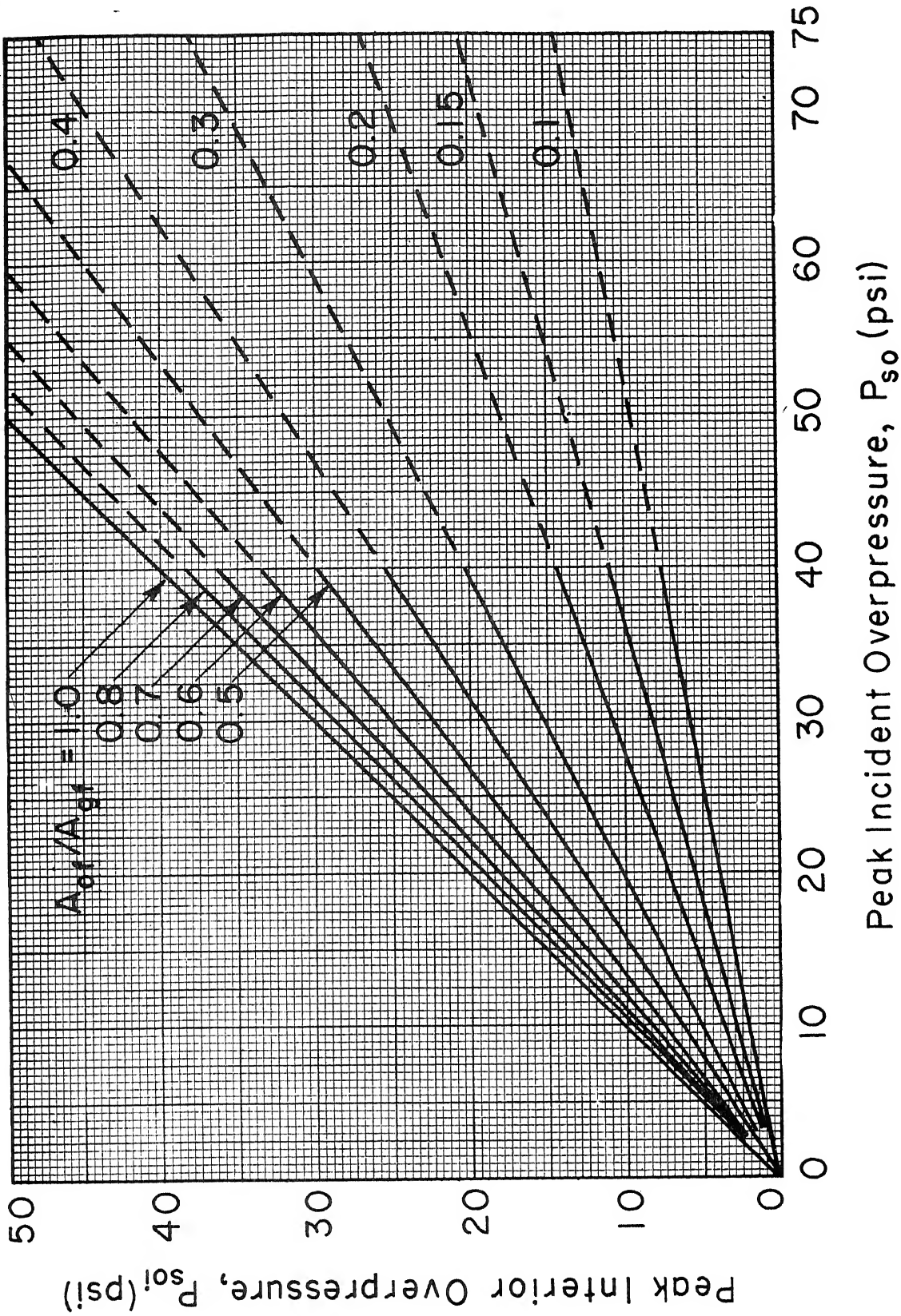


Figure 3.41. Peak interior overpressure vs peak incident overpressure for various percentages of front wall openings.
(Validity of dashed portions of curves uncertain)

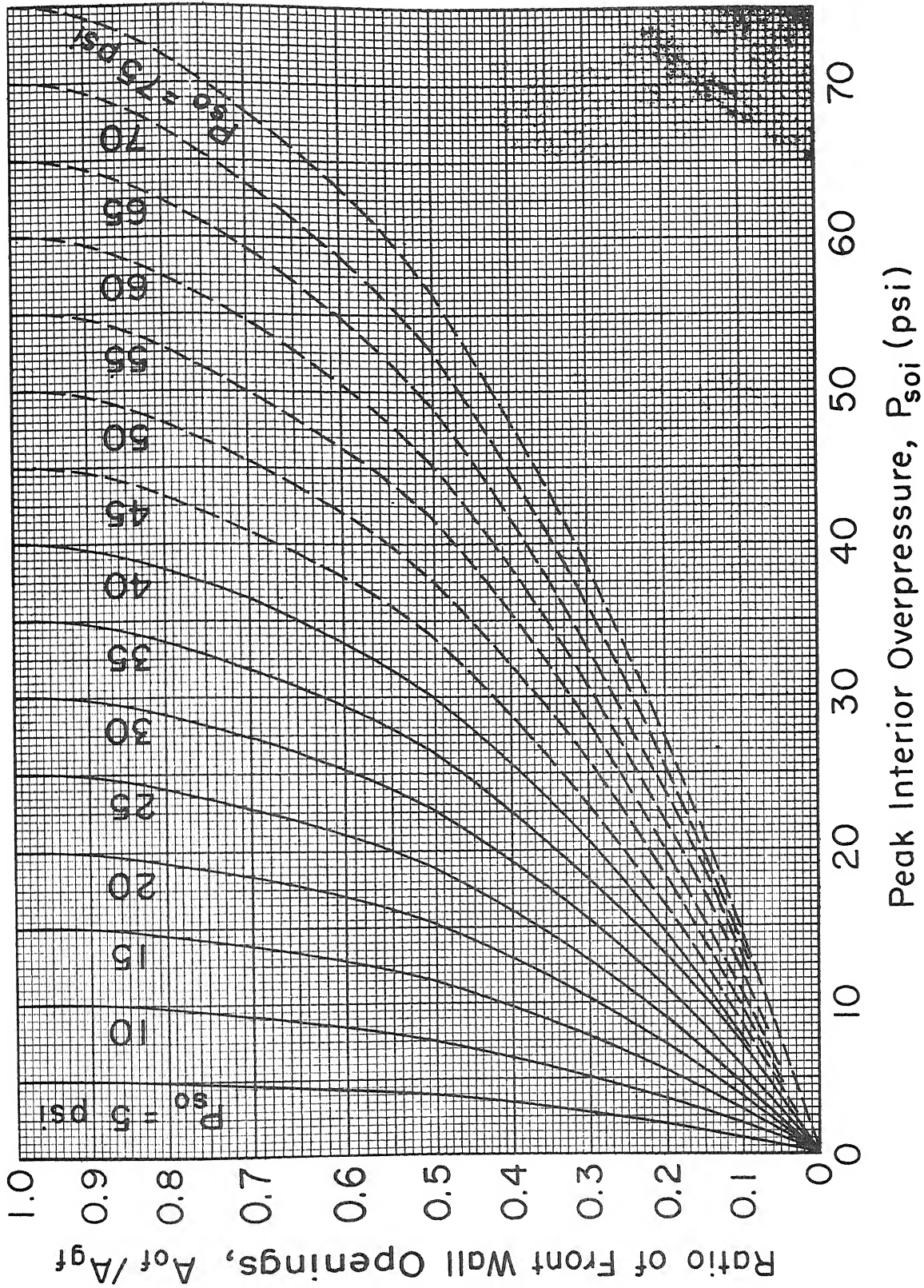


Figure 3.42. Peak interior overpressure vs percentage of front face openings for various peak incident overpressures.
(Validity of dashed portions of curves uncertain)

there is an additional build-up following an initial decay due to the return of the shock wave reflected from the rear wall toward the front wall, while for longer structures this second build-up is absent. It is assumed that the interior blast wave eventually reaches a condition of equilibrium wherein the interior and the incident blast waves have equal overpressures and the back wall interior overpressure equals the drag pressure in the incident blast wave, with the time displacement factor $t_d = L_i/U_{i0}$.

To account for the effect of size of the structure on interior overpressures, two curves of the interior back wall overpressures are given. Figure 3.43 is applicable to structures in which the

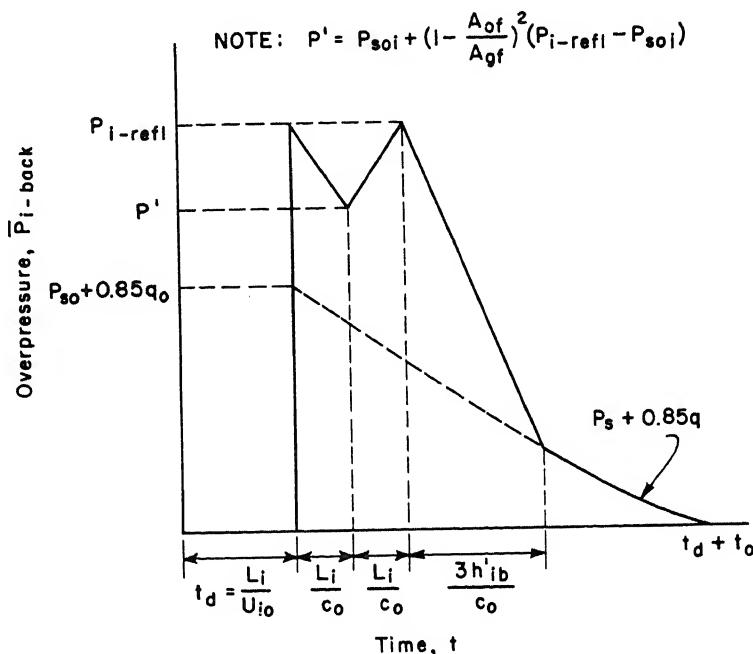


Figure 3.43. Average interior back wall overpressure vs time--small rectangular structure ($L_i/U_{i0} < 0.1t_0$)

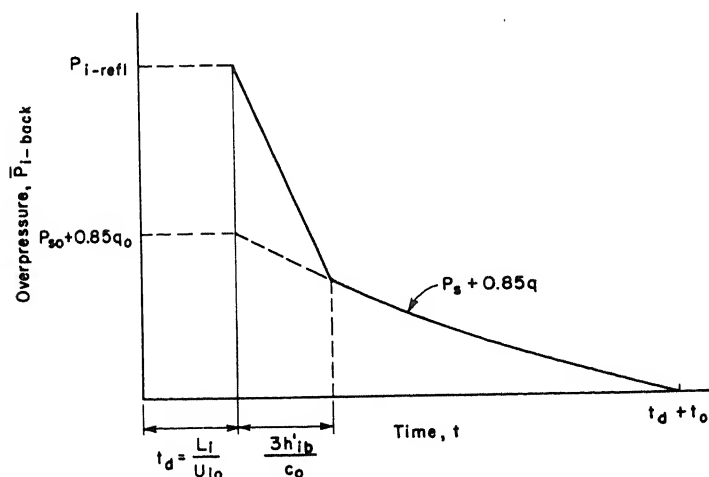


Figure 3.44. Average interior back wall overpressure vs time--large rectangular structure ($L_i/U_{i0} > 0.1t_0$)

time required for the inside reflected shock wave to travel the length of the interior is less than one-tenth the duration of the positive phase of the outside shock wave; i.e., $L_i/U_{i0} < 0.1t_0$. Figure 3.44 is applicable to those structures for which $L_i/U_{i0} > 0.1t_0$. \bar{P}_{i-back} as a function of time is as illustrated in these figures.

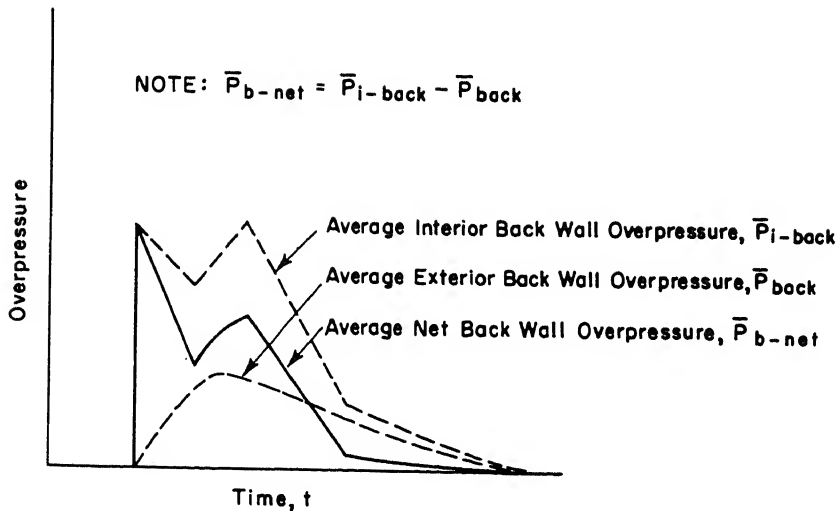


Figure 3.45. Average net back wall overpressure vs time--rectangular structure with openings

f. Average Net Back Wall Overpressure \bar{P}_{b-net} . The average net overpressure acting on the back wall \bar{P}_{b-net} is determined by subtracting the exterior back wall overpressure from the interior back wall overpressure on a common time basis according to the equation

$$\bar{P}_{b-net} = \bar{P}_{i-back} - \bar{P}_{back} \quad (3.21)$$

where \bar{P}_{b-net} , \bar{P}_{i-back} , and \bar{P}_{back} are given in terms of t . Figure 3.45 illustrates graphically the variation of the average net back wall overpressure with time.

g. Average Exterior Roof Overpressure \bar{P}_{roof} . In this paragraph it is assumed that the roof is plane, horizontal, and without roof surface openings. Therefore, the average overpressure vs time curves on the exterior are computed by the methods outlined in paragraph 3-08e and illustrated in figure 3.34. The quantity h' used in these figures should be replaced by h'_f .

h. Average Interior Roof Overpressure \bar{P}_{i-roof} . Here again it is necessary to place the structure being considered into one of the two categories established in the previous paragraphs due to the difference in behavior of the inside shock. For the smaller interiors the average overpressure on the inside of the roof will build up in time L_1/U_{i0} to the initial peak overpressure of the inside shock wave, at which time reflection of the interior shock from the rear face will take place. This reflected shock then travels toward the front wall spreading higher pressures along the underside of the roof. The reflected shock front is destroyed by the vortices at the front face as well as by flow out through

openings and no further reflections occur. The average roof overpressure then decreases from the rear face reflected value to the equilibrium value of P_s , the incident air blast overpressure. Figure 3.46 displays the average interior roof overpressure for those structures in which $(L_i/U_{i0}) < 0.1t_o$.

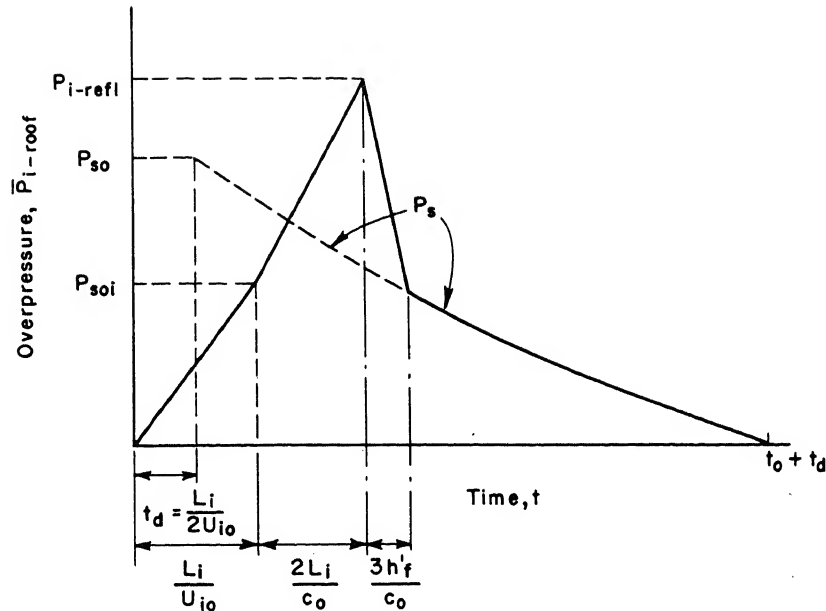


Figure 3.46. Average interior roof overpressure vs time--small rectangular structure $(L_i/U_{i0}) < 0.1t_o$.

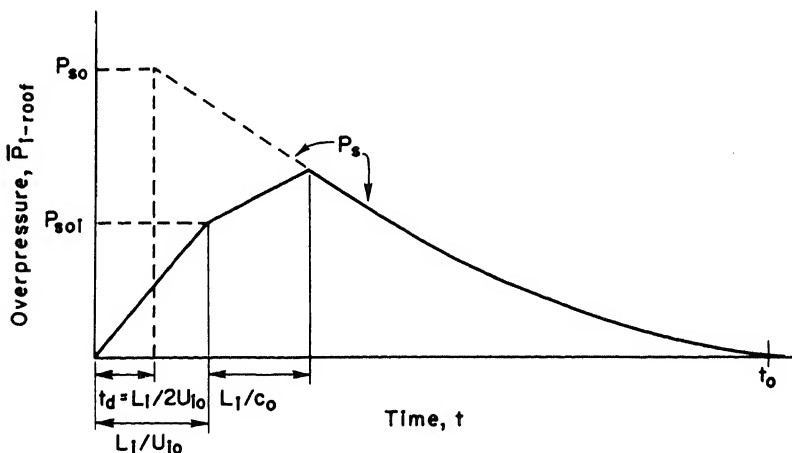


Figure 3.47. Average interior roof overpressure vs time--large rectangular structure $(L_i/U_{i0}) > 0.1t_o$.

Figure 3.47 displays the average interior roof overpressure curve for those structures in which $L_i/U_{i0} > 0.1t_o$. In these structures the average overpressure does not build up to P_{i-refl} since the shock wave reflected from the rear face decays before it can

spread its higher pressures over the whole of the underside of the roof.

i. Average Net Roof Overpressure \bar{P}_{r-net} . The average net overpressure acting down on the roof \bar{P}_{r-net} is determined by subtracting the average interior roof overpressure from the average exterior roof

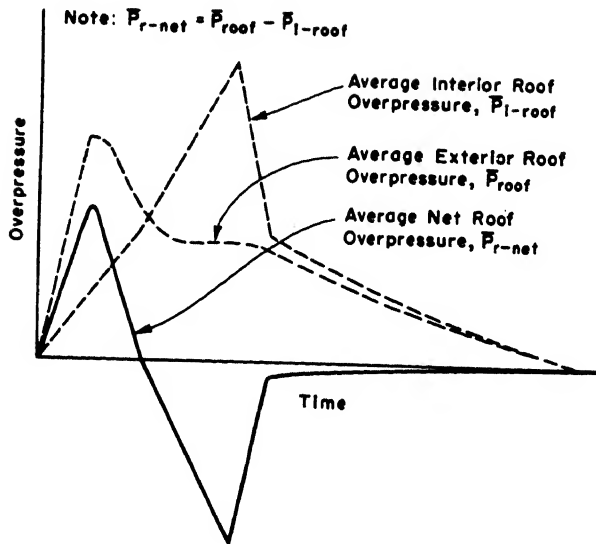


Figure 3.48. Average net roof overpressure vs time--rectangular structure with openings

overpressure on a common time basis according to the equation

$$\bar{P}_{r-net} = \bar{P}_{roof} - \bar{P}_{i-roof} \quad (3.22)$$

Figure 3.48 illustrates graphically the variation of the average net roof overpressure with time.

j. Average Exterior Side Wall Overpressure \bar{P}_{side} The exterior loading on the side can be handled as for closed rectangular structures in paragraph 3-08f, except that the quantity h' should be replaced by h'_f . It is assumed that the side is without openings;

however, even if windows are present, the combined action of exterior and interior pressures may prevent their breakage. In any case, the effect of openings is considered to be negligible.

k. Average Interior Side Wall Overpressure \bar{P}_{i-side} The average interior side wall overpressure is handled in exactly the same manner as the average interior roof overpressure. It is assumed that the side is without openings, as for the exterior side wall overpressures.

l. Average Net Side Wall Overpressure \bar{P}_{s-net} The average net overpressure acting inward on the side wall \bar{P}_{s-net} is determined by subtracting the average interior side wall overpressure from the average exterior side wall overpressure on a common time basis according to the equation

$$\bar{P}_{s-net} = \bar{P}_{side} - \bar{P}_{i-side} \quad (3.23)$$

Figure 3.49 illustrates graphically the variation of the average net side wall overpressure with time.

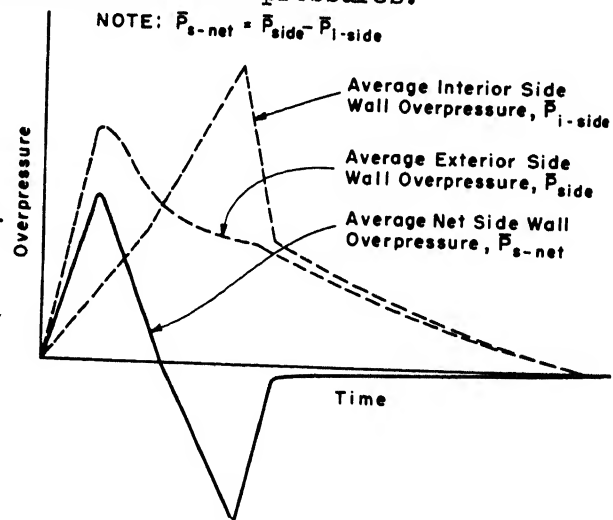


Figure 3.49. Average net side wall overpressure vs time--rectangular structure with openings

3-12 PROCEDURE FOR COMPUTATION OF LOADS ON RECTANGULAR STRUCTURES WITH OPENINGS. Repeat Steps 1, 2, and 3 under paragraph 3-09.

a. Average Exterior Front Wall Overpressure vs Time. Step 1. Determine h'_f from the relation

$$h'_f = \sum \frac{\delta_n h_n A_n}{A_f}$$

Step 2. Determine h' , the clearing height for the front face, treating it as if it were closed. Use $h'_f = h'$, if Step 1 gives $h'_f > h'$.

Step 3. Determine t'_c from the relation $t'_c = 3h'_f/c_{refl}$.

Step 4. Use Steps 1, 2, and 6 to 9 of paragraph 3-09a to obtain the curve of \bar{P}_{front} vs time.

b. Average Interior Front Wall Overpressure vs Time. Step 1. Determine h'_{if} , the weighted average build-up height for the inside front wall.

Step 2. Determine P_{soi} , knowing P_{so} and A_{of}/A_{gf} , from figure 3.41 or figure 3.42.

Step 3. Determine U_{io} , knowing P_{soi} , from figure 3.9.

Step 4. Determine P_{i-refl} , knowing P_{soi} , from figure 3.20.

Step 5. Determine the curve of P_s using figure 3.22 or table 3.1.

Step 6. Plot the curve of $\bar{P}_{i-front}$ vs time as illustrated in figures 3.38 or 3.39.

c. Average Net Front Wall Overpressure vs Time. Step 1. Knowing \bar{P}_{front} and \bar{P}_{back} for a sequence of times t_1, t_2, t_3 , etc., determine $\bar{P}_{f-net} = \bar{P}_{front} - \bar{P}_{back}$ for each value of t .

Step 2. Plot the curve of \bar{P}_{f-net} vs time as illustrated in figure 3.40.

d. Average Exterior Back Wall Overpressure vs Time. Step 1. Determine h'_b from the relation

$$h'_b = \sum \frac{\delta_n h_n A_n}{A_R}$$

Step 2. Determine h' , the clearing height for the rear face, treating it as if it were closed. Use $h'_b = h'$, if Step 1 gives $h'_b > h'$.

Step 3. Determine t'_b from the relation $t'_b = 4h'_b/c_o$.

Step 4. Use Steps 1, 2, and 4 to 8 of paragraph 3-09b to obtain the curve of \bar{P}_{back} vs time.

- e. Average Interior Back Wall Overpressure vs Time. Step 1. Determine h'_{ib} , the weighted average build-up height for the inside back wall. Step 2. Determine P_{soi} , U_{io} , and P_{i-refl} as in paragraph 3-12b. Step 3. Determine $t_d = L_i/U_{io}$. Step 4. Determine overpressure at time $t - t_d = L_i/c_o$ from the relation

$$\bar{P}_{i-back} = P_{soi} + (1 - A_{of}/A_{gf})^2 (P_{i-refl} - P_{soi})$$

Step 5. Determine the curve of $P_s + 0.85q$ as in Steps 1 and 6 to 8 of paragraph 3-09a.

Step 6. Plot the curve of \bar{P}_{i-back} vs time as illustrated in figure 3.43 or 3.44.

- f. Average Net Back Wall Overpressure vs Time. Step 1. Knowing \bar{P}_{i-back} and \bar{P}_{back} for a sequence of times t_1, t_2, t_3 , etc., determine $\bar{P}_{b-net} = \bar{P}_{i-back} - \bar{P}_{back}$ for each value of t .

Step 2. Plot the curve of \bar{P}_{b-net} vs time as illustrated in figure 3.45.

- g. Average Exterior Roof Overpressure vs Time. Step 1. Use Steps 1 to 8 of paragraph 3-09e to determine the curve of \bar{P}_{roof} vs time, but replacing the quantity h' appearing in any of these Steps by h'_f .

- h. Average Interior Roof Overpressure vs Time. Step 1. Determine P_{soi} , U_{io} , and P_{i-refl} as in paragraph 3-12b.

Step 2. Determine $t_d = L_i/2U_{io}$.

Step 3. Determine the curve of P_s using figure 3.22 or table 3.1.

Step 4. Plot the curve of \bar{P}_{i-roof} vs time as illustrated in figure 3.46 or 3.47.

- i. Average Net Roof Overpressure vs Time. Step 1. Knowing \bar{P}_{roof} and \bar{P}_{i-roof} for a sequence of times t_1, t_2, t_3 , etc., determine $P_{r-net} = \bar{P}_{roof} - \bar{P}_{i-roof}$ for each value of t .

Step 2. Plot the curve of \bar{P}_{b-net} vs time as illustrated in figure 3.48.

- j. Average Exterior Side Wall Overpressure vs Time. Step 1. Use the procedure of paragraph 3-09g to determine the curve of \bar{P}_{side} vs time, but replacing the quantity h' by h'_f .

k. Average Interior Side Wall Overpressure vs Time. The curve of $\bar{P}_{i\text{-side}}$ is obtained in the same manner as $\bar{P}_{i\text{-roof}}$, as presented in paragraph 3-12h.

1. Average Net Side Wall Overpressure vs Time. Step 1. Knowing \bar{P}_{side} and $\bar{P}_{i\text{-side}}$ for a sequence of times t_1, t_2, t_3 , etc., determine $\bar{P}_{s\text{-net}} = \bar{P}_{\text{side}} - \bar{P}_{i\text{-side}}$ for each value of t .

Step 2. Plot the curve of $\bar{P}_{s\text{-net}}$ vs time as illustrated in figure 3.49.

LOADING ON STRUCTURES WITH GABLED ROOFS

3-13 LOADING ON GABLED ROOFS. a. Average Front Slope Roof Overpressure \bar{P}_{roof} , Shock Front Parallel to Ridge Line. When the shock wave strikes a roof surface, or the earth cover of

a semiburied structure, pitched as in figure 3.50(a) or (b), oblique reflection of the shock front occurs.

The reflected pressure $P_{r-\alpha}$ is a function of the peak incident overpressure P_{so} and the angle of inclination of the roof θ . The ratio

$P_{r-\alpha}/P_{so}$ is plotted in figure 3.11 as a function of the angle of incidence α , here equal to $90^\circ - \theta$.

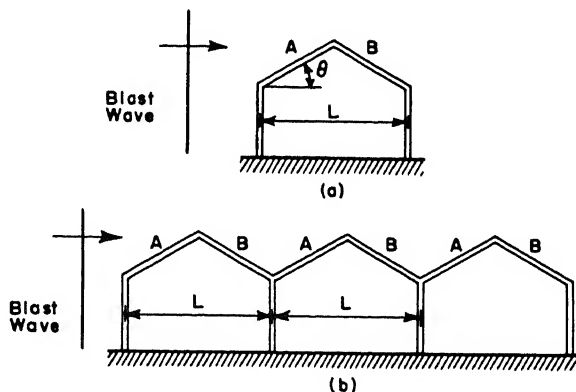


Figure 3.50. Typical gabled roofs

For a given angle of inclination of the roof, the ratio of the maximum average overpressure to the reflected overpressure is a constant when the overpressures are expressed in terms of their deviation from the overpressure in the incident shock wave. This relation is expressed as follows, where K_θ is independent of the peak incident overpressure

$$K_\theta = (\bar{P}'_{\text{roof}} - P_{sL}) / (P_{r-\alpha} - P_{sL}) \quad (3.24)$$

where \bar{P}'_{roof} = peak average overpressure on front slope of each bay at time $t = t_d + L/4U$

L = length of one gabled roof span

P_{sL} = overpressure in the incident shock wave at time $t - t_d$
 $= L/4U_o$

$P_{r-\alpha}$ = reflected overpressure as obtained from figure 3.11

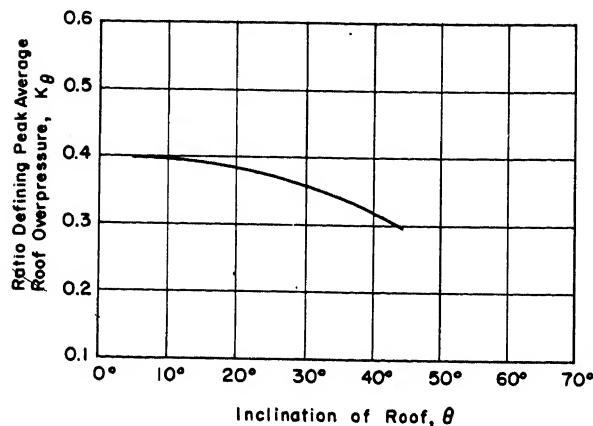


Figure 3.51. Ratio defining peak average roof overpressure vs inclination of roof

The factor K_θ is plotted as a function of θ in figure 3.51. The peak average overpressure on the front roof slope \bar{P}'_{roof} is then computed from the following equation

$$\bar{P}'_{\text{roof}} = P_{sL} + K_\theta(P_{r-\alpha} - P_{sL}) \quad (3.25)$$

The average overpressure on the front slope of the roof builds up linearly from zero at time

$$t = t_d - L/4U_0$$

to the value given by equation (3.25) at time $t = t_d + L/4U_0$. The average overpressure then clears to the drag overpressure at time $t = t_d + 3L/4U_0$ and is given by the relation

$$\bar{P}_{\text{roof}} = P_s + C_D q \quad (3.26)$$

for all times in excess of $t = t_d + 3L/4U_0$, where

\bar{P}_{roof} = average overpressure on the front roof slope

P_s = overpressure in the incident shock wave

t_d = time-displacement factor $\approx L/4U_0$ for front slope of first bay

q = dynamic pressure

C_D = drag coefficient plotted in figure 3.52 as a function of θ [22].

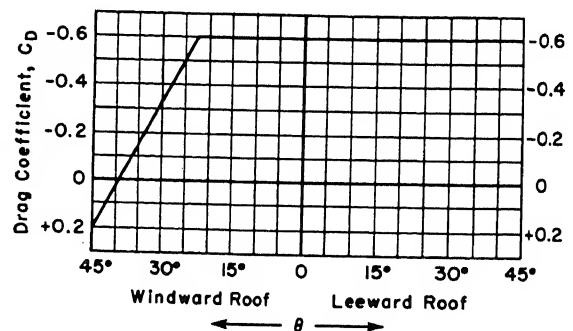


Figure 3.52. Drag coefficient for gabled roofs vs slope angle of roof

The local overpressure vs time curve at a point on the front slope of the gabled roof surface consists of an instantaneous overpressure rise to the reflected pressure $P_{r-\alpha}$ followed by a linear decrease to the drag overpressure, given by equation (3.26), in a clearing time equal to $L/2U_0$. The time displacement for the drag pressure curve is equal to the time required for the shock to travel from the front edge of the structure to the point at which it is desired

to determine the local overpressure.

The local overpressure vs time curve at a point on the rear roof slope consists simply of the drag overpressure given by equation (3.26). The time displacement t_d for the drag pressure curve is equal to the time required for the shock to travel from the front edge of the structure to the point at which it is desired to determine the local overpressure.

Figures 3.53 and 3.54 illustrate average overpressure vs time curves for the front roof slope in the first bay and in any bay. The first bay time-displacement factor t_d is given above, and for any other bay it is the time required for the shock front to travel from the front wall of the structure to a point halfway across the front roof slope of the bay.

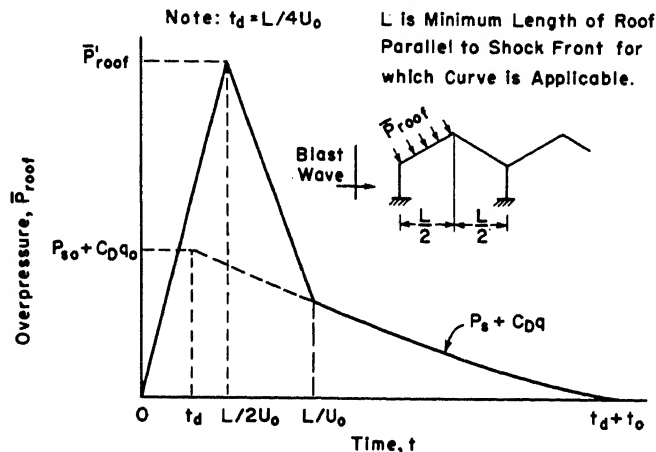


Figure 3.53. Average overpressure on windward roof slope of first bay of gabled structure vs time--ridge line parallel to shock front

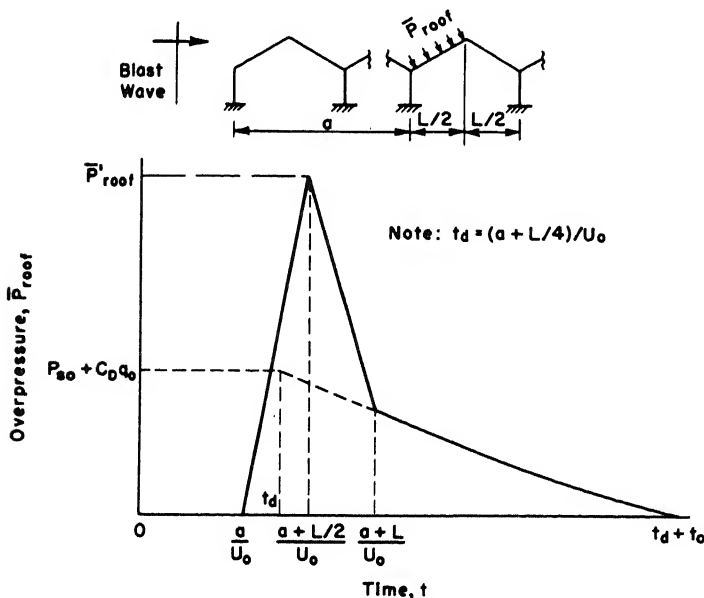


Figure 3.54. Average overpressure on windward roof slope of any bay of a gabled structure vs time--ridge line parallel to shock front

The local overpressure vs time curve at a point on the front slope of the gabled roof surface consists of an instantaneous overpressure rise to the reflected pressure $P_{r-\alpha}$ followed by a linear decrease to the drag overpressure, given by equation (3.26), in a clearing time equal to $L/2U_0$. The time displacement for the drag pressure curve is equal to the time required for the shock to travel from the front edge of the structure

to the point at which it is desired to determine the local overpressure.

b. Average Rear Slope Roof Overpressure \bar{P}_{roof} , Shock Front Parallel to Ridge Line. No reflection takes place on the rear roof slope, slope B of figure 3.50. The overpressure builds up linearly from zero at time

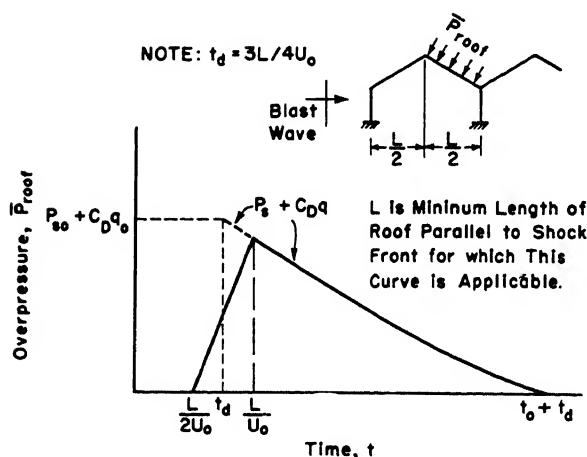


Figure 3.55. Average overpressure on leeward roof slope of first bay of gabled structure vs time--ridge line parallel to shock front

$t = t_d - L/4U_0$, the time at which the shock front reaches the roof peak, to the overpressure as given by equation (3.26) at time $t = t_d + L/4U_0$. For the rear slope of the first bay the time-displacement factor is $t_d = 3L/4U_0$. The average overpressure-time curve on this surface is illustrated in figure 3.55.

The local overpressure vs time curve at a point on the rear roof slope consists simply of the drag overpressure given by equation (3.26). The time displacement t_d for the drag pressure curve is equal to the time required to travel from the front edge of the structure to the point at which it is desired to determine the local overpressure.

c. Average Overpressures, Shock Front Perpendicular to Ridge Line. The overpressures on all surfaces, for the blast wave traveling along the ridge line of the structure, are obtained by the methods outlined in paragraph 3-08. For closed structures, the clearing height h' is taken as the average height of the front wall, or half the width, whichever is the smaller; the build-up height of the back wall is taken as the average height of that wall or half the width, whichever is the smaller. The clearing and build-up heights for gabled structures with openings are computed by the procedures in paragraph 3-11.

3-14 PROCEDURE FOR COMPUTATION OF LOADS ON GABLED ROOFS. Repeat Steps 1, 2, and 3 under paragraph 3-09.

a. Average Front Slope Roof Overpressure in First Bay vs Time, Shock Front Parallel to Ridge Line. Step 1. Determine U_0 , knowing P_{s0} , from figure 3.9.

- Step 2. Determine $t_d = L/4U_o$.
- Step 3. Determine K_θ , knowing θ , from figure 3.51.
- Step 4. Determine P_{sL} , the overpressure in the incident shock wave at time $t - t_d = L/4U_o$. Use figure 3.10 to get t_o and figure 3.22 to find P_{sL}/P_{so} .
- Step 5. Determine $P_{r-\alpha}$, knowing $\alpha = 90^\circ - \theta$ and P_{so} , from figure 3.11.
- Step 6. Determine \bar{P}'_{roof} , the average maximum overpressure on the roof at time $t = t_d + L/4U_o$, from the relation

$$\bar{P}'_{roof} = K_\theta(P_{r-\alpha} - P_{sL}) + P_{sL}$$

- Step 7. Determine C_D , knowing θ , from figure 3.52.
- Step 8. Determine $P_s + C_D q$ by use of Steps 1, 6, and 7 of paragraph 3-09a and the following table.

time, t	$t - t_d$	$(t - t_d)/t_o$	q/q_o	q	$C_D q$	P_s/P_{so}	P_s	$P_s + C_D q$
(1)	(2)	(3)	(4)	(5)	(6)	(7)	(8)	(9)

Column (1) is a sequence of times from $t = t_d$ to $t = t_d + t_o$.

Column (4) is obtained from figure 3.24 or table 3.2 for the values in column (3).

Column (7) is obtained from figure 3.22 or table 3.1 for the values in column (3).

Step 9. Plot the curve of \bar{P}'_{roof} vs time as illustrated in figure 3.53.

b. Average Rear Slope Roof Overpressure in First Bay vs Time, Shock Front Parallel to Ridge Line. Step 1. Determine U_o , knowing P_{so} , from figure 3.9.

- Step 2. Determine $t_d = 3L/4U_o$.
- Step 3. Determine $P_s + C_D q$ by following Steps 7 and 8 of paragraph 3-14a.
- Step 4. Plot the curve of \bar{P}'_{roof} vs time as illustrated in figure 3.55.

LOADING ON EXPOSED STRUCTURAL MEMBERS

3-15 LOADING ON EXPOSED STRUCTURAL FRAMEWORKS. The blast wave loading on structures with open steel frameworks such as bridge trusses, steel towers, or steel industrial buildings following the destruction of frangible walls is caused almost entirely by the drag pressure resulting from the high-velocity blast wind which follows directly behind the shock front. The load due to the unbalanced pressures resulting from reflection and diffraction of the shock front can be neglected because of the extremely short duration of these effects. A structure of this type consists of structural elements whose dimensions are so small that their front face clearing times are less than 10 milliseconds. In addition the members are so small that they are enveloped by the blast wave in a similar short length of time. The total load on the structure due to the drag forces can be obtained by computing the load on all the individual elements of the buildings, front

and back walls and intermediate elements, and adding them together on a common time basis. The total drag overpressure on an element can be computed from the formula

$$\text{Drag overpressure} = C_D q \quad (3.27)$$






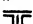

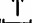
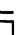
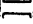

where

C_D = coefficient of drag obtained from figures 3.56 and 3.57. This coefficient is applied to the individual structural elements

q = dynamic pressure due to the air velocity in the incident blast wave at any time $= \rho u^2/2$, and is determined from figures 3.23 and 3.24

$t_d = L/U_0$, where L is the distance from the front portion of the structure to the element for which the load is being computed

DRAG COEFFICIENTS, C_D , FOR VARIOUS STRUCTURAL CROSS-SECTIONS

Shape	Direction of Wind C_D	Shape	C_D
	2.0		2.0
	2.0		1.0
	2.0		2.0
	1.8		2.0
	2.0		2.2
	1.8		

* Standard or Wide Flange Sections

† Built up Sections, either Riveted or Welded

DRAG COEFFICIENTS, $(C_D)_w$, FOR WINDWARD (UNSHIELDED) TRUSS OF BRIDGES

$(C_D)_w$ is given as a function of the solidity ratio, $G=A'/A$, where A is the total area included within the limiting boundaries of the truss, A' is the actual area of the members in a plane normal to the wind direction.

For single span trusses:

$G < 0.25$	$(C_D)_w = 1.8$
$G > 0.25$	$(C_D)_w = 1.6$

For multiple span or very long span trusses:

$0.00 < G < 0.20$	$(C_D)_w = 2.0$
$0.20 < G < 0.30$	$(C_D)_w = 1.8$
$0.30 < G < 0.90$	$(C_D)_w = 1.6$
$0.90 < G < 1.00$	$(C_D)_w = 2.0$

Figure 3.56. Drag coefficients for various structural shapes and trusses

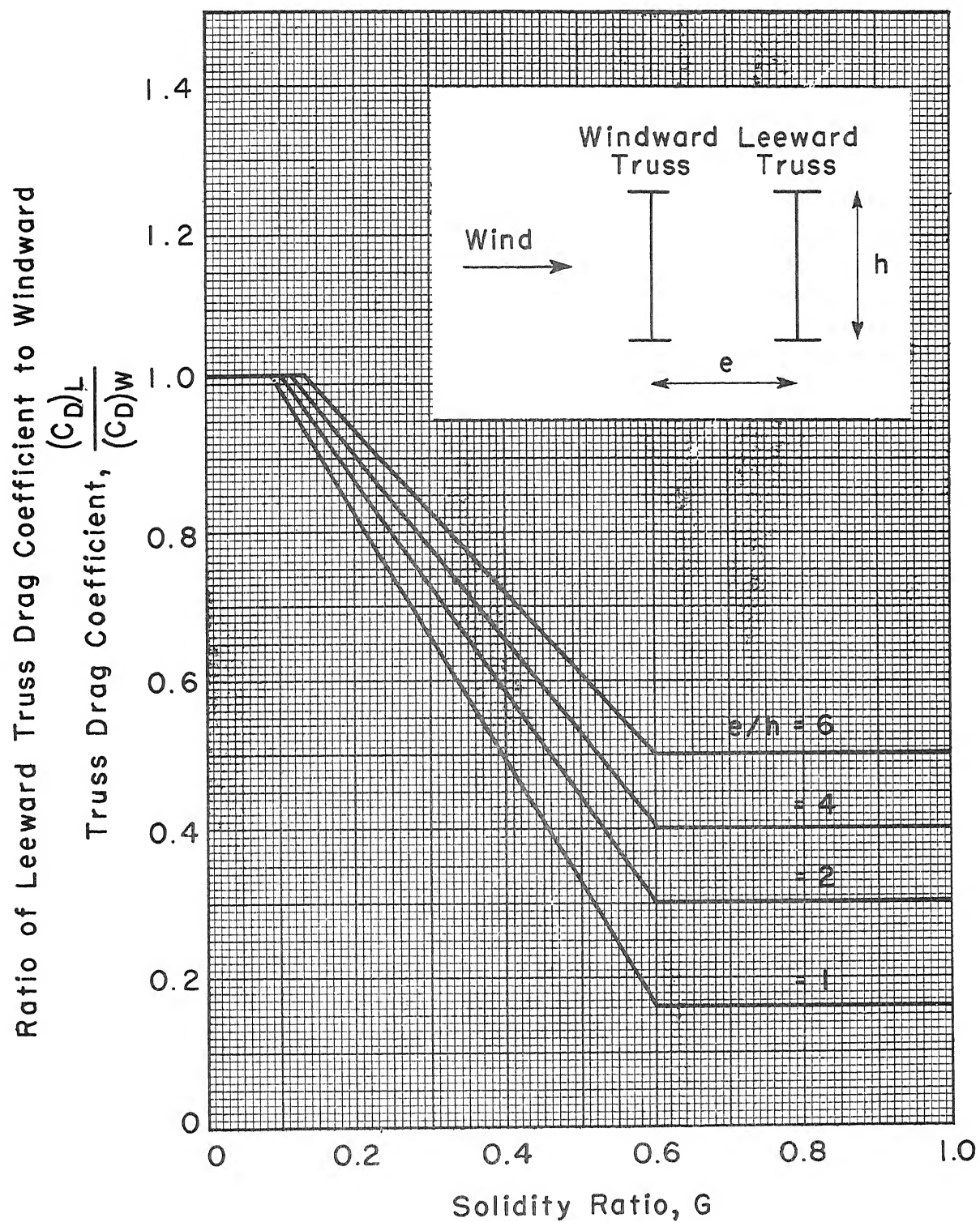


Figure 3.57. Drag coefficients for leeward trusses

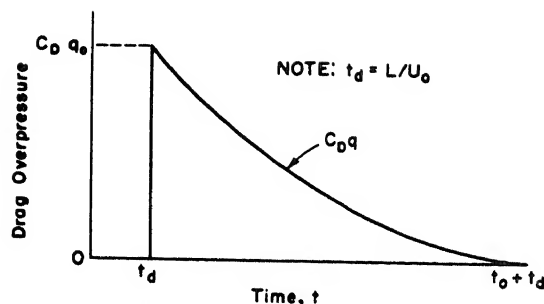


Figure 3.58. Drag overpressure vs time on exposed structural element

Figure 3.58 illustrates the drag overpressure-time curve for an exposed element located at distance L from the front portion of a structure. The total load on the element at any time is obtained by multiplying the drag overpressure (at any time) by the projected area of the member transverse to the direction of travel of the blast wave. The total load on the structure

at any time is obtained by summing the loads on all the individual members, based on time t , referenced to the instant the frontmost elements of the structure are struck by the shock wave.

The overpressure-time curve for the front wall supporting elements of a structure with frangible wall covering is shown in figure 3.59. The overpressure on the front wall prior to the time of failure is determined as previously described for the front wall of a closed rectangular

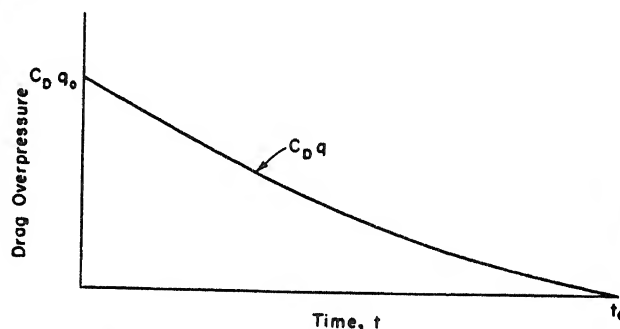


Figure 3.59. Drag overpressure vs time on front wall elements supporting frangible wall panels

structure. The time of failure is actually a very short time for frangible elements compared to t_0 , and the load transmitted to the supporting elements prior to failure may be neglected. After the front wall fails the supporting elements are subjected to the drag overpressures given by equation (3.27). The overpressure-time curve for the back wall supporting elements is similar to that for the front wall except all times are displaced by the time-displacement factor $t_d = L/U_0$, where L is the distance between the front and back wall. After failure of the back wall, the back wall supporting elements are subjected to the drag overpressures given by equation (3.27).

3-16 PROCEDURE FOR COMPUTATION OF LOADS ON EXPOSED STRUCTURAL FRAMEWORKS.
Repeat Steps 1, 2, and 3 of paragraph 3-09.

Step 4. Determine U_o , knowing P_{so} , from figure 3.9.

Step 5. Determine t_d = time for shock wave to travel from reference point to member under consideration.

Step 6. Determine C_D from figure 3.56 or figure 3.57.

Step 7. Determine q_o , knowing P_{so} , from figure 3.23.

Step 8. Determine q , knowing q_o , for a sequence of times from figure 3.24 or table 3.2.

Step 9. Evaluate $C_D q$ for these times.

Step 10. Plot the curve of net drag overpressure vs time as illustrated in figure 3.58.

LOADING ON CYLINDRICAL SURFACES

3-17 LOADING ON CYLINDRICAL ARCH SURFACES. a. Cylindrical Arch Overpressure P_{cyl} , Axis Parallel to Shock Front.

Figure 3.60a is a definition sketch for the notation used in the determination of the loads on a cylindrical arch surface. Structures in this category are illustrated in figure 3.60b. These consist

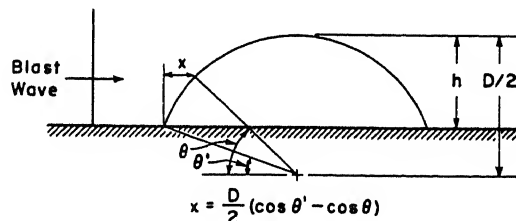


Figure 3.60a. Definition sketch for cylindrical arch notation

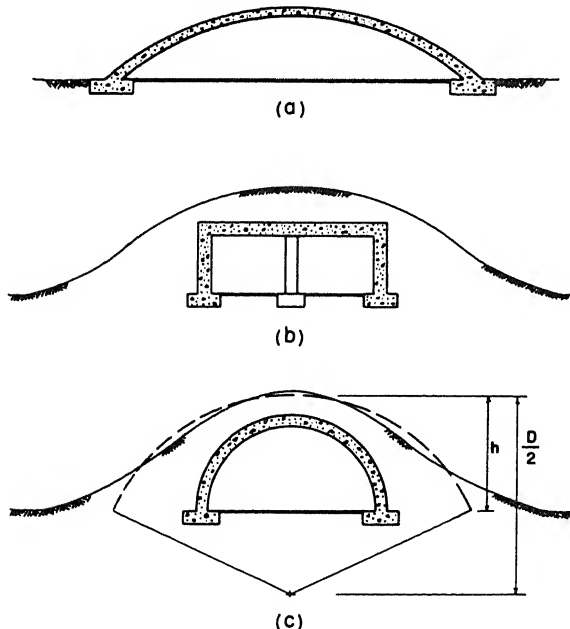


Figure 3.60b. Illustration of structures with cylindrical arch surfaces

of exposed arch structures and surface structures of various shapes covered by an earth fill. If the arch or earth-fill surface is not truly circular, it is approximated by an arc of a circle as illustrated by dashed lines in figure 3.60b(c), and the loads are computed for the equivalent circular surface. Note that in some cases a better approximation of the ground surface is obtained with a gabled roof shape, in which case the loads are computed as

described in paragraph 3-13. Procedures given in this paragraph determine the air blast loading as a function of time on the cylindrical arch surface exposed to the air blast, whether it be the surface of the arch on the exposed structure, or the surface of the rounded fill over the covered structure. With this procedure, zero time is the instant at which the incident shock front first strikes the cylindrical arch surface at its intersection with the horizontal ground surface, along the line defined by $\theta = \theta'$.

Figures 3.61 and 3.62 illustrate the variation of the local overpressure P_{cyl} with time on the surface of a cylindrical arch. Each of these

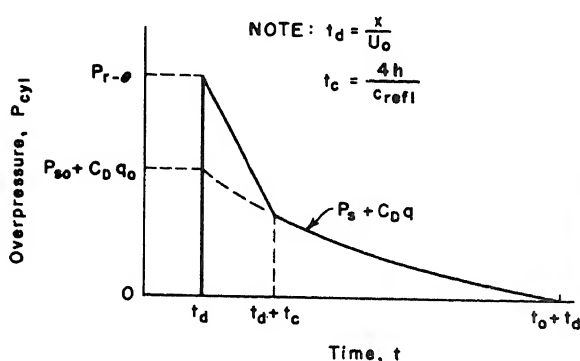


Figure 3.61. Local overpressure on front surface of cylindrical arch vs time--axis parallel to shock front, $0^\circ \leq \theta' < \theta < 90^\circ$

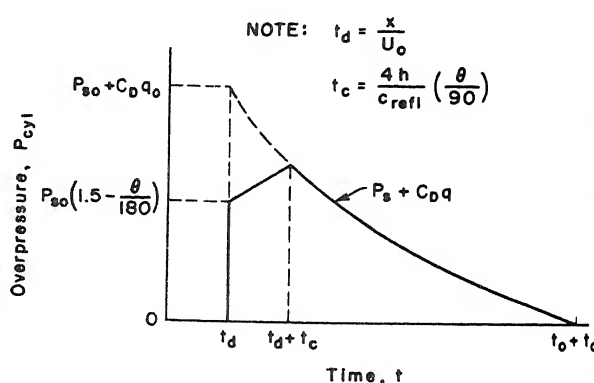


Figure 3.62. Local overpressure on leeward surface of cylindrical arch vs time--axis parallel to shock front, $90^\circ \leq \theta < 180^\circ$

figures is valid only within a certain range of θ values, which are determined by the clearing time peculiar to each. These times and the sequence of overpressures within them are defined as follows:

For $0^\circ \leq \theta' < \theta < 90^\circ$ (figure 3.61): The overpressure at a given point rises instantaneously from zero to $P_{r-\alpha}$ at time $t_d = x/U_0$. The value of $P_{r-\alpha}$ is given in figure 3.11 as a function of α , the angle of incidence of the shock wave. For the cylinder of figure 3.60a, $\alpha = \theta$. Clearing of reflection effects occurs at time $t = t_d + t_c$ where the clearing time t_c is given by

$$t_c = 4h/c_{refl} \quad (3.28)$$

The local overpressure at any point after the clearing of reflection effects is given by equation (3.29). P_{cyl} acts normal to the surface of the arch.

$$P_{cyl} = C_D(q) + P_s \quad (3.29)$$

where q is the dynamic pressure incorporating the time-displacement factor t_d

C_D is the local drag coefficient, which is a function of θ and is obtained from figures 3.63a, b, c, and d and 3.64 as discussed below

P_s is the overpressure in the incident blast wave at any time $t - t_d$

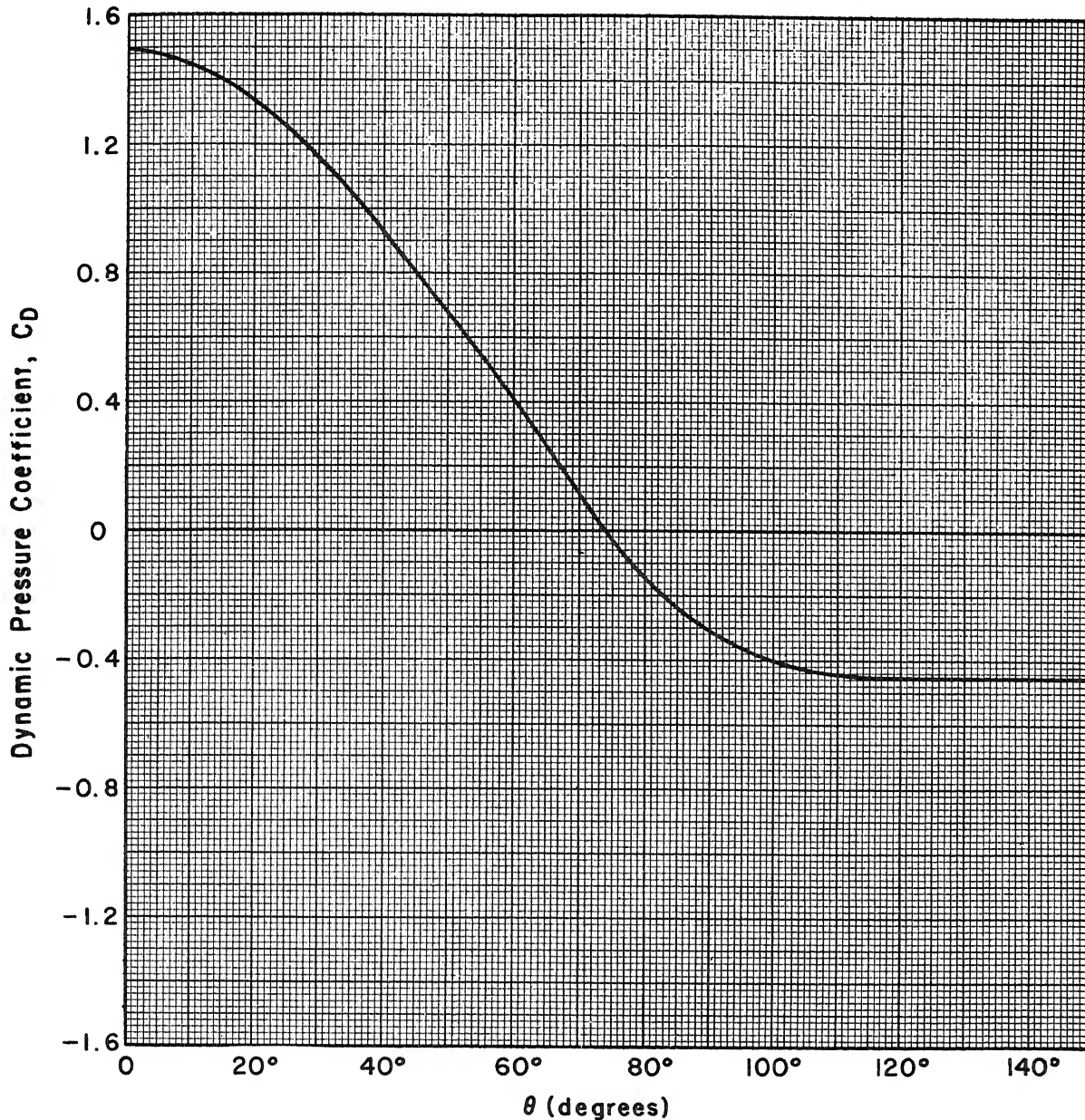


Figure 3.63a. Local dynamic pressure coefficient for cylindrical arch--axis parallel to shock front--supersonic Mach numbers ($M > 1$)

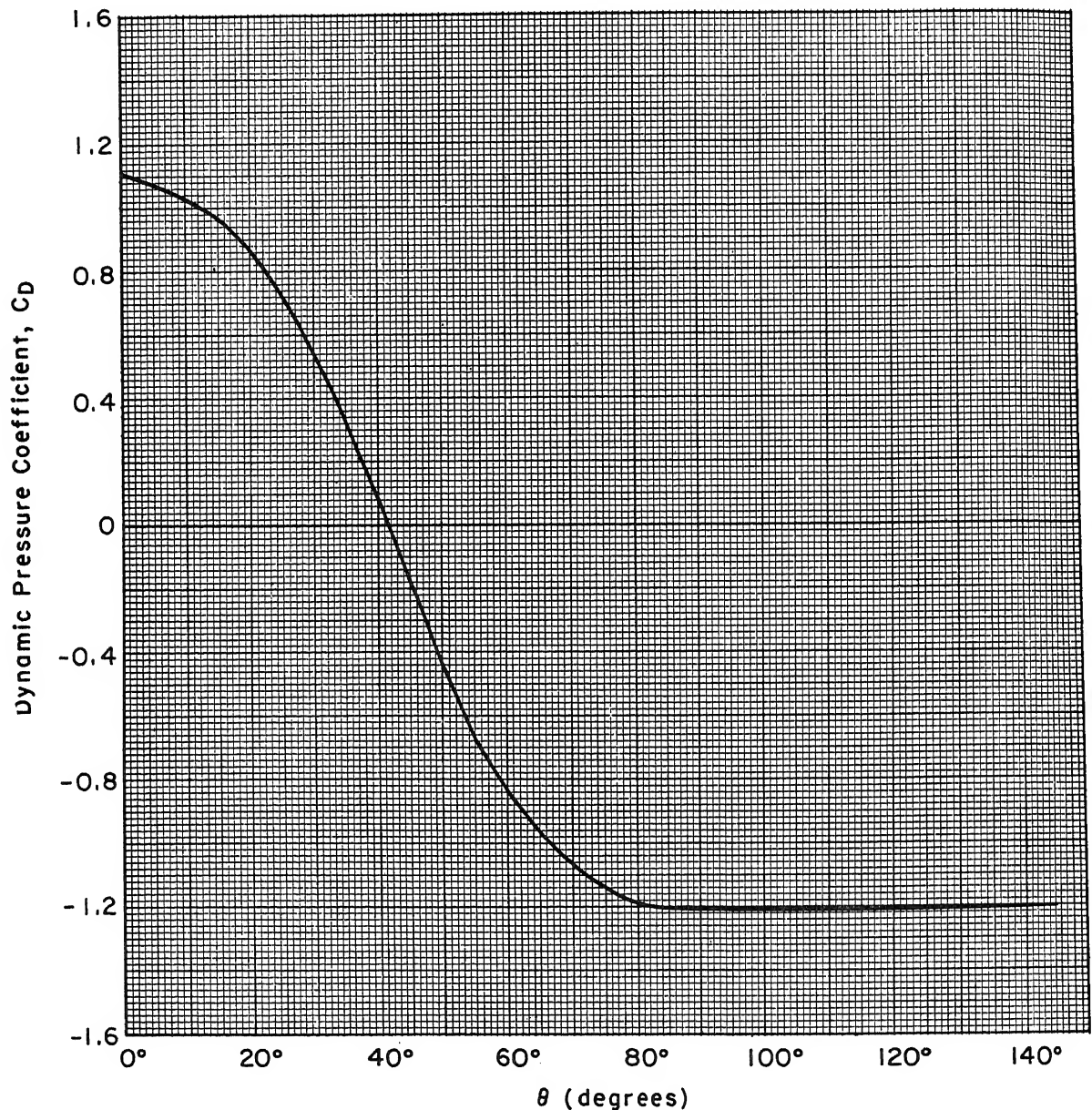


Figure 3.63b. Local dynamic pressure coefficient for cylindrical arch--axis parallel to shock front--high subsonic Mach numbers ($0.4 < M < 1$)

The distribution of dynamic overpressures about an arch is a function of both the Reynolds number R_e and the Mach number M of the high-velocity wind in the blast wave [48, 54]. The Reynolds number, a dimensionless quantity of the type $\frac{u \rho_0}{\mu}$, is a parameter which characterizes the relative importance of viscous action in steady nonuniform flow. Since the

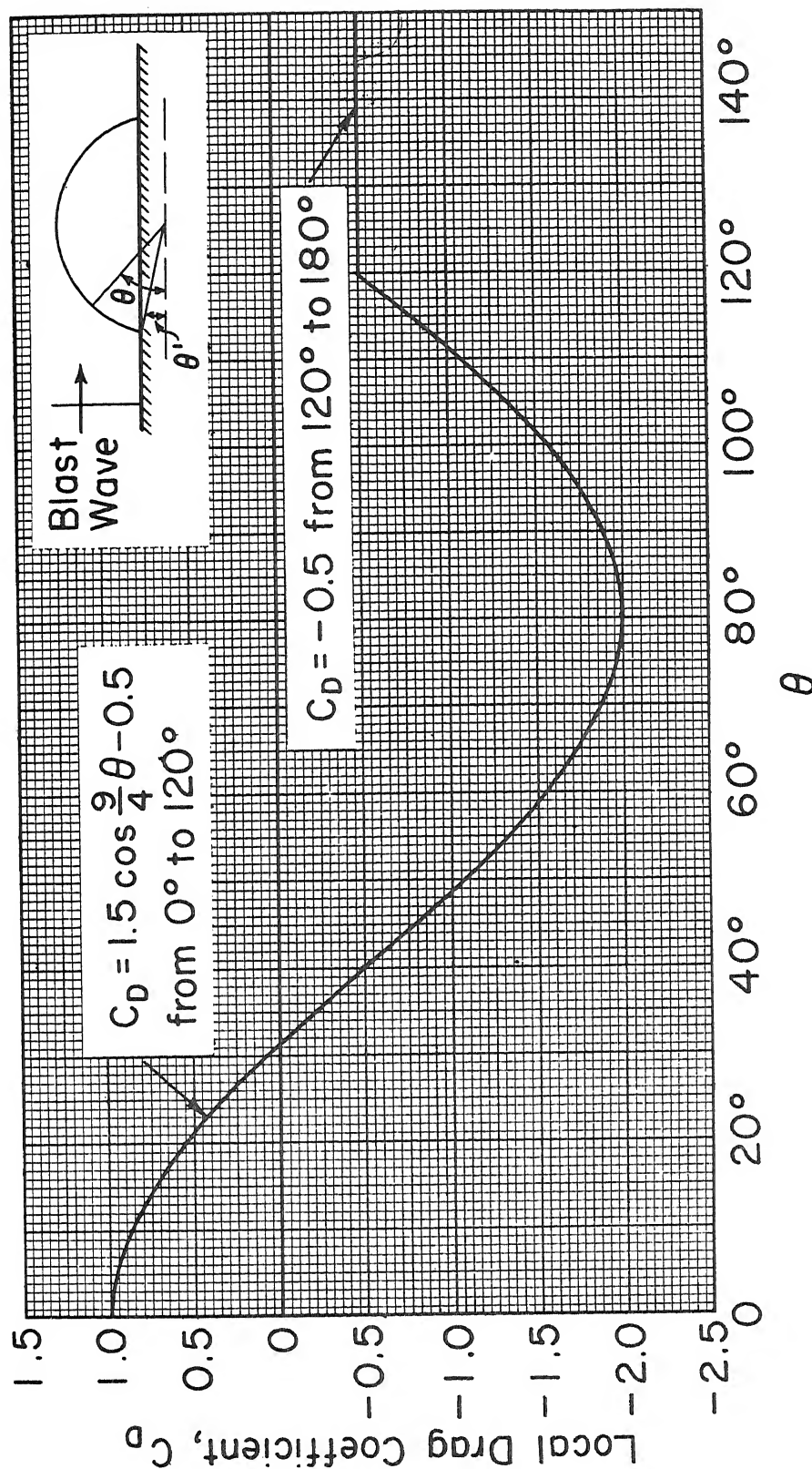


Figure 3.63c. Local dynamic pressure coefficient for cylindrical arch-axis parallel to shock front [$R > 5(10)^5$ and $M < 0.4$]

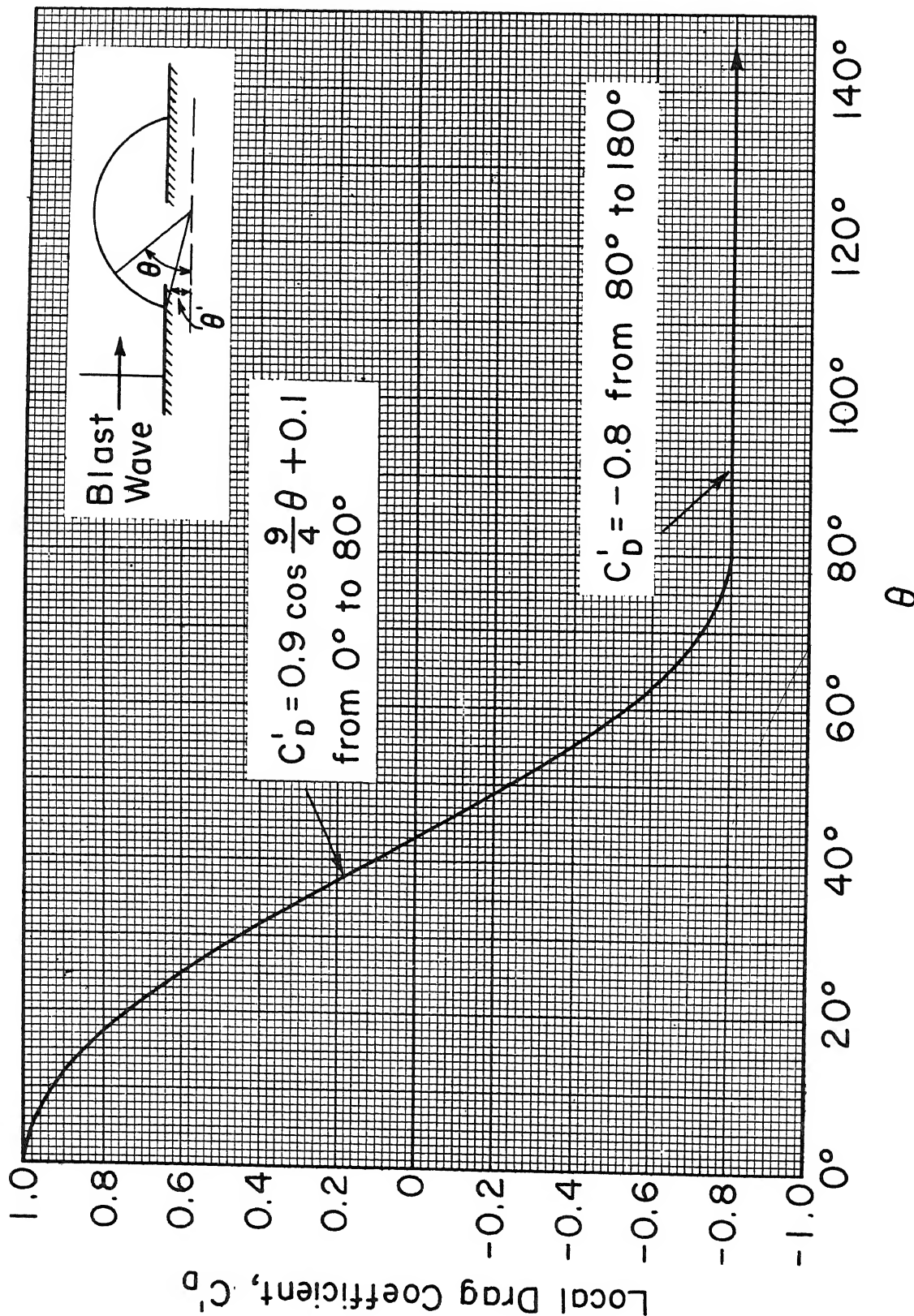


Figure 3.63d. Local dynamic pressure coefficient for infinitely long cylindrical arch parallel to shock front [$R < 5(10)^5$ and $M < 0.4$]

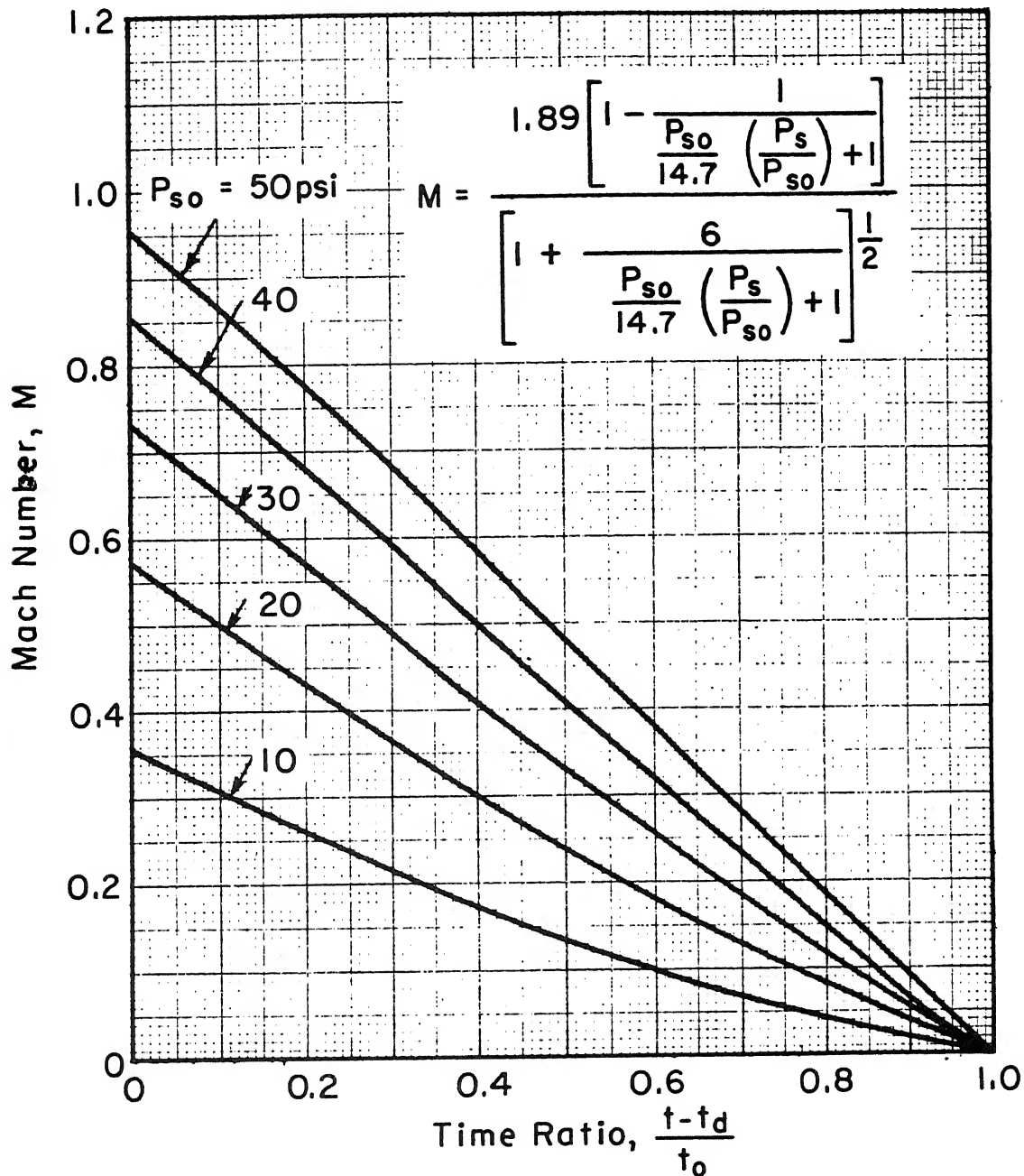


Figure 3.64. Mach number of undisturbed stream vs time ratio for various peak overpressures

viscosity μ and the density ρ appear as a ratio in the Reynolds number, it is convenient to treat this ratio of fluid properties as a property itself. Thus, the Reynolds number involves only the arch diameter D , a velocity u , and the fluid property ρ/μ . The Mach number, also a

dimensionless quantity, is the ratio of the actual velocity to the velocity of sound.

In the following discussion, the distribution of dynamic pressures about the circular arch is assumed to be the same as the distribution about a circular cylinder having the same diameter. Then the results of experimental studies conducted on flow past circular cylinders can be utilized for this problem. This procedure will introduce some error but it is believed to be insignificant compared to the uncertainty associated with the basic data.

For flow at low Mach numbers, the pressure distribution and the total drag force change abruptly for a Reynolds number range between $3(10)^5$ and $5(10)^5$. This transition is very sensitive to the smoothness of incident flow, temperature gradients, and roughness of the surfaces. The explanation advanced for this change in pressure distribution and decrease in drag is that the boundary layer changes from laminar to turbulent at this critical Reynolds number and causes the separation point to move farther back, resulting in the redistribution of dynamic pressure observed.

As the Mach number of the flow is increased, this decrease in total drag and redistribution of pressure at the critical Reynolds number becomes less pronounced until at a Mach number of about 0.4, it no longer occurs. The separation point does not move when the boundary layer changes from laminar to turbulent and is probably fixed by the presence of shock waves. For flows with a free stream Mach number greater than 0.4, the pressure distribution is not influenced by the Reynolds number but it is somewhat dependent upon the Mach number, the distribution being different for supersonic flow than for subsonic flow.

Four pressure distributions are necessary in order that the entire ranges of Reynolds and Mach numbers can be considered. The critical values of Reynolds and Mach numbers are arbitrarily taken as $R = 5(10)^5$, $M = 0.4$, and 1.0. These dynamic pressure coefficients are applicable for steady flow conditions, and since the flow about the arch is far from steady, their use may introduce some additional error. The order of magnitude of the error could be ascertained by comparing the results obtained by this procedure with direct measurements in field tests in which unsteady effects are present.

The expression for the local pressure coefficient when $R < 5(10)^5$ is

$$C_D = \frac{C'_D}{1.2} \left[0.7 + 0.5 \sqrt{1 - 4/(L/D)^2} \right] \quad (3.30)$$

where

C'_D is the local pressure coefficient for an arch infinitely long when $R < 5(10)^5$ (figure 3.63d)

L is the length of the axis of the arch

D is the diameter of the arch

The Mach number is plotted in figure 3.64 and the ratio of Reynolds number to cylinder diameter is plotted in figure 3.65 for a range of incident peak overpressures as a function of $\frac{t - t_d}{t_o}$.

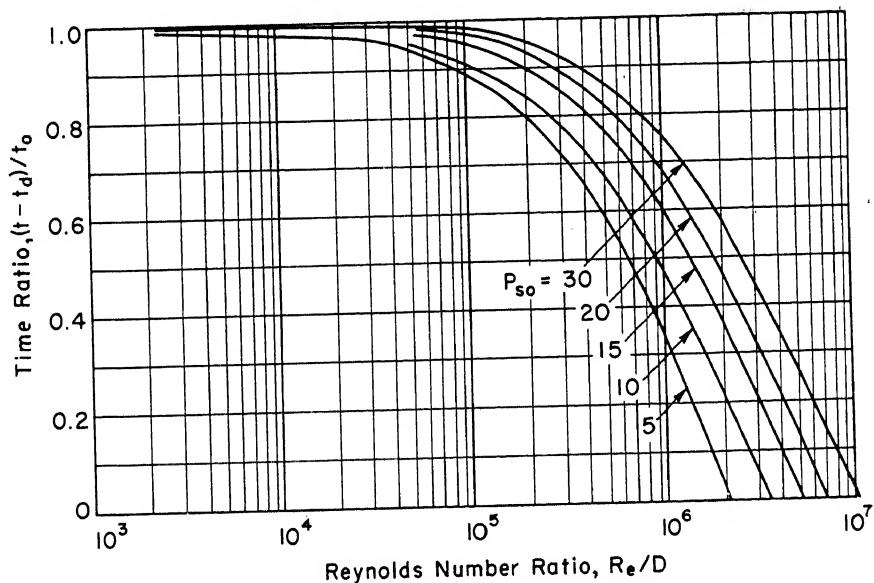


Figure 3.65. Reynolds number ratio of undisturbed stream vs time ratio for various peak overpressures

For $90^\circ < \theta < 180^\circ$ (figure 3.62): The overpressure at any point on the leeward side of the cylinder rises instantaneously from zero to a finite overpressure at time $t - t_d = 0$, given by

$$P_{cyl} = (1.5 - \theta/180)P_{so} \quad (3.31)$$

This initial overpressure clears to the value of P_{cyl} as given by equation (3.29) at time $t = t_d + t_c$, where

$$t_c = (4h/c_{refl})(\theta/90) \quad (3.32)$$

Appendix A, Transonic Drag Pressures, appearing at the end of this manual has been extracted from a report prepared by Amman and Whitney, Consulting Engineers, under contract DA 49-129-Eng-319 with the Chief of Engineers.

A method is outlined and charts included for evaluating pressures on earth-covered aboveground structures that have sloped embankments and a limited flat earth fill over their top. The method is based on aerodynamic principles which have a laboratory background. The results obtained are for a flat-top shock which must be converted to a shock that varies with time when applied to the analysis of structures to resist atomic weapons. The application to shock waves which vary with time can be accomplished in a similar manner described above for the equivalent circle method. At the present time the method outlined in appendix A has not been sufficiently developed to be set forth as a preferred method of analysis. Supplemental data will be available at a future time.

b. Average End Wall Overpressure \bar{P}_{end} , Axis Parallel to Shock

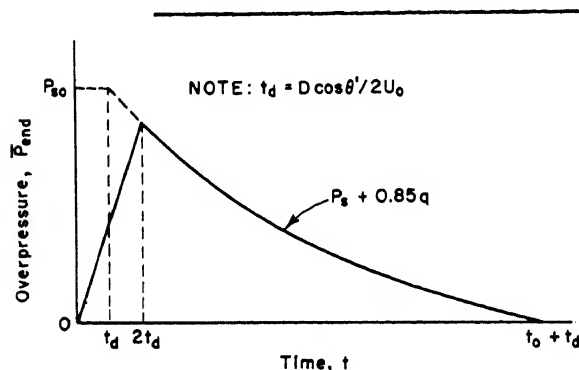


Figure 3.66. Average overpressure on closed ends of cylindrical arch vs time-axis parallel to shock front

Front. The average overpressure \bar{P}_{end} on the ends of a cylinder oriented as in figure 3.60a is given in figure 3.66. It is assumed that the variation of incident overpressure in the time required for the shock wave to travel across the cylinder is linear and that the average overpressure on the ends is equal to the overpressure in the incident

blast wave P_s with the time-displacement factor $t_d = D \cos \theta' / 2U_0$.

c. Local Cylindrical Arch Overpressure, Axis Perpendicular to Shock

Front. The local overpressure at any point on the periphery of the cylindrical arch oriented with its axis perpendicular to the shock front is the overpressure in the incident blast wave P_s with a time-displacement factor $t_d = L' / U_0$ where L' is the distance from the front end to the point at which the overpressure is desired.

d. Average End Wall Overpressure, Axis Perpendicular to Shock Front.

The average overpressure on the front and back ends of a cylindrical arch oriented with its axis perpendicular to the shock front can be computed as outlined in paragraphs 3-08a and 3-08b. The clearing height for the front wall and the build-up height for the back wall are equal to h as shown in figure 3.60a.

3-18 PROCEDURE FOR COMPUTATION OF LOADS ON CYLINDRICAL ARCHES. Repeat Steps 1, 2, and 3 of paragraph 3-09.

a. Local Cylindrical Arch Overpressure vs Time, Axis Parallel to Shock Front. Step 1. Determine $P_{r-\alpha}$, knowing $\alpha = \theta$ and P_{so} , from figure 3.11 for $\theta < 90^\circ$. Initial $P_{cyl} = (1.5 - \theta/180)P_{so}$ for $\theta > 90^\circ$.

Step 2. Determine c_{refl} , knowing P_{so} , from figure 3.21.

Step 3. Determine $t_c = 4h/c_{refl}$ for $\theta < 90^\circ$ or $t_c = (4h/c_{refl})(\theta/90)$ for $\theta > 90^\circ$.

Step 4. Determine U_o , knowing P_{so} , from figure 3.9.

Step 5. Determine $t_d = x/U_o$.

Step 6. Determine $\frac{t - t_d}{t_o}$ at which $M = 1$ from figure 3.64.

Step 7. Determine C_D for times less than this value from figure 3.63a.

Step 8. Determine $\frac{t - t_d}{t_o}$ at which $M = 0.4$ from figure 3.64.

Step 9. Determine C_D for times less than this value but greater than the time determined in Step 6 from figure 3.63b.

Step 10. Determine $\frac{t - t_d}{t_o}$ at which $R = 5(10)^5$ from figure 3.65.

Step 11. Determine C_D for times less than this value but greater than the time determined in Step 8 from figure 3.63c.

Step 12. Determine C_D for times in excess of the value determined in Step 10 from equation (3.30) and figure 3.63d.

Step 13. Determine $P_s + C_D q$ by following the procedure of Step 8, paragraph 3-14a.

Step 14. Plot the curve of P_{cyl} vs time as illustrated in figures 3.61 and 3.62.

b. Average End Wall Overpressure vs Time, Axis Parallel to Shock Front. Step 1. Determine $t_d = D \cos \theta' / 2U_o$.

Step 2. Determine values of P_s for a sequence of times ranging from $t - t_d = D \cos \theta' / 2U_o$ to $t - t_d = t_o$ from table 3.1 or figure 3.22.

Step 3. Plot the curves of P_{end} vs time as illustrated in figure 3.66.

c. Local Cylindrical Arch Overpressure vs Time, Axis Perpendicular to Shock Front. Step 1. Determine t_d , the time required for the shock front to travel from the front end of the arch to the point under consideration.

Step 2. Determine P_s for a sequence of times, with a time-displacement factor t_d .

Step 3. Plot the curve of $P_{cyl} = P_s$.

d. Average End Wall Overpressure vs Time, Axis Perpendicular to Shock Front. Step 1. Determine the clearing height $h' = h$ (see figure 3.63a).

Step 2. Plot the curves of \bar{P}_{front} and \bar{P}_{back} vs time using methods of paragraphs 3-09a and b, respectively.

LOADING ON DOMES

3-19 LOADING ON SPHERICAL DOME SURFACES. The notation convention used to designate a point on the surface of a dome is illustrated in figure 3.67. With the notation adopted, any point on the periphery of a spherical dome is located by the two angles θ and ϕ . Denoting by p any point on the sphere, θ is the angle between the horizontal diameter parallel to the direction of travel of the shock and the radius Op joining the surface point to the geometrical center of the sphere. The elevation of the point p above a horizontal plane through the center of the sphere is $R \sin \theta \sin \phi$, where ϕ is the angle between the horizontal plane through the center of the sphere and the inclined plane containing points O , O' , and p .

The variation with time of the local overpressure P_{dome} normal to the surface of the dome is similar to that for a cylinder as shown in figures 3.61 and 3.62. The overpressure at a given point rises

instantaneously from zero to $P_{r-\alpha}$ at time $t_d = x/U_o$, where $x = (d/2) - R \cos \theta$ with d being the distance across the dome at its base and U_o is the shock front velocity. The angle of incidence at the impinging shock wave is equal to θ . For values of θ less than 90° the reflected overpressure is obtained from figure 3.11; for θ greater than 90° the maximum overpressure is given by the relation

$$P_{\text{dome}} = (1.5 - \theta/180)P_{so} \quad (3.33)$$

The initial maximum overpressures are cleared in time t_c as given by equation (3.34), where h is the height of the dome above its base.

$$t_c = 3h/c_{\text{refl}} \quad \text{for } \theta < 90^\circ \quad (3.34)$$

$$t_c = (3h/c_{\text{refl}})(\theta/90) \quad \text{for } \theta > 90^\circ$$

The local overpressure at any point after the clearing of reflected overpressures is given by equation (3.35).

$$P_{\text{dome}} = C_D q + P_s \quad (3.35)$$

where

q = unit drag pressure incorporating the time-displacement factor t_d

C_D = local drag coefficient plotted as a function of θ in figures 3.68 and 3.69

The ratio of the Reynolds number of the air blast wind to the diameter of the sphere is plotted in figure 3.65 for various incident overpressures as a function of $(t - t_d)/t_o$. At the Reynolds number $R_e = 10^5$, the value of the drag coefficient changes abruptly. The ratio of $(t - t_d)/t_o$ associated with this value of R_e determines the applicability of either

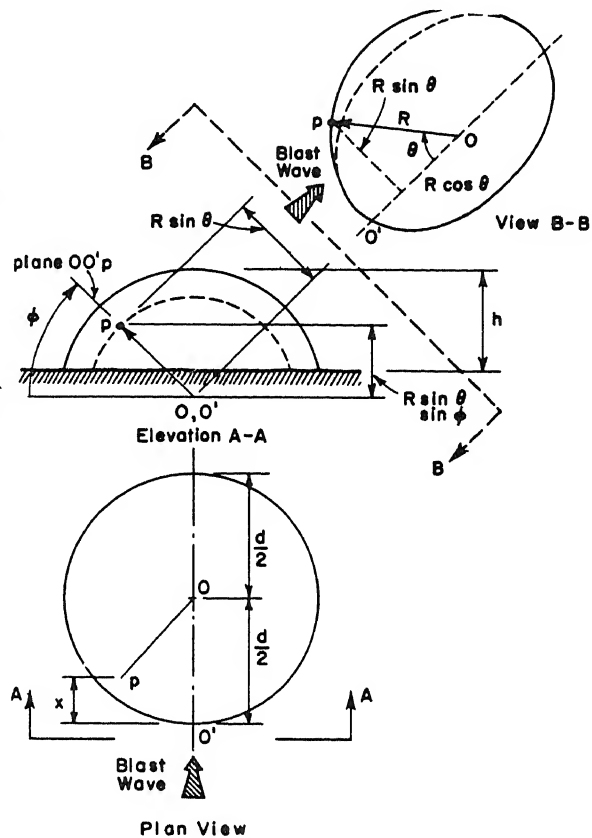


Figure 3.67. Definition sketch for spherical dome notation

figure 3.68 or 3.69 to obtain C_D for use in equation (3.35).

The loading in domes calculated by the methods presented in this paragraph can be in error for large overpressures. Use of the present method should not be made for pressures greater than 15 psi.

3-20 PROCEDURE FOR COMPUTATION OF LOADS ON SPHERICAL DOMES. Repeat Steps 1, 2, and 3 of paragraph 3-09.

Step 4. Determine $P_{r-\alpha}$, knowing $\alpha = \theta$ and P_{so} , from figure 3.11 for $\theta \leq 90^\circ$. Determine maximum $P_{dome} = (1.5 - \theta/180)P_{so}$ for $\theta \geq 90^\circ$.

Step 5. Determine c_{refl} , knowing P_{so} , from figure 3.21.

Step 6. Determine $t_c = 3h/c_{refl}$ for $\theta \leq 90^\circ$ or $t_c = (3h/c_{refl})(\theta/90)$ for $\theta \geq 90^\circ$.

Step 7. Determine U_o , knowing P_{so} , from figure 3.9.

Step 8. Determine $t_d = x/U_o$.

Step 9. Determine $(t - t_d)/t_o$ at which $R_e/D = 10^5/D$, knowing P_{so} , from figure 3.65.

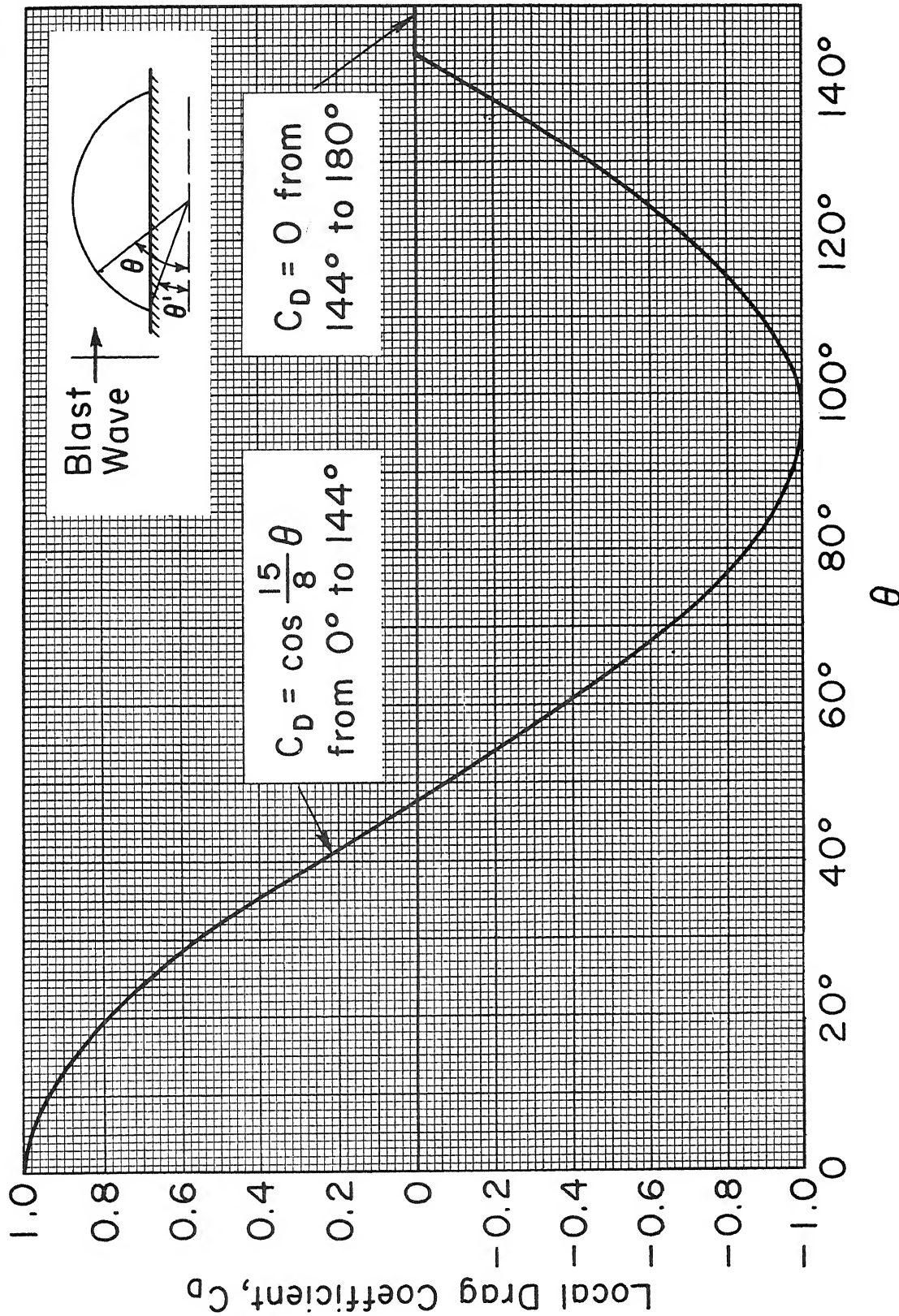
Step 10. Determine C_D for times less than the value of $t - t_d$ obtained in Step 9 from figure 3.68; for times greater than this value from figure 3.69.

Step 11. Determine $P_s + C_D q$ by following the procedure of Step 8, paragraph 3-14a.

Step 12. Plot the curve of P_{dome} vs time for the point selected, as illustrated in figures 3.61 and 3.62.

LOADING ON BURIED STRUCTURES

3-21 LOADING ON BURIED STRUCTURES. The method for determination of earth pressure loading on buried structures is more approximate than that for the loading on surface structures. The soil has an appreciable mass which affects the magnitude of the overpressures acting on a buried structure because of the motion of the structural elements which are in contact with the soil. This is handled by an empirical procedure in which the load is computed independently of the motion of the structural element. However, the mass of the element in contact with the soil is increased by the amount of the mass of the soil adjacent to the structure, but of a thickness not

Figure 3.68. Local drag coefficients for spherical dome, $R_e > 10^5$

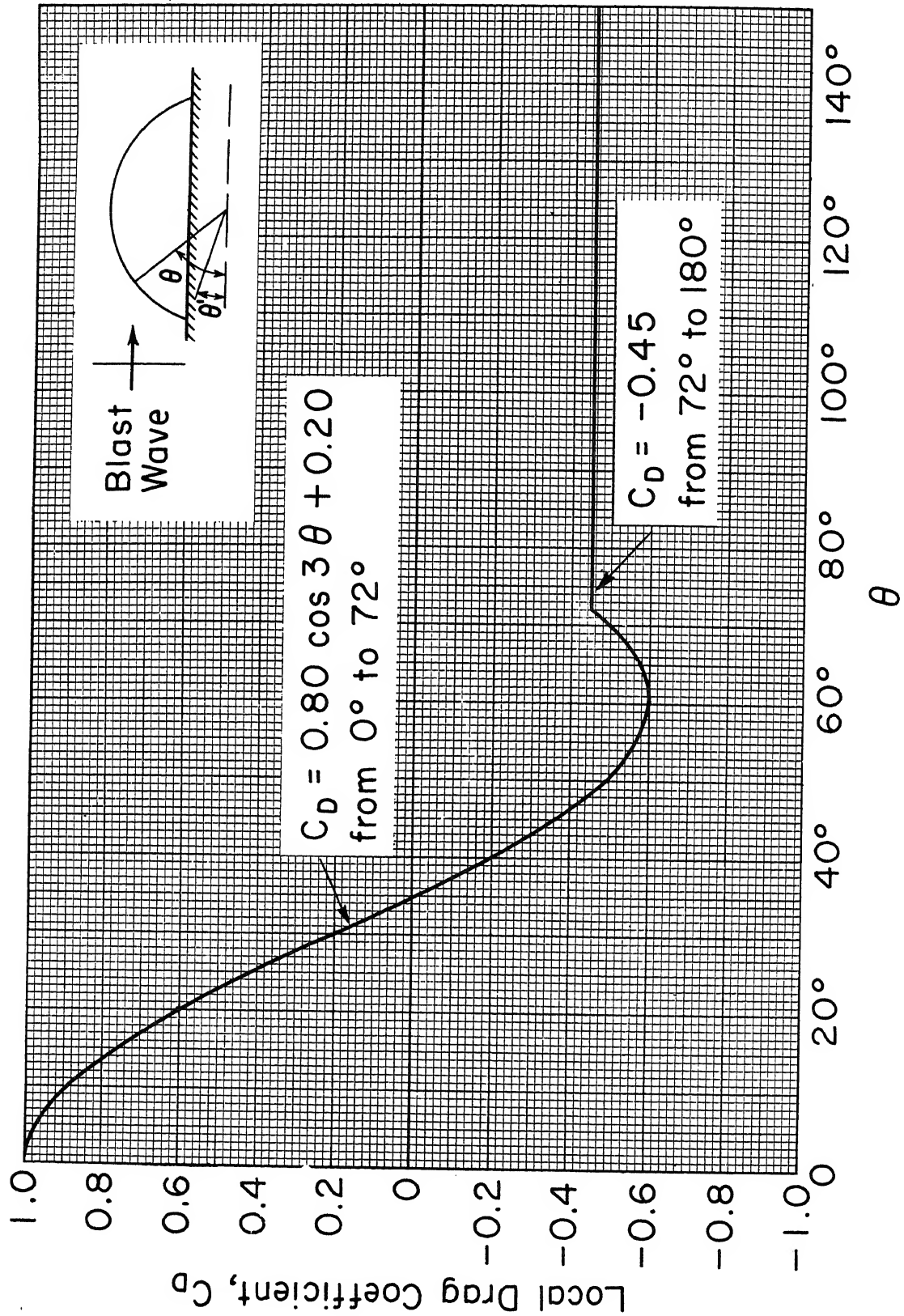


Figure 3.69. Local drag coefficients for spherical dome, $R_e < 10^5$

to exceed the span of the element. Other factors which complicate the situation are "arching action" and wide variations in the density, moisture content, and seismic velocity of the soil with depth and location which affect the transmission of pressure waves through the ground. The treatment below, which neglects "dynamic arching," is largely substantiated by the conclusions of reference [46].

An air blast wave impinging upon the surface of the ground induces underground overpressures of a magnitude approximately equal to the blast wave overpressure at shallow depths of 5 to 20 ft [30] in the ground below which cause earth overpressures on the sides, roof, and bottom of buried structures. The pressure wave thus induced in the ground is propagated at the velocity C_s , the seismic wave velocity in ground (see table 3.3). If the ground surface above the buried structures is located in the region of

Table 3.3. Soil Factors

Soil Type	Soil Weight (lb/ft ³)	C_s , Seismic Velocity (fps)		k, Soil Pressure Factor (Eq (3.40))	
		Min	Max	Min	Max
Top soil (light dry)	85	600	900	262	590
Top soil (moist, loamy silt)	95	1,000	1,300	812	1,370
Top soil (clayey)	100	1,300	2,000	1,420	3,370
Top soil (semiconsolidated sandy clay)	110	1,250	2,150	1,510	4,150
Wet loam	105	-	2,500	-	5,600
Clay (dense wet, depending on depth)	115	3,000	5,900	8,850	34,100
Rubble or gravel	-	1,970	2,600	6,400	11,100
Cemented sand	145	2,800	3,200	9,700	12,600
Water-saturated sand	125	-	4,600	-	22,500
Sand	145	4,600	8,400	26,200	87,000
Sand clay	110	3,200	3,800	10,000	13,900
Cemented sand clay	145	3,800	4,200	17,800	21,700
Clay, clayey sandstone	150	-	5,900	-	45,000
Loose rock talus	130	1,250	2,500	1,750	7,000
Weather-fractured rock	160	1,500	10,000	3,100	140,000
Weather-fractured shale	150	7,000	11,000	63,000	156,000
Weather-fractured sandstone	160	4,250	9,000	23,500	116,000
Granite (slightly seamed)	170	-	10,500	-	160,000
Limestone (massive)	170	16,400	20,200	390,000	590,000

regular reflection, the air blast wave will intersect the ground at an acute angle, which is assumed equal to zero for computational purposes. The induced ground pressure wave front is then horizontal, and moves downward through the soil and past the structure with a vertical velocity C_s .

On the other hand, if the ground surface above the structure is located in the region of Mach reflection, the air shock wave travels parallel to the surface of the ground, and the induced ground pressure wave is assumed to behave as illustrated in figure 3.70. The leading portion of the ground pressure wave is inclined downward at the angle γ , whose sine is C_s/U_o , with the surface of the ground from the intersection of the air shock front with the ground surface. Although in many cases C_s will exceed U_o , it is recommended for computation that the angle of inclination of the ground pressure wave with the earth's surface not exceed 90° which corresponds to the case where $C_s = U_o$. As the ground pressure wave impinges on a buried structure, it first loads the upper front corner and proceeds horizontally across the roof with a velocity U_o in the direction of travel of the air shock wave and simultaneously proceeds vertically down the front side of the structure with a velocity $U_o \times \tan \gamma$. After the ground pressure wave has traveled the length of the roof, it proceeds down the rear side again at velocity $U_o \times \tan \gamma$.

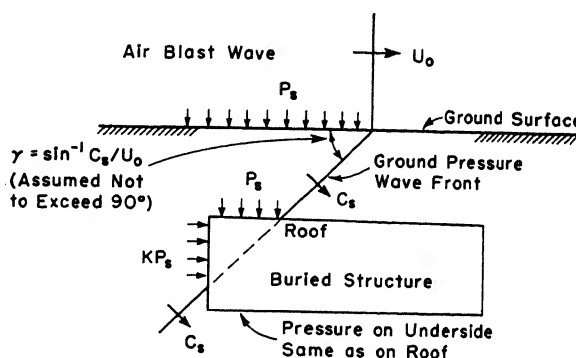


Figure 3.70. Ground pressure wave induced by air blast wave in region of Mach reflection

When the buried structure is located in either the region of regular or Mach reflection, the local overpressure on the roof is approximately equal to the overpressure of the air blast wave on the earth's surface P_s since apparently no appreciable reflection occurs on the surfaces of a buried structure. The lateral overpressure on the vertical sides of a buried structure may be considerably less than the pressures applied at the top surface of the soil depending upon the type of soil and the height of the water table. A value of $0.15P_s$ has been measured in tests at Nevada [46] where the soil was a dry silty clay. Static tests on soils have

demonstrated that the lateral at-rest earth pressure varies from 0.4 to 0.5 of the vertical earth pressure in sandy or granular soils and may become as large as the vertical earth pressure for soft clay soils because of a phenomena called plastic flow [43, 44, and 45]. For the type of dynamic loading contemplated here, dry clay soils will probably behave similar to granular soils because the load will not persist for a sufficient length of time to permit the occurrence of plastic flow. However, it is believed that wet clay soils would behave like a viscous fluid and transmit lateral pressures instantaneously. For design purposes, it is recommended that the lateral overpressure on vertical surfaces of buried structures be taken as KP_s , where K can be evaluated as follows:

$K = 0.25$ for dry cohesionless soils

$K = 0.50$ for medium cohesive soils

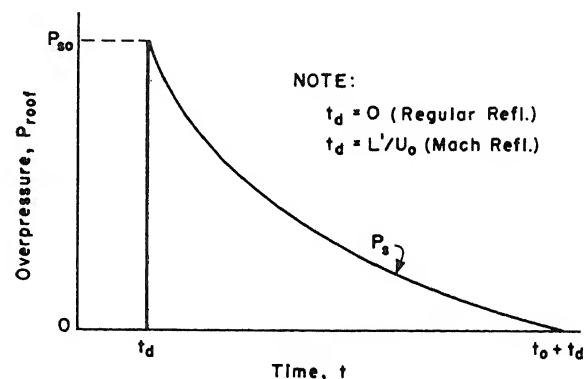
$K = 0.75$ for soft cohesive soils

$K = 1.00$ below water table

a. Local Roof Overpressure P_{roof} . Regular Reflection Region: The local roof overpressure or overpressure at a given point on the roof is equal to the air blast wave overpressure on the ground surface P_s with $t_d = 0$, and where time t is zero when the ground pressure wave strikes the roof of the structure.

Mach Reflection Region: The local roof overpressure is equal to the air blast wave overpressure on the ground surface P_s with $t_d = L'/U_o$ where time t is zero at the instant the ground pressure wave strikes the upper front corner of the structure.

L' is the distance from the point on the roof where the pressure is wanted to the upper front corner of the structure, and U_o is the air shock front velocity. The overpressure-time curve is illustrated in figure 3.71.



b. Average Roof Overpressure \bar{P}_{roof} . Regular Reflection Region: Average roof overpressure is

Figure 3.71. Local roof overpressure vs time for buried structure located in regions of regular and Mach reflection

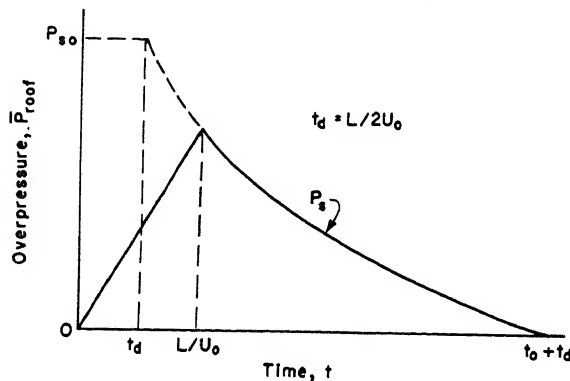


Figure 3.72. Average roof overpressure vs time for buried structure located in region of Mach reflection

identical with local roof overpressure.

Mach Reflection Region: The average roof overpressure is illustrated in figure 3.72. The overpressure rises linearly from zero at time $t = 0$ to P_s , the local overpressure existing at the center of the roof, at time $t = L/U_0$, where $t_d = L/2U_0$ and $L =$ length of roof in direction of travel of

air shock wave.

c. Local Front and Back Wall

Overpressures P_{front} and P_{back} .

Regular Reflection Region: The local front and back wall overpressures are equal to KP_s . The time-displacement factor is $t_d = h'/U_0 \tan \gamma$ where h' is the vertical distance from the roof to the point under consideration. The overpressure-time curve is illustrated in figure 3.73.

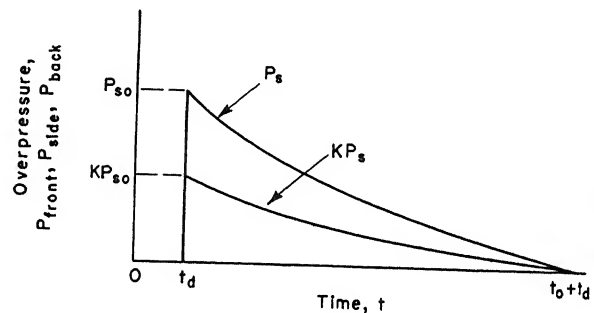


Figure 3.73. Local front wall, back wall, and side wall overpressure vs time for buried structure located in regions of regular and Mach reflection

Mach Reflection Region: The local front and rear wall overpressures are equal to KP_s . The time-displacement factor is $t_d = h'/U_0 \tan \gamma$ for the front face and $t_d = L/U_0 + h'/U_0 \tan \gamma$ for the rear face where h'

and L are as defined above. The overpressure-time curve is illustrated in figure 3.73.

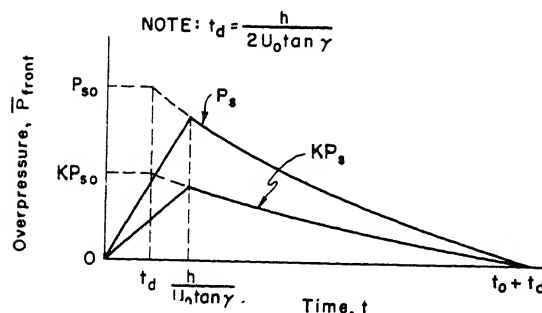


Figure 3.74. Average front wall overpressure vs time for buried structure located in regions of regular and Mach reflection

d. Average Front Wall Overpressure \bar{P}_{front}

Regular Reflection Region: The average front wall overpressure is illustrated in figure 3.74. The overpressure rises linearly from zero at time $t = 0$ to KP_s at

$t = h/U_o \tan \gamma$, where $t_d = h/2U_o \tan \gamma$ and h is the height of the front wall of the structure.

Mach Reflection Region: The average front wall overpressure is illustrated in figure 3.74. The overpressure rises linearly from zero at time $t = 0$ to KP_s at $t = h/U_o \tan \gamma$, where $t_d = h/2U_o \tan \gamma$.

e. Average Back Wall Overpressure \bar{P}_{back} . **Regular Reflection Region:** The average back wall overpressure is identical with the average front face overpressure.

Mach Reflection Region: The average back wall overpressure is illustrated in figure 3.75. The overpressure rises linearly from zero at time $t = L/U_o$ to KP_s at time $t = L/U_o + h/U_o \tan \gamma$.

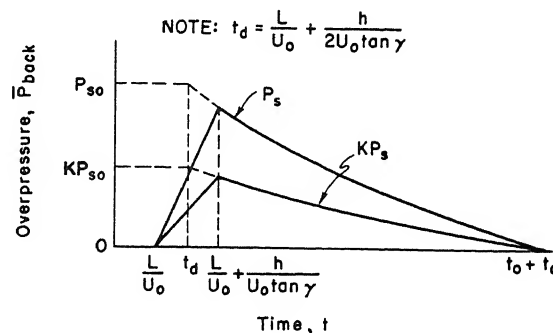


Figure 3.75. Average back wall overpressure vs time for buried structure located in region of Mach reflection

f. Local Side Wall Overpressure P_{side} . **Regular Reflection Region:** The local side wall overpressure is identical with the local front and rear wall overpressures.

Mach Reflection Region: The local side wall overpressure is obtained in a similar manner as that for the front and rear wall local overpressures. The time-displacement factor is $t_d = L'/U_o + h'/U_o \tan \gamma$ where L' is the horizontal distance from the upper front corner of the side wall and h' is the vertical distance from the upper front corner of the side wall to the point at which it is desired to obtain the overpressure. The local side wall overpressure vs time curve is illustrated in figure 3.73.

g. Average Side Wall Overpressure \bar{P}_{side} . **Regular Reflection Region:** The average side wall overpressure is identical with the average front face overpressure.

Mach Reflection Region: The average side wall overpressure is illustrated in figure 3.76. The overpressure rises linearly from zero at time $t = 0$ to KP_s at time $t = L/U_o + h/U_o \tan \gamma$, where $t_d = (L/U_o + h/U_o \tan \gamma)/2$.

h. Overpressure on Underside of Buried Structure. The conclusions

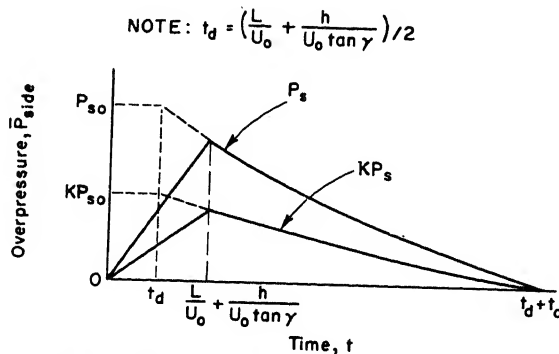


Figure 3.76. Average side wall overpressure vs time for buried structure in region of Mach reflection

reached in reference [52] indicate that the overpressures exerted on the underside of buried structures with an integral floor are of the same order of magnitude as the overpressures on the roof. Therefore, it is recommended that in both the regular and Mach reflection regions the bottom surface of buried structures with an integral floor be designed to

support the identical overpressures applied to the roof of the structure as given in paragraphs 3-21a and b.

3-22 PROCEDURE FOR COMPUTATION OF LOADS ON BURIED STRUCTURES. Repeat Steps 1, 2, and 3 of paragraph 3-09.

Step 4. Determine U_o , knowing P_{so} , from figure 3.9.

Step 5. Determine t_d .

Step 6. Determine P_s from table 3.1 or figure 3.22.

Step 7. Plot the curves of overpressure vs time as illustrated in figures 3.71 to 3.76.

RADIATION

3-23 NUCLEAR RADIATION PHENOMENA. A characteristic of an atomic detonation is the emission of nuclear radiation. This represents approximately 15 per cent of the total energy of a typical air burst. It is expressed in terms of initial radiation and residual radiation.

Initial radiation is defined as the nuclear radiation which is derived directly from the initial fission and fusion reactions of the detonation. It is delivered within approximately the first half minute following detonation and its significant effects are confined to a radius of a few miles from the point of detonation.

Residual radiation applies to the radiation emitted after the first minute by the fission products, unfissioned residues, and to a limited extent by the bomb case fragments and materials such as dust in the air in

which radioactivity has been induced. Residual radioactivity, in the aggregate, is of an enduring nature; however, its intensity decreases by a process of natural radiation decay. The residual radiation produced by an air burst is usually dissipated in the upper atmosphere and does not therefore constitute a hazard on the ground. However, when a nuclear weapon is detonated at or near the ground level large amounts of the surface materials, such as earth or water, are drawn up into the cloud. Radioactive isotopes formed as described above become associated in various ways with these materials which, being considerably heavier than those resulting from an air burst, will fall back to the earth's surface in the local area; the heavier particles falling nearer to the point of detonation and the lighter materials settling out progressively farther downwind. The material so deposited is known as "fallout" and the areas on which it falls are said to be radiologically contaminated. With megaton yield weapons, fallout may extend several hundred miles downwind and cover five to six thousand square miles or more.

Fallout patterns are usually depicted as elongated and cigar shaped. Such a pattern would only be found under idealized conditions which seldom, if ever, would occur. The existence of complicated wind structures, as well as variations of these structures in time and space, may cause extreme distortions in the shape of the fallout pattern. In addition, intensities within the pattern may be extremely irregular.

Nuclear radiations consist of neutrons, gamma rays, beta particles, and alpha particles. The neutrons, which are subatomic particles of neutral charge, are released in the fission and fusion reactions and are produced essentially in the first half second after detonation. Gamma rays, which are high-energy electromagnetic radiations (like X rays), are emitted from the fireball as initial radiation and from fission products and from the capture of neutrons in bomb fragments and other materials as residual radiation. Beta particles, composed of high-speed electrons emitted by the radioactive fission products and alpha particles, identified as the nuclei of helium atoms, originate in the unfissioned residues of plutonium or uranium. Both the neutrons and gamma rays have a long range in air and are very penetrating. Substantial thicknesses of materials of

high density are required to reduce their intensity to harmless levels. In general, initial gamma radiation is more important than neutron radiation for large weapons. However, for weapons of small physical size, neutron and gamma radiation may be of equal significance, depending upon the characteristics of the shielding provided. Beta particles have a very short range in air and relatively little penetration capability. Beta emitters can damage human tissue when taken into the body, and in addition can cause serious burns if they come in contact with the skin. Alpha particles have an even shorter range in air and are stopped by almost any type of barrier. They are a hazard only if their emitters are taken into the body by inhalation, ingestion or, under limited circumstances, through breaks in the skin.

Gamma radiation dosage is measured in terms of a unit called the roentgen *r* which is a standard measure of the ionization caused by gamma rays in their passage through matter and hence of the injury which is caused to a body of living organisms. Initial gamma radiation is a function of weapon yield, air density, and the distance of the burst from the structure. Figure 3.77 gives the intensity of initial gamma radiation at any distance from ground zero for a surface burst.

Neutron radiation dosage, for the purpose of assessing radiation hazard, is measured in rem (roentgen equivalent - mammal) which is the amount of energy absorbed in mammalian tissue which is biologically equivalent in mammals to one roentgen of gamma or X rays. Neutron radiation is a function of the weapon yield, weapon design, air density, and the distance of the burst from the target. Figure 3.79a gives the intensity of neutron radiation at any distance from ground zero for surface burst of fission weapons. Figure 3.79b provides similar data for fusion weapons.

Nuclear radiation can produce a variety of harmful effects in living tissue which may be acute or delayed depending upon the total amount of radiation absorbed and the period of time within which it is received. When radiation is received within a short time (1 or 2 days), the effect is considered to be acute and, under most conditions, is essentially independent of dose rate. When dosage is received over a long period of time, either continuously or in repeated increments, partial recovery takes

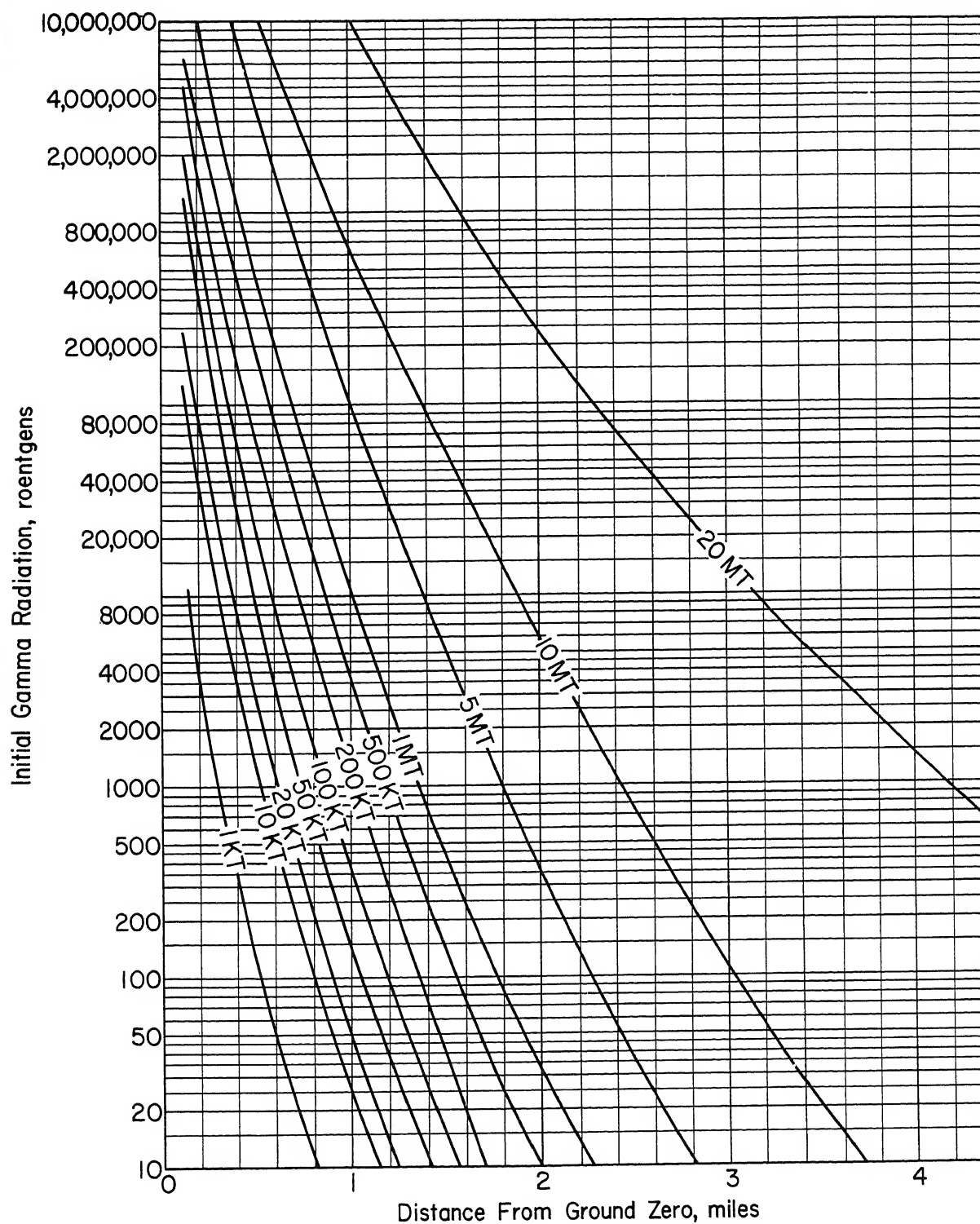


Figure 3.77. Initial gamma radiation, surface burst, 0.9 air density

place. Under these conditions of exposure, larger total doses can be tolerated insofar as early effects are concerned.

Ultimate body damage resulting from nuclear radiation is a summation of the several separate radiation effects involved. Thus, roentgens of gamma radiation received must be added to the roentgen equivalent dosage for man (rem) of neutron radiation received in order to obtain the total dose. The effects of different amounts of radiation received are shown in table 3.4.

A particular effect is associated with a range of doses rather than a specific dose. This does not necessarily mean that any dose within a given range will always result in the effect stated but rather that the dose required to cause the effect will fall somewhere within this range.

Table 3.4. Acute Effects of Whole Body Penetrating on Human Beings

Dose in 1 Week, rem	Effect
150	No acute effects, possible serious long-term hazard
150-250	Nausea and vomiting within 24 hours, normal incapacitation after 2 days
250-350	Nausea and vomiting in under 4 hours. Some mortality will occur 2 to 4 weeks. Symptom-free period 48 hours to 2 weeks
350-600	Nausea and vomiting under 2 hours. Mortality certain in 2 to 4 weeks. Incapacitation prolonged
600	Nausea and vomiting almost immediately. Mortality in 1 week

In the absence of directives which stipulate otherwise, it is recommended that protection provided be sufficient to reduce the combined initial gamma and neutron dose to not more than 50 rems. This will allow for possible later additional dosage received from fallout, within structures or outside during decontamination operations, or traversal through contaminated areas.

3-24 NUCLEAR RADIATION SHIELDING. An important consideration in the design of a protective structure is the provision of adequate shielding against the effects of nuclear radiation. In determining shielding

requirements, separate consideration must be given to initial radiation and residual radiation. However, ultimate body damage resulting from nuclear radiation is a summation of all of the separate radiation effects involved; namely, initial gamma, neutron, and residual gamma radiation.

a. Initial Radiation Shielding. The effectiveness of initial radiation shielding is a function of the composition and geometry of the shielding material, the energy distribution of the radiation at the target, the distance from the detonation source, the angle of incidence of the radiation, and in the case of neutrons, the configuration of the weapon. Initial gamma radiation transmission factors for concrete and earth are given in figure 3.78. Similar factors for neutrons are given in figure 3.80. The curves in these charts are based on the assumption that the radiation is essentially point source and is perpendicular to the slab of shielding material. The transmission factor is the ratio of the radiation dose received behind the shielding material to the dose which would have been received in the absence of the shield.

The factors which determine the effectiveness of an initial gamma shield are density and mass. The transmission factors of materials of known density other than concrete and earth may be estimated by interpolation on a density basis, between the curves shown in figure 3.78.

Neutron attenuation represents a more complex problem in which several different phenomena are involved. First, the fast neutrons must be slowed down into the moderately fast range; the moderately fast neutrons must then be slowed down into the slow or thermal range; following which the thermal neutrons must be absorbed. This absorption process, referred to as radiative capture, is accompanied by the emission of relatively high energy gamma rays which must be absorbed by the shielding medium. Figure 3.80 provides a rough approximation of the neutron attenuation capabilities of concrete and earth. More reliable data are not presently available but studies in this area are in process. Consequently, neutron attenuation data should be checked whenever neutron shielding criteria for specific projects are required.

The procedure for calculating the required shielding thickness for initial radiation is illustrated by the following example:

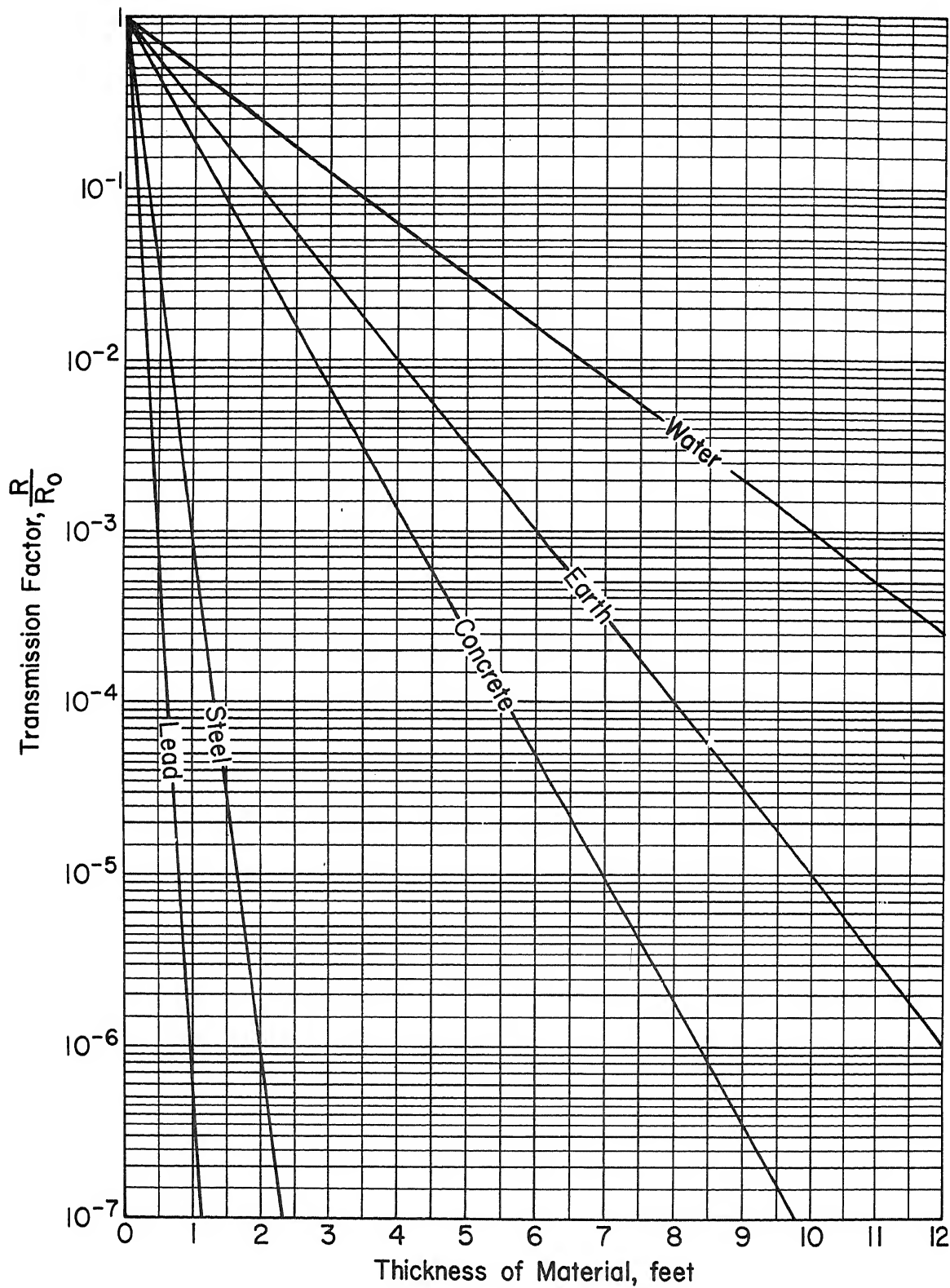


Figure 3.78. Attenuation of initial gamma radiation

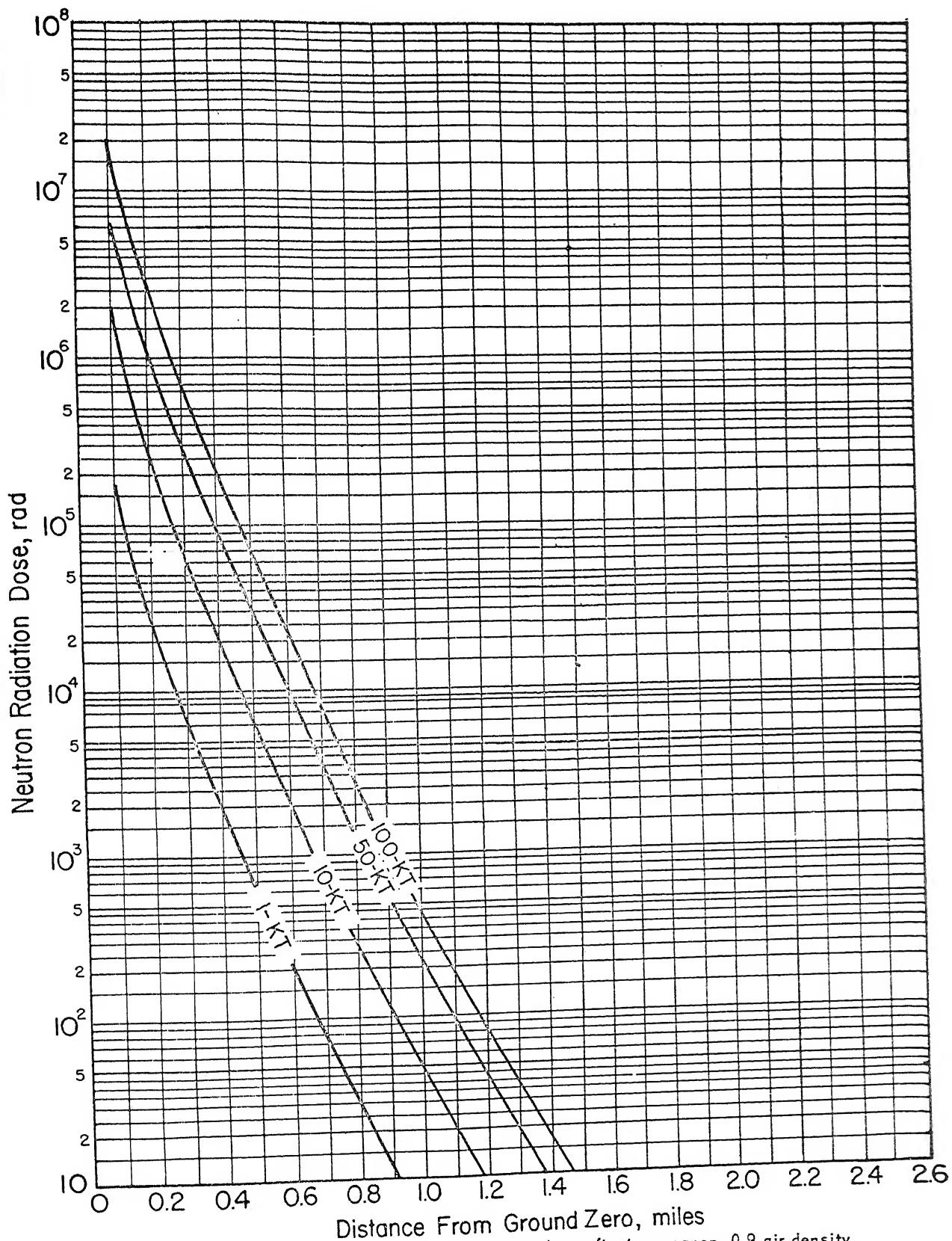


Figure 3.79a. Neutron radiation dose, surface burst, fission weapon, 0.9 air density.

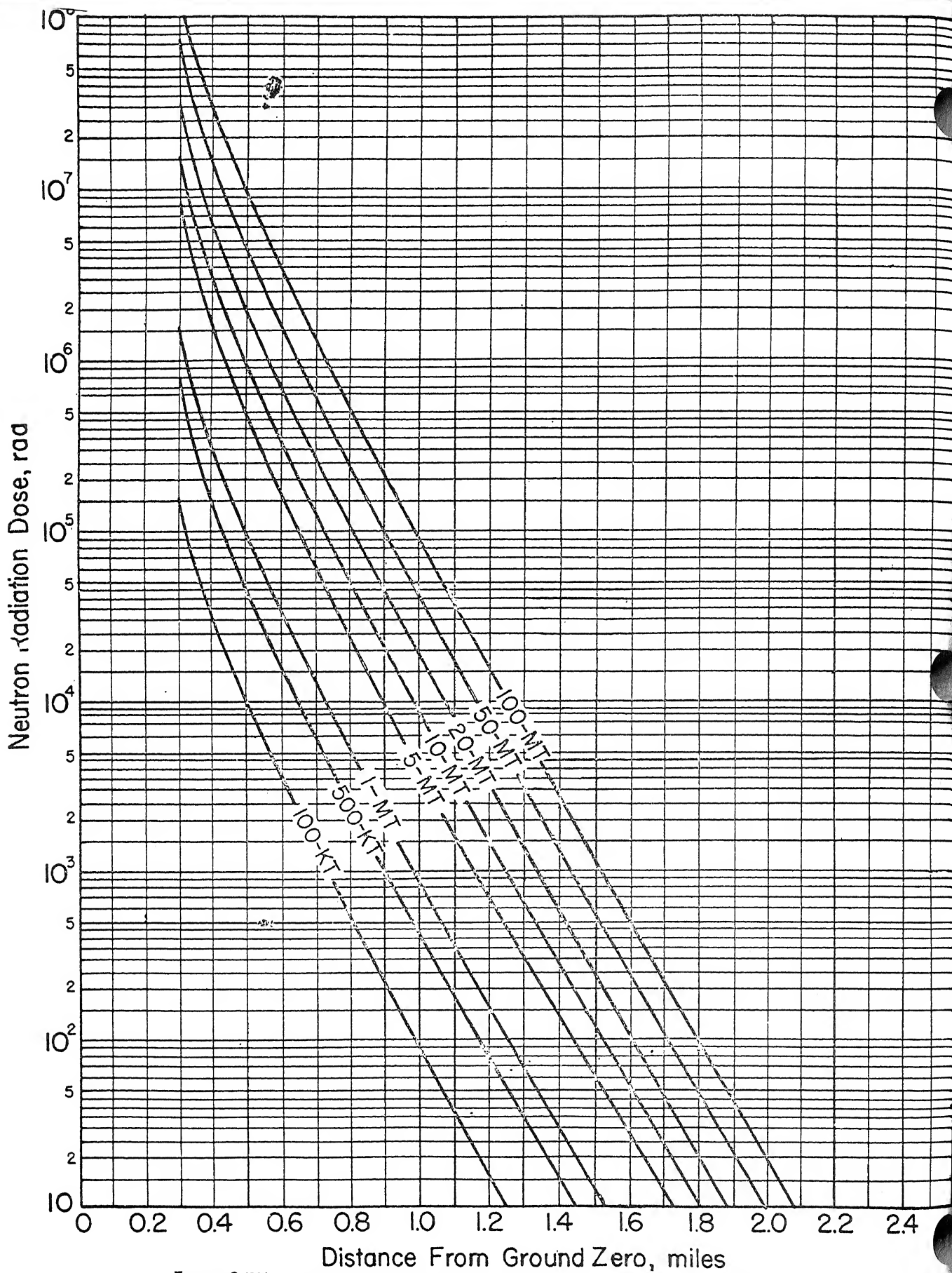


Figure 3.79b. Neutron radiation dose, surface burst, fusion weapon, 0.9 air density.

1 July 59

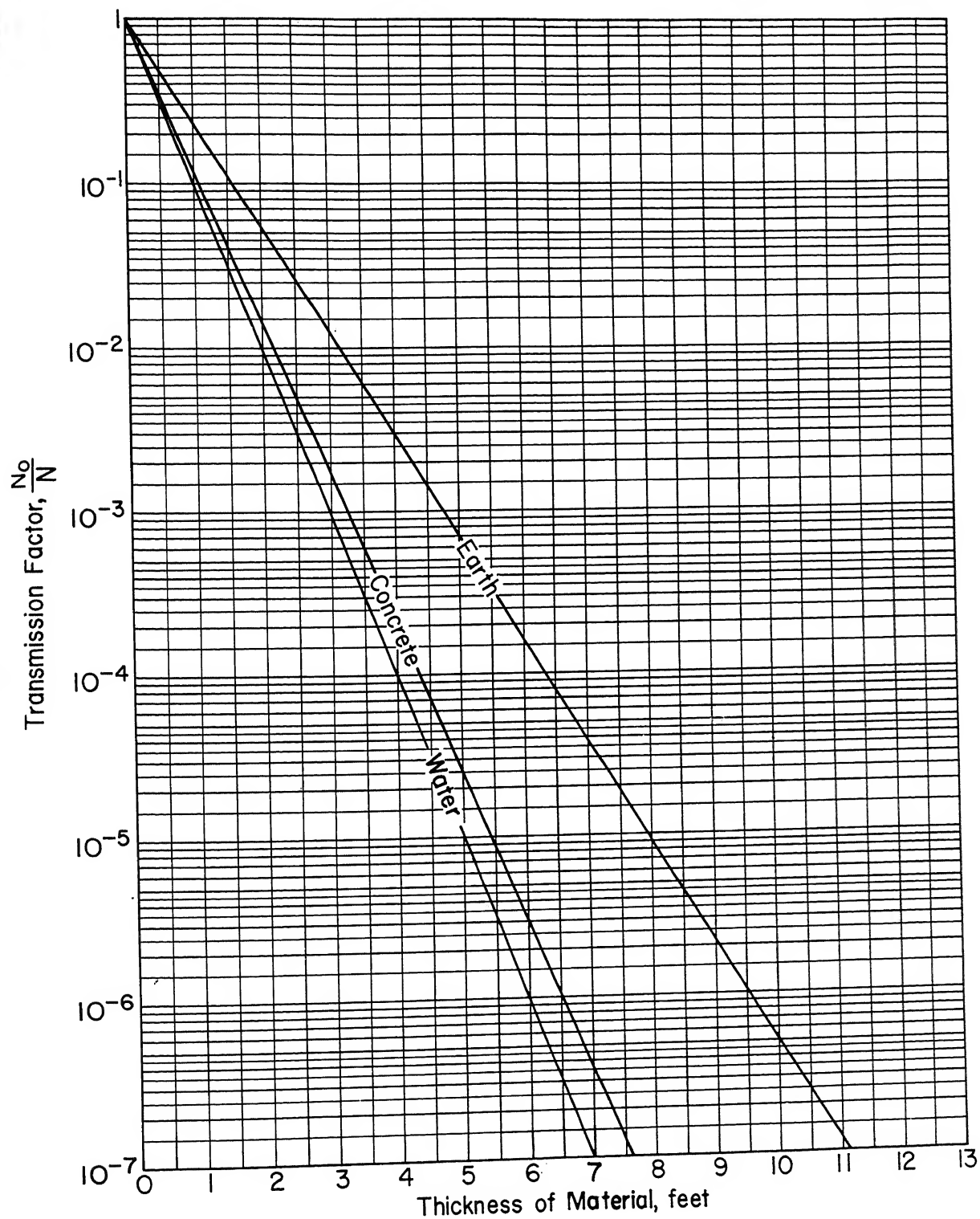


Figure 3.80. Attenuation of neutrons

Problem: A personnel structure is to be designed that will resist a 50-psi incident overpressure. A 12-in.-thick reinforced concrete roof will meet the structural requirement. Determine the earth cover needed to reduce the initial gamma and neutron radiation to an acceptable level of 50 rem. Consider a 100-KT surface burst at a distance that would produce the design overpressure.

The weapon effects data are:

100-KT Surface Burst

50-psi overpressure - distance from ground zero = 0.4 mile
(figure 3.12b)

0.4-mile distance - gamma = 70,000 r (figure 3.77)

0.4-mile distance - neutrons = 100,000 rem (figure 3.79a)

Procedure: From figures 3.78 and 3.80, the transmission value in feet, of concrete and trial thicknesses for the earth cover are found to be as follows:

	<u>12 in. of Concrete</u>	<u>4 ft of Earth</u>	<u>5 ft of Earth</u>
Gamma	0.19	0.01	0.003
Neutrons	0.12	0.003	0.0007

Try 4 ft of earth cover. The amount of radiation transmitted is:

Gamma:	12 in. of concrete, $70,000 \times 0.19$	= 13,300 r
Neutrons:	12 in. of concrete, $100,000 \text{ rem} \times 0.12$	= 12,000 rem
Gamma:	4 ft of earth, $13,300 \times 0.01$	= 133 r
Neutrons:	4 ft of earth, $12,000 \times 0.003$	= <u>36</u> rem
	Total transmitted	169 rem

This is greater than the maximum acceptable level of 50 rem. Try 5 ft of earth cover.

Gamma:	5 ft of earth, $13,300 \times 0.003$	= 39 r
Neutrons:	5 ft of earth, $12,000 \text{ rem} \times 0.0007$	= <u>8</u> rem
	Total transmitted	47 rem

Since this is less than the maximum allowable of 50 rem, 5 ft of earth cover is satisfactory.

b. Fallout Radiation Shielding. The problem of shielding from fallout radiation is different from that of direct radiation. The main differences are:

- (1) Radiation from fallout particles persists for a long period of time but at a delaying rate.
- (2) The radioactive particles are spread over large areas.
- (3) The radiation received at a point on the ground comes partly from the plane area source and partly from scattered radiations or "skyshine."
- (4) The energy of the radiation from fallout is much lower than the initial gamma radiation.

Due to the above characteristics of fallout radiation, the calculation of shielding thicknesses is more complex than for direct radiation and must take into account the time factor and the height, shape, and size of the protected structure together with the location of the point of interest relative to the surrounding structure.

Data and design criteria are contained in references [36] and [49]. A detailed method for evaluating the protection afforded by existing buildings against fallout radiation is given in reference [50]. This method can be adapted for use in the design of shielding for protected areas in new structures.

3-25 THERMAL RADIATION. a. Phenomena. The temperatures in the fire ball of an atomic bomb detonation are very high (approximately 330 billion calories per kiloton), resulting in a large proportion of the energy being emitted as thermal radiation. The thermal energy reaching any particular point is a function of the distance from the detonation, the yield of the weapons, and the scattering and absorption caused by the atmosphere. The amount of atmospheric attenuation is a function of the visibility, or the horizontal distance at which large dark objects can be seen against the sky at the horizon. The principal characteristics of thermal radiation are that it:

- (1) Travels with the speed of light (186,000 miles per second).
- (2) Travels in a straight line.
- (3) Has very little penetrating power.
- (4) Can be easily absorbed or attenuated.
- (5) Can be scattered.
- (6) Can be reflected.

In view of its speed of travel, the time of arrival at a target is almost instantaneous with respect to the detonation. The integrated total thermal energy delivered per unit area is plotted in figures 3.81 and 3.82 as a function of distance from the point of burst for a clear atmosphere (visibility 10 miles). Intensity of thermal radiation falling on any surface is reduced in proportion to the cosine of the angle that the surface makes with one which would be perpendicular to the incidence of radiation. Thus, the intensity on a surface 45 degrees from the perpendicular would be about 70 per cent of that on a comparable perpendicular surface.

b. Scaling. If two atomic bombs with total energy yields of W_1 and W_2 are exploded, the proportion of the total energy emitted as thermal radiation is approximately the same for each weapon, therefore, the thermal radiation energy is proportional to the yield. At a given distance from the detonation the total amount of radiant energy on a unit area is also proportional to the yield and is shown by the expression

$$Q_2/Q_1 = W_2/W_1 \quad (3.36)$$

where Q_1 and Q_2 are the radiant energy on a unit area for the two weapons.

c. Effect on Materials. A surface exposed to thermal radiation will absorb part and reflect part of this radiation. The amount of the absorption depends on the material and especially upon its color, as the darker colored materials will absorb a much larger proportion than light colored materials. The absorption causes the temperature to rise, and damaging effects may result.

The most important physical effects of the high temperatures due to the absorption of thermal radiation are, of course, charring or ignition of combustible materials and the burning of skin. It is very difficult to establish definite conditions under which these effects will or will not occur, and their extent; however, for convenience, it is found necessary to use total energy per unit area criterion.

Table 3.5 gives data relative to critical heat energies which produce various effects on construction material, surrounding foliage, and exposed

1 July 59

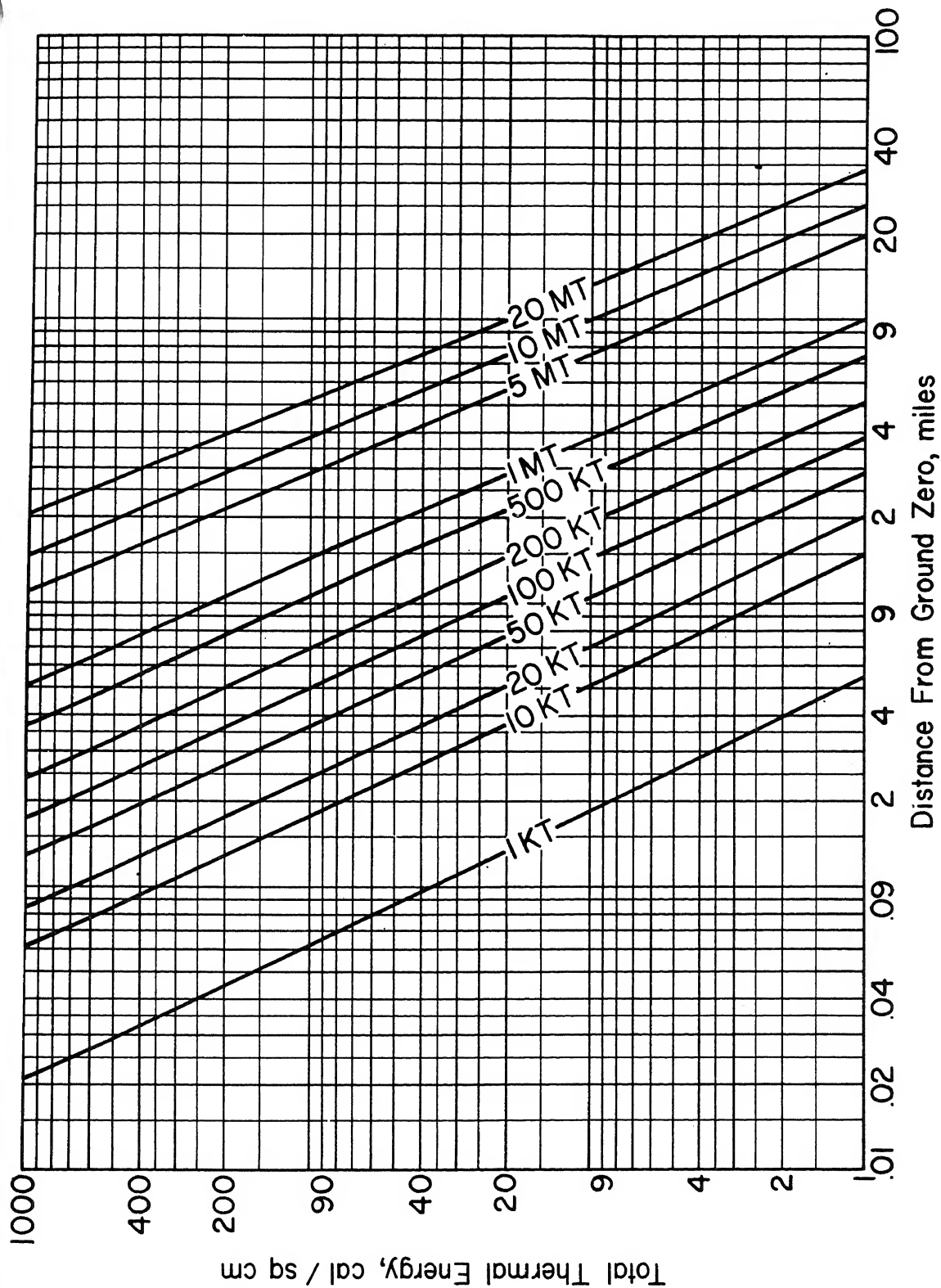


Figure 3.81. Total thermal energy, surface burst, 10-mile visibility

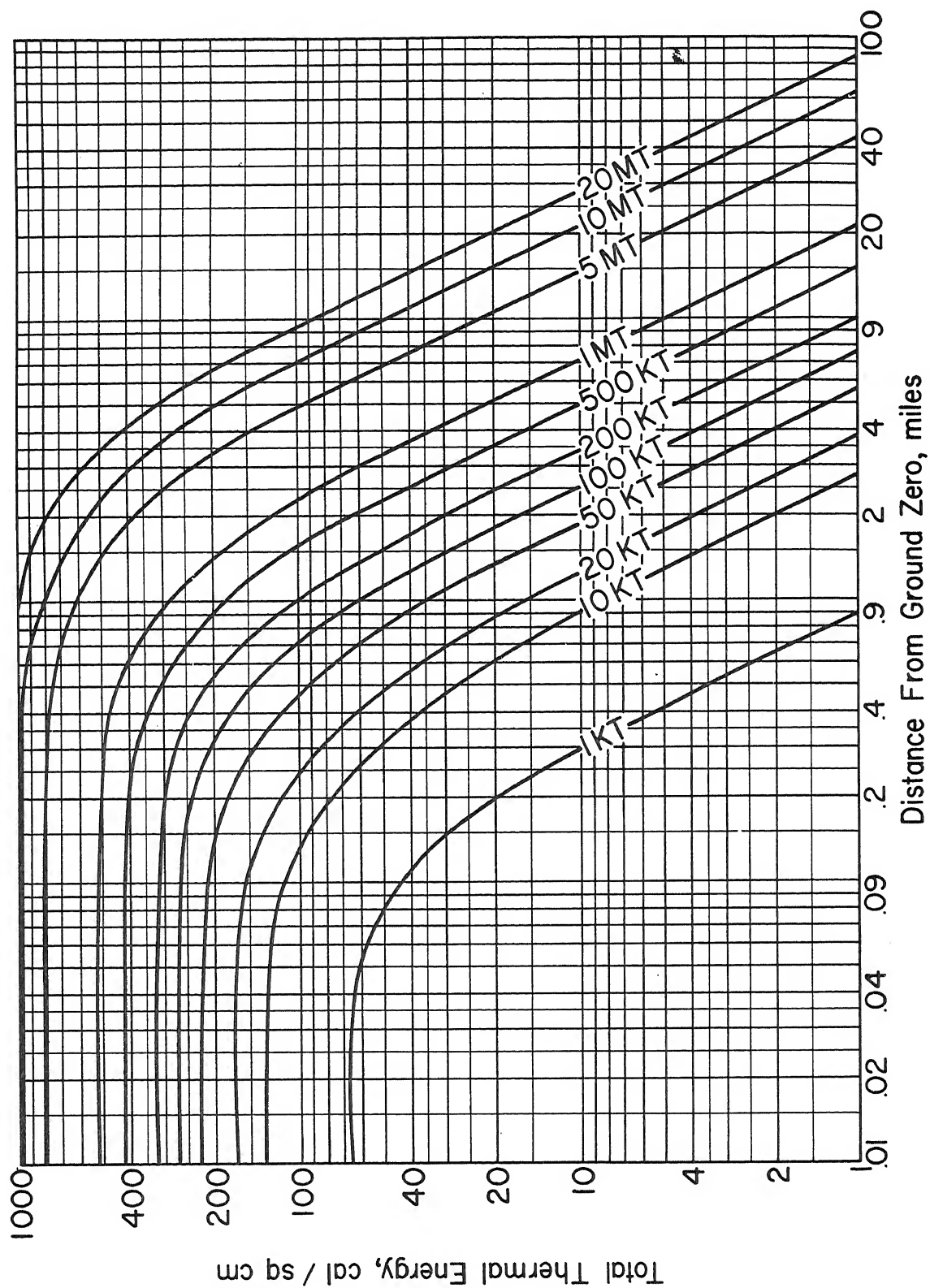


Figure 3.82. Total thermal energy, typical airburst, height = $650 W^{1/3}$, 10-mile visibility

1 July 59

Table 3.5. Critical Thermal Energies, Construction Materials

Material	Type	Damage	Energy, cal/sq cm	
			100 KT	10 MT
Glass	Ordinary window	Highly resistant to heat but brittle and will break at low blast pressures (see reinforced glass)		
Glass reinforced with plastic (shatterproof)	Bakelite, cellulose acetate, lucite, Plexiglas	Surface melts and darkens	70	126
Plastics	USAF window 1/2 in. thick	Dense smoking and flames	430	750
Sand	Siliceous	Explodes (popcorns)	19	35
Sandbags	Cotton canvas filled	Chars, bags fail	18	32
Fiberboard	Corrugated and/or laminated	Flames during explosion	10	18
Plywood	Douglas fir	Flames during explosion	16	20
Wood	Unpainted planks, Douglas fir	Deep charring	18	32
Siding steel, corrugated	28 gage +	Not affected	107	--
Siding-galbestos	22 gage	Flames during explosion	14	28
Electric wire, rubber insulated	12-2-600v	Flames during explosion	13	26
BX armored wire	600v	Not affected up to	107	
Romax nonmetallic	19-2-600v	Charring	8	16
Roll roofing	Mineral surface	Flames during explosion	40	71
Roll roofing	Smooth surface	Flames during explosion	16	20
Grass	Dry	Flames during explosion	7	16
Leaves	Dry fallen	Flames during explosion	5	10

elements of structures. It will be noted that more heat energy is required from the larger weapon than the smaller one to produce the same effect. This is due to the length of the delivery time, which means that in order to produce the same thermal effect in a given material, the total amount of thermal energy (per unit area) received must be larger for a nuclear explosion of high yield than for one of lower yield, because the total energy is delivered over a longer period of time.

Although a serious hazard, injury and damage from thermal radiation can be more easily avoided than can some of the other damaging effects of atomic weapons. Shelter behind any object which will prevent direct exposure to rays from the detonation is sufficient protection. A wall or any other screening object, even clothing, will provide a shield from thermal radiation.

CRATERING

3-26 CRATERING PHENOMENA. When an atomic bomb is detonated near the surface of the ground, a crater is formed in the ground under the explosion as shown in figure 3.83. Two zones of disturbance in the soil around the crater are distinguishable. One, the rupture zone wherein the soil has

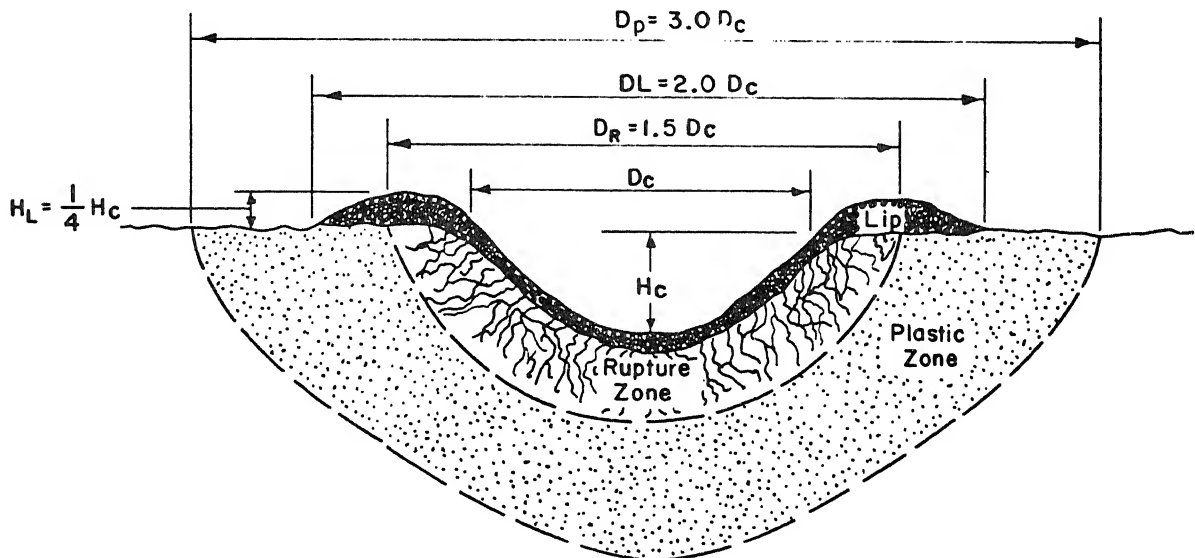


Figure 3.83. Typical crater

been violently ruptured, the other, the plastic zone wherein the soil has been permanently deformed but without visible rupture. If the material consists of rock there will be a rupture zone but little or no plastic zone. Some of the material thrown out of the crater falls back to form a lip around the edge. The height of the lip and the extent of the rupture and plastic zones are functions of the crater diameter and depths, as indicated in figure 3.83.

The limits of the rupture zone represent the closest distance to a cratering explosion at which it is feasible to construct a resistant structure. Due to the detrimental effects of the material thrown out of the crater, the high ground accelerations and displacements, and the high intensity of the blast pressures and radioactivity, it is not considered practicable to design protected structures to resist the effects within the radius of the crater lip or within approximately twice the crater radius. At distances greater than this, the pressure exerted on buried structures by the directly transmitted ground shock is less than the earth pressure caused by the air blast wave. Although the directly transmitted ground shock is initially of higher magnitude than the air blast wave, it is attenuated at a greater rate than the air blast.

The depth and diameter of the crater depend upon the characteristics of the soil and upon the energy yield of the explosion as given by figure 3.84.

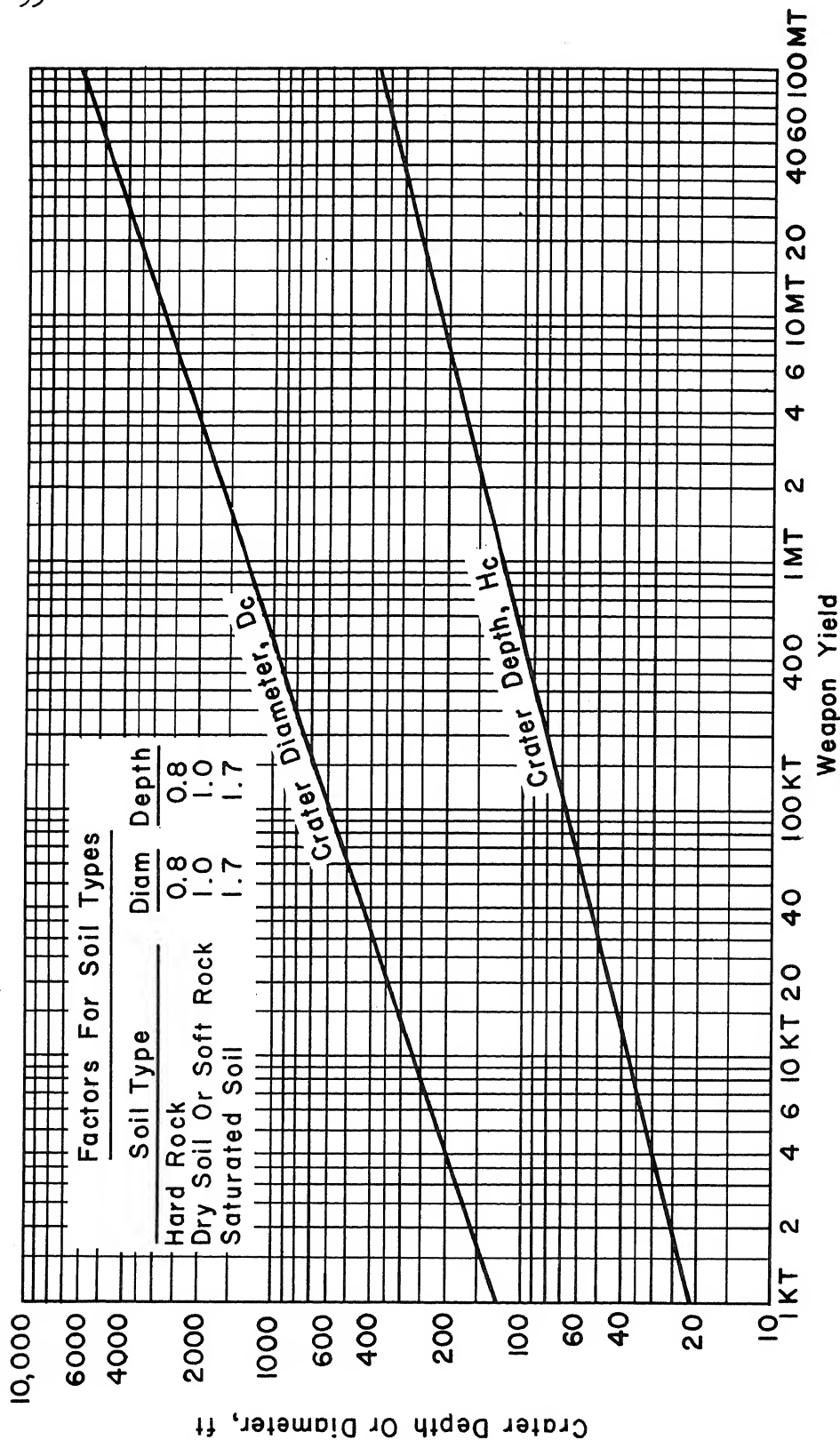


Figure 3.84. Crater diameter and depth for a surface burst. (Apply factors given above for different soil types)

BIBLIOGRAPHY

1. Feigen, M. Air Blast Pressures on a Cantilever Wall. Los Angeles, California: University of California, December 1951.
2. Operation GREENHOUSE, Project 3.3, Vol. I, Pressures and Displacements, Appendix G. Chicago, Illinois: Armour Research Foundation of Illinois Institute of Technology, May 1952. SECRET.
3. Merritt, M. L. Some Preliminary Results of a Study of Diffraction Around Structures at GREENHOUSE. Albuquerque, New Mexico: Sandia Corporation, September 1951. CONFIDENTIAL, RESTRICTED DATA.
4. Bleakney, W. Shock Loading of Rectangular Structures. Technical Report II-11. Princeton, New Jersey: Princeton University, Department of Physics, January 10, 1952.
5. Vortman, L. S. A Procedure for Predicting Two-Dimensional Blast Loading on Structures. Albuquerque, New Mexico: Sandia Corporation, October 1952. CONFIDENTIAL, Specified Distribution only.
6. Penzien, J. Experimental Investigation of the Blast Loading on an Idealized Structure. Albuquerque, New Mexico: Sandia Corporation, December 1951. RESTRICTED.
7. Merritt, M. L. Some Tests on the Diffraction of Blast Waves. Albuquerque, New Mexico: Sandia Corporation, June 1951.
8. Operation GREENHOUSE, Project 3.3, Vol. I, Final Report, Appendix I. Chicago, Illinois: Armour Research Foundation of Illinois Institute of Technology, May 1952. SECRET.
9. Bleakney, W. Rectangular Block, Diffraction of a Shock Wave Around an Obstacle. Princeton, New Jersey: Princeton University, Department of Physics, December 7, 1949.
10. Bleakney, W. The Diffraction of Shock Waves Around Obstacles and the Transient Loading of Structures. Technical Report II-3. Princeton, New Jersey: Princeton University, Department of Physics, March 16, 1950.
11. White, D. R., Weimer, D. K., and Bleakney, W. The Diffraction of Shock Waves Around Obstacles and the Transient Loading of Structures. Technical Report II-6. Princeton, New Jersey: Princeton University, Department of Physics, August 1, 1950.
12. Duff, R. E., and Hollyer, R. N. The Effect of Wall Boundary Layer on the Diffraction of Shock Waves Around Cylindrical and Rectangular Obstacles. Ann Arbor, Michigan: University of Michigan, June 21, 1950.
13. Uhlenbeck, G. Diffraction of Shock Waves Around Various Obstacles. Ann Arbor, Michigan: Engineering Research Institute, University of Michigan, March 21, 1950.
14. White, M. P. Blast Loads on Resistant Rectangular Structures Without Openings. Amherst, Massachusetts: Mimeographed Report, July 21, 1952. CONFIDENTIAL.

15. Operation GREENHOUSE, Air Forces Structures Program, Appendix E, Vol. III. Chicago, Illinois: Armour Research Foundation of Illinois Institute of Technology, August 1951. CONFIDENTIAL.
16. Duff, R. E., and Hollyer, R. N. The Diffraction of Shock Waves Through Obstacles With Various Openings in Their Front and Back Surfaces. Report 50-3. Ann Arbor, Michigan: Engineering Research Institute, University of Michigan, November 1950.
17. Operation GREENHOUSE, Air Force Structures Program, Appendix E, Section I. Washington, D. C.: Armed Forces Special Weapons Project, March 1951. RESTRICTED.
18. Princeton University, Department of Physics. The Diffraction of a Shock Wave Around a Hollow Rectangular Block-Opening Facing Shock. Tentative Report. Princeton, New Jersey: Princeton University, October 26, 1950.
19. Perret, W. R. Operation BUSTER-JANGLE, Attenuation of Earth Pressures Induced by Air Blast. Albuquerque, New Mexico: Sandia Corporation, March 7, 1952. SECRET.
20. Smith, L. G. Photographic Investigation of the Reflection of Plane Shocks in Air. Office of Scientific Research and Development, Report No. 6271. Washington, D. C.: 1945.
21. Bleakney, W. and H. H. Taub, "Interaction of Shock Waves," Reviews of Modern Physics, Vol. 21, no. 4, (1949), pp 584-605.
22. Chien, N., and others. Wind Tunnel Studies of Pressure Distribution on Elementary Building Forms. Iowa City, Iowa: Institute of Hydraulic Research, State University of Iowa, 1951.
23. Howe, G. E., "Wind Pressure on Structures," Civil Engineering, Vol. 10, no. 3, (March, 1940), pp 149-152.
24. Massachusetts Institute of Technology, Department of Civil and Sanitary Engineering. Behavior of Truss Bridges Under Blast From an Atomic Bomb - Phase II, General Study of Truss Bridges. Cambridge, Massachusetts: July 1951. OFFICIAL USE ONLY.
25. Pagon, W. Watters, "Aerodynamics and the Civil Engineer," Engineering News-Record, series of eight articles, Vols. 112-115, (March 15, 1934 to October 31, 1935).
26. Lindsey, Walter E., "Drag of Cylinders of Simple Shape," National Advisory Committee for Aeronautics, Report, 619, 1937.
27. Rouse, H. Fluid Mechanics for Hydraulic Engineers. New York, New York: McGraw-Hill Book Company, Inc., 1938.
28. Am. Society of Civil Engineers, Subcommittee on Wind Bracing, "Wind Bracing in Steel Buildings," ASCE, Proceedings, Vol. 62, no. 3, (March 1936), pp 397-412.
29. Rouse, Hunter, ed., Engineering Hydraulics, New York, John Wiley and Sons, inc., (1950).

1 July 59

Bibliography

30. Perret, W. R. Operation TUMBLER-SNAPPER - Earth Stresses and Earth Strains. Albuquerque, New Mexico: Sandia Corporation, September 15, 1952. CONFIDENTIAL.
31. Bingham, H. H., Weimer, D. K., and Griffith, W. The Cylinder and Semi-Cylinder in Subsonic Flow. Technical Report II-13. Princeton, New Jersey: Princeton University, Department of Physics, July 1952.
32. Normal Reflection of Shock Waves, Explosives Research Report No. 6. Washington, D. C.: Bureau of Ordnance, Department of the Navy.
33. Chandrasekhar, S. On the Decay of Plane Shock Waves. Report No. 423. Aberdeen, Maryland: Ballistics Research Laboratory, Aberdeen Proving Ground, November 8, 1943.
34. Pressure Profiles, a series of five reports which are a reduction of the data in references 10, 11, and 18. Chicago, Illinois: Armour Research Foundation of Illinois Institute of Technology.
35. Chandrasekhar, S. The Normal Reflection of a Blast Wave. Report No. 439. Aberdeen, Maryland: Ballistics Research Laboratory, Aberdeen Proving Ground, December 20, 1943. RESTRICTED.
36. Department of the Army, Pamphlet No. 39-3. The Effects of Nuclear Weapons. Washington, D. C.: U. S. Government Printing Office, May 1957. SECRET.
37. Howard, W. J., and Jones, R. D. Free Air Pressure Measurements for Operation JANGLE by Project 1.4. Albuquerque, New Mexico: Sandia Corporation, February 19, 1952. SECRET, Restricted Data.
38. Armed Forces Special Weapons Project, Operation JANGLE: Summary Report: Weapons Effects Tests. Washington, D. C.: November 1952. SECRET, Restricted Data.
39. Armed Forces Special Weapons Project, Operation JANGLE: Weapons Effects Tests. Preliminary Report. Washington, D. C.: SECRET, Restricted Data.
40. Murphey, B. F. Operation TUMBLER-SNAPPER: Air Shock Pressure-Time vs Distance. Albuquerque, New Mexico: Sandia Corporation, August 1, 1952. SECRET, Restricted Data.
41. Murphey, B. F. Operation BUSTER-JANGLE, Some Measurements of Over-pressure-Time vs Distance for Air Burst Bombs. Albuquerque, New Mexico: Sandia Corporation, March 4, 1952. SECRET, Restricted Data.
42. Gowen and Rerhins, "Drag of Circular Cylinders for a Wide Range of Reynolds Numbers and Mach Numbers," National Advisory Committee for Aeronautics, Technical Note, 2960.
43. Terzaghi, Karl, "A Fundamental Fallacy in Earth Pressure Computation," Boston Society of Civil Engineers, Journal, Vol. 23, no. 6, (April 1936), pp 71-88.
44. Taylor, D. W. Fundamentals of Soil Mechanics. New York, New York: John Wiley and Sons, Inc., 1948.
45. Terzaghi, K., and Peck. Soil Mechanics in Engineering Practice. New York, New York: John Wiley and Sons, Inc., 1948.

EM 1110-345-413
1 July 59

Bibliography

46. Newmark and Sinnamon. Air Blast Effects on Underground Structures. Draft of Final Report, Project 3.8, Operation UPSHOT-KNOTHOLE. Chicago, Illinois: University of Illinois, January 1, 1954. SECRET.
47. Armed Forces Special Weapons Project, Operation BUSTER, Project 2.4-2, The Effect of Thermal Radiation on Materials. Washington, D. C.: 1952. SECRET, Restricted Data.
48. Modern Developments in Fluid Dynamics, High Speed Flow. Vol. II. Great Britain, Aeronautical Research Council, Fluid Motion Subcommittee, Oxford Press, 1953.
49. Departments of Army, Navy, and Air Force, Capabilities of Atomic Weapons. TM 23-200. Washington D. C.: November 1957, CONFIDENTIAL.
50. Departments of Army and Navy, Radiological Recovery of Fixed Military Installations. TM 3-225. Washington, D. C.: 16 April 1958.

FOR THE CHIEF OF ENGINEERS

W. P. LEBER
Colonel, Corps of Engineers
Executive

APPENDIX A

TRANSONIC DRAG PRESSURES

A-01 INTRODUCTION. This appendix is concerned with the calculation of nuclear blast pressures on aboveground earth-covered structures, such as shown in figure A.1, which will be applicable to pressure levels above 25 psig.

Blast loading on structures may be divided into two stages, i.e. the diffraction phase and the enveloped phase. When the pressure at the rear of the surface attains the value of the pressure in the blast wave, the diffraction process may be considered to have terminated, and subsequently, steady state conditions may be assumed to exist until the pressures have returned to the ambient value prevailing prior to the arrival of the blast wave. The dif-

fraction phase pressures on the surface of the earth cover may be computed by methods set forth in EM 1110-345-413 and EM 1110-345-420; however, little information is available concerning the enveloped phase pressures. The enveloped phase pressures consist of the incident pressures plus the dynamic pressures. This appendix presents a solution for obtaining the enveloped phase pressures on wedge-shaped earth covers similar to those shown in figure A.1. The pressures transmitted through the earth to the structure may be computed by methods described in EM 1110-345-413 and EM 1110-345-420

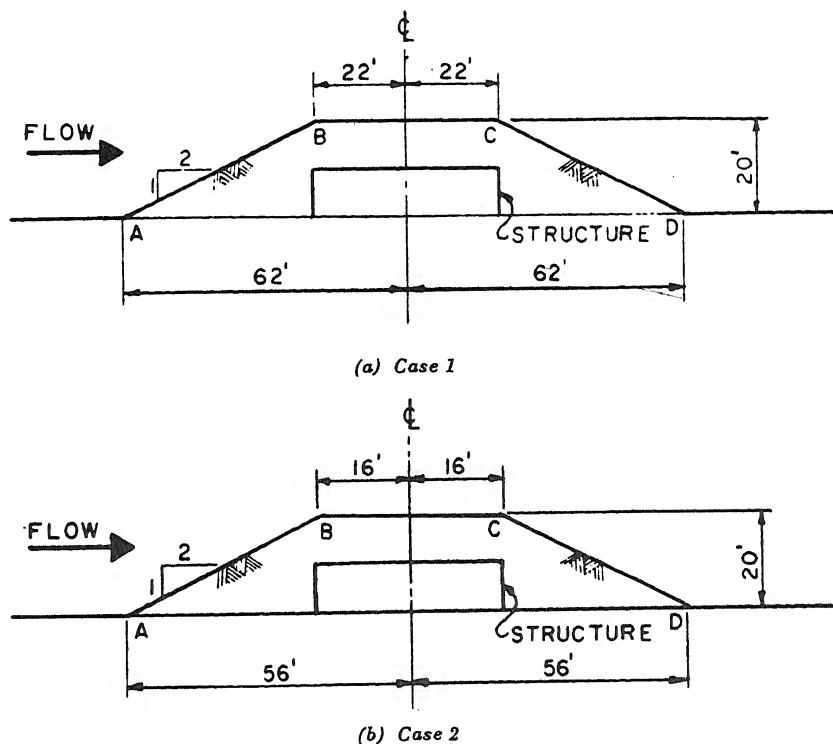


Figure A.1. Aboveground earth-covered structures

or by use of a Mohr's Circle Solution. The results are compared with the equivalent circle solution given in these manuals.

The flows considered are those behind the shock waves whose characteristics are given in table A.1.

Table A.1. Shock Wave Characteristics, 25 psig to 200 psig

Shock pressure, psig	25	50	100	200
Dynamic pressure, psig	12.2	41	123	330
Shock velocity, ft/sec	1756	2216	2927	3985
Sound velocity behind shock, ft/sec	1309	1447	1681	2064
Particle velocity behind shock, ft/sec	868	1375	2082	3059
Temperature at shock, deg Kelvin	379	467	636	968
Density at shock, $\rho \times 10^7$ lb/in. ³	871	1161	1526	1895
Mach number behind shock	0.664	0.951	1.239	1.481
Stagnation pressure behind shock, psia	53.5	116	294	766

The flows and the structures are considered two dimensional. This is conservative with respect to the pressures on the structure. The effect of the structures being finite in the direction perpendicular to the plane of figure A.1 is to reduce somewhat the pressures near the ends of the structure as compared to the pressures computed in the following paragraphs.

A-02 GENERAL FEATURES OF THE FLOW. The general features of the flow depend on the Mach number of the given conditions behind the original shock wave. The Mach number is the ratio of the particle velocity to the velocity of sound. When all parts of a flow have a Mach number less than one, the flow is called subsonic. If the Mach number is everywhere greater than one, the flow is called supersonic. If the Mach number is less than one in some places and greater than one in other parts of the same flow, it is called transonic. All of the combinations of initial flows and the geometries given fall in the transonic range for which both experiments and theory are, unfortunately, relatively scarce and complex.

In the subsonic case the usual concept of pressure coefficients C_p

to be multiplied by the dynamic pressure $1/2\rho V^2$ are applicable. Coefficients given for incompressible flow may be used with less than 1 percent error for Mach numbers from zero to 0.1. This covers the range intended for most wind load coefficients. From Mach numbers 0.1 to 0.5 the incompressible pressure coefficients may be used if first multiplied by $\frac{1}{\sqrt{1-M^2}}$. This is the Prandtl-Glauert rule. (See reference [A.2], p 139). For larger Mach numbers, more elaborate methods must be used.

In the supersonic case the flow pattern is illustrated in figure A.2.

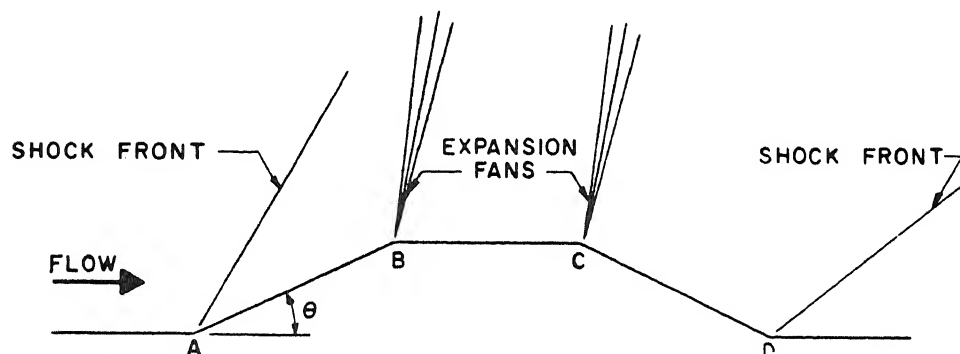


Figure A.2. Supersonic flow

On hitting the corner at A, the flow forms a shock wave which turns the oncoming flow abruptly, so it is parallel to AB. This causes a pressure rise. At B, the flow goes through a Prandtl-Meyer expansion fan which again turns the flow, this time with a pressure reduction. At C there is another expansion fan and then a compression shock wave at D returning the flow to its original direction. The changes of pressure, density, temperature, etc., at each shock and expansion can be conveniently figured using figures A.3 through A.5. The pressure is relatively constant on each of the faces AB, BC, and CD, being of course greatest on AB. The shock wave at A is called an attached shock wave because it starts right at A. As the Mach number decreases toward one, there will be a certain Mach number (figure A.6) at which the attached shock will no longer be possible for the given angle θ . Below this Mach number the shock wave is detached as shown in figure A.7 and the flow will be in the transonic range.

In the transonic flow shown in figure A.7, the flow is supersonic throughout except for the embedded subsonic region EFBAE. The initial

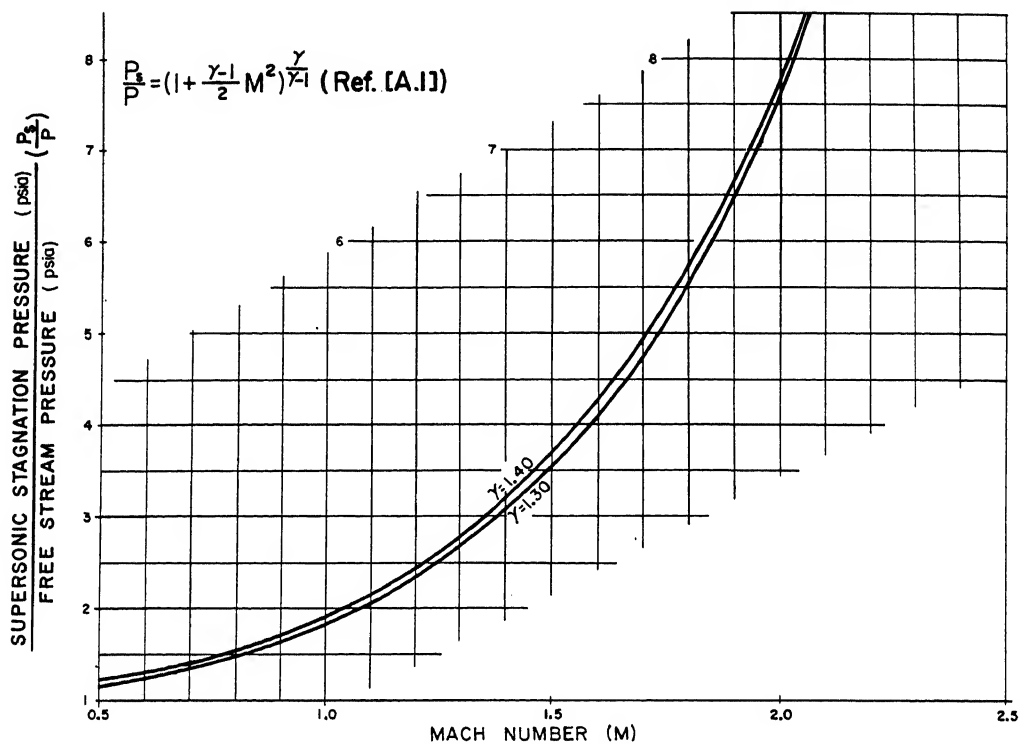


Figure A.3. Ratio of supersonic stagnation pressure to free stream pressure vs Mach number

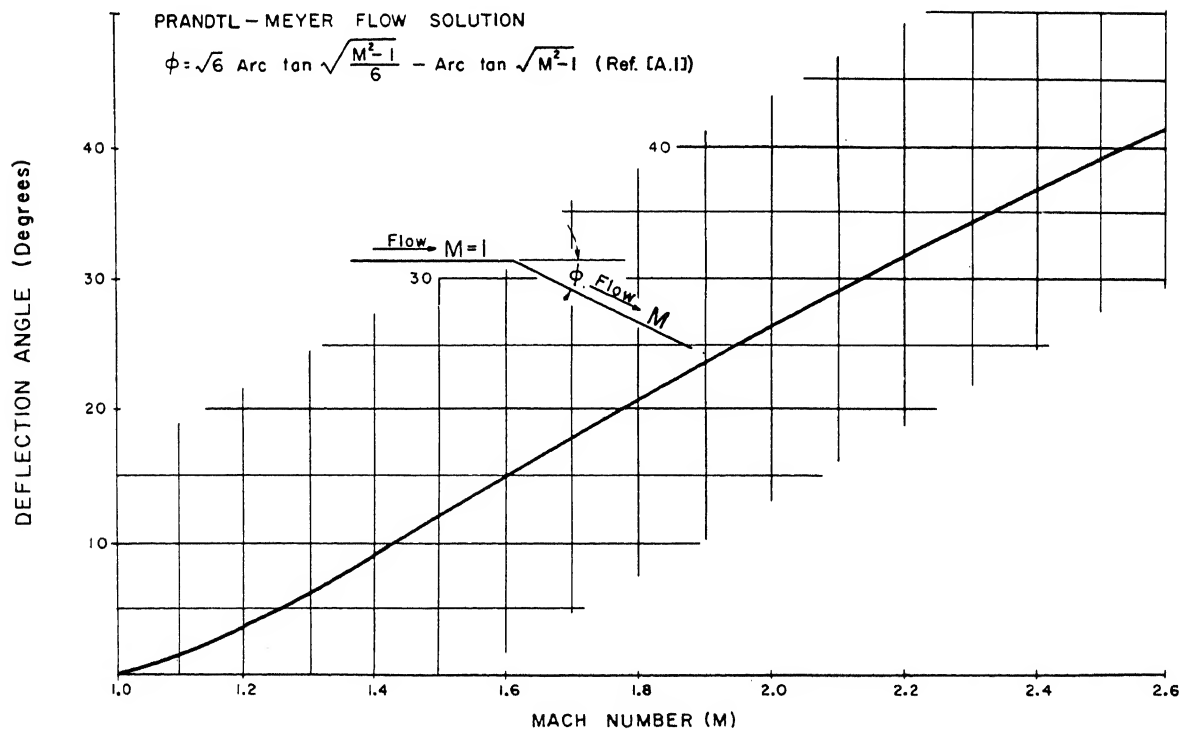


Figure A.4. Deflection angle required to expand to a given Mach number

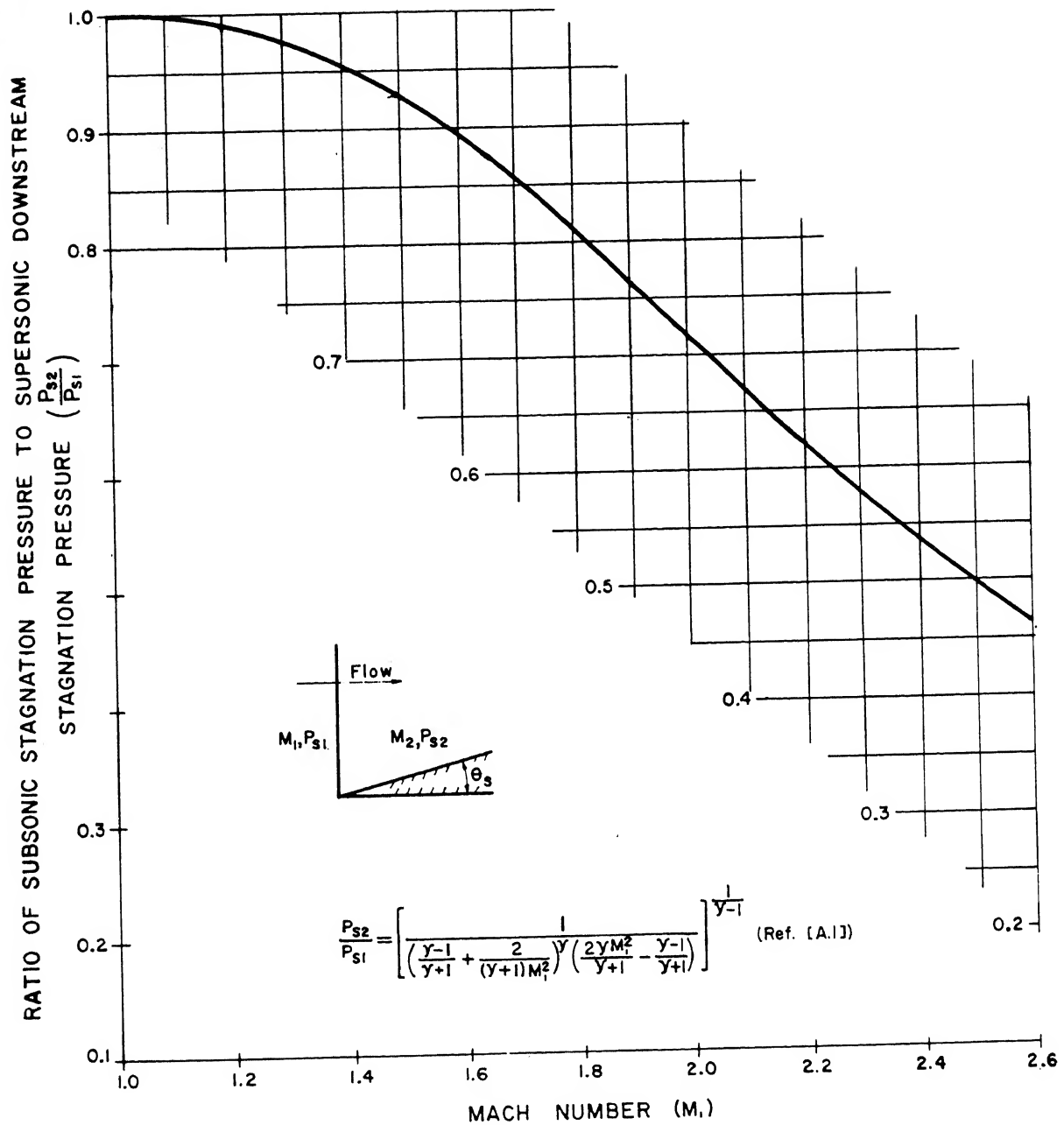


Figure A.5. Stagnation pressure ratio across a normal plane shock (psia)

1 July 59

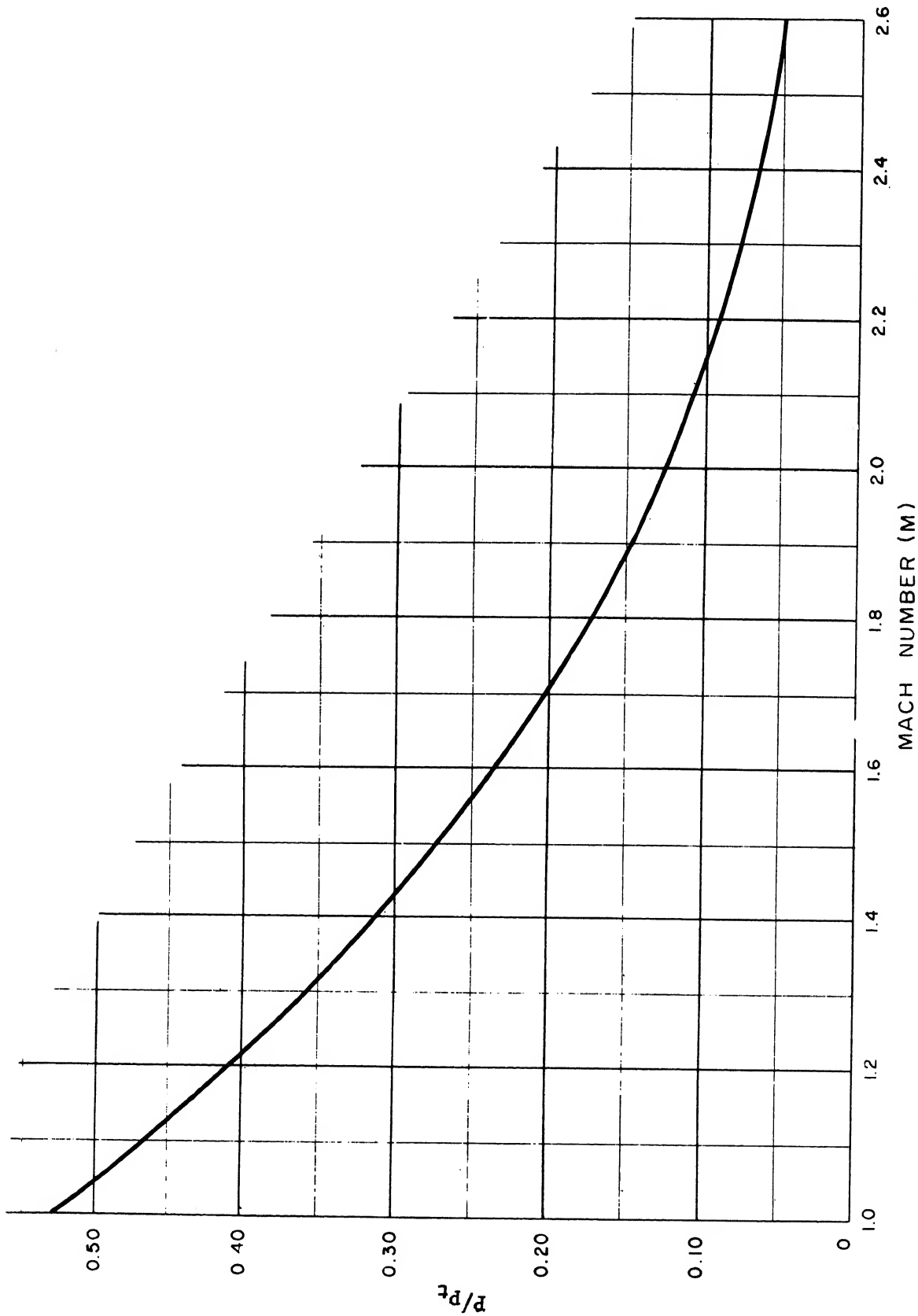


Figure A. 5a. Ratio of static pressure, p , to total pressure, p_t vs Mach number, M . (Reference A. 10)

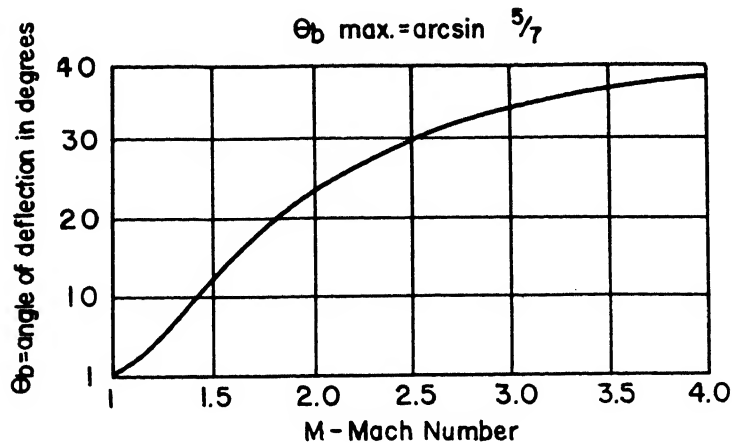


Figure A.6. Maximum deflection angle for which the shock wave will remain attached (reference [3])

flow is assumed supersonic, i.e. $M > 1$. (Reference [A.7].)

As the initial Mach number decreases to 1, the detached shock in figure A.7 forms further ahead of point A. When the Mach number falls below 1, the typical situation in the transonic range is as shown in figure A.8 with

one or more supersonic regions embedded in the subsonic flow. The conditions shown apply to Mach numbers not too close to one. As the Mach number increases and approaches one, the supersonic regions grow and coalesce, finally covering the structure from B to D. In this condition there would be a shock wave starting from D as in figure A.7.

The flows shown in figures A.7 and A.8 have certain features of interest in common. In both cases the pressure at A is equal to the stagnation pressure of the subsonic flow upstream of A. At B the local Mach number is always unity at the start of the expansion fan. These facts have

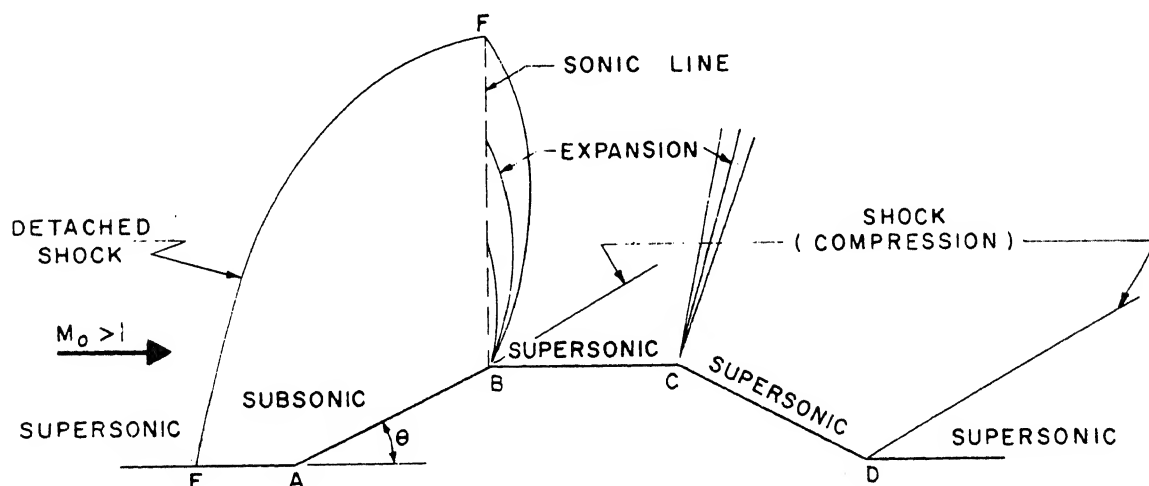


Figure A.7. Transonic flow ($M_0 > 1$)

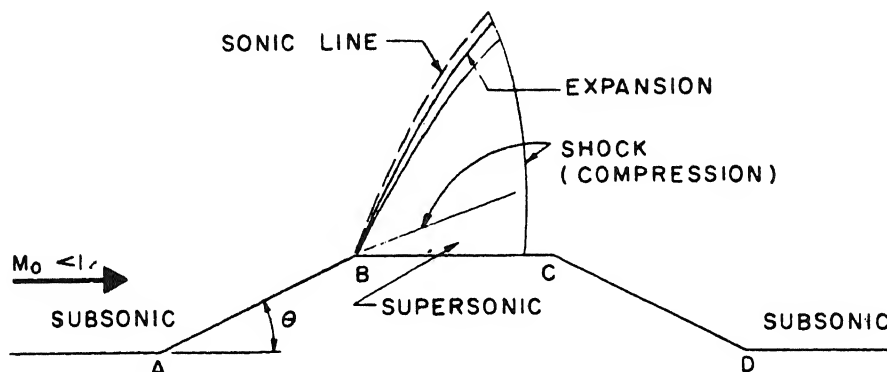


Figure A.8. Transonic flow ($M_0 < 1$)

been established experimentally and theoretically (reference [A.6]).

Further, it has been shown that the pressure distribution on the face AB is the same for a wide range of transonic flows for a given angle θ when the pressure is expressed in terms of the stagnation pressure rather than a pressure coefficient (reference [A.5], p 255). These facts are the basis for the method used below in computing the pressure distribution for the cases at hand.

A-03 METHOD FOR COMPUTATION OF PRESSURES IN THE TRANSONIC RANGE.

a. Cases In Which The Initial Flow Is Supersonic. The two highest pressure shock waves of 100 psi and 200 psi shock pressure yield an initial flow which is supersonic as shown in Table A.1. In these cases the conditions shown in figure A.8 apply.

The first computation is to find the stagnation pressure in the subsonic region. This may be conveniently done using figures A.3 and A.5. This stagnation pressure at point A, (figure A.9) is obtained by first determining the supersonic downstream pressure, P_{s1} , corresponding to the freestream Mach number, $M_0 = M_1$, from figure A.3 (using $\gamma = 1.4$), then using figure A.5 to determine the pressure at A, P_{s2} . For points between A and B, for the particular angle involved ($\theta = 26.6^\circ$) there are fortunately both theory and experiments available giving the ratio of

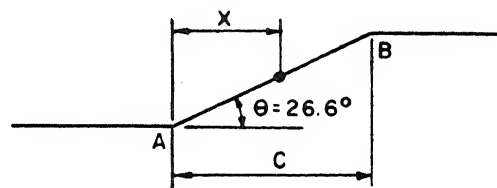


Figure A.9. Definition of x and c

1 July 59

A-03a

the pressure at any point x to the stagnation pressure which occurs at A. These ratios are plotted in figure 16 of reference A.6 and are summarized in Table A.2

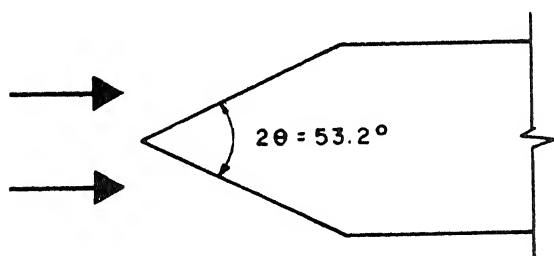
Table A.2. $\frac{\text{Pressure at } x, p}{\text{Pressure at A, } p_s}$ for $\theta = 26.6^\circ$

(From figure 16 of reference [A.6])

$\frac{x}{c}$	$\frac{p}{p_s}$	$\frac{x}{c}$	$\frac{p}{p_s}$
0	1	0.6	0.743
0.1	0.875	0.7	0.723
0.2	0.840	0.8	0.687
0.3	0.822	0.9	0.655
0.4	0.793	1.0	0.528
0.5	0.772		

It will be noted that the experiments and theory in most of the references deal with wedges as shown in figure A.10. The structures considered

herein are effectively one-half of the wedges tested.



The test results and theory available are concerned primarily with the face AB which is the most heavily loaded region and the relatively precise data given in Table A.2 is applicable. Unfortunately, equally precise data is

Figure A.10. Typical wedge profile

not available for the faces BC and CD. On the basis of examination of test results and of the underlying theory the following procedure is suggested as conservative and adequate, though lacking the same precision as the loads on AB.

The pressure at B, on the BC side of the corner may be computed by assuming there is a Prandtl-Meyer expansion fan starting from Mach number one on the downstream side of the corner as the net effect of an over-expansion and compensating compression at the corner. This pressure may be obtained by determining the Mach number, M_2 , on the BC side of the corner corresponding to the deflection angle $Q = 26.6^\circ$ from figure A.4 and then entering figure A.3 with this value to obtain the pressure, P_s . Along the face BC there may be some weak or even quite strong shock waves for which

exact data is not available, but their effect will be to increase the pressure. A reasonable estimate for the cases being considered is that the flow is returned to the pressure of the original supersonic flow upstream of E by the time the corner C is reached. In the absence of exact data a linear distribution of pressure between B and C is assumed.

At C, the pressure on the downstream side may be estimated by assuming a Prandtl-Meyer expansion fan starting from the free stream Mach number. Along the face BD, it is suggested that the pressure be assumed uniform because this region is shielded from the influences that can cause pressure rise along BC. The pressure on CD may be obtained from figure A.4 and A.5a as follows: (1) enter figure A.4 with free stream Mach number to obtain the Prandtl-Meyer angle, θ , (angle thru which a supersonic stream is turned to expand from $M = 1$ to $M > 1$), (2) add θ to the deflection angle (26.6° for our case) to obtain the ratio p/P_t where p is the static pressure on face CD and P_t is the total pressure downstream of C. Since there are only isentropic processes between A and D, P_t is the same as at A, (3) compute p from the ratio p/P_t .

b. Cases In Which The Initial Flow is Subsonic. The shock waves of 25 and 50 psi in Table A.1 have original Mach numbers less than one. In these cases, the pressure at A is the stagnation pressure given in Table A.1 and is obtained from figure A.3 only by entering the figure with the free stream Mach number to obtain the pressure ratio.

The coefficients given in Table A.2 apply for the region AB, using the stagnation pressure as given in Table A.2 for the angle $\theta = 26.6^\circ$

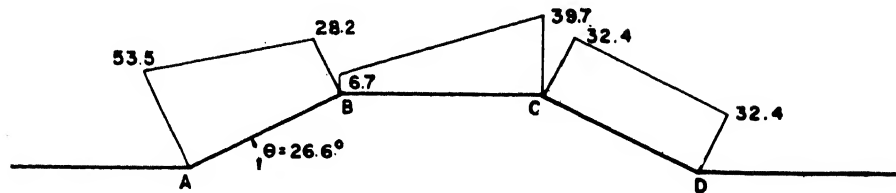
The pressure on the downstream side of B is computed assuming an expansion fan from Mach number one and may be obtained from figure A.3 and A.4 for $\theta = 26.6^\circ$ as for the supersonic case. A linear pressure rise is assumed from B to C, reaching the free stream pressure at C.

The downstream pressure at C is estimated according to their being a separation of the subsonic flow at the corner and with the help of experimental data (reference A.9.) Simple inviscid theory would indicate that the flow expands to zero pressure at the corner and thereafter resumes free stream velocity. However, since for these Mach numbers of approach to an edge of such a large angle as that at C, the flow separates,

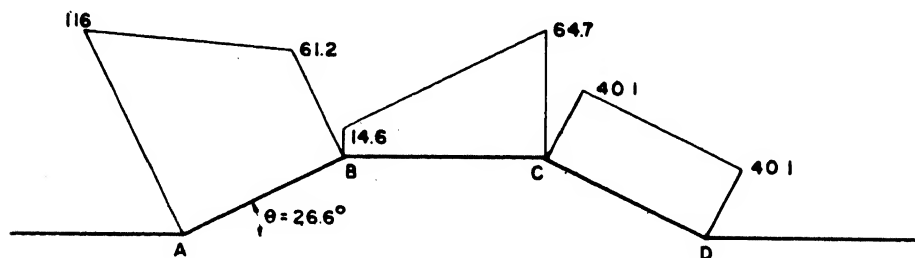
viscous effects can not be ignored (reference A.9). The pertinent data in reference A.9 (page 28 for station 12, 16) applies to a 30° flap deflection at an angle of attack of the flap of -9° . It would be desirable to have data for a leading edge flap deflection of 26.6° and an angle of attack of the flap of 0° but the above data is the closest available at this time. The pressure coefficient, $P = (p - p_o)/q$ indicated by the above test data is between -0.6 and -0.7, where p = the static pressure (psia), P_o = free stream pressure (psia) and q = the dynamic pressure. From another standpoint, if we can apply data from a wedge to represent flow on a half wedge following a straight section, as we did on the forward face AB, then we can apply data from a sharp edged plate at an angle of attack of 26.6° to represent the flow around a sharp corner of 26.6° , with about the same validity. The data on pages 18 and 19 (zero flap deflection) of reference A.9 show that the flow is separated and P is constant over the entire chord for 150, so it surely is also for $\alpha = 26.6^\circ$. The value of P is about 0.6, and this is used for both the 25 and 50 psi cases in this report.

A-04 NUMERICAL RESULTS FOR THE GIVEN CASES. The absolute pressures in pounds per square inch (absolute) are shown in figure A.11 for the given shock waves of 25, 50, 100, and 200 psig, respectively. The exact variation of the pressure along AB in each case may be found by applying the coefficients of table A.2 to the pressure given for point A (figure A.9) in each case. For comparison, the pressure distribution obtained using the equivalent circle method described in EM 1110-345-413 and EM 1110-345-420 is shown for the 25-psig level, and the 200-psig level in figures A.12 and A.13. The values given in figure A.11 are based upon a "flat top" shock but the preceding method is also easily applied to shocks which vary with time.

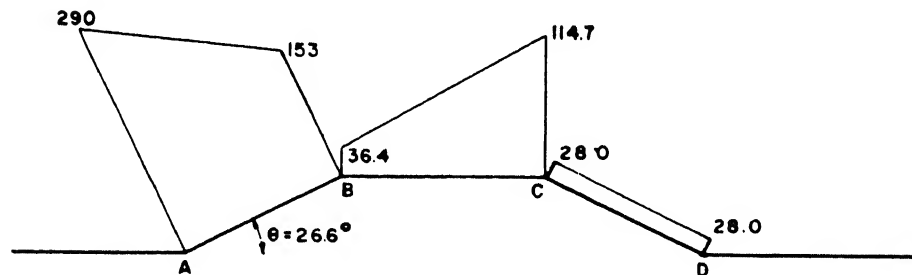
The pressures given are intended to apply to both of the structures shown in figure A.1(a) and figure A.1(b). The difference in the length of BC in the two cases will, in fact, make little difference to the pressure distribution and the available information does not provide any basis for computing these variations. It would be desirable to have a solution for flow over a double-wedge profile of 53° nose angle, but we have not been able to locate any data for this range.



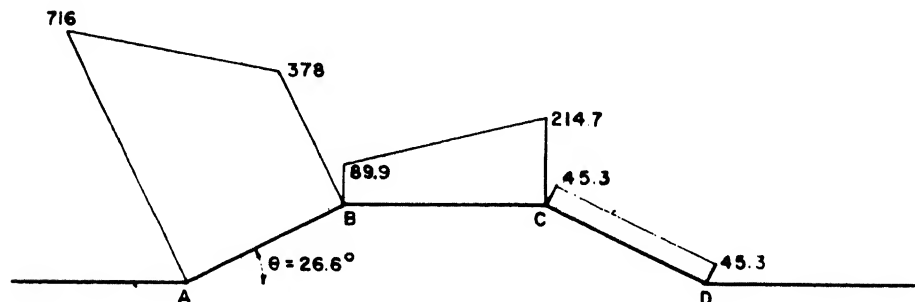
PRESSURES, PSI ABSOLUTE, FOR 25PSIG SHOCK WAVE



PRESSURES, PSI ABSOLUTE, FOR 50PSIG SHOCK WAVE

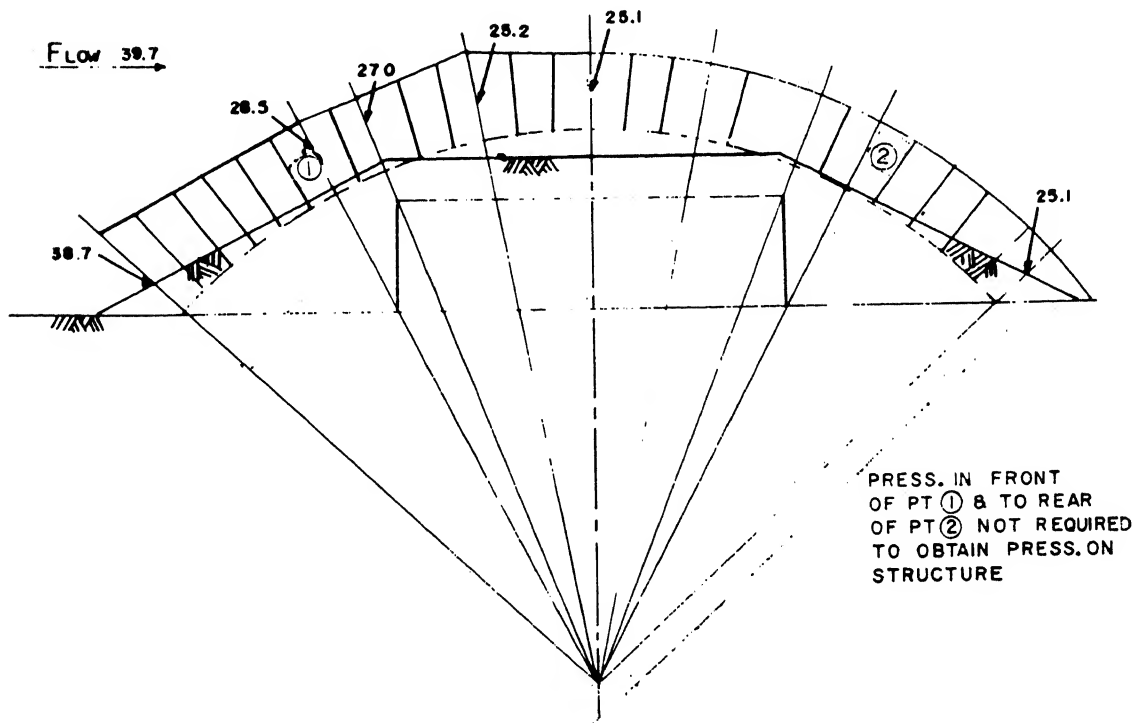
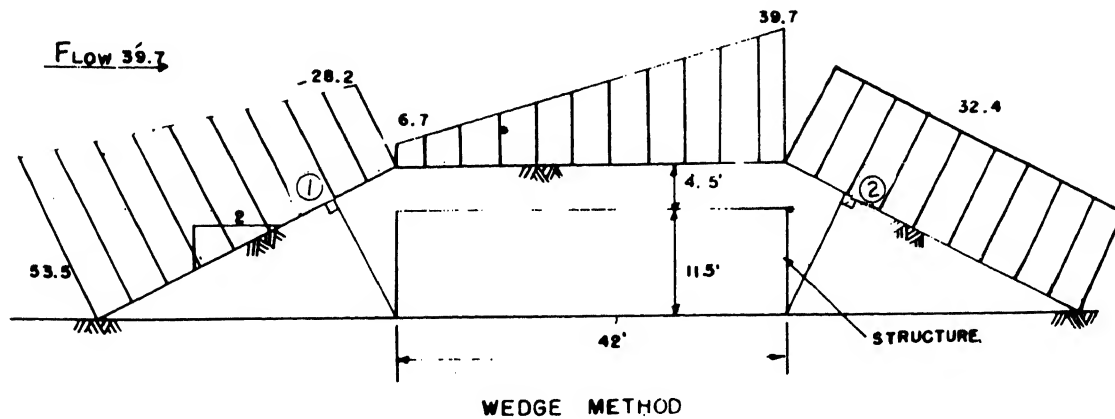


PRESSURES, PSI ABSOLUTE, FOR 100PSIG SHOCK WAVE



PRESSURES, PSI ABSOLUTE, FOR 200PSIG SHOCK WAVE

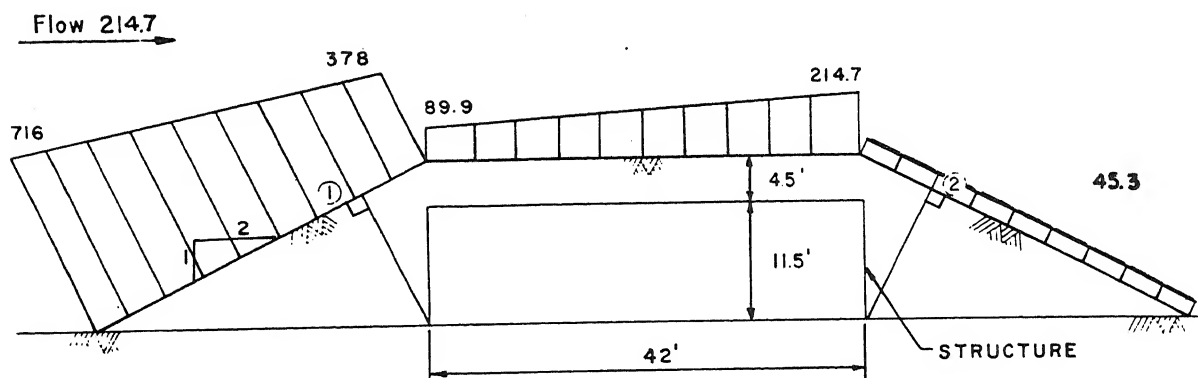
Figure A.11. Steady state pressures for the structures in figure A.1



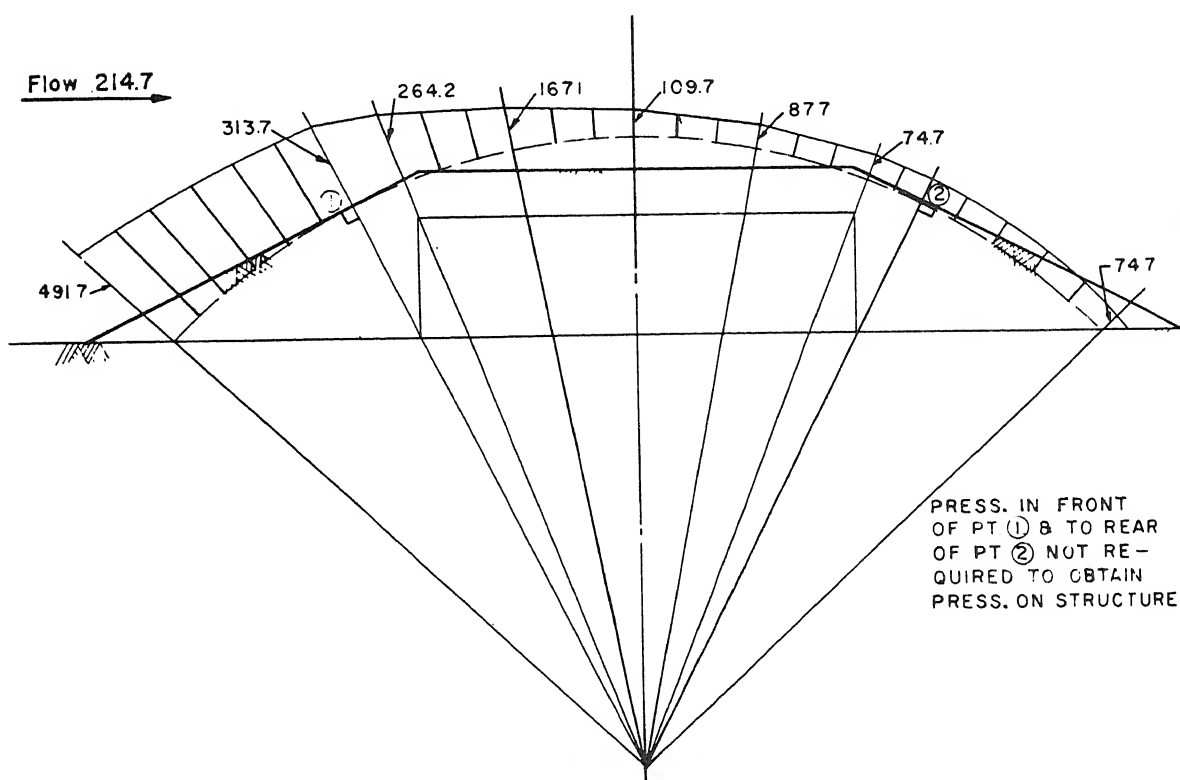
EQUIVALENT CIRCLE METHOD (EM 1110-345-413 AND EM 1110-345-420)

NOTE: ALL PRESSURES ARE PSI ABSOLUTE

Figure A.12. Comparison of wedge method with equivalent circle method, pressure = 25 psig



WEDGE METHOD



EQUIVALENT CIRCLE METHOD (EM 1110-345-413 AND EM 1110-345-420)
NOTE ALL PRESSURES ARE PSI ABSOLUTE

Figure A.13. Comparison of wedge method with equivalent circle method, pressure = 200 psig

A-05

EM 1110-345-413

1 July 59

A-05 REMARKS CONCERNING DOME OR CONICAL-SHAPED STRUCTURES. The above analysis has been concerned with structures which are long enough compared to the dimension in the direction of flow to be considered two dimensional. A dome or conical-shaped structure does not fall in this category and the coefficients suggested above should not be used for such cases, although this would certainly be conservative as far as the heavily loaded windward side is concerned.

Field measurements on full scale structures of this type were made during the 1957 nuclear test series conducted at the Nevada Test Site, but were not available at the time of this report.

REFERENCES

BOOKS

- A.1. Daily, C. L. and Wood, F. C. Computation Curves for Compressible Fluid Problems. New York, New York: John Wiley and Sons, Inc., 1949.
- A.2. Liepmann, H. W., and Puckett, A. E. Introduction to Aerodynamics of a Compressible Fluid. New York, New York: John Wiley and Sons, Inc., 1947.
- A.3. Miles, E. R. C. Supersonic Aerodynamics. New York, New York: McGraw-Hill Book Company, Inc., 1950.

Articles and Reports

- A.4. Liepmann, H. W., and Bryson, A. E. "Transonic Flow Past Wedge Sections." Journal of the Aeronautical Sciences, Vol. 17, No. 12, (December 1950), pp 745-755.
- A.5. Griffith, W. "Shock-Tube Studies of Transonic Flow Over Wedge Profiles." Journal of the Aeronautical Sciences, Vol. 19, No. 4, (April 1952), pp 249-257.
- A.6. Bryson, A. E. "An Experimental Investigation of Transonic Flow Past Two-Dimensional Wedge and Circular-Arc Sections Using a Mach-Zehnder Interferometer." Report 1094, National Advisory Committee for Aeronautics, 1952.
- A.7. Vicenti, W. G., and Wagoner, C. B. "Transonic Flow Past a Wedge Profile with Detached Bow Wave." Report 1095, National Advisory Committee for Aeronautics, 1952.
- A.8. "Design of Structures to Resist the Effects of Atomic Weapons", EM 1110-345-413 and EM 1110-345-420, Engineer Manual - Corps of Engineers, U. S. Army.
- A.9. Cleary, J. W. & J. A. Mellanthin, "Wind-Tunnel Tests of a 0.16 Scale Model of the X-3 Airplane at High Subsonic Speeds - Wing and Fuselage Pressure Distribution", NACA RM A50D07, June 22, 1950.
- A.10. Ames Research Staff, "Equations, Tables & Charts for Compressible Flow", NACA Report 1135, 1953.
- A.11. Spreiter, J. R., "Theoretical & Experimental Analysis of Transonic Flow Fields", NACA - University Conference on Aerodynamics, Construction and Propulsion, Vol. II - Aerodynamics, October 20-22, 1954.

References

EM 1110-345-413

1 July 59

- A.12. Anon, "Transient Drag and Its Effect on Structures", Final Report,
Project MR 1013, American Machine and Foundry Company, February
25, 1955 (Confidential).
- A.13. Spreiter, J. R. & A. Y. Alksne, "Thin Airfoil Theory Based on
Approximate Solution of the Transonic Flow Equation", NACA,
TN 3970, May 1957.

DEPARTMENT OF THE ARMY
US ARMY AG PUBLICATIONS CENTER
1655 WOODSON ROAD
ST. LOUIS, MISSOURI 63114

OFFICIAL BUSINESS
PENALTY FOR PRIVATE USE \$300

POSTAGE AND FEES PAID
DEPARTMENT OF THE ARMY
DOD 314

